UNIVERSIDADE D
COIMBRA

Josephine Blersch

BIOCOMPATIBLE NANOPARTICLES TO MODULATE CELL ACTIVITY

Tese no âmbito do Doutoramento em Biologia Experimental e Biomedicina, ramo de Biotecnologia e Saúde, orientada pelo Professor Doutor Lino da Silva Ferreira e Doutor Akhilesh Rai, apresentada ao Instituto de Investigação Interdisciplinar da Universidade de Coimbra.

Janeiro de 2021

Josephine Blersch

BIOCOMPATIBLE NANOPARTICLES TO MODULATE CELL ACTIVITY

Tese no âmbito do Doutoramento em Biologia Experimental e Biomedicina, ramo de Biotecnologia e Saúde, orientada pelo Professor Doutor Lino da Silva Ferreira e Doutor Akhilesh Rai, apresentada ao Instituto de Investigação Interdisciplinar da Universidade de Coimbra.

Janeiro de 2021

PROLOGUE

ABSTRACT

RNA-based medicines have distinct advantages in comparison to conventional drugs such as small molecules or other biomolecules in terms of specificity, potency, number of accessible targets, manufacturing, among others. However, several obstacles need to be addressed before the clinical translation of RNA-based therapeutics such as targeting and intracellular delivery. The main objective of this thesis was the development of biocompatible light-triggerable nanoparticle libraries to improve cell targeting and intracellular delivery of RNA-based medicines, for both *in vitro* and *in vivo* applications. The two nanoparticle libraries (each one of them were obtained from poly(amido amine) polymers) were synthesized by high-throughput strategies via Michael-type addition. In one of the libraries (160 NP formulations), the polymers were sensitive to light because they incorporated in their backbone a photo-cleavable linker (PCL) while, in the other (110 NP formulations), the polymer backbone was not sensitive to light but was modified with a pendent photo-cleavable molecule. In both cases, the polymers were precipitated in aqueous solution to form nanoparticles which were then complexed with siRNA or miRNA molecules. NP dissociate at different rates once activated by UV or a blue laser. A significant number of NPs showed more than 75% decrease in concentration after 10 min of light activation. In a High Content Screening, the NP library was screened for a fast transfecting carrier (with less than one hour of cell-material contact) in a model system (anti-GFP siRNA), that cause higher gene silencing than a commercial agent with boosted efficacy using light activation. More than a third of light-triggered NPs was found with increased gene silencing efficacy (up to 500%) in comparison to commercial transfection agent (Lipofectamine RNAiMAX) without compromised cell viability. Several candidates were further characterised in secondary tests regarding their specificity to skin cells (with some NPs that were more internalised by a specific type of cell than others) and endolysosomal escape. Functional studies before and after light activation with therapeutic relevant siRNA and miRNA prove applicability of the carriers for *in vivo* experimentation. Moreover, we have confirmed the advantages of one of the candidate formulations in a wound healing animal model, for the delivery of a recently identified skin regenerative miRNA. This thesis describes a powerful platform with the first light-activatable nanoparticle library with remote activation and efficient *in vivo* non-coding RNA delivery in wound healing. The results presented here are an exciting first step towards the translation of light-triggerable polymeric carriers for RNA-based therapeutics delivery.

Keywords: gene delivery, RNAi therapeutics, light-triggerable materials, nanomaterials, external trigger, modulation of cell activity, wound healing, *in vivo* microRNA delivery

RESUMO

As terapias baseadas em moléculas de RNA apresentam vantagens quando comparadas com medicamentos convencionais, tais como pequenas moléculas ou outras biomoléculas, em termos de especificidade, potência, número de alvos acessíveis, fabricação, entre outros. No entanto, vários obstáculos precisam de ser ultrapassados antes da translação clínica destas terapias baseadas em RNA, tais como a entrega direcionada e a entrega intracelular. O principal objetivo desta tese foi o desenvolvimento de bibliotecas de nanopartículas (NPs) biocompatíveis e responsivas à luz para aumentar a eficácia da entrega intracelular de moléculas de RNA, para aplicações in vitro e *in vivo*. As duas bibliotecas de nanopartículas (cada uma delas foi obtida a partir de polímeros de poli (amido amina)) foram sintetizadas através de estratégias de alto rendimento via reação de adição do tipo Michael. Numa das bibliotecas (160 formulações de NPs), os polímeros são sensíveis à luz uma vez que foi incorporado na sua estrutura um grupo foto-clivável (PCL), enquanto que na outra biblioteca (110 formulações de NPs), a estrutura do polímero não era sensível à luz, mas foi modificado com uma molécula pendente foto-clivável. Nas duas bibliotecas, os polímeros foram precipitados numa solução aquosa para formar nanopartículas, sendo posteriormente complexadas com moléculas de siRNA ou miRNA. Uma vez irradiadas com luz UV ou um laser azul, as NPs desintegram-se e libertam o siRNA ou o miRNA. Um número significativo de NPs mostrou uma diminuição na concentração superior a 75% após 10 min de ativação com luz. Numa triagem de alto conteúdo, as bibliotecas de NPs foram testadas para encontrar uma formulação que tivesse uma transfecção rápida (com menos de uma hora de contato célula-material) num sistema modelo (siRNA anti-GFP), causando um silenciamento eficaz do gene, quando comparado com um agente comercial. Mais de um terço das NPs irradiadas com luz mostraram uma eficácia superior do silenciamento do gene (máximo até 500%) em comparação com o agente de transfecção comercial (Lipofectamine RNAiMAX), sem com isso comprometer a viabilidade celular. As formulações mais eficazes foram também caracterizadas em testes secundários quanto à sua especificidade para células da pele (com algumas NPs que foram mais internalizados por um tipo específico de célula do que outros) e escape endolisossomal. Estudos funcionais, antes e depois da ativação de luz, usando siRNA e miRNA com relevância terapêutica comprovam a aplicabilidade das formulações para experimentação *in vivo*. Além disso, confirmamos as vantagens de uma das melhores formulações em um modelo animal de cicatrização de feridas, para a entrega de um miRNA regenerativo de pele. Esta tese descreve pela primeira vez uma biblioteca de nanopartículas ativáveis remotamente por luz para a entrega eficiente de RNA não codificante *in vivo* na cicatrização de feridas. Os resultados aqui apresentados

demonstram um passo promissor para a translação de formulações poliméricas foto-ativáveis pela luz na entrega de terapias baseadas em RNA.

Palavras chaves: entrega de genes, Terapia RNAi, materiais foto-ativáveis por luz, nanomateriais, estímulo externo, modulação da atividade celular, cicatrização de feridas, entrega de microRNA *in vivo*

KURZZUSAMMENFASSUNG

RNA-basierte Arzneimittel haben im Vergleich zu herkömmlichen Arzneimitteln, wie kleinen Molekülen oder anderen Biomolekülen, deutliche Vorteile. Unter anderem hinsichtlich der Spezifität, Wirksamkeit, Anzahl zugänglicher Ziele und Herstellung. Vor der klinischen Übersetzung von RNA-basierten Therapeutika müssen jedoch einige Hindernisse, wie gezielte Arzneimittelabgabe (Targeting) und intrazelluläre Verabreichung, überwunden werden. Das Hauptziel dieser Arbeit war die Entwicklung einer Bibliothek biokompatibler lichtaktivierbarer Nanopartikel (NP) zur Verbesserung des Zell-Targetings und der intrazellulären Abgabe von RNA-basierten Arzneimitteln für In-vitro- und In-vivo-Anwendungen. Die entstandenen zwei Nanopartikelbibliotheken (jede bestehend aus Poly(amido amin)-Polymeren) wurden durch Hochdurchsatzstrategien unter Verwendung von Michael-Addition synthetisiert. In einer der Bibliotheken (160 NP-Formulierungen) wurden durch den Einbau eines photospaltbaren Linkers (PCL) in das Grundgerüst, lichtempfindliche Polymere hergestellt. Für die Andere Bibliothek (110 NP Formulierungen) wurde das (nicht lichtempfindliche) Polymer mit einem photospaltbaren Molekül (Photo-Antenne) modifiziert. In beiden Fällen wurden die Polymere in wässriger Lösung ausgefällt um Nanopartikel zu bilden, die dann mit siRNA- oder miRNA-Molekülen komplexiert wurden. Die NP dissoziieren mit unterschiedlichen Geschwindigkeiten, sobald sie durch UV- oder einen blauen Laser aktiviert werden. Eine signifikante Anzahl von NP zeigte nach 10 Minuten Lichtaktivierung eine Konzentrationsabnahme von mehr als 75%. In einem High Content Screening wurde die NP-Bibliothek in einem Modellsystem (Anti-GFP-siRNA) auf einen schnell transfizierenden Träger (mit weniger als einer Stunde Zellmaterialkontakt) gescreent, der eine höhere Gen-Stummschaltung (Gen-Silencing) mit verstärkter Wirksamkeit durch Lichtaktivierung erzielt als ein kommerzielles Mittel. Mehr als ein Drittel der durch Licht aktivierten NP wurde mit einer erhöhten Gen-Silencing-Wirksamkeit (bis zu 500%) im Vergleich zu einem kommerziellen Transfektionsmittel (Lipofectamin RNAiMAX) ohne Beeinträchtigung der Lebensfähigkeit der Zellen gefunden. Mehrere Kandidaten wurden in Sekundärtests hinsichtlich ihrer Spezifität für Hautzellen (mit einigen NP, die von einem bestimmten Zelltyp stärker internalisiert wurden als andere) und ihrem endolysosomalen Austritt weiter charakterisiert. Funktionsstudien vor und nach Lichtaktivierung mit therapeutisch relevanter siRNA und miRNA belegen die Anwendbarkeit der Träger für *In-vivo*-Experimente. Darüber hinaus wurden die Vorteile einer der Kandidatenformulierungen in einem Tiermodell für Wundheilungsstudien, hinsichtlich der Abgabe einer kürzlich identifizierten hautregenerativen miRNA, bestätigt. Diese Arbeit beschreibt eine leistungsstarke Plattform mit der ersten lichtaktivierbaren Nanopartikelbibliothek mit

Fernaktivierung und effizienter *in vivo* Abgabe nicht-kodierender RNA bei der Wundheilung. Die hier vorgestellten Ergebnisse sind ein aufregender erster Schritt zur Translation lichtauslösbarer polymerer Träger für die Abgabe von RNA-basierten Therapeutika.

Schlagwort: Gentransfer, RNAi Therapeutika, photoaktivierbare Materialien, Nanomaterialien, Fernaktivierung, Modulierung der Zellaktivität, Wundheilung, *in vivo* microRNA Abgabe

ACKNOWLEDGEMENTS

To my advisor Dr. Lino Ferreira, I want to express my sincere gratitude, for his valuable guidance and continuous support. I want to acknowledge his encouragement of my creativity and free thinking, his critical comments and trust that I received throughout the research work.

I want to thank all the members of the NanoDrug Network, especially our collaborators from the NanoDrug project Prof. Karsten Haupt and Prof. Klaus Liedl who were always available to discuss this project. I want to thank Prof. Haupt and Carlo Gonzato, for the help in polymer characterization. Especial thanks to Prof. Liedl and Julian Fuchs who gave me the possibility to learn programming, facilitating the analysis of High Content Screening Data while a 3 month stay in Innsbruck. This experience was a seed, driving my curiosity and paving the path for my present and future.

I want to acknowledge the support of my co-supervisor Akhilesh Rai and the help and contribution of the project team. Especially to Vitor Francisco who supported the project in its final stages. Thank you for your help and contribution to this work. Thanks to Adrian Jimenez, Malwina Kotowicz, Catarina Rebelo, Helena Antunes, Susana Simoes, Ermelindo Leal, Miguel Lino and Sandra Pinto, for your contribution, your hands and support. Also, I want to acknowledge Vitor Francisco and Filipe Rodrigues who continue the research work in the LIghtBRARY project.

The whole group and former group members from the Biomaterials and Stem cell-based Therapeutics lab I would like to thank for their support and the time we spend together in Cantanhede and Coimbra. The proximity in which we worked and the stimulatory environment gave me the opportunity to discuss science, getting insights, finding answers and to learn about close connected fields that broadened my knowledge and opened my mind.

I want to thank my current team of the immunX project and the LAT members at the German Center for Neurodegenerative Diseases in Bonn under the leadership of Philip Denner and Eugenio Fava, for giving me trust, support and an incredible opportunity to grow and advance in the field of High Content Screening, Data Science, Immunology and Nanomedicine.

I want to acknowledge here the theatre company Marionet, where my participation started for a public outreach activity as Marie Curie Fellow, which developed into a passion. In the first play, "E agora Frankenstein?" ("And now, Frankenstein?") where Marry Shelley's Frankenstein, developed from a scientist steeling body parts from the cemetery, to a passionate stem cell engineer, supported by European Commission funds, I could barely pronounce all the words correctly in Portuguese. Over the years and plays, my language improved until the moment where I could actively drive discussions and write scenes as for the last play where I participated "Luz de perdição" ("Light of perdition") and "Luz_Livro" ("Light_Book"). I want to thank Mario Montenegro for all his time, the spirit with which means he is driving the amateur-science-theatre group to the stage and all the laughter. I would like to thank all the amazing researchers and actors I have met and got friends in this context. Art and science are connected in various means. One definitely is theatre.

I want to thank my dear friends Gabriela Mesquita, Margarete and K.P. Engelland, Andrea and Norbert Erbe, Malwina Kotowicz, Paula Nosari, Michela Comune, Catarina Rebelo, Cristiana Paulo, Sezin Aday, Sarah Hartmann, Mehrzad Zargarzadeh, Julian Chollet/mikroBIOMIK, Dietmar Götze and Martin Kleppe who believe in me, encourage me and support me on my way. Thank you, Tobias Pranter, for not giving up by my side, for your help, your support that brought me here and for your hand in mine. I am thankful for each day we spent together. I feel grateful to be surrounded by such amazing personalities. Especially the camaraderie from the strong women by my side gave me the force that I needed. Thank you!

I want to thank my companions Paula Nosari (Drums, Music & Therapy), Mafalda Soares (Vocals & Light Design), Gabriela Mesquita (Triangle & Contractuality) from the "*DreiFrauenPunkRockBand e um triangulo aus Coimbra*" for being with me (Guitar, Vocals & Science)!

My Portuguese family at the "Casa das Bonecas" where I had the chance to live in their garden, in the middle of peaceful nature. Thank you, Manuela & Enginheiro João Benjamin & your family, my neighbour Sonja with Gabi and Blimunda.

With deep gratitude I want to thank my family - my mother Silvia, my father Erhard, my sister Katharina Franziska and my brother Tobias - for giving me support on my way. For giving me strength, believing in me and being close even far away on this journey in Portugal.

FINANCIAL SUPPORT

The research leading to this thesis has received funding from the European Commission and the European Research Council under the European Union's Seventh Framework Programme (FP/2007-2013) within the projects NANODRUG (Novel nanomaterials for drug delivery to the skin | Marie-Curie Actions, Initial Training Network | project no 289454, 2011-2015) and NanoTrigger (ERC Grant Agreement no. 307384). Further this project received funding from ERA Chair project (ERA@UC, reference: 669088) through EU Horizon 2020 program and POCI-01-0145-FEDER-029414 (acronym: LIghtBRARY) project, through Compete 2020 and FCT programs.

PUBLICATIONS AND COMMUNICATIONS

Awards

Winner of Marie Curie Early Stage Researcher European Fellowship (September 2012).

Provisory Patent

Blersch J. and Ferreira L., Light-triggerable Nanoparticles and the uses thereof, PAT20191000026512

Publications

Blersch, J., Francisco V., Rebelo C., Jimenez, A., Antunes H., Gonzato C., Pinto S., Simoes S., Liedl K., Haupt K., Ferreira L., "A light-triggerable nanoparticle library for the controlled release of non-coding RNAs", Angewandte Chemie, 2020, Volume 59 (5), p. 1985-1991.

Blersch, J., Francisco, V., Rebelo, C., Jiménez-Balsa, A., Antunes, H., Pinto, S., Simoes, S., Rai, A., Ferreira, L., "A light-triggerable formulation to control the stability of pro-angiogenic factor-1α (HIF-1α)", Nanoscale, 2020 (12), p. 9935-9942.

Francisco, V., Rebelo, C., Rodrigues, A.F., **Blersch, J.,** Fernandes, H., Ferreira, L., "A high-throughput screening platform to identify nanocarriers for efficient delivery of RNA- based therapies.", Methods, 2020, doi.org/10.1016/j.ymeth.2020.12.002.

Estronca. L., Francisco, V., Pitrez, P., Honório, I., Carvalho, L., Vazão, H., **Blersch, J**., Rai, A., Nissan, A., Simon, U., Grãos, M., Saúde, L., Ferreira, L., "Induced pluripotent stem cell-derived vascular networks to screen nano-bio interactions.", Nanoscale Horizons, accepted for publication 2020.

Comune, M. Rai, A., Chereddy, K.K., Pinto, S., Aday, S., Ferreira, A.F., **Blersch, J.,** Cunha, R., Rodrigues, R., Simões, P.N., Preat, V., Ferreira, L.," Antimicrobial peptide-nanoscale therapeutic formulation with high skin regenerative potential". Journal of Controlled Release, 2017 (262) p. 58-71.

Oral Communications

Blersch, J., Jiménez-Balsa, A., Rebelo, C., Henriques-Antunes, H., Francisco, V., Kotowicz, M., Pinto, S., Rai, A., Haupt, K., Liedl, K., Ferreira, L. S., Efficient non-coding RNA delivery in wound healing by photo-triggerable nanoparticles, 53rd Annual Scientific Meeting of the European Society for Clinical Investigation (ESCI), 22-24 May 2019, Coimbra, Portugal.

Blersch, J., Jiménez-Balsa, A., Rebelo, C., Henriques-Antunes, H., Francisco, V., Kotowicz, M., Pinto, S., Rai, A., Haupt, K., Liedl, K., Ferreira, L. S., A photo-triggerable NP library for skin cell targeting and efficient in-vivo small non-coding RNA delivery in wound healing, 29th European conference on Biomaterials, 9-13 September 2018, Maastricht, Netherlands.

Blersch, J., Jiménez-Balsa, A., Rebelo, C., Henriques-Antunes, H., Francisco, V., Pinto, S., Rai, A., Haupt, K., Liedl, K., Ferreira, L. S., HT-Screening identifies light-triggerable NP formulation for efficient in-vivo non-coding RNA delivery in wound healing, XII Spanish-Portuguese Conference on Controlled Drug Delivery, Tailoring drug delivery systems to the patients´ needs, 14-16th January 2018, Coimbra, Portugal.

Blersch, J., Jiménez-Balsa, A., Rebelo, C., Henriques-Antunes, H., Francisco, V., Pinto, S., Rai, A., Haupt, K., Liedl, K., Ferreira, L. S., Light-triggerable Nanoparticles for efficient in-vivo non-coding RNA delivery in wound healing, 10th International Meeting of the Portuguese Society for Stem Cells and Cell Therapies, 12-14th October 2017, Covilhã, Portugal.

Blersch, J., Using High Content Imaging to determine the bioactivity of a NP library for noncoding RNA delivery, 5th Nanodrug International Scientific Meeting, July 2015, Algero, Italy.

Blersch, J., Using biocompatible NPs as delivery platform for microRNAs, 4th Nanodrug International Scientific Meeting, February 2015, Innsbruck, Austria.

Blersch, J., Using biocompatible NPs as delivery platform for microRNAs, 3rd Nanodrug International Scientific Meeting, July 2014, Coimbra, Portugal.

Blersch, J., Using biocompatible NPs as delivery platform for microRNAs, 2nd Nanodrug International Scientific Meeting, September 2013, Biarritz, France.

Posters

Blersch, J., Francisco, V, Rebelo, C, Jiménez-Balsa, A., Henriques-Antunes, H. Kotowicz, M., Gonzato C., Pinto, S., Simoes S., Liedl K., Haupt K., Ferreira L. S., A photo-triggerable NP library for skin cell targeting and efficient in-vivo small non-coding RNA delivery in wound healing, 14th Microsymposium on Small RNA Biology, May 15-17th 2019, Vienna, Austria.

Blersch, J., Jiménez-Balsa, A., Rebelo, C., Henriques-Antunes, H., Francisco, V., Pinto, S., Rai, A., Haupt, K., Liedl, K., Ferreira, L. S., HT-Screening identifies light-triggerable NP formulation for efficient in-vivo non-coding RNA delivery in wound healing, MCAA General Assembly & Annual Conference 2&3 February Leuven, Belgium.

TABLE of CONTENTS

ACRONYMS AND ABBREVIATIONS

°C	|	Degree Celsius
2D	|	2-dimensional
3D	|	3-dimensional
A	|	nucleobase arginine
A2780	|	human ovarian carcinoma cells
A7r5	|	Rat aortic smooth muscle cells; fibroblasts
AAV	|	adeno-associated virus
ABOL	|	4-amino butanol
Ag	|	silver
Ago2	|	argonaute 2
AMD	|	age-related macular degeneration
ApoB	|	apolipoprotein B
ApoE	|	apolipoprotein E
ARPE	|	human retinal pigment epithelial cells
ASGPR	|	asialoglycoprotein receptor
ASO	|	antisense oligo nucleotide
ATP	|	adenosine triphosphate
Au	|	gold
Azo	|	azobenzene
BAB	|	blood-aqueous barrier
BALB/c	|	albino inbred mouse
bEnd3	|	immortalized brain endothelioma cells
BRB	|	blood-retinal barrier
C57BL/6	|	genetic background inbred mouse
C. elegans	|	Caenorhabditis
CBA	|	cystaminebisacrylamide
CD	|	cyclodextrin
COS-7	|	monkey kidney fibroblasts
CPP	|	cell penetrating peptides
CTGF	|	connective tissue growth factor
Cy5	|	flourescent chromophor 649/666 nm Ex./Em.
d	|	days
Da	|	Dalton
db/db	|	diabetic genetic mouse model
DIO	|	diet-induced obese
dL	|	deci liter
DLS	|	Dynamic Light Scattering
DMEM	|	Dulbecco's modified Eagle's Medium
DMSO	|	dimethyl sulphoxide
DNA	|	deoxyribonucleic acid
DOTAP	|	Dioleoyl-3-trimethylammonium propane
DPc	|	dendrimeric phthalocyanine
DPPC	|	1,2-dipalmitoyl-sn-glycero-3-phosphocholine
DR	|	diabetic retinopathy
DS	|	degree of substitution
dsRNA	|	double stranded RNA
EC	|	endothelial cell
ECM	|	extracellular matrix
EDA	|	diamno ethane
EEA1	|	early endosome antigen 1
EGFR	|	epidermal growth factor receptor
EggPC	|	Egg phosphatidylcholine
EGM-2	|	Endothelial cell growth medium-2
EMA	|	European Medicines Agency (EU)
EMF	|	electromagnetic field
EOMA	|	mouse endothelial hemangioendothelioma cells
ESC	|	endothelial stem cells
FACS	|	flourescence activated cell sorting
FBS	|	fetal bovine serum
FDA	|	Food and Drug Administration (US)
FGF	|	fibroblast growth factor
FL2	|	Fidgetin-like 2
G	|	nucleobase guanine
g	|	gravitational field strength
Gal8	|	galectin-8
GalNAc	|	N-acetyl galactosamine
GAPDH	|	Glyceraldehyde 3-phosphate dehydrogenase
GBM 319	|	human brain cancer cells
(e)GFP	|	(enhanced/emerald) green flourescent protein
GM3	|	ganglioside-monosialic acid 3

GNP	gold nanoparticles
GPC	Gel Permeation Chromatography
GSH	glutathione reductase
h	hour(s)
H-NMR	proton nuclear magnetic resonance spectroscopy
HA	hyaluronic acid
HaCaT	human keratinocytes
hATTR	hereditary transthyretin-mediated amyloidosis
HBV	hepatitis B virus
HCI	High-Content Imaging
HCS	High-Content Screening
HCT	human epithelial colorectal carcinoma cells
HDR	high dynamic range
HEK293	human embryonic kidney epithelial cells
HeLa	human epithelial, adenocarcinoma cells
hESC	human embryonic stem cell
hESdCs	human embryonic stem cell-derived cells
HIF-1α	hypoxia inducible factor one alpha
hMSCs	human mesenchymal stem cells
HMVEC	primary human microvascular endothelial cells
HNSCC	human head and neck squamous cell carcinoma
HSV	herpes simplex virus
HT	High-Throughput
HTS	High-Throughput Screening
hUCBMNCs	human umbilical cord blood mononuclear cells
HUVEC	human umbilical vein endothelial cells
Hz	Hertz
ICG	indocyanine green
ICR (CD-1®)	Albino mouse with high incidence of retinal degradation
IGF	insulin like growth factor
IL	interleukin
k	kilo
LAMP1	lysosomal-associated membrane protein 1
LbL	layer-by-layer
LC	liquid cristal
LC3	Microtubule-associated protein
LCST	lower critical solution temperature
LNA	locked nucleic acid
LNP	lipid or lipid-like nanoparticle
LODER	Local Drug EluteR ™
M	molecular weight
MCF-7	human epithelial adenocarcinoma cells
Me	Methyl group
mg	miligram
min	minutes
miR	microRNA
MMP	matrix metalloproteinase
MnSOD	manganese superoxide dismutase
MRI	Magnetic Resonance Imaging
MRSA	Methicillin-resistant Staphylococcus aureus
MSC	mesenchymal stem cells
mRNA	messenger RNA
MW	molecular weight
NC	no carrier
ncRNA	non-coding RNA
NEP	nanochannel electroporation
NHDF	normal human dermal fibroblast
NIR	near infrared
nm	nanometer
NO	nitric oxide
NP	nanoparticle
NPE	1-(2-nitrophenyl)ethyl
nt	nucleotide
NVOC	4,5-dimethoxy-2-nitrobenzyl chloroformate
o-NB	ortho-nitrobenzyl
O_2	oxygen
OECs	outgrowth endothelial cells
OTE	off target effect
PAA	poly(amido amine)

PAMAM	poly(amido amine) dendrimer
PATK	poly(amino ketal)
PBAE	poly(β-amino ester)
PBS	phosphate buffered saline
PC	Pachyonychia Congenita
PCI	photochemical internalisation
PCL	photo cleavable linker
PCN	photochromic nucleoside
PCSK9	proprotein convertase subtilisin/kexin type 9
PDGF	platelet derived growth factor
pDMAEMA	poly(dimethylaminoethyl methacrylate)
PDT	photodynamic therapy
PE	polyethylene
PEG	polyethylene glycol
PEG-DMG	1,2-Dimyristoyl-rac-glycerol, methoxypolyethylene Glycol
PEG-DSPE	methoxy-polyethylene glycol-distearoylphosphatidylethanolamine
PEI	polyethyleneimine
PEO	EOMA
PFPAM	Perfluorpropane-Albumin Microsphere
PH1	primary hypoxaluria Type 1
PHD2	prolyl hydroxylase domain protein 2
PI	propidium iodide
PLA	poly(lactic acid)
PLK-1	polo-like kinase-1
PLys	poly lysine
PP	poly propylene
ppm	parts per million
PS	polystyrene
PS	photosensitizer
PUVA	UVA photochemotherapy
qRT-PCR	quantitative real time Polymerase chain reaction
RES	reticuloendothelial system
RISC	RNA induced silencing complex
RNA	ribonucleic acid
RNAi	RNA interference
ROS	reactive oxygen species
RT	room temperature
SC	stem cell
sd-rxRNA	self-delivering nucleic acid
SEC	size exclusion chromatography
SEM	standard error of the mean
SHH	sonic hedgehog
shRNA	short hairpin RNA
siRNA	short interference RNA
SNA	spherical nucleic acid
SPION	super paramagnetic iron oxide
SPR	Surface Plasmon Resonance
SS	disulfide linkage
ssDNA	single stranded DNA
STZ	streptozotocin
TAT	trans-activator of transcription
TEM	Transmission Electron Microscopy
TGF-β	Transforming growth factor beta
TLR	toll-like receptor
TMS	tetramethylsilane
TNF-α	tumour necrosis factor alpha
TTR	transthyretin
U	nucleobase uracil
UCNP	up-conversion nanoparticle
UTMD	ultrasound-targeted microbubble distruction
UTR	untranslated region
UV	ultraviolet
VEGF	vascular endothelial growth factor
vis	visible
XIAP	x-linked inhibitor of apoptosis protein
YFP	Yellow flourescent protein
β-Gal	β-Galactosidase
ζ	Zeta
µm	micrometer

LIST OF FIGURES

LIST OF TABLES

CHAPTER I – AIMS AND OUTLINE OF THIS THESIS

RNA-based medicines have high therapeutic potential, as targets are not restricted by translation (as cell surface markers, enzymes), but any mRNA sequence can be targeted with high specificity. This gives RNAi therapeutics "extraordinary drug-like properties"[1] with distinct advantages in comparison to conventional drug therapies (e.g. small molecules or other biomolecules) in terms of specificity, potency, number of accessible targets and manufacturing. In 2018, it was approved by FDA the first RNAi medicine based on siRNA encapsulated in lipid nanoparticles. In the meantime, several clinical trials are running with miRNA-based formulations. A general limitation of the RNAi formulations is related to their toxicity (infusion/immune reaction) and lack of efficacy. Toxicity is due to the high dosage that needs to be administered, since efficiency in intracellular delivery is lacking. Endosomal escape of leading formulations for siRNA delivery was shown to be as low as 2% *in vitro* and *in vivo*[2], limited by a very short timeframe after endocytosis[3].

The main objective of this thesis was the development of biocompatible light-triggerable nanoparticle libraries to improve cell targeting and intracellular delivery of RNA-based medicines, for both *in vitro* and *in vivo* applications. The significance of the work is attested by: (i) the first demonstration of a light-triggerable NP library for small ncRNA delivery with fast transfection and rapid endosomal escape properties, (ii) the demonstration of the superior uptake and transfection efficiency in skin cells with small noncoding RNA (both siRNA and microRNA) in comparison to commercial standard (Lipofectamine RNAiMAX) and (iii) the increased bioactivity through light activation (as shown in skin wound healing).

The PhD thesis is divided in five chapters. A general overview is given in **Chapter I**. It includes the presentation of the problem addressed by the thesis and discusses significant contributions to advance the state of the art.

Chapter II reviews the state of the art of RNAi therapeutics and triggerable nanomaterials for gene delivery. A focus is given on endosomal escape of NP formulations for siRNA delivery. Different approaches of polymer libraries screened for gene delivery are reviewed as well. The last section of the chapter focuses on light-triggerable formulations for gene delivery including application in treatments of ocular and skin diseases. **Chapter III** describes the development of a library of light-triggerable polymeric NPs for the delivery of small non-coding RNAs with activity in wound healing. The NPs were obtained from polymers containing a photo-cleavable linker in their backbone. The chapter reports the intracellular trafficking properties of

one of the formulations and its increased efficiency in delivering pro-migratory microRNA-150. Finally, it describes the bioactivity of the formulation in an acute wound healing mouse model. **Chapter IV** gives information about synthesis and characterization of a light-triggerable NP library bearing the photosensitive compound as antenna pendant to the polymer chain. The chapter reports the activity of the NP library containing a siRNA in a reporter cell system and then the bioactivity of the top formulations in skin cells. Finally, it describes the application of the lead formulation in regenerative medicine, showing results of pro-proliferative, pro-migratory and pro-angiogenic activity of light activated NPs in combination with PHD2 siRNA in endothelial cells. A general discussion of results from Chapter III and IV is provided in **Chapter V** with the presentation of future opportunities for the material developed in this thesis.

CHAPTER II – STATE OF THE ART

The key element for the effect of any medication is the delivery of the drug to its site of action and to ensure its bioactivity. Two major issues need to be addressed; the first is the delivery to the location where the drug is needed, the second is the protection of the drug to guarantee its bioactivity. Efficiency of the medication is dependent on both. Therefore, drugs need a delivery system. The drug delivery system determines pharmacokinetic and pharmacodynamic. Non-specific toxicity and immunogenicity should be minimised and biorecognition needs to be ensured.

Multidisciplinary approaches and potentially the combination of various methods is necessary to design a carrier system for controlled drug delivery. Several parameters need to be considered for the design of a system. Firstly, the drug and its physicochemical properties such as solubility, charge and protein binding characteristics need to be analysed. Second the route of delivery (defines the technology) and the target site (specific organ, tissue, cell type) as well as the disease pathologies and patient´s needs (i.e. acute or chronic disease)[4].

Efficiency of a drug is given if the drug reaches the target site in its optimal therapeutic dose. Sustained release systems were developed in 1950's[5] to provide therapeutic doses over prolonged time periods by gradual drug release after an initial bolus to reach the therapeutic dose. Drug plasma levels can be held constant until 12 h (or with implants for months) after the administration[5]. This might be advantageous for systemically delivered drugs. However, many pathologies are restricted to a certain site in the body and systemic delivery might lead to severe side effects. Controlled delivery systems allow to minimize unwanted side effects with maximisation of the applied dose at the target site. There are three modes of controlled drug delivery: (i) targeted delivery – to a specific cell type, tissue, organ, (ii) modulated release – variable release rate with control by environmental parameters, biofeedback, sensor input or external control device and (iii) controlled release – in a predetermined rate, or at a specific time, with a specific release profile, control over location and time or spatiotemporal control over the release[5]. External triggers such as light, ultrasound and magnetic stimulation allow high levels of spatiotemporal control.

The focus of this work is on the delivery of RNA antisense (RNAi) therapeutics, which is a "hard-to-deliver" category of molecules. RNAi drugs as microRNA and short interference RNA (siRNA) are very potent therapeutics due to their high specificity and selectivity for targets that are independent of the cellular expression system, giving the possibility to interfere in the regulation of any mRNA target. Delivery vehicles are necessary to protect RNAi therapeutics

from degradation, to promote cell and tissue uptake and to avoid toxicity. From the discovery of gene suppression by RNA interference in 1998 by Craig Mello and Andrew Fire in *C. elegans* [6], it took twenty years until the clinical approval of Onpattro® (patisiran), the first RNAi drug in 2018[7,8].

1 GENE DELIVERY OF RNAi THERAPEUTICS – The promise in anti-sense

1.1 Definition & Mechanisms

RNAi are molecules (described in animals, plants and protozoa) that regulate gene expression on a post-transcriptional level. This process is triggered by sequence specific non-coding double stranded RNAs such as endogenous microRNA and synthetic short interference siRNA with around 19-25 nucleotides (nt) size. Upon binding, the targeted mRNA transcripts are cleaved, degraded or translation is suppressed[9]. 1400 endogenous and highly conserved microRNAs are described in mammals with functions from development to apoptosis.

Mechanistically, short hairpin pri-miRNAs are translated from the genome, processed by RNAse III Drosha to 70-100 pre-miRNAs and exported from the nucleus via Exportin-5 to the cytoplasm (Figure 1). The RNAse III Dicer binds to double strand RNAs (dsRNA) and short hairpin RNAs (shRNA) and breaks them into shorter double stranded fragments (~21 nt

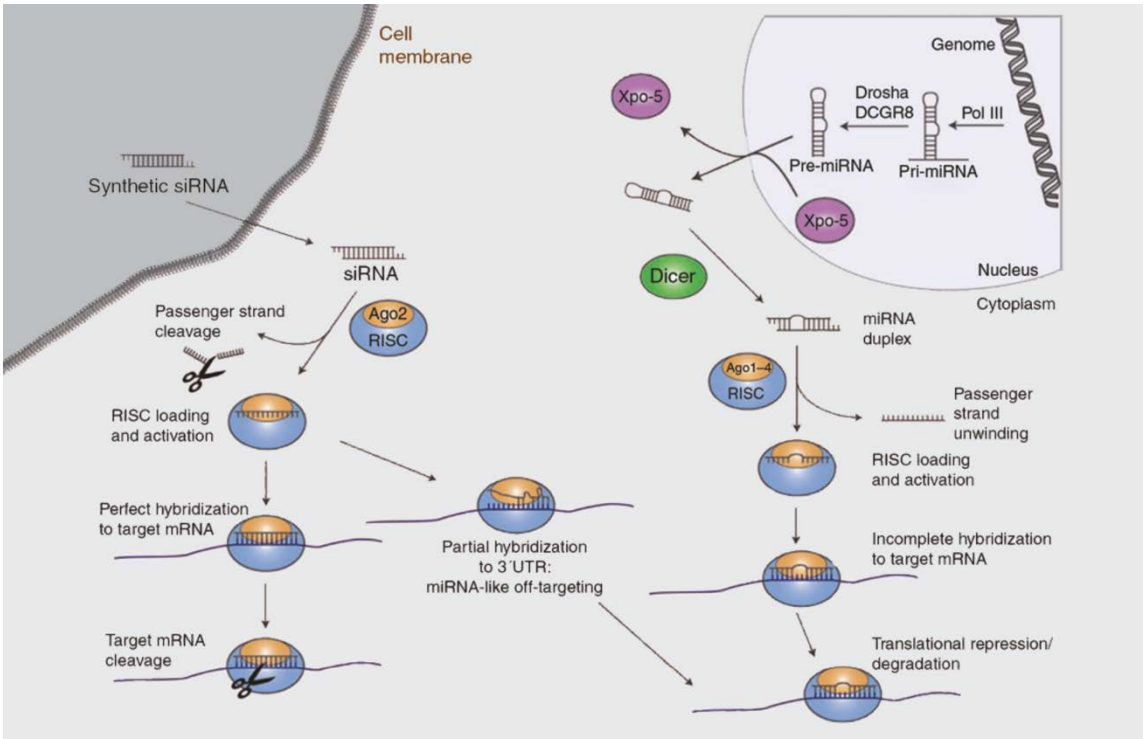

Figure 1: RNA silencing mechanism for endogenous microRNA (right side) and exogenous dsRNA and siRNA (left side). Adapted from Kanasty et al., Molecular Therapy, 2012.[10]

fragments with 2-nt overhangs on 3'-terminus)[10]. The dsRNA guide is associated with the RNA induced silencing complex (RISC). Passenger (sense) and guide (antisense) strand are unwound and the guide is loaded in the RISC, with 5'-terminus bound to PIWI domain of Argonaute 2 (Ago2) protein and 3'-terminus by the PAZ domain of Ago2. The passenger strand is degraded[11]. Through the antisense strand, RISC recognizes the mRNA target and binds (through Watson-Crick base paring) to its 3' untranslated region (3' UTR). The "seed sequence" at the 5'-end of the antisense strand extends for microRNA from 2-7 nucleotides, whereas full sequence homology is needed for siRNA binding. Translational repression occurs if microRNA-RISC binds to the mRNA target. Cleavage and full degradation occurs, if longer microRNA sequences (central microRNA region binds) or siRNAs bind to the mRNA target[12]. Consequentially (through the short "seed sequence"), one microRNA can have regulatory impact in multiple targets and siRNA act with high specificity on one target mRNA.

1.2 Barriers & Limitations

Very often off target effects (OTE) weaken RNAi action, or lead to unintended and unpredicted non-specific silencing on other mRNAs, that can reduce therapeutic efficiency or lead to adverse side-effects like cell death[13]. Causes can be dependent or independent from dsRNA sequences. Theoretically, siRNA act via full complementary binding to the target mRNA. In reality, incomplete siRNA binding to the target can occur, leading to a "microRNA-like" action, giving possibility to regulate via OTE hundreds of genes with significant impact[14]. These effects might be dose-dependent[15], whereas with lower concentrations, less OTE is observed[16].

Table 1: Overview of extra- and intracellular barriers

Extracellular barriers	Intracellular barriers
Circulation in the bloodstream, enter in the target tissue, avoidance of immune response (e.g. uptake by reticuloendothelial system (RES), TLR activation)[21]	Internalisation
Avoid excretion	Endosomal escape
Diffusion through extracellular matrix	Unpacking from the delivery system
Stability and protection from nuclease degradation[22]	Release of the nucleic acid cargo in the cytoplasm or nucleus
Cellular association / adhesion on cell surface	Loading to the RISC[16]

To develop therapeutic siRNA, optimisation (via bioinformatic methods[9]) is a must to achieve high mRNA target sequence specificity. When designing a siRNA, the "asymmetry rule" needs to be taken in consideration, i.e., the U/A content in the 5'-terminus needs to be adjusted,

since guide and passenger strand are selected by the RISC through thermodynamic stability. RNA strands with a less stable 5'-terminus (high U/A content) act as guide[17]. Less RNAi silencing efficacy can also occur through too high dosage, leading to saturation of RNAi pathways that can cause inhibition of endogenous shRNA processing and through that to toxicity[18,19]. If therapeutic dose is optimised, microRNA can act clinically efficient on the target without perturbing endogenous microRNA[20]. Moreover, dsRNA are shown to provoke unspecific immune reactions by activation of interferon system[21–23]. The immunostimulatory capacity of siRNA is shown to be sequence dependent with 5'-UGUGU-3' as one motif, among others, leading to recognition by toll-like receptors (TLRs)[24]. To circumvent activation of the innate immune response, siRNA and microRNA can be chemically modified or loaded into viral and non-viral vectors.

To protect small non-coding RNAs from degradation by nucleases present in serum and cytoplasm and to increase dsRNAs half-life *in vivo*, a broad range of chemical modification were developed since RNAi's discovery in the 1980s (reviewed by Deleavey[25], Gooding[26] and Watts et al.[27]). Importantly, activity should not be compromised by the modification. Position, type and charge changes of and through modifications need to be considered. Most prominent modifications comprise sugar modifications as 2'-*O*Me at 5'-terminus with reduction of off-target silencing[28], phosphate (internucleotide) linkages[29] or base modifications. A combination of 2'-*O*Me and 2'-fluoro nt was shown to not only improve stability and reduce immunostimulation, but also to increase potency *in vitro*[30]. However, 2'-fluoro modifications are also shown to cause cell death[31]. Chemical modifications can improve several parameters (nuclease stability, reduction of OTEs) towards successful development of RNAi therapeutics. Though, efficient intracellular delivery of the nucleic acids therapeutics is critical for translation of the technology to the clinic.

1.3 Delivery of small non-coding RNAs

The biggest challenge for small non-coding RNAs is to accumulate in the target tissue and to cross the plasma membrane with endosomal escape as the bottleneck for RNAi efficiency. Small non-coding RNAs, as siRNA and microRNAs, are hydrophilic, negatively charged molecules with ~14-15 kDa molecular weight. Plasma membrane permeability is restricted to small (<1 kDa), neutral or slightly hydrophobic molecules, to protect the cellular machinery from "invading RNAs"[32]. Delivery systems need to be developed to facilitate internalisation of dsRNA. Delivery systems protect dsRNA from enzymatic degradation, reducing the need for chemical modification and thus risking activity. Physical methods as iontophoresis[33], gene gun (laser assisted transfection)[34], electroporation[35] can be used for *in vitro* gene transfection or as local delivery systems to penetrate the skin barrier. Those methods induce reversibly the destabilization of the

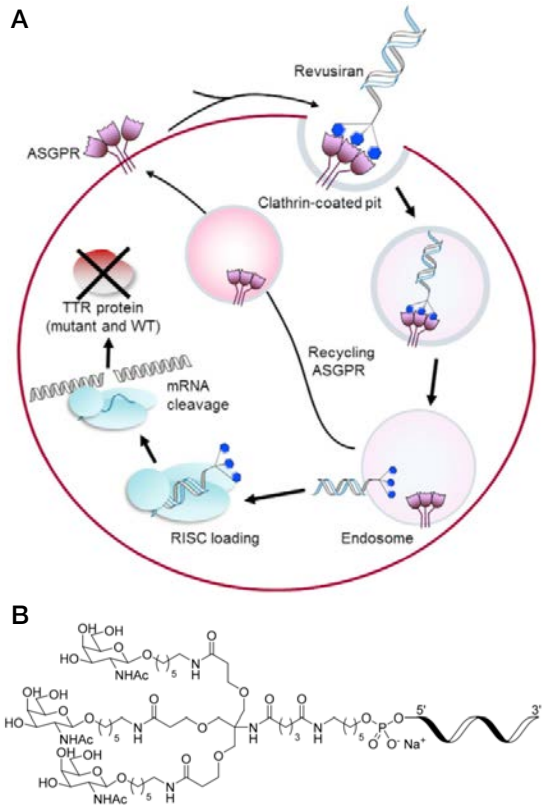

Figure 2: (A) Mechanism of GalNAc-siRNA trafficking. (B) GalNAc structure consistent of triantennary N-acetyl galactosamine ligand with trishexylamin linker. Adapted from Zimmermann et al., Molecular Therapy, 2017[46] and Cedillo et al., Molecules, 2017[49].

plasma membrane and allow permeation of the dsRNA into the cell. Limitations are the possibility to destroy the membrane integrity, the time that is needed for an effective treatment and the size of the lesion. Viral vectors represent nature's most optimised method to enter a host genome and were the first methods applied in gene therapy[36]. Virus such as adenovirus, adeno-associated virus (AAV), lentivirus, retrovirus and herpes simplex virus (HSV-1) can be easily modified with the sequence of interest and are shown to achieve high transfection efficacy. However, those vectors can induce severe toxicity, immune response and oncogenicity[37], leading to the failure of many clinical trials[38]. Most clinical trials comprise retro- and adenovirus formulations for cancer treatment[39]. The first human gene therapy on an AAV vector, Glybera®, approved 2012 by the European Medicines Agency (EMA) was withdrawn from the market 2017[40] because it was too expensive with $1 million in average per treatment[41]. No viral formulation for microRNA delivery is currently in clinical trial stage. Whereas conjugated systems with peptides (for increased cell permeation or with protein transduction domains[42,43]), aptamers[44], or N-acetyl galactosamine (GalNAc)[45] are in late stage clinical trials or already approved for clinical use by the American Food and Drug Administration (FDA)[46]. GalNAc can be recognised by asialoglycoprotein receptor (ASGPR; highly expressed in hepatocytes) followed by clathrin mediated endocytosis[47]. ASGPR recycling occurs in very short time (15 min)[48] making the target/ligand pair very efficient

(see scheme Figure 2). The conjugate structure was optimised for the number of GalNAc antennas and the size of the linkage[46,49]. Any kind of DNA or RNA species can be conjugated with GalNAc and used for hepatocyte targeted delivery[50]. The first FDA approved RNAi (siRNA) drug Onpattro® from Alnylam in 2018[7] for treatment of polyneuropathy (hATTR; hereditary transthyretin-mediated amyloidosis) is a siRNA-GalNAc conjugate on a lipid nanoparticle (LNP) carrying siRNA against TTR (transthyretin) mRNA to the liver. However, the LNP induces an immune response so that the patients need to take steroid, acetaminophen and antihistamines to decrease the chance of immune reactions prior to the treatment with Onpattro®. The treatment also leads to a decrease in vitamin A levels and patients are advised to supplement with daily allowance of vitamin A[51]. To reach beyond the liver, other nanoparticle (NP) carriers were developed. Lipidic formulations are the most advanced in clinical trials but also cyclodextrin NPs and spherical nucleic acids[52,53] are in clinical trials[54]. More recently extracellular vesicles (exosomes) are used to deliver small ncRNA. They offer high therapeutic potential, but allow very few control about the composition of their content[55].

1.4 Application of RNAi therapeutics & Clinical Trials

The clinical advantage of RNAi is that siRNA and microRNA act on a post-transcriptional level, which allows to reach "undruggable" protein targets, giving "extraordinary drug-like properties" to RNAi therapeutics[1]. Furthermore, RNAi is a natural process, active in any mammalian cell, the process is more specific, has longer duration (more than six months after a single injection[56]) and has much higher potency (more than 100 fold) in comparison to common antisense oligonucleotides or ribozymes[57]. This makes RNAi a safe technology with high

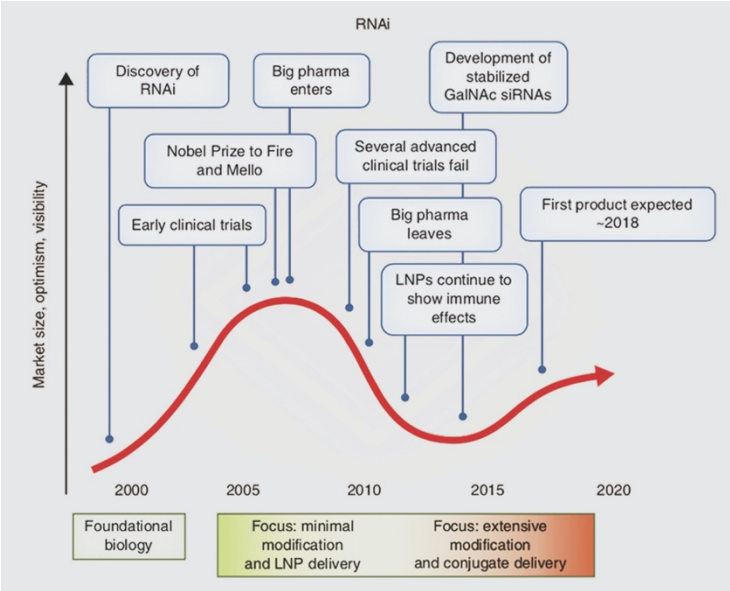

Figure 3: Timeline and market response of RNAi therapeutics development. Adapted from Khvorova et al., Nature Biotechnology, 2017[72].

therapeutic index. In 2003 multiple companies started out to foster clinical application of RNAi. Front line Strategic Consulting (San Mateo, CA, USA) estimated the RNAi market on a value of $38 billion in 2004 with an expected annual market growth of at least 30%[1]. In spite of high investments from big pharma, first clinical trials with unmodified siRNA failed due to a lack of efficacy and toxicity[58,59]. Immune reactions were not only observed in trials with naked siRNA but also with the first NP carriers, causing infusion reaction[60]. Fail of clinical trials and economic crisis in 2008 led big pharma to step out[61] of RNAi, quit their RNAi programs and let biotech companies as Alnylam go, which in turn had to refocus their work (a timeline over RNAi therapeutics development is drawn in Figure 3). John Maraganore, CEO from Alnylam: "We had conquered delivery to the liver, so we decided to make that our strategy, and it turned out that many genetic orphan diseases have their basis in the liver." Positive clinical results from Alnylam with LNP carriers and GalNAc ligand, delivering siRNA with PCSK9 target to treat TTR-mediated amyloidosis, together with data from other companies (Regulus, Arrowhead and others) lead to huge investments of big pharma in the RNAi companies. In 2014 Alnylam achieved 3.4% share in the biotech industry with a market capitalisation of about $5.9 billion[62,63], with established $8 billion today (June 2019)[64], after FDA approval of Onpattro® in August 2018[65]. Besides Onpattro®, three more antisense oligonucleotide drugs got approval by FDA, nusinersen (Spinraza®; spinal muscular atrophy; 2016), mipomersen (Kynamro®; hypercholesterolemia; 2013), eteplirsen (Exondys 51®; duchenne muscular dystrophy; 2016)[66]. Products in the pipeline of RNAi companies as QP-1002 for the treatment of kidney injury and PF-655 to treat age-related macular degeneration, both from Quark Pharmaceuticals and inclisiran, a PCSK9 inhibitor developed by Alnylam will reach larger patient populations. Clinical data of inclisiran highlights 50% knockdown in target cells being persistent until 6 months post administration[56]. Though the long persistency might rise consequences in a longer term since there is interference in a natural pathway by the treatment. Possible toxicity through imbalances in microRNA levels caused by occupation of the RISC complex with the therapeutic RNA[67].

To date, there are 315 ongoing clinical trials involving RNA therapeutics including siRNA[68] and the global market for RNA drugs is expected to reach $10 billion until 2024[68]. Analysis of formulations used for siRNA and miRNA delivery in clinical trial stage (clinicaltrials.gov last accessed 10th May 2019; see Figure 4B with Table 2 and Table 3) reveals that more than half of the studies are conducted with naked siRNA or miRNA (naked = without carrier vehicle but chemically modified) or conjugated to GalNAc. The increased use of GalNAc is related to positive clinical data by Alnylam and the FDA approval of Onpattro® in 2018[7]. LNPs are clinically the most advanced, nevertheless steroid pre-treatment is necessary to get a grip on immune-activation and toxicity can be observed despite the steroid treatment[69,70]. Development

of polymeric NP carriers, as CALAA-01 by Calando Pharmaceuticals with promising data in clinics are on hold due to low efficiency and unspecific toxicity[71]. Most studies focus on the liver as LNP and GalNAc conjugates are most efficient in hepatocytes (Figure 4). Much work has to be done in the development of therapies targeting other organs. Table 2 tries to highlight clinical trials of siRNA-based therapies with ophthalmologic and skin targets. Those are discussed in a later chapter of this work.

In summary, the main risks of siRNA drugs are (i) off-targeting causing (severe) side effects (can be optimised in *in vitro* assays[31]), (ii) unpredictable effects due to high siRNA levels competing intracellularly with "natural" microRNA RNAi machinery, (iii) accumulation of stable siRNAs in endolysosomal compartment causing cytotoxicity[65,72]. The challenge remains over the delivery of RNAi inducing short, double stranded RNA to the cytoplasm of cells at the disease site. Big improvement is still necessary for pharmacokinetics and pharmacodynamics and targeting of extra hepatic tissues[73]. Fambrough fosters the A,B and C system for the development of siRNA delivery systems, which includes step A as "accumulation", step B "binding and internalisation" and C as "cytoplasmic release"[74]. In the delivery of RNAi therapeutics, the delivery system plays the most crucial role.

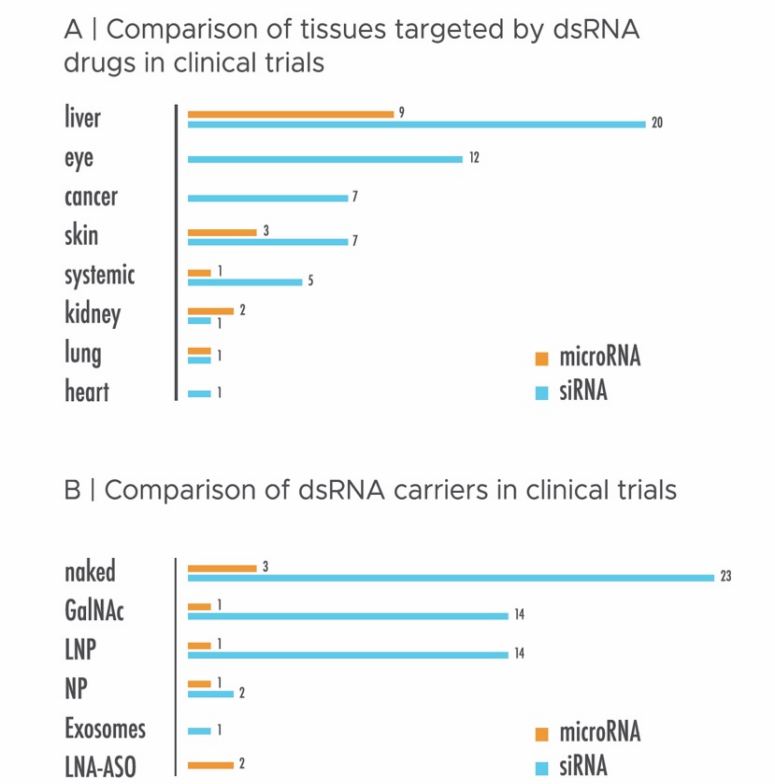

Figure 4: Analysis of clinical trials involving siRNA and microRNA by (A) target tissue and (B) carrier of the small dsRNA. Data from clinicaltrial.gov, last accessed May 2019.

Table 2: Selected siRNA therapies in clinical trials.

Drug	Target gene	siRNA carrier	Target tissue	Disease specification	Stage - Status	Clinical trial No.	Company
ALN-CC5 Cemdisiran	CC5	GalNAc-siRNA	kidney	proteinuria with IgA Nephropathy /Berger Disease /Glomerulonephritis /Hemoglobinuria	II - recruiting	NCT03841448 NCT02352493	Alnylam Pharmaceuticals
ALN-AS1 Givosiran	ALAS1	GalNAc-siRNA	kidney	Acute hepatic porphyria	III - ongoing	NCT03338816	
ALN-RSV01	RSV-N	NC	lung	Respiratory syncytical virus infection	II - completed	NCT01065935	
ALN-TTRSC Revusiran	TTR	GalNAc-siRNA	systemic	hATTR-PN /hATTR-CM	III - terminated	NCT02319005	
ALN-TTR02 Patisiran	TTR	LNP	systemic	hATTR-PN /hATTR-CM	III - completed	NCT02939820	
ALN-AT3SC Fitusiran	AT	GalNAc-siRNA	systemic /blood	Hemophilia A&B	III - recruiting	NCT03549871	
Lumasiran Illuminate-A	GO	GalNAc-siRNA	kidney	primary hypoxaluria Type 1 (PH1)	III - recruiting	NCT03681184	
MSCs derived Exosomes with KRAS G12D siRNA	KRASG12D	Exosomes	cancer	Metastatic Pancreatic Adenocarcinoma / pancreatic Ductal Adenocarcinoma	I - not yet recruiting	NCT03608631	M.D. Anderson Cancer Center / National Cancer Institute (NCI)
OLX10010	CTGF	NC	skin	Hypertrophic Cicatrix	I - recruiting	NCT03569267	Olix Pharmaceuticals Inc.
Bevasiranib	VEGF	NC	eye	AMD	III - withdrawn	NCT00557791	OPKO Health Inc.
Bevasiranib siRNA Cand5	VEGF	NC	eye	Diabetic Macular Edema	II - completed	NCT00306904	
TD101	K6α	NC	skin	Pachyonychia Congenita	I - completed	NCT00716014	Pachyonychia Congenita Project
PF-655	VEGF	NC	eye	CN /Diabetic Retinopathy /Diabetic Macular Edema	II - completed	NCT01445899	Quark Pharmaceuticals
QPI-1002	p53	NC	heart	Cardiac Surgery /Delayed Graft function	III - recruiting	NCT03510897 NCT02610296	
RXI-109	CTGF	NC	eye /skin	AMD /CN /subretinal fibrosis /Hypertrophic scar	II - ongoing	NCT02599064 NCT02246465	Rxi Pharmaceuticals Corp.
siG12D-LODER	KRAS	LODER polymer	cancer	Pancreatic Ductal Adenocarcinoma /Pancreatic Cancer	II - recruiting	NCT01676259	Silenseed Ltd.

Continuation Table 2:

Drug	Target gene	siRNA carrier	Target tissue	Disease specification	Stage - Status	Clinical trial No.	Company
STP705	TGF-β1 COX-2	NC	skin	Hypertrophic Scar	II - recruiting	NCT02956317	Sirnaomics
SYL1001	TRPV1	NC	eye	Dry Eye Disease	III - completed	NCT03108664	Sylentis, S.A.
Bamosiran	β2-AR	NC	eye	Open Angle Glaucoma /Ocular Hypertension	II - completed	NCT02250612 NCT01739244	
Inclisiran ALN-PCSSC	PCSK9	GalNAc-siRNA	systemic /kidney	renal impairment (hypercholesterolemia)	III - recruiting	NCT03851705	The Medicines Company

CC5	Cysteine proteinase inhibitor	CTGF	Connective tissue growth factor
ALAS1	Delta-aminolevulinate synthase 1	K6a	Keratin 61
RSV	Respiratory syncytial virus	COX-2	Cyclooxygenase-2
AT	Ataxia-telangiectasia	TRPV1	Transient receptor potential cation channel subfamily V member 1
GO	Glycolate oxidase		
TTR	Transthyretin	ß2-AR	ß2-Adrenoreceptor
hATTR-PN	Hereditary Amyloidosis with Polyneuropathy	PCSK9	Protein convertase subtilisin/kexin 9
hATTR-CM	Hereditary Amyloidosis with Cardiomyopathy		
KRAS	KRAS Proto-Oncogene, GTPase		

Table 3: Selected clinical trials involving miR and antagomiR therapeutics.

Drug	microRNA	microRNA carrier	Disease	Intervention	Phase – Status	Clinical trial No.	Company
RG-125 /AZD4076	antimiR-103/107	GalNAc-antimiR	liver	subcutaneous injection	II - ongoing	NCT02826525	AstraZeneca
TargomiR /mesomiR-1	miR-16	EDV-NP	lung /cancer	systemic /injection	I - completed	NCT02369198	EnGenelC Ltd.
MRG-106 /cobomarsen	antimiR-155	LNA-modified ASO	blood /cancer	systemic /local	I - recruiting	NCT02580552	miRagen Therapeutics Inc.
MRG-110	antimiR-92a	ASO	skin	local /intradermal injection	I - completed	NCT03603431	
MRG-201	miR-29	mimic	skin		I - completed	NCT02603224	
MRX34 /miR-Rx34	miR-34	LNP (liposome)	liver /cancer	systemic /injection	I - terminated	NCT01829971	Mirna Therapeutics
MRX34 /miR-Rx34	miR-34	LNP (liposome)	skin /cancer		I -withdrawn	NCT02862145	
RG012 /Lademirsen	antimiR-21	ASO	kidney	subcutaneous injection	II - suspended (2019)	NCT02855268	Regulus Therapeutics Inc.
Miravirsen /SPC3649	miR-122	LNA-modified ASO	liver	systemic /injection	II - completed	NCT01200420	Santaris Pharma A/S

EDV-NP nonliving bacterial minicells

2 Nanotechnology and Nanomedicine

Nanoparticles (NP) (Ø 1-1000 nm)[75] are especially suitable to develop drug carriers for therapeutic use. NP are also used for applications as biosensor for diagnosis, as imaging (contrast) agent and for theranostics (combination of therapy and diagnosis). There is a large variety of materials and architectures being from natural, organic or inorganic sources (Figure 5). After approval of the first nanodrug in 1995 (Doxil®, Doxorubicin loaded, liposomal NP for the treatment of metastatic breast cancer)[76], the FDA approved already 51 nanodrug formulations for various applications, comprising liposomal, polymeric, micellar, inorganic NPs and nanocrystals with growing approval of protein drugs for clinical trials. The number of clinical trials including nanodrug formulation is growing exponentially with increasing diversity and complexity of the formulations[77].

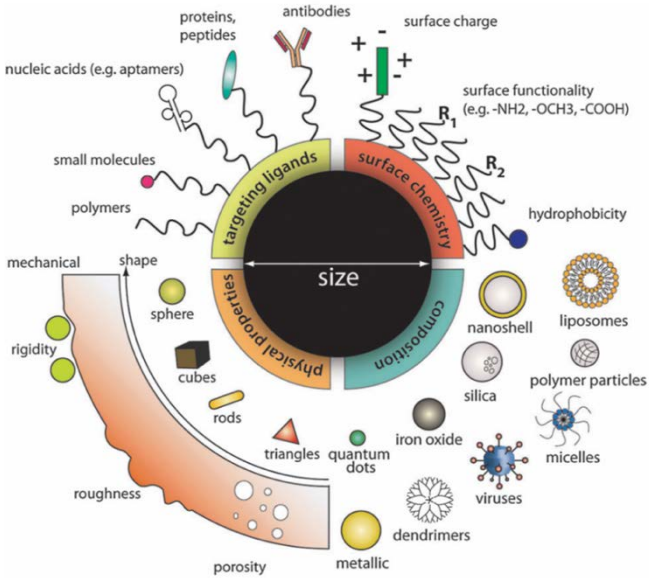

Figure 5: Characteristics and diversity of nanoparticle composition, physical properties and surface chemistry. Adapted from Chou et al., Chem. Soc. Reviews, 2011[90].

The design of a nanocarrier requires the selection of a set of chemical and physical properties which are dependent on the application of the carrier, the administrative route and the drug payload (Figure 5). Nanocarriers offer through high surface area/volume ratio (often with large inner surface area through porosity[78]) the possibility to (i) carry large drug doses with low particle carrier concentration (reducing the effective dose, minimizing toxicity), (ii) immobilize and carry highly hydrophobic drugs and (iii) load combinations of drugs. Drugs can be either entrapped in the carrier´s structure or adsorbed on the carrier by electrostatic interaction, but there also exists the possibility to covalently bind the drug onto the carrier[79,80]. If the nanomedicine

is administered systemically, decoration of the NP with polyethylene glycol (PEG, or other hydrophilic polymers as poloxamer, dextran, polyvinylpyrrolidone or surfactants) may be helpful to avoid (i) NP aggregation, (ii) unspecific protein adsorption, (iii) immunogenicity and (iv) opsonisation (leading to phagocytosis and clearance) thus improving circulation time in the blood stream[81,82]. When NPs are dispersed in biological media they immediately interact with serum proteins. The composition of the NP-protein complex changes dynamically depending on the binding constants of the proteins present in the biological media and the physicochemical properties of the NP[83,84]. This corona can cover surface functionalities of the nanocarrier in such way, that the desired ligand function (e.g. ligand specific targeting) can be lost[85]. Pre-coating of the surface with PEG[81,86], nucleic acids or proteins[87] can stabilize the NPs by better control of the protein corona on the NP. But PEGylation of the nanocarrier can also over-stabilize the NP and hide relevant factors on the NP surface relevant for molecular recognition.[88,89]

Targeting ligands (e.g. antibodies, aptamers and peptides as transferrin and vitamins as folate[85,90]) equivalent to specific cell surface markers can be immobilised on the outer surface of the NP to increase specificity of drug release and minimize undesired side effects as toxicity in non-disease affected areas. Ligands as transferrin[91,92] can be used to significantly increase the cellular uptake of gold NPs by transferrin receptor mediated endocytosis, as it was reported by Yang et al.[92].

For the intracellular delivery of small and macromolecules, efficient internalisation and drug release in the specific cell compartment is the limiting step for the drugs activity. Size, shape[93] and surface chemistry affect the endocytosis of NP formulations[90,94,95]. To understand what the cell "sees" from the NP-protein complex, zeta (ζ)-potential and hydrodynamic radius (by dynamic light scattering, DLS) measurements can be conducted. This is essential to understand the NP-cell interaction[96].

3 Endocytosis mechanism, intracellular trafficking and endosomal escape

Endocytosis is the mechanism, by which any type of cells communicates with their biological environment. Through this energy dependent process, cells can internalize nutrients, biomolecules, signalling molecules and NPs by engulfment of the material through invagination of the plasma membrane (Figure 6). Subsequently vesicles, called endosomes (phagosomes in the case of phagocytosis), are formed, where the material is encapsulated by a lipid bilayer from the former plasma membrane[97]. The endosomes undergo then an intracellular trafficking mechanism (Figure 6) delivering the cargo to specialised vesicular structures, where the cargo is either delivered to (i) the intracellular compartment, (ii) recycled and secreted to the extracellular milieu, or (iii) in the case of polarised cells, the cargo is delivered across cells (called "transcytosis")[97]. The pathways of endocytosis are differentiated in pinocytosis with uptake of fluids and solutes as receptor (clathrin- and caveolae-) mediated endocytosis, macropinocytosis (receptor independent) and phagocytosis for the uptake of large particles (mainly macrophages, neutrophils, monocytes, dendritic cells)[98,99].

The uptake of NPs into cells is dependent on multiple factors of the NP's nature such as size, shape[93], surface chemistry (zeta potential)[90,94–96] and the type of cell and its machinery, since

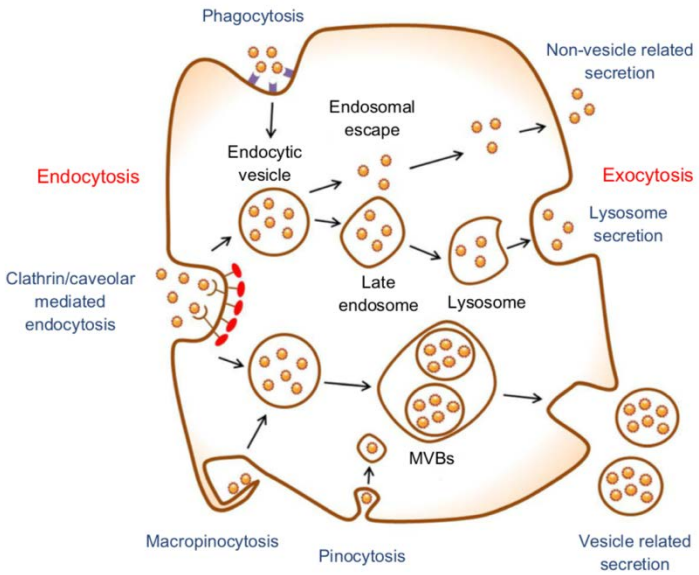

Figure 6: Schematic representation of intracellular Nanoparticle trafficking. Cellular internalisation can follow different processes and depends on the characteristics of the nanoparticle. Larger NP are internalised via micropinocytosis, smaller NP follow endocytosis mechanisms dependent on NP interaction with membrane proteins such as clathrin or caveolin. Upon interaction of NPs with membrane proteins, such as clathrin or caveolin, endocytic vesicles are formed. Maturation of endosomes to late endosomes and lysosomes as well as other internalisation pathways are depicted here. Adapted from Oh et al., Int. J. Nanomedicine, 2014.[94]

various cell types can internalize the same NP by different endocytic pathways[100,101]. There are few studies analysing NP internalisation in different cell types[100–102.] The studies are not comparable since NP type and experimental condition vary each time. In 2008, Xia et al. found that polystyrene NP show different levels of colocalisation with LAMP1 (a marker of endolysosomal compartment) with highest rates for endothelial cells (46%) and hepatocytes (51%) in comparison to macrophages (33%), epithelial (8%) and pheochromocytoma (7%) cells after NP pulse of 6 h. This study shows cell type dependency for NP uptake mechanism and magnitude of internalisation[100]. Cell type preferences of NP internalisation of different types of human and murine cells were shown by Voigt et al., after 2 h of NP cell contact. The study confirms elevated endosomal NP uptake in endothelial cells found by Xia et al. with independency of species (mouse vs. human). Furthermore, they show preferences of cell types to certain chemistries. Cellular internalisation showed generally higher levels using poly(vinyl sulphonic acid) in comparison to poly(acrylic acid) NPs[102].

The critical step determining potency of intracellular drug delivery from a nanocarrier, is the process of endosomal escape. The endosomal compartment is due to ATP mediated proton accumulation generally more acidic in comparison to the intracellular space (pH 7.4). While the maturation of the endosome, the compartment gradually acidifies from ~pH 6.0 until ~pH 4.5 in lysosomes[97]. Nanocarriers composed by polycations as polyethyleneimine (PEI) and other polyamines with pH buffering capacity cause the "proton sponge" effect leading to the disruption of the endolysosomal compartment[103].

3.1 Enhancing endosomal escape

For direct transfection to the cytoplasm (without passing through the endolysosomal compartment) the following methods may be used: (i) electroporation, where a pulsed electric field is applied, giving the possibility to transfect mammalian cells with DNA[104,105], mRNA[106] or siRNA[107,108], or (ii) laser assisted photoporation, where transient nanochannels/pores are formed in the plasma membrane of the cell to allow the entrance of genetic material[109,110]. Unfortunately, these methods are not applicable in an *in vivo* context. To enhance endosomal escape of a nanocarrier several strategies can be applied[2,111,112] but the most used one is based in the conjugation of the surface of the NP with cell penetrating peptides. Surface decoration or conjugation with cell penetrating peptides (CPP) such as penetratin™, TAT and MPG[113] have been shown to enhance siRNA delivery *in vitro* and also *in vivo*. TAT peptide has already been tested in several clinical trials for the treatment of hearing loss[114] (Phase III; NCT02809118; NCT register from https://clinicaltrials.gov), myocardial infarction[115] (Phase II; NCT00785954) and

intraocular inflammation and pain[116] (Phase III; NCT02235272)[117]. Moschos et al. showed that p38 MAP kinase siRNA covalently conjugated to either cholesterol, penetratin™ or TAT, reduced mRNA expression *in vitro*. When applied *in vivo* only cholesterol-siRNA conjugates show silencing efficacy, penetratin™-siRNA conjugate treatment led to activation of the immune system[118]. Therefore, although cell-penetrating peptides may increase gene silencing efficacy, they may activate the immune system. Using covalently bound TAT peptide, Kanazawa et al. show effective *in vivo* gene silencing in tumour bearing mice[119] and rat brains[120]. They demonstrated significantly increased uptake of PEG polycaprolactone copolymer with covalently linked TAT and electrostatically bound siRNA (MPEG-PCL-Tat) in rat neuronal cells (RN33B) *in vitro* and in an *in vivo* rat model after intranasal administration[120]. This work shows successful siRNA brain delivery facilitated by TAT peptide.

3.2 Endosomal escape and the controversial discussion of the proton sponge hypothesis

In a study by Boussif et al. (1995) the effect of cationic charged polymers in endosome rupture was demonstrated. Using a polyplex of PEI/DNA they show, that protonation of nitrogen atoms of PEI lead to a positive charge excess followed by ATPase driven proton accumulation which leads to osmotic swelling (by passive cytosolic chloride influx, diffusion of water and swelling of the PEI because of charge repulsion effects) of the vesicle and finally rupture of the endosomal bilipid membrane with following cargo release[103]. However, in a study conducted by Benjaminsen et al. (2013) where they used a pH sensitive (pH 3.2 – 7.0) nanoprobe to be colocalised with PEI NPs, no significant changes in the pH after PEI transfection in the lysosomes until 24 h was observed. They hypothesised that PEI served as a "proton sponge"; however, the V-ATPase could stabilize the pH by its function as proton pump. They concluded that the proton sponge effect could not be the main phenomenon causing polyplex releasing from the endolysosomal compartment[121]. Likewise, there have been contradictory results on the endosomal escape mechanism of cationic lipid nanoparticles (LNP). Lu et al. showed in 2009 that inhibition of various endocytosis pathways (in kidney cells) did not alter the knockdown of the target gene, though cholesterol depletion from plasma membrane decreased significantly target gene knockdown[122]. These results suggest, that siRNA delivery via cationic lipid carriers occurs via direct fusion of lipoplexes and the plasma membrane. By using RNA interference and chemical inhibitors, Gilleron et al. and Sahay et al. have proven cellular uptake of LNP in HeLa cells through macropinocytosis[2,123].

3.3 A spotlight on the endosomal escape of siRNA-NP formulations

Most of the NP are shown to be internalised via endocytosis[98], still the main obstacle remains in clarifying the intracellular trafficking of NP-siRNA formulations. In particular, determining the mechanism and efficiency of endosomal escape. Classical methods to assess cytosolic siRNA delivery comprise experiments of biological activity or quantitative fluorescence microscopy (further methods are reviewed by Martens et al.[124]). Biological activity of siRNA can be determined by using model systems composed of a stable expressed reporter protein (such as GFP or luciferase) and siRNA against that reporter[125]. If cytosolic delivery of siRNA via a nanocarrier occurred, the reporter protein will be silenced, and the extent of protein expression (fluorescence or qRT-PCR) can be taken as quantitative measure for endosomal escape[126]. In fluorescence microscopy, colocalisation experiments between labelled siRNA with stained endolysosomal compartment can be performed[126,127]. These are indirect methods; direct measures are difficult since siRNA concentrations in a therapeutic range are often below the detection limit (sensitivity) of the quantitative method. Exact quantification of cytosolic release of siRNA from endosomes remains challenging. The first studies addressing this issue quantitatively were published by Gilleron et al.[2] and Sahay et al.[3] in 2013. Using fluorescent or nanogold (6 nm) labelled siRNA (against GFP) formulated with LNP (ionizable lipid, disteroylphosphatidyl choline, cholesterol, PEG-DMG[128]) applied in clinical trials (and approved by FDA) and a combination of

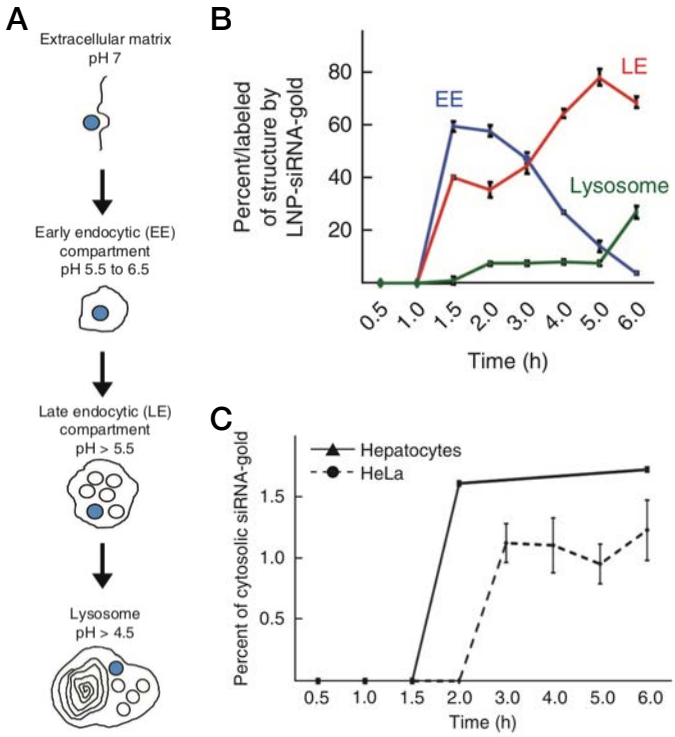

Figure 7: (A) LNP intracellular trafficking. (B) Quantification of LNP-siRNA-gold labelled intracellular compartments from electron microscopy images after NP pulse of 3 hours in HeLa cells. (C) Comparison of cytosolic siRNA-gold content in hepatocytes (in vivo) and HeLa cells (in vitro). Adapted from Gilleron et al., Nature Biotechnology, 2013[2].

fluorescence and electron microscopy, Gilleron et al. determined the cytosolic siRNA concentration in hepatocytes *in vitro* and *in vivo* until 6 h post-administration (Figure 7). They found that less than 2% of the initial siRNA dose can be found until this timepoint, suggesting that the remaining quantity is trapped in the endolysosomal compartment[2]. These results were confirmed by the comparison with a formulation that shows lower knockdown efficacy, but same internalisation properties[129]. The study showed that endosomal escape properties were decisive for gene silencing efficacy. Furthermore, by blocking endosomal progression pharmacologically (with bafilomycin), Gilleron observed no changes in cytosolic siRNA concentration (~1.2-1.4 %)[2]. This indicates that siRNA release may occur at an early stage of endosomal progression. By high resolution confocal microscopy, Sahay et al., quantified colocalisation of cationic LNPs conjugated to fluorescence labelled siRNA (Alexa Fluor 647) with endosomal markers for early endosomes (EEA1), late endosomes/lysosomes (LAMP1), late endosomes/lysosomes (LAMP2) and markers for tubulovesicular endocytic recycling (Rab11) in HeLa cells (Figure 8). After 3 h pulse with cationic LNP, two-fold increased colocalisation with late endosomal/lysosomal markers in comparison to those marking the early endosomal compartment. In a time-course of 15 min steps the trends reveal decline of colocalisation with EEA1 and increase with LAMP1 and 2, suggesting that most siRNA is localised and possibly trapped in late endosomes[3]. These results confirm the hypothesis by Gilleron et al. that the time window for endosomal escape is at initial stages of intracellular trafficking.

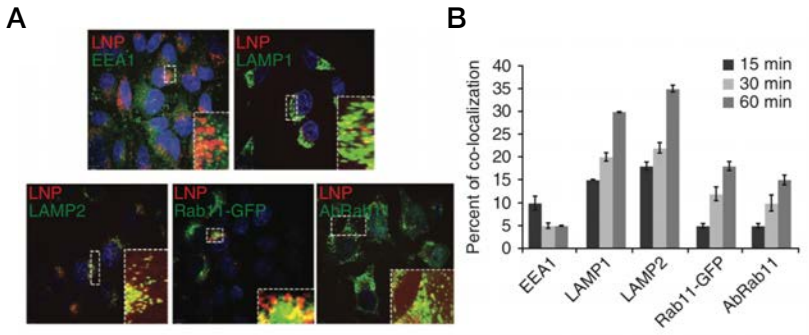

Figure 8: (A) Representative images and (B) colocalisation quantification of LNP-siRNA647 with endolysosomal markers after 3 h transfection of HeLa cells. Adapted from Sahay et al., Nature Biotechnology, 2013[3].

Further progress in the timeframe determination of siRNA cytosolic release from endosomes and the characterisation of these vesicles was achieved 2015 by Wittrup and co-workers[130]. Transfected with lipoplex siRNA-AF647 and using high dynamic range (HDR) fluorescence microscopy, increased fluorescence intensity from endosomes short before siRNA release could be observed. Generally, siRNA release occurred in the first 5-15 min after internalisation from (maturing) endosomes with $EEA1^{-}Rab5^{+}Rab7^{+}Rab9^{\pm}LAMP1^{-}$. Lysosomal marker LAMP1 was positive about 40-50 min after siRNA release from the vesicle. Wittrup et al.

also confirmed earlier findings, that gene delivery vehicles (as cationic polyplex and lipoplex) can activate macroautophagy[131,132]. They showed that LC3 (a central structural membrane protein of autophagosomes[131]) was recruited to the siRNA releasing endosome in few minutes. From a series of galectins (endosomal glycan detector), Wittrup observed that galectin-8 recruitment to the siRNA releasing vesicle occured 5-10 seconds after release and could be used as marker for siRNA releasing endosomes. When LNP-siRNA (ionizable lipid, disteroylphosphatidyl choline, cholesterol, PEG-DMG[128]) were used, fluorescence signals were too low to detect signal in the cytoplasm. The authors used galectin-8 as a marker for vesicles releasing siRNA. Releasing endosomes were characterised by galectin-8 and endosomal marker colocalisation. siRNA release occurred from $EEA1^{-}Rab5^{+}Rab7^{\pm}Lamp1^{-}$ with a subset positive for autophagy marker LC3 within 10 min. No more release events were observed when vesicles were positive for LAMP1. In total, about 3.5% of siRNA was released to cytoplasm. This means that most of the studies trying to determine endosomal escape focus on a time span, where most release events might have had occurred already, so most of the siRNA material is located in late endosomes/lysosomes (as shown in the study of Sahay et al. as well.).

In summary, the studies presented here showed that (i) internalisation occurs within the first hours of cell-material contact, (ii) the window for endosomal escape lies within the first 15 min after internalisation, (iii) siRNA in late endosomes/lysosomes (from ~30-50 minutes) remains trapped in lysosomes and that (iv) galectin-8 can be used as marker for siRNA releasing endosomes. In addition, the above studies showed low endosomal escape efficacy of clinically applied siRNA nanoformulations and thus the need to further invest in the development of materials for rapid and efficient cellular uptake and endosomal escape.

4 High-throughput screening of stimuli-sensitive compound libraries – The run for increased transfection efficacy

To overcome barriers of gene delivery and to increase transfection efficacy, strategies involving internal and external triggers have been developed to activate drug release from nanocarriers. These can be specifically designed to respond with a structural change to the stimulus. Physiological stimuli are correlated to microenvironmental changes (e.g. temperature, pH, specific enzymes) as pathologic situations (cancer, inflammation, diabetes, cardiovascular, degenerative) and can be exploited to endogenously (internal) trigger drug release (Figure 9A)[133]. On-demand control over the drug release can be achieved using external (extracorporeal) physical triggers such as light, magnetic or electric pulses, or ultrasound[134]. Sensitive components can be

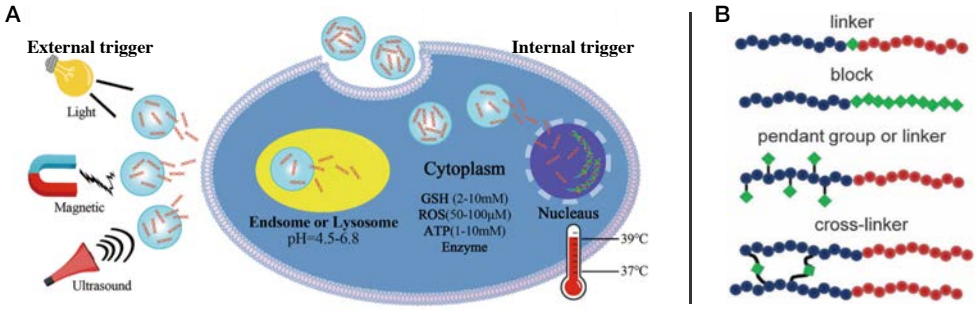

Figure 9: (A) Schematic representation of external and internal triggers used to activate drug release from nanocarriers. Adapted from Li et al., Topics in Current Chem., 2017[133]. (B) Trigger sensitive compounds (green) can be incorporated in various manners into drug carriers. Adapted from Kelley et al., Chem. Soc. Rev., 2013[135].

incorporated into the NP structure, as a linker, pendent group or incorporated in the core of the NP structure (Figure 9B)[135]. Stimulus application leads to physical changes such as swelling, aggregation, charge reversal or chemical changes such as degradation, alterations in solubility and phase transition in the NP to release the drug cargo. An overview of trigger sensitive NP platforms for gene delivery is given in Table 4.

In the last 15 years, researchers have initiated the use of NP libraries to identify the most efficient and rapid formulations for cell transfection of RNAi [111,112]. HTS techniques were adapted to screen compound libraries with nanomaterials reacting to internal stimuli for increased transfection efficacy (see Table 6-8). Anderson, Akinc, Green and co-workers developed in 2003 high throughput screening methods employing combinatorial parallel synthesis and multiparametric analysis of polycations, lipidoids and LNPs for the delivery of pDNA[111,136–138], siRNA[112] and mRNA[139]. To develop large compound libraries, it is necessary to pick synthetic routes, where no additional solvents, catalysts or protection/deprotection steps are necessary and where starting material is commercially available. This approach allows rapid optimisation and adaption of parameters as NP/polymer composition for the specific application. To facilitate NP

synthesis, (i) poly-/or lipoplexes[111] are formed by co-precipitation of polymer/lipid with DNA/RNA material, or (ii) the therapeutic material is immobilised on the surface of the NP by electrostatic interaction[112]. To analyse such large compound libraries, homogenous read-out methods through luminescence or fluorescence are used, to classify materials for cytotoxicity and compound bioactivity. More recently high content imaging has emerged as a method to allow multiparametric readouts in high throughput screening. Through this methodology several NP formulations entered in clinical trials and are already approved for therapeutic use by EMA and FDA[140].

Table 4: Trigger sensitive (nano-)materials for gene delivery (pDNA/microRNA/siRNA/ASO).

Type of trigger			Sensitive compound	Material	Drug	Type of NP	Application/ Benefit	Reference
Internal stimulus	Chemically	pH	Ester	Poly(β-amino ester)	DNA /VEGF	Polyplex	NP Library transfecting ECs, hMSCs with enhanced angiogenesis	Shmueli et al.[138], Yang et al.[139]
			Oxime	siRNA lipoplex with aminoxy lipid surface	siRNA or pDNA	Lipoplex	High NP stability with improved silencing efficacy	Carmona et al.[140]
			Calcium phosphate (CaP)	CaP	DNA	Inorganic NP	Lowering intracellular calcium disturbance while transfection	Neumann et al.[141]
			Ketal	Ketal linked poly(β-amino ester)	NFα-siRNA	Polyplex	Acid cleavable linker and pH buffering capacity lead to higher endosomal escape	Guk et al.[142]
			Ionizable polar amine groups	Lipid-like material	TR-siRNA	Lipoplex	Stable TTR silencing in mice and nonhuman primates	Love et al.[143]
		Redox	Disulphide linked PEI	Poly(L-lysine)-PEG copolymer-ssPEI	IAP siRNA	Polymeric NP	Easy degradability, improved therapeutic efficiency	Cheng et al.[144]
			Phospho-thioethanol	siRNA-S-S-PE in PEG-PE micelles	GFP siRNA	Micelle	Stabilisation without compromising transfection efficacy	Musacchio et al.[145]
			Azobenzene	PEG2000-Azo-PEI-DOPE	GFP siRNA	Polyplex	Hypoxia targeted delivery by PEG cleavage, GFP silencing in tumours after i.v. injection	Perche et al.[146], Kiyose et al.[147]
		pH&Redox	(S-S-functionalised) ssPEI	mPEG-b-PLA-PHis-ssPEI	Cl2 siRNA	Polyplex	Breast tumour (MCF-7) growth-inhibition; Superior endosomal escape, enhanced diassembly	Zhu et al.[148]
		Enzyme	Matrixmetallo proteinase 2 (MMP2)	MMP2-sensitive copolymer PEG-pp-PEI-PE	Survivin siRNA	Micelle	Tumour targeting via up-regulated tumoural MMP2	Zhu et al.[149]
		ROS	Thioketal	Poly(amino thioketal)	siRNA	Polyplex	ROS triggered disassembly	Shim et al.[150]
	Physically	Temperature	Swelling/deswelling of the nanocapsule; cold- shock	Pluronic/PEI2K nanocapsule PEG-siRNA complex	EGF siRNA	Polymeric NP	Increased endosomal escape and gene silencing	Lee at al.[151]
			Sol-gel transition	PEI-poly(organo phosphazene)	Cyclin B1 siRNA	Polyplex	Gelation in target tissue; sustained release; *in vivo* anti-tumour effect by cyclin B1 silencing	Kim et al.[152]

Continuation Table 4:

Type of trigger			Sensitive compound	Material	Drug	Type of NP	Application/ Benefit	Reference
External stimulus	Electrically	**Nanochannel electro-poration)**	Focused electric field on small area of cell membrane	DOTAP, EggPC, PEG-DSPS	CL-1 siRNA/ pDNA	Lipoplex	Non-endocytic path by direct channel formation for nanocarrier entry; improved silencing	Boukany et al.[108]
		Conductive polymer	Arylsulphonamide cleavage upon electric stimulus	Poly(cyclopentadithiophene)-DNA	DNA	DNA	Electrochemically controlled gene delivery	Gautier et al.[153]
	Magnetically	**Guidance**	SPION	Dextran-coated SPION	PLK1 siRNA	Metallic NP	Selective uptake in tumour cells and simultaneous MRI detection	Mahajan et al.[154]
		Heating	Magnetite NP core	Dextran-coated iron oxide NP	Covalently bound DNA	Metallic NP	Release of DNA by EMF activation without heating of the surrounding	Derfus et al.[155]
	Ultrasound	**Ultrasound-targeted Microbubble Destruction**	Polymeric thin film with C3F8 gas core	PFPAM-PEI-shRNA complex	HD2 shRNA	Micro-bubble	Non-invasive targeted method	Zhang et al.[156]
			Lipid thin film with C3F8 gas core	Phospholipid bubble filled with C3F8	HD2 shRNA	Micro-bubble	Prevention of myocardial infarction by PHD2 silencing	Zhang et al.[157]

TR	Thyroid hormone receptor	DOPE	1,2-Dioleoiyl-sn-glicero-3-phosphoethanolamine
IAP	Alkalie phosphatase	DOTAP	1,2-di-(9Z-octadecenoyl)-3-trimethylammonium-propane
Cl2	Liver ribonuclease A	EggPC	egg yolk phosphatidylcholine
PLK1	Polo-like Kinase 1	PEG-DSPS	distearoylphosphatidylethanolamine
HD2	Histone deacetylase	PFPAM	Perfluoropropane-Albumin Microsphere

4.1 Nanomaterials using internal triggers to enhance drug release

Carriers, which are activated to release their drug cargo upon (i) pH changes, (ii) enzyme substrate reactions and (iii) temperature, are called self-regulated systems, where the "release rate is controlled by feedback information, without any external intervention"[141]. Self-regulated systems often use characteristics of the pathologic zone to trigger activity of the nanocarrier e.g. low pH in tumour tissue, high temperature caused by inflammation or increased redox potential o presence of specific enzymes characteristically for the pathology. Carriers will be locally activated by sensing the microenvironment and release the cargo "on demand"[134]. In the last decade, the most significant contributions were done in the development of pH and redox sensitive materials.

4.1.1 pH sensitive libraries for gene therapy

pH responsive materials have been attracting major attention since the acidic pH in the endolysosomal compartment (endosomes pH≈5.5-6, lysosomes pH≈4.5-5) can be used as trigger to activate drug release. The slightly acidic tumour microenvironment (pH≈6.5-7.2) caused by the "Warburg effect" (anaerobic glycolysis in hypoxia and accumulation of acidic metabolites as lactic acid)[142] can be utilised.

Table 5: Studies involving pH sensitive polymer libraries for gene delivery.

Material	Drug	Cell type	Screening readout	Advance	Benefit	Reference
Poly(β-amino ester)s (PBAE)	DNA	COS-7	Luciferase expression	Combinatorial synthesis and HT testing of PBAEs; hits with hydrophobic chain in crosslinker and hydroxyl groups in the side chain	2350 polymers; 26 with higher transfection efficacy as L2000 and >40 polymers more effective as PEI; 2 with 2-fold increase.	Anderson et al.[111], 2003
	DNA	COS-7	Luciferase expression	Optimisation of MW, end-group and polymer/DNA ratio; oxygen content and hydrophobicity are parameters improving transfection	Higher transfection (4-fold) efficacy as PEI and L2000; pH buffering capacity of PBAEs; endosomal escape	Akinc et al.[136,137], 2003
	DNA	COS-7	Luciferase expression MTT	Hit: C32: C: 1,4-butanediol-diacrylate 32: 5-aminopentanol	>500 compounds; intra tumoural injection of C32-pDNA with 4-fold increase transfection as jetPEI; effective *in vivo* prostate cancer treatment	Anderson et al.[149,150], 2004, 2005
	pDNA	HUVECs	Luciferase expression GFP expression	Longer carbon chain as significant parameter Hits: C32, JJ32, E28	COS-7 transfection is not a predictable parameter for the transfection efficiency in other cell types	Green et al.[138], 2006
	pDNA	COS-7	Luciferase expression	Parallel end-capping of C32; hits with hydrophilic amine capping	Improved gene delivery *in vivo* as unmodified C32 and JetPEI	Zugates et al.[151,152], 2007
	pDNA	hESCs	GFP reporter	C32 with diamine end-capping 1,3-diaminopentane	4-fold increase gene delivery efficacy as L2000; maintaining hESCs viability, morphology, undifferentiated state	Green et al.[153], 2008
	pDNA	MDA-MB 231	GFP reporter	B4S4 modified endgroups or MW; hit with piperazine endgroup (E7)	Transfection of hard to transfect breast cancer *in vitro*	Kim et al.[154], 2014
Polymeric cationic core-shell NPs	Firefly siRNa	HeLa	Renilla and firefly luciferase reporter	NP hits contain tertiary amines with more than 1 reactive site and amines with buffering capacity	HT-screening of structurally different 1536 NP. Dual reporter for silencing (firefly) and cytotoxicity (Renilla)	Siegwart et al.[155], 2011
Dendrimer	Cy5.5, Tie2, Itgb1 siRNA	ECs (HMVEC)	Tie2 mRNA expression	PAA / poly(propylenimine) dendrimers modified with short hydrophobic lipid tails; hit with amide bond and pK_a=5.5	Successful siRNA delivery to lung endothelial cells in vitro and *in vivo*	Khan et al.[156], 2015
Dendrimer with acid degradable ester moieties	siRNA let-7g miR	HeLa Tumour mice	Luciferase Tumour-growth	Modulating core, generation, periphery; hit: 5A2SC8 -tertiary ethylene amine core-octane thiol periphery	HT-screening of 1512 dendrimers with 6% silencing luciferase and high viability for late-stage cancer treatment	Zhou et al.[157], 2016

MTT colorimetric metabolic cell viability assay
Tie2 Tyrosine-protein kinase receptor
Itgb1 Integrin beta-1

There are two major approaches to design pH-responsive materials. Firstly, the use of polymers with ionizable functional groups (e.g. amine, pyridine, piperazine, carboxylic or sulphonic acids etc.) that change physical characteristics upon protonation or deprotonation. Second, the use of acid-cleavable linkers such as imine, hydrazine, acetal, ortho-ester or ketal acid groups[143–145]. The most classic material for gene delivery is the polycation polyethylenimine (PEI). Transfection efficiency using PEI is highly dependent on the molecular weight and branching degree of the polymer. It was observed, that transfection efficiency of *in vitro* systems using PEI/DNA polyplexes increases with increasing molecular weight of PEI[146] but decreases *in vivo* because of cytotoxicity[147]. This shows the conflict between transfection efficacy and cytotoxicity[148] and suggests also the development of more straight forward methods for material synthesis to allow a less iterative approach. Michael addition of diacrylates with amines to poly(β-amino ester)s (PBAEs) fulfil requirements to be used for combinatorial synthesis of polycation libraries. A huge number of compounds of diacrylates and amines is commercially available giving the possibility to vary the physicochemical properties of the polymers as much as possible. Molecular weight of PBAEs can be controlled by the ratio of diacrylate to amine. In an acidic environment, PBAEs degrade through hydrolysis of ester bonds in the polymer backbone and contribute by pH buffering capacity to increased endosomal escape properties through the proton sponge effect. Many compound libraries of PBAEs were screened as summarised in Table 5. All of them identified increased gene transfection efficacy with PBAE for pDNA transfection in comparison to PEI or other agents with lower cytotoxicity profiles. Analysis of structure-function relationships have shown that amine terminated PBAEs with hydroxy functions in the side chains and high molecular weight (MW) are the most effective for gene delivery[136,137]. Amine endcapping is shown to increase the efficiency even more[151–153]. Amine endcapped PBAE C32 (identified by Anderson et al., 2004[149]) composed of 1,4-butanediol diacrylate (compound C) and 5-aminopentanol (compound 32) with 1,3-diaminopentane endcapping was demonstrated to increase gene delivery to human embryonic stem cells (hESCs) 4-fold in comparison to a commercial agent, Lipofectamine 2000 (L2000) while maintaining stem cell morphology and undifferentiated state[153].

1536 structurally different polymeric cationic core shell NPs with an ionizable cationic amine core for the delivery of siRNA were screened by Siegwart et al.[155]. SiRNA was bound electrostatically in the core or the shell of the NP. In a secondary screen the effect of the amine structure on NP internalisation in HeLa cells was analysed. It was observed, that tertiary alkyl amines (dimethyl > diethyl > dibutyl) show higher internalisation levels in comparison to secondary alkyl amines (methyl > ethyl). Also, formulations with pendant tertiary amines as piperazine and pyrrolidine structures showed high ability to condense siRNA and high cellular

uptake levels. However, for *in vivo* application, modification with cholesterol was necessary to achieve silencing in liver hepatocytes[155].

Table 6: pH sensitive libraries of lipids and lipid-like materials for gene delivery.

Material	Drug	Cell type	Screening readout	Advance	Benefit	Reference
Cationic lipidoids	Firefly-siRNA/ 2'OMe-miR ApoB	HeLa/ HepG2/ Mice Rat Primates	Firefly and renilla luciferase reporter	Novel one-step synthesis route for parallel synthesis of lipidoids from alkyl-acrylate, alkyl-acrylamide and amino molecules identifying design criteria (i) amide linkage, (ii) >2 alkyl tails, (iii) tail 8-12 carbons, (iv) secondary amine	1200 NP, with 17 formulations tested *in vivo* for factor VII silencing in rodent liver and ApoB siRNA to nonhuman primates with 85% silencing of ApoB RNA in livers; stable silencing in liver, lung and peritoneal macrophages in all 3 species.	Akinc et al.[112], 2008
Lipid-like material	Firefly-, TTR-siRNA	HeLa Mice Primates	Firefly and renilla luciferase reporter	Parallel one-step synthesis of amino alcohols via epoxid ring-opening (polar amine head and nonpolar hydrocarbon tail)	126 compounds; siRNA directed liver gene silencing; simultaneous administration and silencing of 5 genes in mice liver; stable silencing of transthyretin in nonhuman primates	Love et al.[158], 2010
Lipid NP (LNP)	Firefly-, TTR-, PCSK-9-siRNA	HeLa	Firefly and renilla luciferase reporter	Parallel two-step lipid thiol-yne synthesis	Multiparametric analysis identifying pK_a as main parameter determining LNP function and activity	Alabi et al.[159], 2013
LNPs	mRNA ssDNA sgRNA	HEK293-Cre-recombinase reporter /Mice	Cre protein production and sequencing	mRNA with ssDNA barcodes on LINPs	New screening technology (FIND) for mRNA delivery *in vivo*. From >250 LNPs, two were identified to deliver mRNA to endothelial bed.	Sago et al.[139], 2018

Much success was achieved in the development of lipid or lipid-like materials (LNPs) for gene delivery (exemplary studies see Table 6) when the FDA approved the first LNP siRNA drug (Patisiran from Alnylam) in 2018[7]. Alnylam was the partner in the development of novel one-step synthesis routes of lipid-like[158] materials and lipidoids[112] for parallel synthesis to deliver siRNA. LNPs can contain ionizable groups to provoke endosomal burst or can fuse with the endosomal membrane (by structural similarity to lipids in the plasma membrane) which leads to destabilisation of the membrane and endosome burst[160]. Alabi et al. hypothesised the pK_a as main parameter predicting and determining LNP efficacy for gene delivery[159]. Amide linkages as well as alkyl tails with 8-12 carbons and secondary amines in the composition of the LNP were identified as important design criteria for efficient and biocompatible carriers[112].

4.1.2 Redox sensitive polymer libraries for gene therapy

To achieve redox sensitivity, disulphide (R-S-S-R') linkages can be incorporated into the material. Disulphide moieties are rapidly cleaved by glutathione (GSH) or thioredoxin reductases which leads to degradation/fragmentation of the material and induces drug release. Intracellular GSH concentration (~1-20 mM) is about 1000-fold higher in comparison to the extracellular environment (~0.002 mM) and serves as such as a specific trigger for intracellular drug release[161].

Polymer libraries to screen for bioreducible polycations were prepared by Michael-type addition of bisacrylamides and amines to poly(amido amine)s (PAA). The effects of chemical functionalities in PAAs for non-viral gene delivery are extensively reviewed[162]. Cystaminebisacrylamide was identified in several screenings as the lead bisacrylamide[163,164]. Exemplary studies are summarised in Table 7. Tzeng et al. designed a polymer library of amine endcapped PBAEs for siRNA delivery to human mesenchymal stem cells (hMSCs), inhibiting osteogenesis by delivery of B-cell lymphoma (Bcl)-like protein 2 (BCL2) siRNA. The cystamine containing polymer was identified with highest ability to complex siRNA and to induce sustained gene silencing[165]. Kozielski et al. demonstrate, that disulphide modified PBAE R647 can deliver GFP siRNA more efficiently without causing cytotoxicity to human brain cancer cells, while the non-bioreducible analogue 647 with similar physical properties and siRNA binding capacity doesn't impact GFP expression and causes toxicity[166].

Table 7: Redox responsive and bioreducible polymer libraries for gene delivery.

Material	Drug	Cell type	Screening readout	Advance	Benefit	Reference
SS-PAA	pDNA	COS-7	β-Gal	Best PAA with N,N'-cystaminebisacrylamide (CBA) and ABOL	Disulphide containing formulations (CBA) with higher transfection efficacy and lower toxicity	Lin et al.[163], 2006
SS-PAA	pDNA	COS-7	β-Gal	Disulphide in the diamine and variation in the crosslinkers	4-fold increased transfection efficacy in comparison to PEI and pDMAEMA	Piest et al.[169], 2008
Au-SS-siRNA coated with PBAE library	siRNA	HeLa	Dual luciferase	AuNP-siRNA-PBAE C32-221	Cellular uptake of PBAE modified formulation but no uptake with AuNP or AuNP-siRNA	Lee at al.[170], 2009
SS-PBAEs	siRNA	hMSCs	eGFP silencing	Cystamine (SS) terminated PBAEs with superior silencing effect	Control of hMSC differentiation with prolonged silencing of BCL2 *in vivo*	Tzeng et al.[165], 2012

ß-Gal	ß-Galaktosidase
pDMAEMA	poly(2-dimethylaminoethyl methacrylate) (pDMAEMA)
ABOL	4-amino-1-butanol

Lin et al. identified a PAA of N,N'-cystaminebisacrylamid (CBA) and 4-amino butanol (ABOL) as best polymer for gene transfer of pDNA to COS-7 cells[167]. Vader et al. used this polycation to transfect human head and neck squamous carcinoma (HNSCC) cells with epidermal growth factor receptor (EGFR, overexpressed in squamous carcinoma) siRNA. However, they couldn´t observe efficient siRNA condensation and transfection. Only modification with 25-50% of diaminoethane (EDA) lead to efficient EGFR silencing, indicating, that more cationic charge was necessary to condense siRNA. Additionally, they found, that polymer/siRNA weight ratios need to be optimised to guarantee that there is enough "polymer" to keep increased endosomal escape properties[168]. Further examples can be found with enzyme sensitive materials.

4.1.3 Enzyme sensitive materials

Upregulated expression and accumulation of specific enzymes can be exploited to induce enzyme-specific drug release. Such enzymes include proteases, glycosidases and phospholipases. Matrix metalloproteinase 2 (MMP2) is known to be upregulated in cancer, leading to cancer progression and metastasis. Therefore, it is used as biomarker in diagnosis and can be used as trigger for drug release in the cancerous tissue. Zhu et al. developed a MMP2 sensitive micellar NP for the co-delivery of siRNA and a hydrophobic drug. The nanocarrier is formed by self-assembling of MMP2 responsive copolymer, PEG-peptide-PEI-1,2-dioleoyl-sn-glycero-3-phosphoethanolamine. Quantifying the siGLO siRNA labelled cells 2h after *intra venous* injection, a 2.4 fold increase in labelling of total tumour cells was observed with the MMP2 sensitive micelle, concluding selective tumour targeting and drug release by the MMP2 sensitive micelle in comparison to non-sensitive micelle[171].

4.1.4 ROS triggered materials

Another phenomenon which can be explored for internal triggered drug release is the increased production of reactive oxygen species (ROS) (such as hydroxyl radicals, H_2O_2 and superoxide) in tumour cells or chronic wounds in comparison to a healthy environment[172]. Shim et al. designed a polycationic nanocarrier functionalised with a cancer cell targeting peptide. Thioketal functionalities in the poly(amino ketal) (PATK) polymer backbone will be cleaved by ROS, leading to the disassembly of the polyplex and release of the DNA to the cytosol. Enhanced targeting and gene transfection was proven in prostate cancer cells[173].

4.1.5 Temperature sensitive materials

Temperature differences from ambient to body temperature (~37 °C) and pathologically increased temperature in inflammation or cancer (~40-42°C) can be utilised as internal stimulus to activate drug release from a nanocarrier system. The most advanced nanocarriers are thermosensitive liposomes, which undergo conformational changes in the lipid bilayer by phase transition of the lipids. The phase transition depends on the lower critical solution temperature of each lipid[134]. ThermoDox®, a thermosensitive liposomal formulation for doxorubicin delivery is currently evaluated in a Phase III clinical trial for treatment of hepatocellular carcinoma. Yet, no thermosensitive formulation carrying siRNA is reported in clinical trials[174].

An injectable thermosensitive and biodegradable polyplex hydrogel for long-term delivery of siRNA was developed by Kim et al.[175]. Low MW PEI and poly(organo phospazene) conjugated by an ester linkage formed soluble polyplex about 100 nm in size with siRNA. Via sol-gel transition of the organo phosphazene at body temperature, the hydrophobic interactions

increased, and a hydrogel is formed (gelation occurs in the target tissue). Performing *in vivo* experimentation in a tumour xenograft model, sustained cyclin B1 silencing could be observed upon one single injection of polyplex hydrogel with cyclin B1 siRNA[175]. This system can be used in many pathologies, where the target tissue is limited to a very defined area.

An opposite strategic approach was used by Lee et al.[176] in the development of a nanocapsule, that responds with volume expansion to a cold shock. Swelling of the Pluronic F127/PEI2K nanocapsules from 118 nm at 37 °C to >400 nm at 15 °C leads to physical induced burst of the endosomal compartment and delivery of siRNA cargo to the cytosol. Significantly increased silencing of GFP and VEGF (vascular endothelial growth factor) in cancer cells (HeLa, PC-3 prostate adenocarcinoma) was demonstrated using this method[176].

4.2 More control through externally triggerable materials?

To overcome limitations as the heterogeneity of local environment at the disease site and patient specificity external triggers as (i) electric stimuli, (ii) magnetic induction, (iii) ultrasound activation and (iv) light can be used to initiate drug release from a nanocarrier. This allows modulation of drug dosing in real time as well as spatiotemporal and remote control over the drug release. Therapeutic efficiency can be increased by the use of such active trigger. Furthermore, using an external trigger may not require ligand targeted delivery since the location can be determined by directing the external energy source. Therefore, it is necessary to know exactly the location of the disease affected area. There are also possibilities to activate large areas by external triggers such as illumination of the whole skin in UV chambers. Different energy sources and many types of materials were already explored for gene delivery[177]. A summary can be found in Table 4.

4.2.1 Electrically triggered systems

Application of electric fields in physiological media induce redox reactions or ionisation. Consequences are bond cleavage or carrier deformation. Microchip-type devices already exist for medical use allowing control over magnitude and also pulse duration of the electric field[178]. Conductive materials as carbon nanotubes, polypyrrole or conductive hydrogels can be used for electroresponsive drug delivery. However, only very few studies involve this technology for gene delivery[179]. Using a conductive polymer, Gautier et al. designed a nanoformulation for electrochemically controlled delivery of covalently bound DNA. The responsive polymeric-DNA matrix is immobilised on an electrochemical probe (Pt). The poly(cyclopentadithiophene) polymer

properties allow promotion of the electric stimulus in physiological media, resulting in the reduction and cleavage of the arylsulphonamide linker[180].

A classic technique for cell transfection is electroporation. Transient pore formation of the plasma membrane is induced by application of pulsed electric fields with relatively high voltage[181]. This technique is used very frequently but has been shown to impact cell viability negatively and result in low transfection efficiency. Boukany et al. developed a novel method called nanochannel electroporation (NEP) where a nanochannel is formed in the plasma membrane as consequence of a very focused electric field to a small area of the plasma membrane. By that, a strong local gradient on the nanoscale permits exogenous material the direct passage to the cytoplasm[182]. Transfecting lung cancer cells (A549) with lipoplexes carrying MCL-1 siRNA via NEP, Boukany et al. could demonstrate direct transfection to the cytoplasm, no impact in cell viability and about 3-fold increase of MCL-1 silencing in comparison to classic (non-NEP) transfection methods[108].

4.2.2 Magnetically activatable materials

Magnetic fields can penetrate deep into tissue and are applied in diagnostic methods as magnetic resonance imaging (MRI). Penetration depth can be adjusted by frequency and therefore allows additional spatial control. A major class of NPs are manufactured on the base of materials responsive to magnetic fields which can be used for gene delivery (other applications are reviewed by Eloy et al.[179]). Electromagnetic energy in the range of 350-400 kHz penetrates very efficiently into tissue (15 cm; 99%) and doesn´t lead to energy absorption by water, thus doesn´t lead to unspecific (background) tissue heating[183]. In magnetic NPs, such as superparamagnetic iron oxide (SPION) particles, the materials magnetic dipole aligns with the external magnetic field which leads to heating of the NP. Derfus et al. took advantage of this effect to show that DNA bound through hydrogen bonding to a complementary DNA strand that was covalently immobilised on the SPION can be released through magnetic field activation[184] (Figure 10). This technology allows heat (i.e. NIR heating of gold shells) controlled release of several types of biomolecules from one carrier[185].

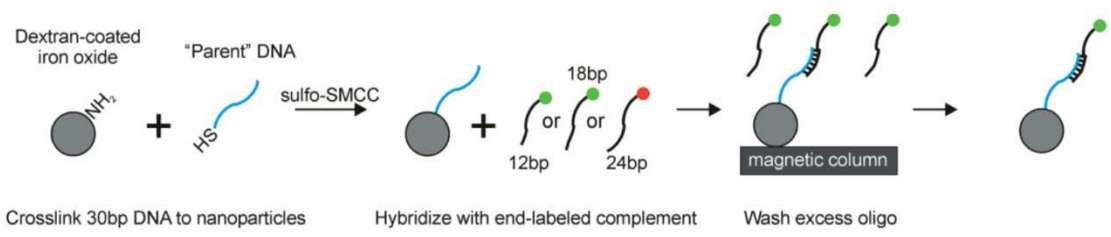

Figure 10: Mechanism of DNA immobilisation by DNA hybridisation on SPIONs. Adapted from Derfus et al., Advanced Materials, 2007[163].

4.2.3 Ultrasound activated materials

Another non-invasive method that is used in diagnostics is ultrasound. Mechanistically, ultrasound can provoke drug release from nanocarriers by cavitation through thermal or mechanical changes in the NP structure. The gas filled cavity of microbubbles responds with nucleation, growth and oscillation to ultrasound stimuli. This leads to pore formation and disruption of cell membranes. High energy ultrasound (>3 MHz) waves however can cause damage of irradiated tissue. Thus, parameters of ultrasound activation need to be optimised carefully. A technique used for gene delivery is called ultrasound-targeted microbubble destruction (UTMD). Zhang et al. used this technique to deliver PHD2 shRNA to H9C2 (cardiac) cells under normoxia (21% O_2) and hypoxia (1% O_2). The microbubble transfection complex consists of perfluoro propane-albumin microspheres (PFPAM; commercially available ultrasound contrast agent) and PEI/RNA polyplexes. Exposure time and ultrasound intensity were optimised to achieve maximum transfection efficacy without compromising cell viability (cytotoxicity if intensity >1.5 W/cm^2 and exposure time > 30 s). Using these settings, significant gene silencing of PHD2 with significant increase in HIF-1α mRNA (which is a direct target of PHD2), was observed, with additionally increased efficiency under hypoxic conditions[186]. Zhang et al. improved this microbubble system by development of a cationic microbubble which allowed to increase RNA drug load for ultrasound-mediated localised myocardial delivery. Cationic microbubbles were prepared from DPPC (1,2-dipalmitoyl-sn-glycero-3-phosphocholine), DC-cholesterol and DSPE-PEG2000 (1,2-distearoyl-sn-glycerol-3-phosphoethanolamine-N-[maleimide-PEG]) and filled with C_3F_8 gas. Transfecting myocardial cells (H9C2) with microbubble/eGFP plasmid complex showed 9-fold increased GFP fluorescence intensity in comparison to plasmid alone and 3-fold increased GFP fluorescence intensity in comparison to ultrasound-mediated transfection, were measured. Microbubble/PHD2-shRNA transfection in H9C2 cells lead to significant silencing of PHD2 mRNA with upregulation of HIF-1α, proving efficient *in vitro* delivery. The PHD2-shRNA microbubbles were then injected in the tail vein of Sprague-Dawley rats. Stable silencing of PHD2 mRNA and upregulation of associated mRNA as HIF-1α, VEGF and bFGF with improved heart function until four days post treatment in scar/border zones of myocardium tissue, was observed[187]. These studies show effective ultrasound-mediated RNAi treatment *in vivo*.

5 A focus on Light triggerable materials for gene therapy

In comparison to other external stimuli, light is an especially appealing non-invasive trigger. Light is energy in form of electromagnetic waves. The spectrum of the visible light ranges from 400 to 700 nm (Figure 11). Light triggered release systems allow high degree of spatial and temporal control for drug delivery and provide rapid, on-demand drug delivery which can reduce toxic (side) effects and enhances drug efficacy. There are plethora of molecules responding to different wavelengths of the light spectrum[188,189]. Target wavelength, excitation intensity and precise location for the irradiation can be easily controlled. Light is non-invasive, inexpensive and easy to produce. Especially (near infrared) NIR light offers the advantage to penetrate deeper (up

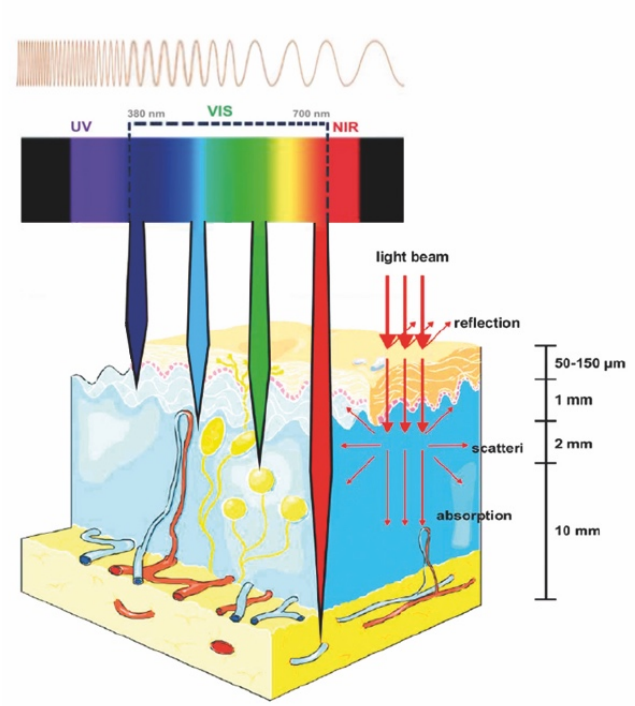

Figure 11: Schematic human skin section indicating penetration depths of light with different wavelengths from the visible electromagnetic spectrum. Red arrows on the right side show light reflection on the epidermis and light scattering and absorption in the dermis. Adapted from Chen et al.[188], Chemical Reviews, 2016 and Silva et al., JCR, 2019. [189]

to 10 mm[190] as can be seen in Figure 11) into the tissue, being less harmful to cells in comparison to UV light[191]. On the other hand, blue light has a lower wavelength, the energy is higher and thus less exposure time is needed. When using light triggered systems, balancing potential harm with benefit is required. Many systems in nature use light as energy source to induce photochemical processes (e.g. chlorophyll light absorption in plant photosynthesis[192], the visual cycle of cis-trans photoisomerisation of rhodopsin[193]). Photoconversion of 7-dehydrocholesterol to vitamin D (cholecalciferol) by UV (<310 nm) absorbed in the skin is crucial for normal growth, skeletal development and calcium absorption[194].

5.1 Phototherapy in the clinic

Phototherapy belongs to the classic clinical treatments for several diseases, such as mood and sleep disorders, neonatal hyperbilirubinemia, cutaneous T-cell lymphoma, inflammatory chronic skin conditions and wound treatments. Mood and sleep related physiological mechanisms are triggered through skin exposure by UV light: vitamin D synthesis, serotoninergic/melatoninergic system and immune system. However, research on phototherapies beneficial effects on SAD (seasonal affective disorder), mood and depression still lack statistical evidence (because of suboptimal study design, few analysed subjects, group heterogeneity). Significant negative correlations can be found between vitamin D levels and depression[195]. About 6-15% of all new-born children suffer from neonatal hyperbilirubinemia (jaundice; total serum bilirubin >12 mg/dl), requiring treatment. Bilirubin, a metabolite resulting from degradation of the hemo group of haemoglobin, is usually cleared by the liver. Several reasons can cause hyperbilirubinemia (acidosis, birth asphyxia, impaired albumin/bilirubin binding, liver diseases among others). Light therapy is the treatment for light to mild forms. Upon skin exposure to blue light (most effective 460-490 nm), the unconjugated bilirubin is converted to bilirubin photoproducts, that are excreted[196,197]. Cutaneous T-cell lymphoma as Sézary syndrome or mycosis fungoides involve treatment of either broadband (270-390 nm, peak 313 nm), narrowband UVB (sharp emission peak 312 nm), ultraviolet A (315-400 nm) or psoralen plus UVA photochemotherapy (PUVA). Also, excimer xenon chloride laser emitting at 308 nm are used for therapy of cutaneous T-cell lymphoma. All treatments are efficient leading to cure or control over the disease[198]. NB-UVB and excimer lasers are also used for treatment of inflammatory dermatologic diseases such as psoriasis and atopic dermatitis[199], where depletion of skin-infiltrating immune cells is needed in the therapeutic strategy[200,201]. UVB treatment in the depigmentation disorder in vitiligo leads to melanocyte stem cell activation and functional development[202]. Acne vulgaris treatment by skin disinfection with UV 407-420 nm targets porphyrins in *P. acnes* bacteria that cause skin eruptions. Light therapy in this context is as effective as oral antibiotic treatment[203]. Furthermore, UVC (200-280 nm) light is shown to have antimicrobial effect and is applied to acute wound infections in order to kill pathogens without damaging the host tissue[204].

5.2 Limitation

Excessive light exposure can lead to damages as skin cancer and tissue damage through local heating. Skin cancer prevalence is increased with increased sun exposure time. Specially the UVB part of the spectrum is known to cause DNA damage (mutation) and abnormal regulation of signal transduction, enhancing the risk developing (non-) melanoma skin cancer[205]. Lan et al.

recently found, that exposure to mildly elevated environmental heat can protect keratinocytes against subsequent UVB-induced DNA damages[206].

Thus, to apply light as a trigger in a therapeutic setting, irradiance and exposure time need to be optimised to avoid long-term side effects. The wavelength of the sensitive moiety in the drug delivery system needs to be fitted to the pathology and the anatomic target. By adjusting beam location and timing of the application, further toxicity can be prevented.

5.3 Photo activatable nanomaterials

Several strategies exist to create light-triggerable materials as can be seen in a tabular overview in Table 8. Most studies involve UV and NIR light as trigger. Generally, light activation induces either the dissociation of the carrier or uncaging of bioactive molecules. This can occur by cleavage (photo-cleavage, -uncaging or -decrosslinking) or isomerisation (azobenzene or spiropyran) of the light sensitive compound. Heat generation (mostly in noble metal NPs) induced through light absorption is another common mechanism to provoke drug release from a nanocarrier (Figure 12).

5.3.1 Surface Plasmon Resonance (SPR), Photothermal effect

Noble metal (e. g. gold) NPs are the most prominent example for indirect photo-responsive delivery systems. If excited by a specific wavelength, the energy from the photons will be absorbed by the electrons of the noble metal NP (particles, shells, rods, cages) and transit from ground state to excited state. Subsequent relaxation of excitation energy leads to nonradiative decay which results in heating of local environment. This is called surface plasmon resonance (SPR)[207]. Photothermal agents and absorbing photons, leading to SPR can be organic dyes (ICG)[208] or noble metal NPs such as gold (Au) NPs (summarised in Figure 12). The release process

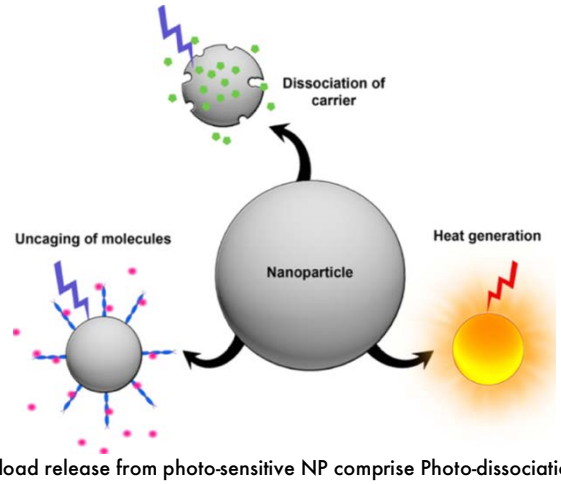

Figure 12: Strategies for payload release from photo-sensitive NP comprise Photo-dissociation, uncaging and heat generation of noble metal NPs. Adapted from Bansal et al., Acc. Chem. Res, 2014[212].

is then initiated by thermo-responsive agents[209]. Through e.g. thermo-de-hybridisation as such of oligonucleotides, de-capping or conformation changes in liposomes, when changing to lower critical solution temperature (LCST)[210,211]. The advantage of these drug delivery systems is that the excitation wavelengths mostly range in the near infrared. Efficiency of photo absorption in NIR is very high, leading to high success probabilities for the indirectly induced release. However, non-specific heating can cause tissue damage of the irradiated area and laser characteristics need to be adapted to not harm the tissue[212].

Especially gold NPs are used to deliver nucleic acid cargos like siRNAs through thiol-Au linkage[170]. Lee at al. showed already in 2009 spatiotemporal controlled release of thiol modified

Table 8: Light-triggerable nanomaterials for gene delivery.

Mechanism	Wavelength (UV, vis, NIR)	Responsive molecule	Material	Drug	Application/ Benefit	Reference
Plasmonic (SPR)/Photo-thermal effect	453 nm/vis	AuNP	AuNP	siRNA eGFP	Gold nanoparticle mediated laser transfection (GNOME) with functional gene knockdown	Heinemann et al.[214]
	800 nm	AuNP	Au-nanoshell-SS-siRNA-lipid bilayer	siRNA GFP	Less laser power for siRNA release and enhanced endosomal escape through TAT-lipid	Braun et al.[215]
	NIR	ICG	Non-ionic surfactant Span80, DOTAP, ICG	siRNA / antimiR-138	Small ncRNA delivery to stem cells	Yang et al.[216]
	765 nm NIR	ICG	PS-$CaCO_3$-chitosan-alginate polyelectrolyte microcapsule	siRNA Akt	Combined thermal and gene therapy for controlled tumour *in vivo* gene silencing	Rui et al.[208]
SPR / Photo-dehybridisation	780 nm NIR	Au nanorod	Au nanorod with miR hybridised on complementary DNA	miR-302a, miR-155	Controlled delivery of more than one microRNA	Lino et al.[185]
Photosensitiser (PS)/ Photochemical Internalisation (PCI)	680 nm vis	Dendrimeric phtalocyanine	PEG-PAsp(DET)-PLys micelle	pDNA	pDNA efficacy protected by compartmentalisation of PS and pDNA	Nomoto et al.[218]
	vis	Aggregation-induced emission (AIE) PS	AIE-Aminoacrylate-oligoethylenimine	DNA	Enhanced endosomal escape through ROS production for controlled DNA unpacking	Yuan et al.[219]
PS / PCI / Photo-isomerisation	365 nm UV / >450 nm vis	Spiropyran	Imidazol-PEGMA-spiropyran copolymer	pDNA	reversibly controllable aggregation-induced enhanced photosensitisation and emission (AIEPE)	Ji et al.[220]
Photo-isomerisation	Up-conversion NIR/UV	Azo-host-guest interaction	$NaYF_4$:Yb/Tm/Er UCNP	siRNA GFP	Breast cancer	Chen et al.[221]
	365 nm UV / >400 nm	Azo-host-guest interaction	Azo-host, cyclodextrin (guest) – DNA - PEG	pDNA	PEG shell detachment and DNA release; improved stability in the bloodstream	Li et al.[222]
	365 nm UV / >400 nm	Azo	Azo- aminoglycoside (neomycin)	pDNA	Reversible on-off switching for controlled drug release	Deka et al.[223]
	365 nm UV / >400 nm	Azo	Azo-PDMAEMA (polycation)	pDNA	Improved uptake/gene expression in COS-7, HepG-2 and CHO-K1 cells	Li et al.[224]
	365 nm UV / >400 nm	Azo	D-threoninol-Azo-tethered DNA	DNA /T7 promoter	Reversible photo-regulation of gene transcription by T7-RNA polymerase	Asanuma et al.[225]
	254 nm/ 365 nm	Photochromic nucleoside (PCN)	2'-deoxyguanosine PCNs	Oligonucleotide/DNA	Reversible photo-regulation of gene transcription and molecular trace	Ogasawara et al.[226]

Continuation Table 8:

Mechanism	Wavelength (UV, vis, NIR)	Responsive molecule	Material	Drug	Application/ Benefit	Reference
Photocleavage	980 nm Up-conversion NIR/UV	o-NB PCL and Hypocrellin A (PS)	$NaYbF_4$-$mSiO_2$ UCNP	siRNA PLK1 and ROS	enhanced apoptosis of cancer cells and light induced ROS for endosomal escape	Zhang et al.[227]
	320 nm UV	o-nitro PCL (NPE)	AgNP-PCL-ASO	ASO	Increased hybridisation activity	Brown et al.[228]
	365 nm UV	o-NB	Hydrophobic core–o-NB-cationic head-siRNA micelle	siRNA Luciferase	Enhanced binding on the NP and controlled release	Li et al.[229]
	365 nm UV	o-NB	mPEG-b-P(APNBMA)$_{23.6}$ polyplexes	pDNA / siRNA	Increased stability of siRNA on NP and controlled release	Foster et al.[230], Green et al.[231]
	365 nm UV	o-NB	PAMAM-oNB-cholesterol Amphiphilic dendriplex	Circular DNA	Circular DNA immobilisation and controlled release	Lai et al.[232]
Photo-cleavage/de-crosslinking	UV	o-nitro-benzyl and thiol-acrylate bond	PEG-hydrogel	noggin siRNA / miRNA-20a	Induced osteogenic differentiation of hMSCs by controlled and efficient target knockdown	Huynh et al.[233]
Photocages	365 nm UV	Bifunctional. coumarin PCL (NPE)	2'-OMe modified and linked sense and antisense strand	antimir- lys-6	First light activated antimir with validation *in vivo* (zebrafish)	Zheng et al.[234]
	385 nm UV	NPE	2'-OMe, cholesterol, NPE modified RNA	antimiR-92a	Improved angiogenesis and chronic wound healing	Lucas, Schäfer et al.[235,236]

AIE	Aggregation-induced emission	PCL	Photocleavable linker
Azo	Azobenzene	o-NB	ortho-Nitrobenzyl
NPE	1-(2-nitrophenyl) ethyl	GNOME	Gold nanoparticle mediated laser transfection
PCN	Photochromic nucleoside	PLK-1	Polo-like kinase 1

rod shaped gold NPs (GNPs) through low power laser irradiation at NIR of 785 nm, which is the absorption peak of Au-nanorods[213]. Figure 13 shows specific RNA silencing of the target gene (ERBB2) by NIR activation of GNPs in comparison to negative Controls (no NP + no NIR, no NP + NIR, scramble NP + NIR). However, analysis of non-activated GNPs with ERBB2 siRNA was not performed, which leaves possible leaching of the siRNA from the carrier unclear. The authors also mention limited cellular uptake of the GNPs as parameter to be improved[213]. Lino et al. developed a system for the controlled release of two different microRNA immobilised on gold nanorods by DNA hybridisation. NIR induced SPR leads to local heating of the nanorod. When the melting temperature of the hybridised DNA pair is reached, hydrogen bonding between the homologous ssDNA break and the ssDNA modified microRNA is released. For the controlled release of two different microRNAs, ssDNA with different length and in consequence differing melting temperature were used. In human outgrowth endothelial cells (OECs) the sequential release of miR-155 and miR-302a was shown to impact proliferation and survival of OECs. The authors could show that application of this technology in an acute wound healing mouse model,

leads to significant faster wound healing kinetics. The use of such a system is of high benefit as only one carrier and one light source need to be used to deliver various biomolecules[185].

5.3.2 Photosensitiser

In the clinic Photosensitisers (PS) are used in photodynamic therapy (PDT) for psoriasis[201], vitiligo[200] and various types of cancer[237]. PS are chromophores that generate reactive oxygen species (ROS) as free radicals through relaxation after excitation with a laser source[238]. Molecules reach through light absorption an excited state, which allows energy transfer to oxygen and production of singlet oxygen and other free radicals (superoxide, peroxide, hydroxyl radical). This reaction occurs in close proximity to the PS, allowing controlled ROS phototoxicity in target cells and/or tissue[239]. The photochemical induced disruption of endolysosomal membranes and subsequently enhanced cytoplasmic delivery is called photochemical internalisation (PCI). PCI gained much interest, since a high quantity of nanocarriers (especially for gene delivery) get trapped in the endolysosomal compartment[240]. Nomoto et al. developed photo-activatable polyplex micelles for gene (pDNA) transfer in solid tumours after systemic administration. The micelle consists of three compartments from a triblock copolymer (PEG-PAsp(DET)-PLys), where

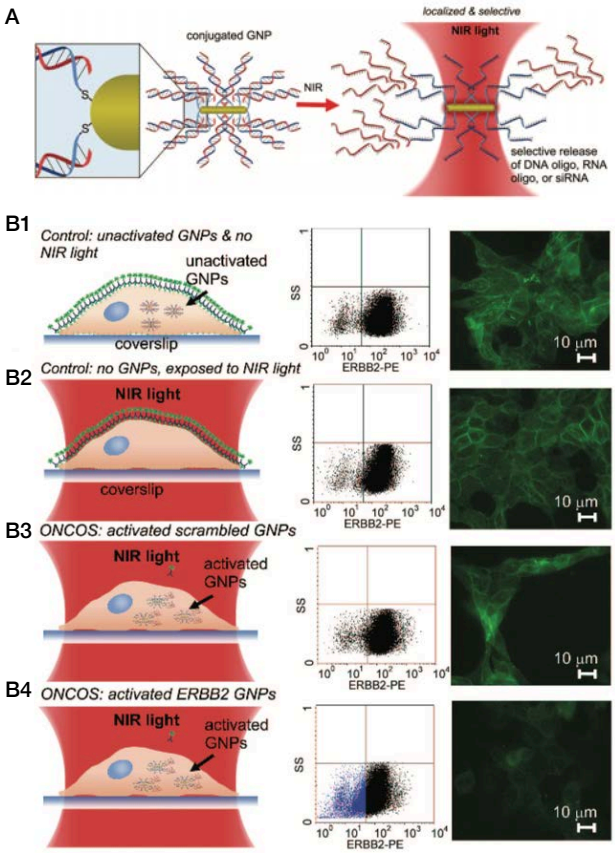

Figure 13: NIR heat induced controlled release of siRNA from Au NPs. (A) mechanistic scheme, (B) controlled ERB2 silencing through NIR activated ERB2 GNPs (B4) in comparison to non-activated (B1) scramble sequence (B3), GNP only (B2) and control condition with no NP but light trigger (B2). Adapted from Lee et al., Nano Letters, 2009[162]

PS and DNA are in different compartments, to protect the DNA from degradation by ROS. On the third and outer layer is a PEG shell, shielding the micelle from unspecific interactions with blood components. The middle layer contains a dendrimeric phthalocyanine photosensitiser (DPc). Peripheral carboxyl groups are facilitating intracellular trafficking in endo-/lysosomes to deliver the DNA to the nucleus. Subsequent protonation of carboxyl groups through acidic pH in endolysosomal compartment leads to release of DPc. Photo activation of DPc provokes destabilisation of endolysosomal membranes through ROS production, facilitating endosomal escape. The pDNA is condensed to the poly lysine (PLys) block of the triblock copolymer to form the core of the NP. These characteristics were confirmed by structured illumination microscopy and confocal laser microscopy with time-laps until 12h. Colocalisation between lysosomes and pDNA decreases until 12 hours indicating endolysosomal escape of the NPs. Using that system in HeLa cells the efficiency of transfection and gene transfer after light activation was shown to be up to 100-fold increased. DPc-TPMs carrying pDNA for a YFP-type reporter mVenus were injected intravenously in mice bearing a solid tumour (subcutaneous HeLa or HCT 116 tumour). NP were activated by light (680 nm laser) 24 h post injection. mVenus expression in the tumour tissue at 3 days after light activation, was only found in irradiated tumours. With 4.4-fold (in HeLa), 6-fold (in HCT 116) increased fluorescence in comparison to non-irradiated tumours[218]. Nomoto et al. demonstrate a light controlled NP system for systemic administration with light controlled and PCI mediated gene transfer. However, gene expression is only shown after light irradiation, the carrier also shows weak gene expression in vascularised organs such as lung, liver, spleen and kidney, reducing the carrier's quality for spatial controlled gene delivery.

5.3.3 Photoisomerisation

Photoisomerisation is defined as the mechanism of conformational change in a molecule induced by irradiation with light of a specific (or range) wavelength. This requires the presence of a chemical bond with limited rotation (double bond) and energy absorption by the molecule to allow the conformational change. Most photoisomerisation reactions are reversible, indicating the reason for these compounds to be called "photoswitches". Photoisomerisation are generally fast reactions with high yields. Chromophores that undergo this reaction are stilbenes,

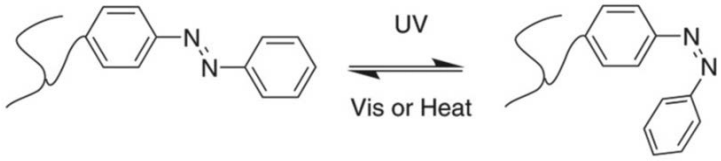

Figure 14: Photoisomerisation mechanism of azobenzene from trans (left side) to cis isomer. Adapted from Weis et al., Macromol. Rapid Com., 2018[245].

spiropyrans[241,242] and azobenzenes, however azobenzenes are the most ubiquitous chromophores.

The photo-induced *cis-trans* isomerisation in azobenzenes (as shown in Figure 14) when incorporated e.g. in a surfactant, photoisomerisation leads to morphological changes of the aggregates, the surface tension and the hydrophilicity[243,244]. Azobenzenes can be easily functionalised and incorporated in macromolecules such as polymers, peptides, proteins and even DNA[243,245–247].

One of the first studies where an azobenzene moiety was introduced in an amphiphilic block copolymer was conducted by Wang et al.[246]. The azobenzene moiety was introduced to the hydrophobic block. Micelles were formed by addition of the non-solvent water, where the hydrophobic block aggregates in the core or of a bilayer membrane. The elongated *trans*-form of the block containing the azobenzene undergoes a conformational change to contracted *cis* form by UV irradiation. The contracted *cis* form destabilizes the LC (liquid crystal) phase and phase transition to more fluid isotropic state occurs. This more fluidic isotropic state makes the hydrophobic core (or membrane) mechanically weaker, deformable or can lead to disintegration. The more stable micellar state can be recovered by visible light exposure, when the conversion from *cis* to *trans* state occurs[246]. This example shows the possibilities, how photocontrol can be "advantageous in the creation of self-assembled monolayers"[243].

Triggering wavelengths can be tuned until NIR depending on the groups next to the azobenzene functionality (Push-Pull-Type Azopolymers)[245]. Another way to use NIR light for photoactivation are transducers as up-conversion NPs (UCNP). Chen et al. recently published their work on up-conversion NPs for photo-controlled release of GFP siRNA by azobenzene mediated host-guest interaction[221]. Azobenzene modified siRNA was complexed via host-guest interaction to β-cyclodextrin (CD) functionalised $NaYF_4$:Yb/Tm/Er UCNPs. Upon NIR activation, the core (transducing/upconverting the light) emits UV light, leading to photoisomerisation of the azobenzene and subsequently siRNA release through unmatched host-guest interaction. Further surface modifications were conducted to increase stability (PEG), targeting (GE11 peptide specific for EGFR) and internalisation (pH responsive TH peptide). Chen et al. show region specific and photo controlled GFP knockdown in a 2D and 3D MCTS tumour cell model. E11 and TH peptides however were necessary to increase cellular uptake and endosomal escape[221]. However, 20 min of laser irradiation are necessary to reach about 80% of gene silencing efficacy. Furthermore, exact quantifications of gene silencing efficacy are missing. Overall, photoisomerisation and related physicochemical changes are giving various possibilities for photoinduced drug release. However, structural parameters (block length, functional groups on azobenzene) might hinder efficient photoisomerisation and subsequent physicochemical changes to induce drug release, to result in an inefficient process[248].

5.3.4 Photocleavage

Photo-responsive chemistries as cleavable moieties are of big benefit, allowing high flexibility for the incorporation of the moiety. In contrast to the previous described methods, as photoisomerisation, photocleavage is an irreversible reaction. Chemistries facilitating this reaction are shown in Figure 15, other groups as indoline and quinoline can be used as well. Pyrene containing moieties, covalently bound via ester linkages are shown to form light-breakable polymeric micelles with a switch in hydrophobicity after photolysis, leading to micelle disruption[248].

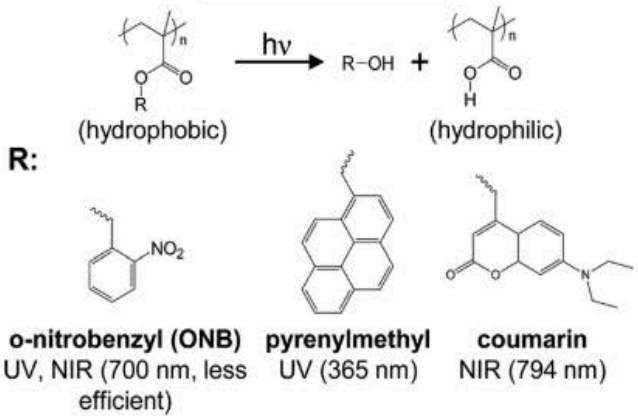

Figure 15: Chemical functionalities for photocleavage with physicochemical hydrophobic/hydrophilic switch. Adapted from Kelley et al., Chem. Soc. Rev., 2013[135].

The most prominent moiety is the ortho-nitrobenzyl (o-NB) group. O-NB derivatives (mainly for photoprotection purposes) can have absorption maxima ranging from ~340 to ~430 nm[249]. Generally, UV light is most efficient to cleave o-NB, even though NIR and two-photon absorption can be used for the cleavage reaction, but with less efficiency[250]. For NIR activation or two-photon absorption other moieties are more favourable[251]. Up-conversion NPs (NIR to UV) can be used as well to activate photocleavable linkers (PCL), as shown in a study by Zhang et al.[227]. PLK1 siRNA was immobilised electrostatically on $NaYF_4$:Tm,Yb@$NaYbF_4$ UCNPs coated with mesoporous silica that was functionalised with a PCL (o-NB derivate) to covalently link a PEG tape to minimize leakage and degradation. Upon irradiation (980 nm upconverted by the UCNP core to 345-475 nm) and photocleavage of PCL, the PEG tape tears off and siRNA can be released from the surface (and the mesopores). With this system, Zhang et al. show ~40% gene silencing of PLK1 mRNA in comparison to no irradiation. After additional immobilisation of a photosensitiser hypocrellin A (HA), gene silencing efficacy increases up to ~70% with 3-fold increased silencing in comparison to no irradiation. With that functionalisation the carrier was more competitive in comparison to Lipofectamine 2000. In a xenograft tumour mouse model, the PLK1 siRNA released from the carrier (UCNP-PEG/HA/siRNA) significantly inhibited proliferation and tumour growth[227]. However, activation of the carrier implies irradiation with

NIR for 40 min (1 W/cm^2). Currently no UCNP is in clinical trial phase and the European Upconversion Network (COST Action CM1403) recommends intense toxicity evaluation to rule out possible harmful effects from the chemical composition and typically small size of UCNPs[252]. A less complex light triggerable system are the amphiphilic polymeric NPs. The photosensitive group can be integrated as photo-antenna (= pendant group) on the polymer chain[230,231,242], or as a linker into the polymer backbone[253–256] or respectively between the polymer blocks[230,231]. Li et al. demonstrate a self-assembly amphiphilic UV-sensitive NP containing a o-NB linker between hydrophobic tail (forming NP's core) and cationic head. SiRNA can condense to the cationic shell of the NP (see scheme Figure 16A). Upon UV activation and cleavage of the o-NB bond, the cationic shell will be cleaved from the NP core, facilitating siRNA release[255]. For activation of the o-NB ester linkage, only 300 seconds with 365 nm (intensity: 10 mW/cm^2) were necessary as shown through proton shifts in ^{1}H-NMR (ethyl proton shift in ester/acid proximity) and UV-Vis absorption spectra changes (peak intensity decrease at 345 nm). To show cellular internalisation (MDA-MB-231), FAM labelled siRNA was condensed to the NPs and increased FAM fluorescence was detected by flow cytometry after 3 and 5 hours of incubation with the NPs (Figure 16C). The authors also show, that light activated siLuciferase-NPs decrease luciferase expression in MDA-MB-231 Luciferase reporter cells about 1.6-fold (ca. 80% luciferase expression without light activation to 50% after light activation; see Figure 16D)[255].

Photocleavage of o-NB groups via UV trigger are also applied to release small molecules as retinoic acid[257] and others for cancer therapy and small ncRNA from di-block copolymer

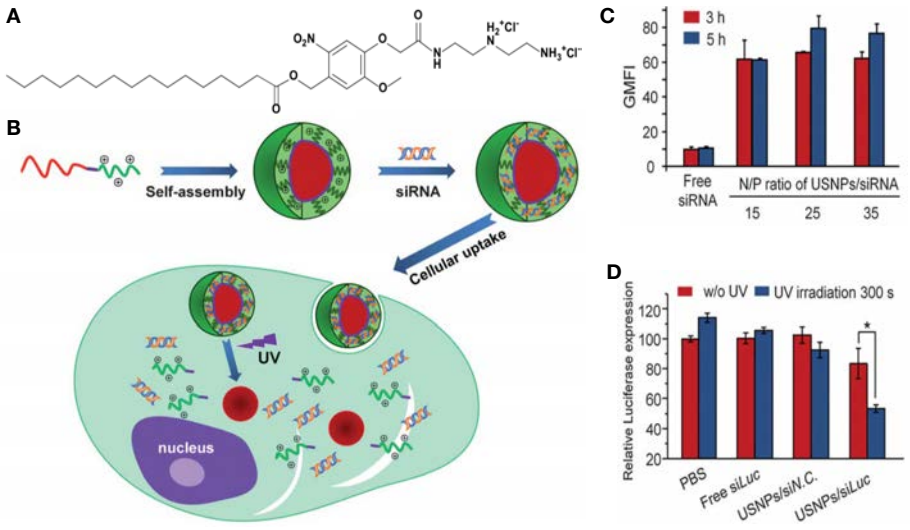

Figure 16: (A) chemical structure of o-NB containing amphiphilic molecule. (B) schematic representation of NP formation and function. (C) Uptake of FAM-siRNA complexes in MDA MB-231 cells quantified by FACS at 3 and 5h transfection time. (D) UV induced gene silencing of siLuciferase NPs in MDA MB-231-Luc cells. Adapted from Li et al., RSC Adv., 2014[255].

assemblies[230] or PEG-thio-acrylate-hydrogels for hMSC (human mesenchymal stem cells) osteogenesis[233,258].

5.3.5 Photocages

Photoactivation via cleavable o-NB and NPE (1-(2-nitrophenyl) ethyl) groups can also be used to cleave caging groups from nucleic acids, microRNAs and antimiRs[234–236,259,260]. Other chemical moieties for photo-uncaging are extensively reviewed by Brieke et al.[261]. Photocages are structures, where a photo-cleavable moiety is covalently bound to a biologically active compound to suppress its physiological activity. The first study involving spatiotemporal controlled antimiRs with successful photoactivation/photo-uncaging *in vivo* (C. elegans) was shown by Zheng et al. in 2011[234]. A bifunctional linker on coumarin base with NPE light cleavable site (as shown in Figure 17), connects antimiR with a blocking strand (with the "seed sequence" of the microRNA). Upon light activation (UV), photolysis of the NPE group occurs and, the uncaged coumarin group gains fluorescent activity and the blocking strand is no more covalently bound to the antimir. Through higher binding affinity, the targeted microRNA binds to the antimir and the blocking strand will be released, leading to microRNA degradation and inhibition of the microRNA regulated pathway. However, the principle did not work for all microRNAs tested. The authors hypothesised, that duplexes of antimir and blocking strand with melting points above 60°C remain hybridised after light activation and are ineffective for microRNA inhibition *in vivo*.

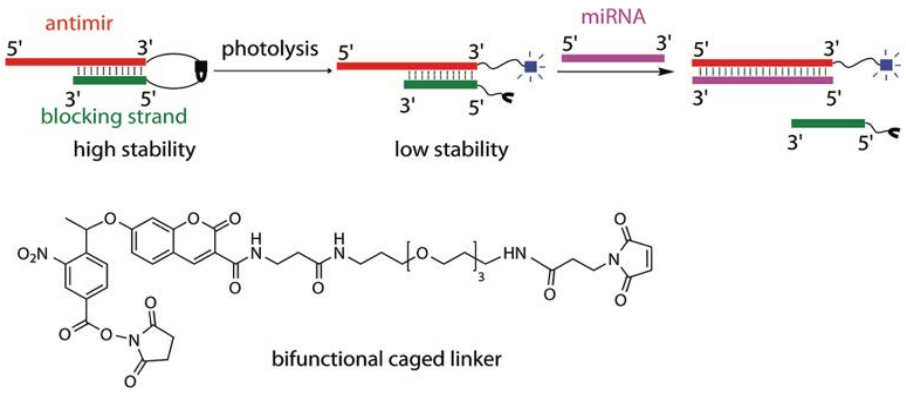

Figure 17: Design of caged antimiR (cantimir) for photo-controlled inhibition of microRNA with a bifunctional linker on coumarin base. Adapted from Zheng et al., ACS Chem. Biol., 2011[234].

Schäfer et al. designed a system of NPE modified 2'-*O*ME-RNA oligonucleotides, that hybridize with absolute complementary to miR-92a after uncaging through UV activation[236]. NPE photolabile groups were attached to nucleobases. The modified RNA oligo with three to six photocaged nucleotides, cannot hybridize to target microRNA. 6 caging groups are necessary to abolish antimir activity UV activation of HUVECs transfected with caged antimir, lead to efficient miR-92a inhibition (70% reduction) and consequently increased expression of ITGα5 target gene

(1.3-fold) with increased angiogenic activity (1.5-fold increased sprout length from HUVEC spheroids) in comparison to non-activated antimiR[236]. The work by Schäfer et al. shows for the first time the therapeutic potential of light induced antimiRs. However, to achieve 90% silencing of miR-92a, 50 nM antimiR are necessary, which is a relatively high dose. In order to activate the antimir 25 minutes of UV irradiation (365 nm, 5-6 mW) are necessary, which increases the risk of UV induced DNA damage.

5.4 Application of light triggerable nanomaterials for local administration to the eye

5.4.1 Clinical trials

RNAi therapeutics targeting ocular diseases were the first to enter clinical trial stage. The first clinical trial was conducted 2004 for the treatment of age-related macular degeneration with siRNA targeting VEGF (NCT0072284). About a third of all RNAi clinical trials are targeting ocular diseases[262]. The main foci are on age-related macular degeneration (AMD), diabetic retinopathy (DR), choroidal neovascularisation and glaucoma (see Table 9).

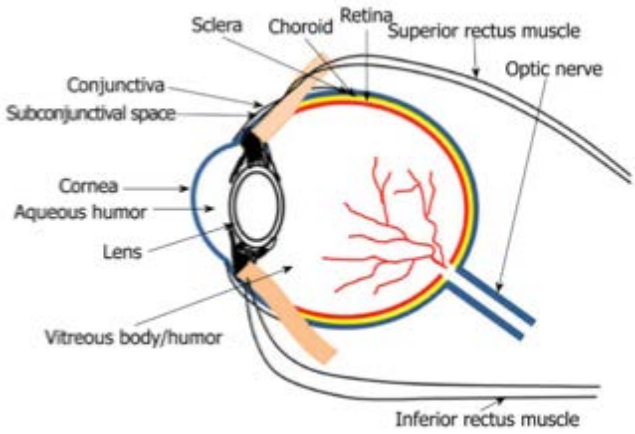

Figure 18: Anatomy of the eye. Adapted from Patel, World J. of Pharmacol., 2013[266]

Administration of the drug to the eye (Figure 18) is facilitated by the accessibility of the organ. Administration routes comprise topical application, intraocular administration via intravitreal injection to the anterior or posterior segment of the eye. Systemic administration is less advantageous, because of low drug permeability through the blood-retinal (BRB) and blood-aqueous (BAB) barrier and consequently low drug bioavailability in the eye (2%), including risk of unspecific toxicity through accumulation in other organs[263]. For the ease of administration and patience compliance, most of ocular therapeutics (90%) are formulated for topical application as ophthalmic solution or ointment. This method is efficient to reach the anterior segment with aqueous humor, iris-ciliary body and lens. Nevertheless, most (95%) of the dose is cleared[264]

through eye protection mechanisms as reflex tearing and blinking and natural processes as nasolacrimal drainage and tear turnover[265]. Additionally, the enzymatic environment of the aqueous humor composed of esterases, aldehyde and ketone reductases may compromise drug half-life. The posterior segment of the eye is separated by corneal and conjunctival epithelium and present a physical barrier for drug delivery. Intravitreal injections are the preferred administration route to reach the posterior segment (retina, choroid). The limitation are risks associated with the surgery such as haemorrhages, retinal detachment and infection among others[266], that reduce patient compliance as well. However, plethora of conditions, such as AMD, DR, choroidal neovascularisation, are affecting the posterior segment. RNAi therapeutics with sustained gene target silencing would be of benefit, additionally reducing the frequency of intravitreal injections. Despite the effort in clinical trials in the field, no formulation reached maturity to be approved by the regulatory authorities.

Table 9: Selected clinical trials for local treatment of ocular or skin diseases with RNAi therapeutics.

Drug	Target/ microRNA	RNA Carrier	Target Tissue	Disease Specification	Phase – Status	Clinical Trial No.	Company
Bevasiranib	VEGF	NC	eye	Age Related Macular Degeneration	III- withdrawn	NCT00557791	OPKO Health Inc.
Bevasiranib siRNA Cand5	VEGF	NC	eye	Diabetic Macular Edema	II - completed	NCT00306904	
PF-655	VEGF	NC	eye	Choroidal Neovascularization /Diabetic Retinopathy	II - completed	NCT01445899	Quark Pharmaceuticals
SYL1001	TRPV1	NC	eye	Dry Eye Disease	III - completed	NCT03108664	Sylentis, S.A.
Bamosiran	β2-AR	NC	eye	Open Angle Glaucoma /Ocular Hypertension	II - completed	NCT02250612 NCT01739244	
RXI-109	CTGF	NC	eye /skin	Age-related macular degeneration /subfoveal choroidal neovascularization /subretinal scarring /subretinal fibrosis /Hypertrophic scar	II - ongoing	NCT02599064 NCT02246465	Rxi Pharmaceuticals Corp.
OLX10010	CTGF	NC	skin	Hypertrophic Cicatrix	I - recruiting	NCT03569267	Olix Pharmaceuticals Inc.
TD101	K6a	NC	skin	Pachyonychia Congenita(PC)	I - completed	NCT00716014	PC Project/ Transderm
STP705	TGF-β1 & COX-2	NC	skin	Hypertrophic Scar	II - recruiting	NCT02956317	Sirnaomics
MRG-110	antimiR-92a	ASO	skin	wound healing / promote angiogenesis	I - completed	NCT03603431	miRagen Therapeutics Inc.
MRG-201	miR-29	mimic	skin	wound healing /scar formation	I - completed	NCT02603224	
MRX34 /miR-Rx34	miR-34	LNP (liposome)	skin/ cancer	Melanoma	I - withdrawn	NCT02862145	Mirna Therapeutics

RNAi therapies in clinical trials for age-related macular degeneration, diabetic retinopathy and choroidal neovascularisation are all related to angiogenesis, which is triggered by VEGF, promoting blood vessels growth. In AMD, the leakiness of these vessels triggers degenerative processes of the retinal epithelium, in severe cases leading to blindness. The first clinical RNAi trial with siRNA targeting VEGF for the treatment of age-related macular degeneration was conducted 2004 (Bevasiranib by OPKO health, NCT0072284). In early 2009, Phase III trials with that compound were withdrawn (NCT00557791). Cho and Kleinmann showed that non-targeting siRNAs (of at least 21 nt length) can inhibit blood (and lymphatic) vessel growth by activation of TLR3 in a mouse model and in human choroidal endothelial cells[58,267]. Meaning that anti-angiogenic effect is sequence and target independent. This also implies that siRNA treatment may induce further unanticipated side effects. Quark Pharmaceuticals then picked up on the VEGF target and developed a short siRNA with 2'-*O*Me modification on each pair of oligonucleotides in the sequence, preventing TLR3 activation[268]. With this formulation, Quark showed improvements in visual acuity in patients with wet AMD. In this phase II trial, it was also shown, that co-RNAi treatment with ranibizumab (which is the frontline of AMD treatment) had better results as ranizibumab alone (NCT00713518). However, there were no statistical differences between the groups[269].

Nevertheless, the high therapeutic potential of siRNA and besides positive safety data from clinical trials, none of the formulations for ocular application showed sufficient efficiency until today. All these trials do have in common, that the formulations were administered locally by intravitreal injection. siRNAs were naked and not formulated with a delivery system. The lack of efficiency might be due to that factor. It is decisive for efficacy that siRNAs are delivered in their active form. The enzymatic environment might destabilize siRNA and the high viscosity of the vitreous (2-4-fold higher than water[270]) might prevent siRNAs mobility and probability to reach the target cells. Therefore, it is important to develop efficient carriers to transport active siRNA to the target cells.

5.4.2 Pre-clinical development of more efficient carriers for ocular siRNA delivery

With the acquisition of OPKO by RXi Pharmaceuticals, Bevasiranib got reformulated in RXi's key technology, the self-delivering nucleic acids (sd-rxRNA). Byrne et al. describe significant silencing efficacy of target mRNA in mouse and monkey eyes after intravitreal injection with no changes in morphology and function of the retina. Sd-rxRNA are asymmetric RNA duplexes, consisting of 19 nt guide strand and less than 15 nt passenger strand with a tail of 6-8 nt that is phosphothiorated (Figure 19)[271]. The sd-rxRNA does not need any further transfection agent[272].

Sd-rxRNA not targeting VEGF, but CTGF (connective tissue growth factor) for the treatment of AMD, choroidal neovascularisation, subretinal scarring and fibrosis are active in clinical trials (NCT02599064).

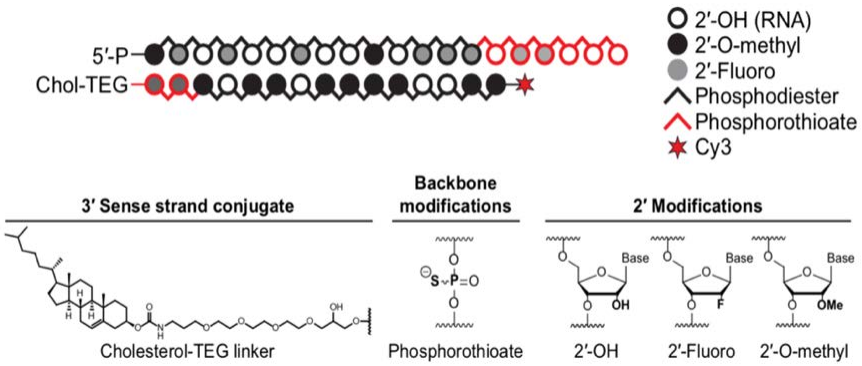

Figure 19: Structure of sd-rxRNAs. Adapted from Ly et al., Nuc. Acid Res., 2017[271].

A variety of nanomaterials for drug delivery to the eye are in development and in preclinical tests, such as liposomes, microparticles, NPs, aptamers, dendrimers among others. For gene delivery of pDNA and siRNA to the eye, polymeric NPs and liposomes are in large number[273]. Extensive reviews were published by Bisht[274], Joseph[275] and Saraiva[273]. Vercauteren et al. explored the use of p(CBA-ABOL) (CBA: cystaminebisacrylamide, ABOL:4-amino butanol) for pDNA transfection to the human retinal pigment epithelium. Transfecting ARPE-19 cells, the authors demonstrated, that polyplex are internalised via a flotillin mediated endocytosis. Knocking out this pathway inhibition of gene transfection can be observed[276]. Martens et al. demonstrate the use of poly(amido amine)s for retinal gene therapy by coating p(CBA-ABOL) with an anionic hydrophilic shell of hyaluronic acid (HA). Polyplex with pDNA with a negative surface charge are efficiently internalised via CD44-mediated endocytosis in ARPE-19 cells. Mobility, in the vitreal network, polyplex uptake and pDNA transfection can be tuned by molecular weight of HA[277]. These studies demonstrate the usability of poly(amido amine)s for gene delivery to the eye.

5.4.3 Light-triggered release system for ocular delivery

The physical characteristics of light and the transparency of the cornea make light-triggered drug delivery suitable to treat ocular disorders, with benefits as site-specific control and high accuracy and safety of the drug release process. So far, there are no publications about trigger sensitive nanoformulations for ocular delivery of siRNA.

The first reported formulation for successful *in vivo* light-triggered drug delivery to the eye describes a polymeric nanoformulation to deliver the anti-angiogenic drug nintedanib[254].

Nintedanib inhibits VEGF, PDGF and FGF receptor[278] and by that vessel formation in animal model of laser-induced choroidal neovascularisation. The NP formulation can be detected by fluorescence microscopy for up to 30 weeks in the intravitreal compartment. Application of the light-trigger (365 nm laser) leads to quinone-methide rearrangement by energy absorption of the o-nitrobenzyl group with subsequent degradation of the polymer into fragments, disassembly of the NPs and release of the cargo[253]. Huu et al. show that nintedanib released from light-activated NPs at 10 weeks post-injection maintained higher bioactivity inhibiting vessel growth in Brown Norway rat eyes in comparison to biodegradable PLGA NP with encapsulated nintedanib[254]. With this work the authors demonstrate applicability and safety of light activatable nanocarriers for intravitreal drug delivery. Furthermore, the sustained biological effect highlights the clinical relevance. Two liposomal formulations (Visudyne®, QLT Inc. and Photrex™, Miravant Med Tech.) for photodynamic therapy of AMD already exist in the market[279]. Nevertheless, healthy cells suffer from toxicity of the photosensitiser. Lajunen et al. describe a liposomal formulation containing gold NPs and ICG (indocyanine green) that is non-toxic and efficiently internalised by human retinal epithelium (ARPE-19) cells (almost 100% of cells labelled with liposomes). Drug release comparing between light activation and no activation was assessed with calcein as model drug and with SYTOX® (Thermo Fisher). After light activation with NIR (9.7 W/cm^2, 2min), the authors observed an increase of about two fold in mean calcein or SYTOX® fluorescence[210].

Another way to avoid frequent intravitreal injections for treatments of the posterior segment of the eye, are intravitreal implants. Sustained drug release can be achieved until a maximum of one year. Typically, they are constituted of polymeric material (i.e. PVA/EVA polymer; Vitrasert®, Auritec Pharm, Inc.), but their use is restricted to small molecule drugs and removal of the implants is controversially discussed[280]. Biodegradable light-responsive *in situ* forming injectable implants (ISFIs) would eliminate risks to the associated surgery of implant removal[281]. Tyagi et al. developed a light activatable polymeric gel based on polycaprolactone dimethacrylate (PCM) and hydroxyethyl methacrylate (HEMA) where gelling is induced via UV photoirradiation of 10 min. 40 days after suprachoroidal injection, no changes in morphology or structure could be found in histological section of Sprague-Dawley rats. Release of bevacizumab from the gel was sustained until 60 days after suprachoroidal injection[282]. Even though the authors did not observe toxicity, free radicals are generated while the photo-crosslinking demonstrating possible limitation of this technique.

In summary these studies show viability of light-triggered NPsfor ocular delivery. Yet there has not been shown any study for light-triggered RNAi in the eye.

5.5 Application of light triggerable nanomaterials for local administration to the skin

The largest organ where light triggered materials for local drug delivery can be applied is the skin. With 15% of adult body weight it is the largest human organ. The skin consists of three layers, the epidermis, the dermis and the hypodermis (schematic representation in Figure 20). The epidermis (~50 µm) serves as protective shield to the outer environment being a chemical, physical and immunological barrier. It mainly consists of keratinocytes that will differentiate and cornify gradually over their lifespan, evolving into the stratum corneum, the outermost skin layer[283]. Much light will be scattered on and in the stratum corneum. Most of the UV-B (315-280 nm) light is absorbed in the epidermis[284]. The tissue layer below the epidermis is called dermis. It is rich in extracellular matrix, giving elasticity and tensile strength, blood and lymph vessels, hair follicles and sweat glands. The connective tissue is mainly formed by fibroblasts. Macrophages and neutrophils are also residing in the dermis, playing an important role in maintaining skin tissue homeostasis[283]. With several millimetres thickness all UV (incl. UV-A, 380-315 nm) and visible irradiation (380-750) will be absorbed in this layer, only infrared light is able to penetrate to the hypodermis[284]. The main role of the third skin layer, the hypodermis (also termed subcutaneous tissue) is fat storage. It mainly consists of fibroblasts, adipose cells and macrophages. Larger blood- / lymph vessels and nerve bundles are found here[283].

Possible target diseases for RNAi therapies for skin conditions are allergic skin disease, psoriasis, vitiligo, pachyonychia congenita (trial with K6α siRNA[285], NCT00716014), acute and chronic wounds, hypertrophic scar (NCT03569267, NCT02956317) and melanoma[262], clinical trials are listed in Table 9. A phase I study in 2016 with miR-34 (MRX34, Mirna Therapeutics, now Synlogic) in a liposomal formulation for treatment of melanoma was withdrawn shortly after its start due to 5 immune related serious adverse events (NCT 02862145). MicroRNA therapies for the treatment of wounds, promoting angiogenesis (NCT03603431) and preventing scar formation (NCT02603224) are in clinical trial phase I.

Table 10: Comparison of acute and chronic wounds.

Level / Characteristic	acute wound	chronic wound
Bacteria	low	high (MRSA)
Inflammatory cytokines	low	high
Protease / ROS	low	high
ECM	intact	degraded
Mitogenic activity	competent	impaired/senescent

Analysis of the 2014 Medicare (American health insurance program) reports revealed costs of $28.1-96.8 billion for treatments of acute and chronic wounds (including infection and wound as second diagnosis)[286]. The Global Burden of Disease (GBD)

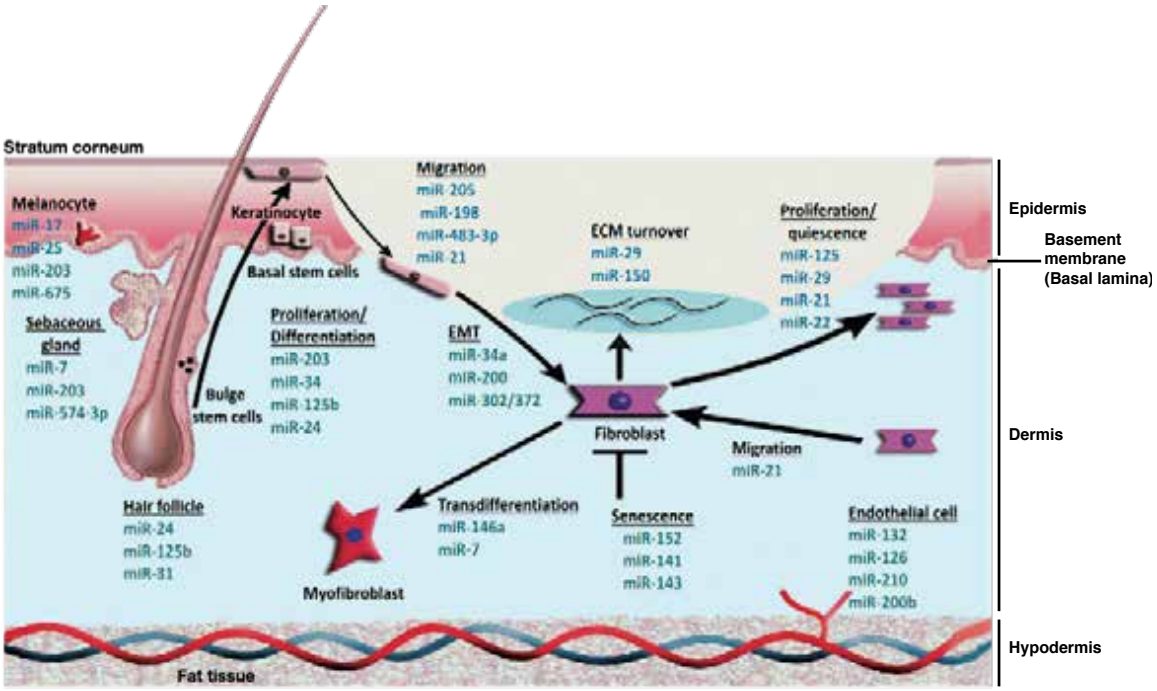

Figure 20: Structure of the skin and role of microRNA in skin homeostasis and wound healing. From the stratum corneum and the epidermis as outermost layers build of keratinocytes with embedded Langerhans cells and hair follicles connecting to the dermis which mainly consist of fibroblasts and extracellular matrix rich in collagen. The dermis also hosts tissue resident macrophages that are important for cell signalling processes. From the subcutaneous layer blood vessel reach into the dermis. Adapted from Miller et al. Adv. Drug. Del. Rev., 2015[296].

study showed increase of 10% in the prevalence for skin and subcutaneous diseases (not including diabetes) from 2006 to 2016[287,288]. Prevalence of diabetes (growth of 23.6% of diabetes mellitus from 2006 to 2016) and with that prevalence of chronic wounds as foot ulcers (15-25%) will increase globally. The type 2 diabetes market is expected to reach $64 billion until 2026 (from $28.6 billion in 2014)[289].

Acute and Chronic Wounds – preclinical evaluation of RNA therapeutics

A wound is defined as "all manner of tissue damage resulting in the disorder of the original tissue structure and homeostasis"[290]. If a "wound is not continuously progressing towards healing"[291] in a timely manner, it is categorised as chronic wound (Table 10). Benefits and disadvantages of classical and novel treatments including stem cell-based therapies are summarised in Table 11[292]. The wound healing process is based on a complex regulatory framework, involving several cell types[290], cytokines, growth factors[293] and hormones[294]. It can be divided in Coagulation and Inflammation phase, the proliferative phase and tissue remodelling phase. MicroRNAs play an important role influencing all cell types and all processes in tissue homeostasis and wound healing. An overview is given in Figure 20 and reviewed by F. Fahs[295], K. J. Miller[296] and E. J. Mulholland[297]. Several microRNA are shown to be specifically up- or downregulated in acute and/or chronic wounds (e. g. of diabetic patients) and therefore can serve for therapeutic targeting. Because of high protease activity and strong oxidative environment in the wound, the use of nanoparticulate carriers is of high benefit to protect microRNAs and siRNAs from degradation and to increase therapeutic efficiency in the wound healing process. Studies pointing

out local RNAi therapeutic approach in wound healing are described hereinafter, a summary of microRNA delivering nanomaterials for the treatment of acute and chronic wounds can be found in Table 12.

Forthwith injury, damaged ECM, damaged tissue cells release signalling cues that lead to accumulation of immune cells in a timely manner, where timed cytokine and signalling molecule release from immune cells is crucial for the healing process.

Coagulation and Inflammation

Platelets initiate coagulation cascade and provide initial fibrinogen-derived extracellular matrix (schematic overview, see Figure 21. They secrete cytokines as TGF-β1 and platelet derived growth factor (PDGF) that activate MSCs and fibroblasts and recruit and activate further immune cells (neutrophils and macrophages) to the injury site. Circulating neutrophils additionally leak through damaged blood vessels into the wound. Neutrophils are also responsible for the elimination of microbes through secretion of antimicrobial peptides, proteases and reactive oxygen species (ROS). Overproduction of ROS causes DNA damage and can lead to necrosis.

Table 11: Treatments of acute and chronic wounds approved by the regulatory authorities.

Treatment / Product	**Benefit**	**Disadvantage**
Gauze	Standard care, inexpensive	Ineffective to protect against microbial invasion
Adhesive dressings	Allow the wound to breathe through exchange of oxygen and water vapour through semi-permeable membrane Prevents from contamination	No debridement if dressings are not changed frequently
Antibiotic / Antiseptic (acetic acid, superoxide) / antimicrobial silver coatings	Fights infection	Microbial Resistance Toxicity leading to prolonged inflammation
Recombinant human (rh) growth factors (rhPDGF (Regranex®), rhFGF, rhEGF, platelet rich plasma)	Highly efficient; data from phase III trial with rhPDGF gel for the treatment of patients with diabetes (type 1 and 2) and chronic ulcers (daily topic application). 43% of trial population showed total wound closure and 32% time decrease for healing process in comparison to placebo control group.	Limited efficacy through lack of stability by degradation in the harsh enzymatic environment in the wound. Clearance before action Possible (systemic) side effects Risk of immune reaction (antibody formation) Costly
Extracellular matrix / Xenograft (Primatrix®, Oasis®) Human skin grafts (Graftjacket®, DermaCELL®)	promotes development of granulation tissue, angiogenesis and tissue regeneration by serving as matrix for cellular ingrowth, rich in active biochemical molecules such as growth factors or collagen and hyaluronan that are important for skin regeneration.	Vascularization/angiogenesis rates uncertain No cells present Allogenic cell sources do have the risk of disease transfer
Skin substitute (Apligraf®, Dermagraft®) Stem cell therapy (autogenous – bone marrow derived SCs; allogenic – amniotic matrix with MSCs, Grafix®)	Living skin equivalent constructed of matrix (collagen, polyglactin) seeded with cells as human neonatal fibroblasts among others, with the benefit of actively producing growth factors and cytokines to rescue the wound healing process.	Donor variability; low engraftment and stability; susceptible to proteases Low shelf life Allogenic cell sources do have the risk of disease transfer Costly
Negative pressure therapy, hyperbaric oxygen therapy	Provokes wound contraction, can be used in combination with cellular or acellular matrix therapy	Danger of skin pressure lesions (by inappropriate placement of tubing)

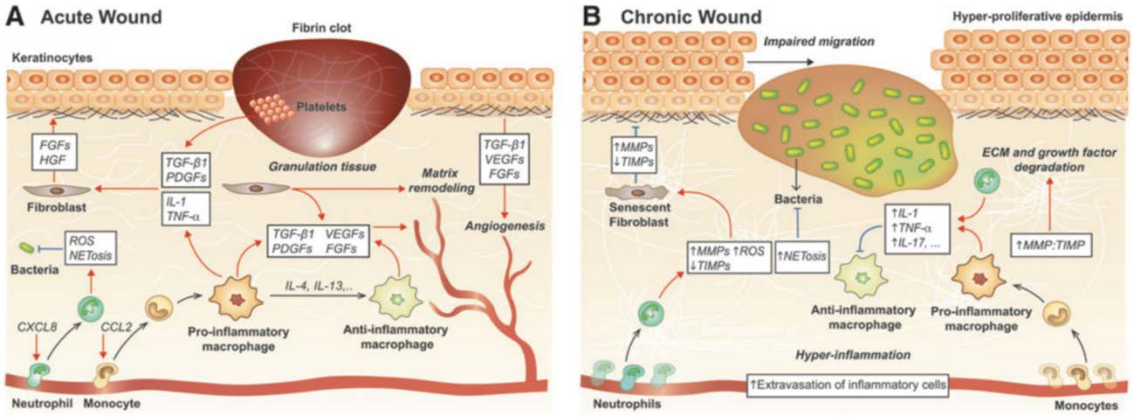

Figure 21: Differences between immune cell signalling in acute (A) and chronic (B) wounds. Adpapted from Larouche et al., Adv. In Wound Care, 2018[298].

Neutrophils also secrete growth factors, such as VEGF, leading to increased proliferation of fibroblasts, keratinocytes, endothelial cells and serves as a chemotactic agent for the recruitment of monocytes[298].

Monocytes differentiating to macrophages and tissue resident macrophages have a key signalling role in wound healing through the orchestrated release of growth factors. While the process occurs a phenotypic shift from pro-inflammatory macrophages (M1) to pro-resolution macrophages (M2) can be observed. Macrophages of the M1 subtype remove cellular debris and secrete factors as IL-1, fibroblast growth factor (FGF-2), PDGF and VEGF, leading to further recruitment of immune cells and proliferation of fibroblasts, keratinocytes and macrophages[298]. Pro-inflammatory macrophages also release nitric oxide (NO) via activation of ***NOS***[299,300]. Inflammation-associated NO is crucial for wound healing by the toxic effect to microbes and parasites, but mainly through its role as signalling molecule for the recruitment and proliferation of hematopoietic stem cells (EPCs) to the wound bed[301]. Deficient protein synthesis of endothelial NO synthase (eNOS) in diabetic mice, was shown to accumulate O_2^-, leading to tissue damage. Gene therapy with single dose of eNOS or manganese superoxide dismutase (***MnSOD***) was shown to reduce O_2^- wound levels and accelerates wound healing[302,303]. Sonic hedgehog (SHH) was shown to be an indirect activator of eNOS. Gene therapy with SHH has been shown to accelerate wound healing in diabetic mice, enhancing NO function[304]. Additionally, SHH stimulates EPCs proliferation and migration by inducing the release of angiogenic factors such as VEGF or angiopoietin-1. Increased proliferation, migration, adhesion and tube formation of endothelial progenitor cells was found after topical administration of SHH in wounds of db/db mice[305]. Park et al. used PBAE NPs for SHH delivery. They demonstrate accelerated wound healing kinetics and two-fold increase of microvessel density and epidermis thickness in acute wound healing mouse model[306].

Proliferative Phase - Tissue formation – Reepithelialisation

Various triggers activate keratinocytes and fibroblasts from the wound-edge, to migrate into the damaged tissue. Vulnerable migrating cells are protected from the oxidative environment in the wound bed via pathways as glutathione-Nrf2-thioredoxin, regulating inflammation-triggered ROS. Nrf2 signalling is impaired in chronic diabetic wounds. Ceradini et al. demonstrate by using topical ***Keap1*** siRNA therapy formulated in LNPs, activation of Nrf2 and rescue of intracellular redox dysregulation through hyperglycaemia. *Keap1* siRNA therapy improves keratinocyte viability, neo-vascularisation (increased VEGF expression), decreases intracellular ROS (increased expression of antioxidants MnSOD-1 and NQO-1) and leads to overall accelerated wound healing kinetic (full wound closure in db/db mice at day 22 with treatment in comparison to 31 days untreated)[307,308]. Independently of the oxidative state in the wound (ROS, NO), damage of the skin results in an ischemic injury site through microvasculature disruption. Hypoxia leads to activation of hypoxia inducible factor 1α (HIF-1α), which is the central regulator of hypoxia response and an efficient therapeutic target for the treatment of ischemic disease such as wound healing and myocardial infarct[309]. Chronic hypoxia though, delays the wound healing process. It is of utmost importance, that wound dressings are semi-permeable for oxygen[310]. Expression of HIF-1α is regulated by prolyl hydroxylase domain protein 2 (***PHD2)***, an oxygen sensor, that triggers HIF-1α degradation in normoxia[311]. RNA silencing of PHD2 stabilizes HIF-1α and can be used as therapeutic strategy to enhance HIF-1α regulated impaired processes in the wound healing process such as proliferation, migration, angiogenesis through upregulation of VEGF, FGF, TGF-β1 and 2 and others (see Figure 22)[312,313], having an

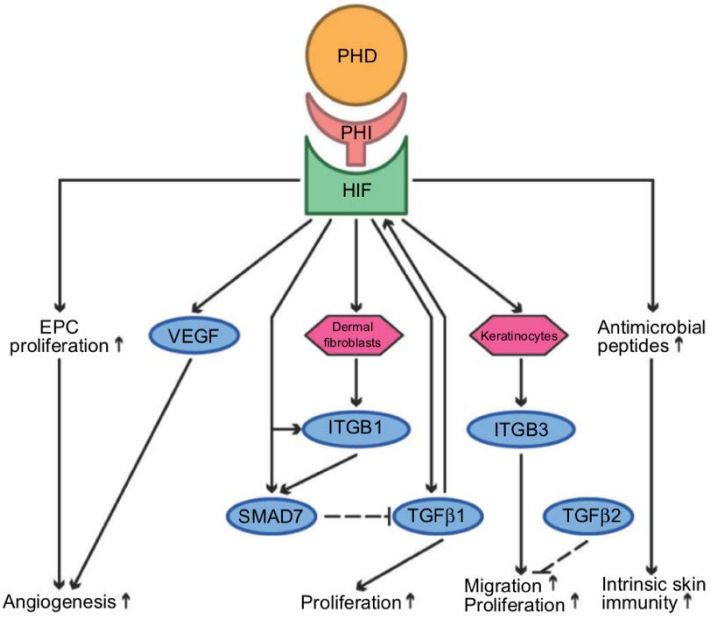

Figure 22: PHD dependency of HIF signaling in wound healing. Adapted from Harnoss et al., Hypoxia, 2015[313].

impact on most cell types involved in the wound healing process. Implantation of PHD 2 silenced fibroblast was shown to lead to improved wound healing in diabetic mice[314]. Martin et al. developed a ROS-degradable poly(thioketal urethane) scaffold for local delivery of PHD2 siRNA complexed in polymeric NPs to promote healing of chronic (diabetic) wounds. Scaffolds were implanted to full excisional wounds on the back of STZ induced diabetic Sprague-Dawley rats and histological analysis was conducted at different timepoints. 4 days post implantation, PHD2 mRNA silencing efficacy was determined to 40% with almost two-fold increase in HIF-1α protein and 60% increase in VEGF protein expression in comparison to the untreated and scramble sequence controls. Seven days after implantation increased formation of mature blood vessels

Table 12: Local, nanoparticle-mediated delivery of microRNA therapeutics for the treatment of acute and chronic full thickness excisional wounds.

microRNA	Carrier	Genetic Target	Study Outcome	Role in Wound Healing	Author
miR-21	miR-21 overexpressing keratinocyte-microvesicles	MMP-1/3, α-SMA, N-cadherin, IL-6/8	Increased migration, differentiation of fibroblasts, enhanced EC angiogenesis and pro-inflammatory response resulting in accelerated wound healing kinetics in diabetic (STZ-induced) Sprague-Dawley (SD) rats	R / A	Li et al., 2019[326]
antimiR-26a	naked, LNA (locked nucleic acid)	miR-26, ID1, SMAD1, p27	Accelerated wound closure with increased amount of granulation tissue and neo-vascularisation in diabetic (db/db) mice	R /A	Icli et al., 2016[327]
antimiR-92a	Photocaged antimiR	miR-92a, Itga5, Sirt1	Increased proliferation and angiogenesis with enhanced wound healing kinetics in diabetic (db/db) mice	R / A / P	Lucas et al., 2017[235]
miR-132	Liposome-pluronic F-127 gel	NFkB	Increased keratinocyte proliferation, reduced inflamation and accelerated healing kinetics in human *ex vivo* wound model and diabetic (db/db) mice	R / P	Li et al., 2017[328]
miR-146a	Cerium Oxide NPs	IRAK1, NFkB pathway	Accelerated healing kinetics and vascularisation in diabetic (db/db) mice and (hperglycemia) porcine model	I	Zgheib et al., 2019[329]
miR-150	Lipoplex	MYB	Increased proliferation of epidermal keratinocytes and EC, with accelerated wound healing kinetics of acute wounds (C57BL/6 mice)	R	Henriques-Antunes et al., 2019[330]
miR-155	Naked/miR-155 plasmid DNA	TIMP-1, MMP-2	Enhanced keratinocyte migration and increased wound closure kinetic in (SD) rats	R	Yang et al., 2017[331]
antimiR-210 antihypoxamiR	LNPs	miR-210	Accelerated reepithelialisation with clear epithelial hyperplasia and increased keratin-14 when injected in ischemic wounds (bi-pedicle flaps in C57BL/6 mice)	R / Hypoxia	Ghatak et al 2016[318]
miR-223	Adhesive hydrogel with miR loaded HA particles	TNFα, IL-1/6, Arg-1	Drives polarisation of macrophages to anti-inflammatory (M2) type / accelerated wound healing in (CD-1) mice, with increased collagen deposition, vascularisation, amount of M2 macrophages	R / I	Saleh et al., 2019[332]
antimiR-378a	PEGylated Au NP	miR378a / integrin-β3, vimentin	Enhanced fibroblast mobility leading to accelerated reepithelialisation and wound closure kinetic in (CD-1) mice	R	Li et al., 2014[333]

R	Reepithelialisation	Sirt1	Sirtuin 1
A	Angiogenesis	IRAK1	Interleukin 1 Receptor Associated Kinase 1
I	Inflammation	MYB	MYB proto-oncogene transcription factor
P	Proliferation	TIMP-1	Metalloproteinase inhibitor 1
a-SMA	a-Smooth Muscle Actin	SD	Sprague-Dawley
ID1	DNA-binding inhibitor ID1	IL	Interleukin
Itga5	Integrin alpha-5 precursor		

(increase in angiogenesis markers collagen IV and alpha smooth muscle actin), proliferation (KI67 staining) and higher amount of granulation tissue in comparison to scramble RNA containing scaffolds, could be determined in the histological sections. This data proves viability of local PHD2 silencing for the treatment of chronic wounds[315]. Also ***p53*** silencing in db/db mice (p53 siRNA encapsulated in an agarose gel[316]) was shown to stabilize HIF-1α, improving wound healing kinetics after application at d1 and d8, through increased expression of vasculogenic cytokines as VEGF[317].

MicroRNA sensitive to the state of tissue oxygenation and hypoxia are termed "hypoxymiRs". Several microRNAs are found to stabilize (miR-92, miR-424) or destabilize (e.g. miR-20b, miR-199a) HIF-1α[297]. In a formulation with LNPs consisting of DOTAP, DODAP and SPC and gramicidine peptide to enhance endosomal escape ($AFGLN_{miR-210}$), ***antimiR-210*** conduces cell proliferation in ischemia to an active state. Ghatak et al. demonstrate accelerated reepithelialisation with clear epithelial hyperplasia and increased keratin-14 when $AFGLN_{miR-210}$ was injected intradermally in the wound-edge of full excisional ischemic wounds (bi-pedicle flaps in C57BL/6). Seven days post treatment scramble and carrier-only control show only very low levels of cell proliferation (KI67, IVIS imaging on repTOP™mitoIRE mice), while proliferation was rescued in wounds treated with antihypoxamiR $AFGLN_{miR-210}$[318].

Pro-resolution macrophages release anti-inflammatory TGF-β1 and promote ECM reorganisation by secreting metalloproteinases (MMPs). In chronic venous leg ulcers from diabetic patients it was shown that ***MMP-9*** is significantly overexpressed, leading to inactivation of growth factors and impairment of the formation of granulation tissue[319,320]. Castleberry et al. developed a layer-by-layer (LbL) film comprising a degradable part of PBAE and dextran sulphate and an MMP-9 siRNA containing layer composed of chitosan. Bandages of the LbL film were applied on full excisional wounds in a diabetic (db/db) mouse model. MMP-9 mRNA was reduced about 80% in tissues harvested at d14 in comparison to the untreated and the scramble siRNA condition with reduction of protease activity of 60%. Wound closure kinetics were accelerated and increased amounts of granulation tissue was found in histological sections, as well as increased collagen deposition (5-fold)[321]. This and other[322] siRNA delivery platforms show the therapeutic potential of MMP-9 silencing for chronic wound healing.

Besides anti-inflammatory growth factors as FGF and interleukin-10 (IL-10), M2 macrophages and T cells also secrete insulin like growth factor IGF-1. Insulin or IGF-1 bind to IGF-1 receptor (IGF1R) or insulin receptor (IR) which activates IGF1/insulin signaling. IGF1R activation leads to increased HIF-1α expression and downstream VEGF expression, promoting neovascularisation. Insulin resistance in type 2 diabetes inhibits IGF1R signaling and

macrophages and T-cells are shown to be deficient in IGF-1 secretion[323,324]. Topical application of IGF-1 can revert this effect[325]. Wang et al. identified ganglioside-monosialic acid 3 (GM3; an epidermal glycosphingolipid) and ***GM3*** synthase (GM3S) as key regulator for the inhibition of insulin/IGF-1 signaling under hyperglycemia or after TNF-α trigger. GM3S and GM3 were found to be overexpressed in tissue samples of human diabetic foot skin (4-fold) and skin of diet-induced obese (DIO) (3-fold) and db/db (2-fold) mice[334]. Randeria et al. developed a strategy involving spherical nucleic acid (SNA) for the delivery of GM3S siRNA[53]. GM3S siRNA is immobilised via disulphide bridges to Au NPs as can be seen in Figure 23. By silencing GM3S, they could observe activation of IGF1R and EGFR as well as significant increase in migration and proliferation of keratinocytes after treatment with GM3S siRNA SNA, even under high glucose levels, that typically inhibit keratinocyte migration. GM3S SNA treatment (every other day 50 nM) of full excisional wounds in a diabetes mouse model (high-fat diet induced, diabetes proven by glucose tolerance test) lead to significantly improved wound healing kinetics (closed at day 12) in comparison to untreated (closed day18), naked scramble siRNA and GM3S siRNA. Differences were statistically visible from day 4, analyzing the wound area and from day 6 on, when analyzing the epidermal gap[53].

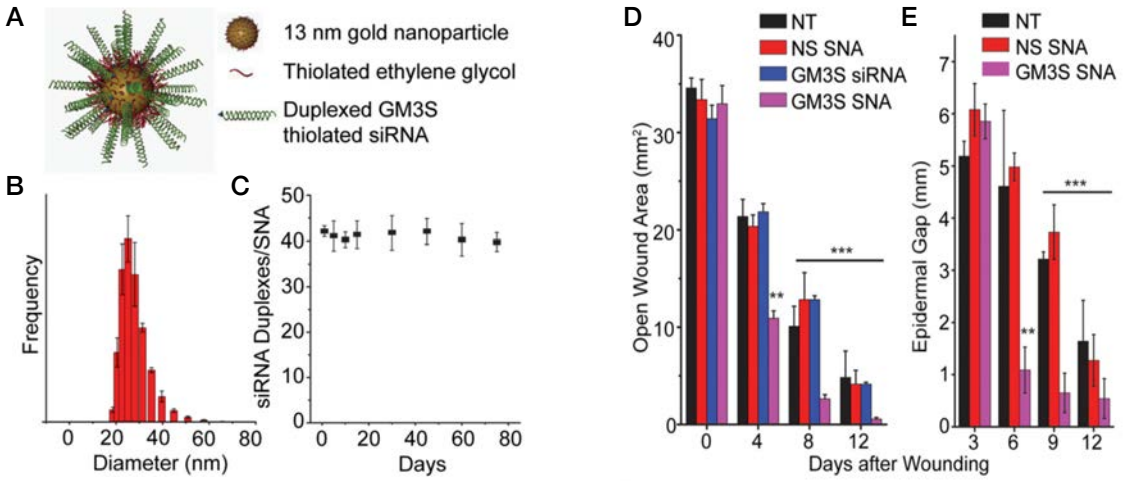

Figure 23: GM3S siRNA Spherical Nucleic Acid to accelerate the wound healing process of chronic wounds. (A) Schematic representation. (B) Size distribution and stability (C) of GM3S SNAs. Wound closure (D) and Epidermal Gap (E) of GM3S SNA treatment in full thickness excisional wounds on db/db mice. Adapted from Randeria et al., PNAS, 2015[53].

Cellular migration is the key tissue movement in reepithelialisation. Keratinocytes and fibroblasts from the wound edge are activated through factors (i.e. growth factors as EGF, TNF-α, IL-1 but also chemoattractant as insulin) to invade the wound zone with provisional ECM[335]. Cell migration was shown to be stimulated by silencing of Fidgetin-like 2 (***FL2***), a microtubule severing enzyme[336,337]. FL2 silencing leads to an increased area of focal adhesion complex, which is correlated to increased cell migration velocity (motility and directionality). Using FL2 siRNA

containing NPs (siRNA containing silica gel), Charafeddine et al. demonstrate two-fold increased migratory capacity of keratinocytes and fibroblasts *in vitro* and significantly accelerated wound closure of full thickness murine wounds (BALB/c). FL2 mRNA was depleted about more than 50% at day 2 post-treatment, persisting until day 8 (about 10% FL2 mRNA) in comparison to FL2 mRNA levels of untreated wounds[336,338].

Increased fibroblast motility accounting for accelerated wound healing kinetics were also found through silencing of miR-378a. Li et al. developed a NP of ***antimiR-378a*** (miR-Pirate378a) conjugated PEG-SH bound on 10 nm Au-NPs. MiR-378a targets integrin-β3- and vimentin were found to be upregulated in cells treated with antimiR-378a, leading to increased cell migration capacity. Significantly improved wound healing kinetics were found of full thickness excisional wounds in the back of CD-1 mice treated with antimiR-378a NPs, in comparison to non-miR containing NPs (significant at day 4 and 6)[333].

These studies highlight the importance of cell migration of keratinocytes and fibroblasts during reepithelialisation.

Tissue remodelling – Scar formation

Fibroblasts and myofibroblasts from the wound edges aim to close the wound quickly to restore the protective skin structure. Extensive wound contraction while healing can lead to reduction of skin elasticity, impaired motion, or loss of function of the affected tissue[339]. Elevated TGF-β levels are shown to stimulate fibrosis through increased (i) proliferation of fibroblasts, (ii) production of ECM components as fibronectin, collagen and integrins among others and (iii) inhibition of protease activity, leading to stabilisation of ECM[340]. Connective tissue growth factor (***CTGF***) expression is selectively induced through activation by TGF-β in fibroblasts[341]. In scar formation, CTGF regulates production of dense collagen matrix (increased expression of collagen) and increased expression of alpha smooth muscle actin[339]. Overexpression of CTGF leads to hypertrophic scarring. Silencing of CTGF with siRNA formulations reduces scar contraction[342,343] in acute wounds and third degree burn wounds. Two formulations (RXi-109 and OLX10010) are evaluated in clinical trials for their effectiveness to prevent hypertrophic scars (NCT03569267, NCT02246465) after revision surgery. Preliminary data of treatment with RXi-109 show improvements in the appearance in comparison to placebo controls[344] (however, RXi-109 is not mentioned in the product pipeline of Phio Pharma, formerly RXi Pharma).

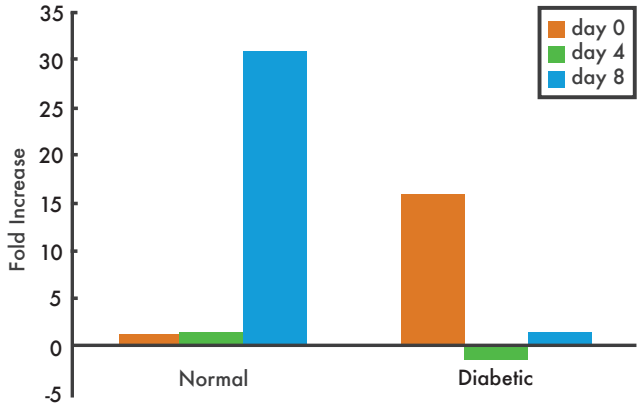

Figure 24: Fold increase of miR-21 expression measured by qRT-PCR in wound tissue of healthy and diabetic mice at different timepoints. Adapted from Madhyastha et al., Int. Wound J., 2012[345].

Tissue remodelling can take up to one year and more. Macrophages, myofibroblasts and other cells undergo apoptosis and leave the tissue. ECM remodelling occurs mainly via secretion of MMPs and signaling molecules from fibroblasts, rebuilding stronger and more robust tissue. Madhyastha et al. found high expression levels of miR-21 at late stages of wound healing, where full thickness excisional wounds in the back of ICR mice were already almost closed[345]. Analysis of microRNA expression in wound tissue of normal (ICR) and diabetic (KKAY) mice over a time course of 8 days revealed, that expression patterns underly temporal control. Especially in the case of miR-21 high expression levels were found at day 8 in healthy animals, whereas highest expression in tissue from diabetic animals was found at day 0 followed by decreased expression until day 8, as can be seen in Figure 24[345]. This study demonstrates the necessity to analyze time dependent patterns of gene and microRNA expression over the course of wound healing.

5.5.1 Light triggerable nanoformulations for RNAi delivery in wound healing

By using light activatable nanoformulations for gene/ncRNA delivery, the necessary temporal control over drug release is given. This approach allows to match drug release exactly with physiologically timed expression patterns. Furthermore, local activation of RNA therapeutics by light-triggered release decrease systemic RNA silencing and with that possible systemic side effects.

With photocaged microRNA, Lucas et al. demonstrate increased biological activity of antimiR-92a *in vivo*[235]. When caged antimiR-92a was injected intradermally in murine skin explants, miR-92a silencing was selectively observed when the formulation was activated with the UV trigger (385 nm, 10 min). For *in vivo* wound healing experiments in a chronic wound healing model (full thickness excisional wounds in db/db mice), treatments were topically applied at the day of the surgery and by intradermal injection to the wound margin at day 4 and 7. Light activation was performed 10 minutes post treatment. Wound closure of treatment with light

activated antimiR-92a was similar to non-caged antimiR-92a. However, increased wound closure with the treatment was not statistically significant in comparison to control groups. Significant differences could be determined when analysing epidermal gap at day 6 and amount of granulation tissue at day 11. Improvement in the wound healing by light-triggered antimiR-92a was due to enhanced proliferation and vascularisation by miR-92a target (Itag5, Sirt1) de-repression[235].

By subcutaneous transplantation of OECs transfected with gold nanorods for NIR controlled release of two different microRNAs, in full thickness excisional wounds, Lino et al. demonstrated the impact of sequential microRNA release, using pro-angiogenic (miR-155) and pro-proliferative (miR-302a) miRNA. If miR-155 release was triggered with the first stimulus at day 0 and miR-302a with the second stimulus at day 1 (sequence 1), wound healing kinetics did not show significant differences to OECs alone. If miR-302a is released on the first trigger (sequence 2), wound closure kinetics immediately increased, with significance at day 4 and 5 and increased OEC engraftment [185]. This study shows for the first-time therapeutic potential of sequential release of two microRNA using one wavelength as release trigger *in vivo*.

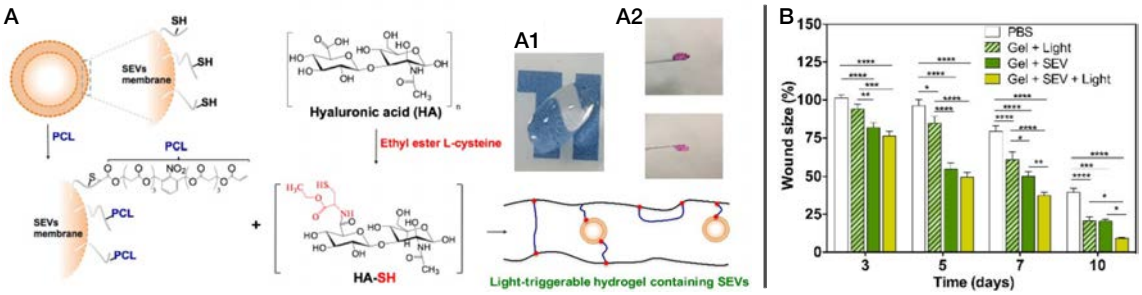

Figure 25: (A) Schematic representation of exosomes immobilised via PCL in light sensitive HA gel; swollen in PBS (A1) and DMEM (A2). (B) Wound closure of full thickness excisional wounds in STZ induced diabetic mice topically treated with PBS, HA gel and UV trigger, HA-exosome gel with and without UV trigger. Adapted from Henriques-Antunes, ACS Nano, 2019[330].

Henriques-Antunes et al. developed a platform based on exosomes immobilised by a photocleavable linker (PCL) in a hyaluronic acid (HA) gel (Figure 25). Exosomes were isolated from human umbilical cord blood mononuclear cells (hUCBMNCs) after a hypoxia stimulus. $CD34^+$ hUCBMNC exosomes have high therapeutic efficiency, increasing proliferation, migration and survival in fibroblast and keratinocytes and network complexity in endothelial cells. Passive release of exosomes from the light sensitive HA gel showed to accelerate wound healing kinetics in a diabetic mouse model (type I). From day 7 differences with the light trigger become statistically significant. miRNAs were found to be responsible for exosomes bioactivity and RNASeq revealed highest expression levels of miR-150-5p. *In vitro* validation proofed increased

proliferation and migration of keratinocytes after miR-150-5p transfection and enhanced cell survival of fibroblasts under hypoxia, with identification of c-MYB as miR-150-5p target. Application of miR-150-5p in an acute wound healing mouse model showed faster wound healing kinetics as saline control[330]. This work shows another example of how light triggered release of bioactive substances can turn the wound healing process more efficient, but there is still much work to do.

The work presented in this thesis focuses in the identification of the chemical composition of small non-coding RNA bearing NPs to (i) target skin cells, (ii) increase efficiency of endosomal escape and by that to (iii) enhance wound healing activity mediated through miR-150 and PHD2 siRNA.

In previous studies high-throughput screening was used to identify NPs with increased intracellular release of non-coding RNA[123, 352-355] from lipoplex or polyplex, however without the possibility of remote control. By using NP libraries with high diversity in terms of chemical composition, size and geometry, formulations can be identified for enhanced cell targeting. Lacking hypothesis of structures beneficial to increase endosomal escape of NPs make the design and screening of NP libraries favorable to identify the most efficient carrier for rapid and effective intracellular siRNA release[111,112]. Here we implement two strategies of introducing light cleavable moieties, either as photo-antenna[257] or into the backbone[357] of poly(amido amine)s. NPs can be formed of the cationic PAAs and negatively charged small non-coding RNA condensed onto the NP. Light exposure of the NP will lead to cleavage of the photo-sensitive moiety leading to the disassembly of the NP. Through the diversity of chemical compositions of the PAAs and the different integration sites of the photosensitive moiety, high variance of physico-chemical parameters and biological activity of released small non-coding RNA are expected. Short timeframes for endosomal escape identified in previous work from Sahay et al.[3] took us to carry out the RNAi screening with short times (< one hour) of cell-material contact for transfection. For successful application of light-activatable RNAi therapeutics in skin regeneration, carriers need to be internalised in the cell type, where RNAi targets alter cell function. Therefore, the leading candidates will be tested for their tropism to skin cells in keratinocytes, dermal fibroblasts and endothelial cells. In this data-driven way we hypothesize to develop more efficient formulations that can be evaluated in the context of wound healing through combination with physiologically relevant miR-150 and PHD2 siRNA.

CHAPTER III – A LIGHT-TRIGGERABLE NANOPARTICLE LIBRARY FOR THE CONTROLLED RELEASE OF NON-CODING RNA

*Josephine Blersch[a], Vitor Francisco[a,b], Catarina Rebelo[a,b], Adrian Jimenez[a], Helena Antunes[a,b], Carlo Gonzato[c], Sandra Pinto[a], Susana Simões[a], Klaus Liedl[d], Karsten Haupt[c], Lino Ferreira[a,b]**

[a]Center for Neuroscience and Cell Biology, University of Coimbra, Coimbra, Portugal

[b]Faculty of Medicine, University of Coimbra, 3000-548, Coimbra, Portugal

[c]Campiegne University of Technology, CNRS Institute Enzyme and Cell Engineering, 60203 Compiègne Cedex, France

[d]Faculty of Chemistry and Pharmacy, Leopold-Franzens, University Innsbruck, Austria

Published in: ***Angewandte Chemie***, 2020, **59(5)**, 1985-1991 †

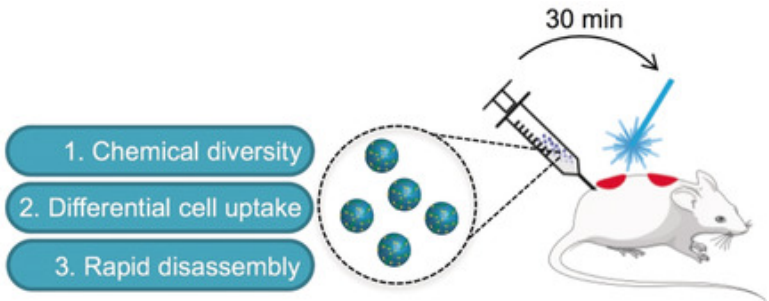

Figure 26: Graphical Abstract.

1 ABSTRACT

RNA-based therapies offer a wide range of therapeutic interventions including for the treatment of skin diseases; however, the strategies to deliver efficiently these biomolecules are still limited due to obstacles related to the cellular uptake and cytoplasmic delivery. Herein, we synthesised a triggerable polymeric nanoparticle (NP) library composed by 160 formulations, presenting physico-chemical diversity and differential responsiveness to light. Six formulations were more efficient (up to 500%) than commercial Lipofectamine in gene knockdown activity. These formulations had differential internalisation by skin cells and the endosomal escape was rapid (minutes range) as shown by the recruitment of galectin-8. The NPs were effective in the release of siRNA and miRNA. Acute skin wounds treated with the top hit NP complexed with miRNA-150-5p healed faster than wounds treated with scramble miRNA. Light-activatable NPs offer a new strategy to deliver topically non-coding RNAs.

† Reproduced from Blersch et al.[379] with permission from John Wiley and Sons (License No. 4879430268089)

2 INTRODUCTION

The capacity to regulate intracellular gene expression with RNA-based therapeutics such as small interfering RNAs (siRNAs) or miRNAs has enormous potential for the treatment of many diseases[2,32,346]. Unfortunately, the intracellular delivery of RNA-based therapeutics is difficult because of their susceptibility to enzymatic degradation and low capacity to cross cell membrane without a vector/carrier. Several delivery strategies have been developed in the last years for the rapid (to facilitate *in vivo* translation) and efficient (to escape the endolysosomal compartment) delivery of RNA-based therapeutics based on NPs, scaffolds, nano-needles, among others[2,32,346]. NPs that either encapsulate or carry RNA-based therapeutics in their surfaces can stabilise the RNA molecules, target potentially specific cell populations and deliver intracellularly the cargo. Unfortunately, NP formulations still offer limited success in terms of endolysosomal escape and temporal delivery of the cargo[347]. For example, in the most efficient formulations, the escape of RNA molecules from the endolysosomal compartment is below 2%[2,130]. Moreover, with the exception of few cases[215,348–351], most of the formulations do not allow temporal delivery of the cargo and yet this issue seems very important because for effective knockdown, RNA molecules should be released from the endosomal compartment shortly (≈15 min)[130] after endocytosis.

The hypothesis of this study is that rapid and efficient delivery systems for RNA intracellular delivery requires the development of NP libraries for the identification of formulations that facilitate cell internalisation while enabling temporal control in the delivery of RNA, with potential advantages in terms of endolysosomal escape. Previous studies have used high-throughput screening to identify NPs to release intracellularly non-coding RNAs[123,352–355]; however, without enabling remote control by an external stimulus such as light. Several strategies have been reported to make light-triggerable NP delivery systems[356]. A frequently used approach is to introduce light cleavable molecules, such as o-nitrobenzyl groups, on the polymer backbone[357]. Light exposure of the NPs leads to the cleavage of the photo-sensitive moiety followed by the disassembly of the formulation.

3 RESULTS and DISCUSSION

Here, we have prepared and characterised a light-triggerable NP library for the controlled intracellular delivery of RNA-based therapeutics. The preparation of such NP library required the use of simple synthetic schemes to be implemented in a high-throughput way, avoiding long

purification steps. Thus, we have selected Michael-type addition chemistry to produce polymers with chemical diversity[123,130,353]. We have synthesised a photo-cleavable linker, based on *o*-nitrobenzyl chemistry, which was reacted with a set of bisacrylamide and amine monomers. The synthesised polymers were precipitated in water to form NPs and then complexed with non-coding RNAs (siRNA or miRNAs). The NPs were characterised for their size, zeta potential, light disassembly properties, cellular internalisation and gene knockdown activity. The formulations with high activity were characterised for their endolysosomal escape. For proof of concept, we demonstrate the efficacy of the formulation in a wound healing animal model using miRNA-150-5p, a miRNA recently identified by us to be involved in keratinocyte proliferation and migration

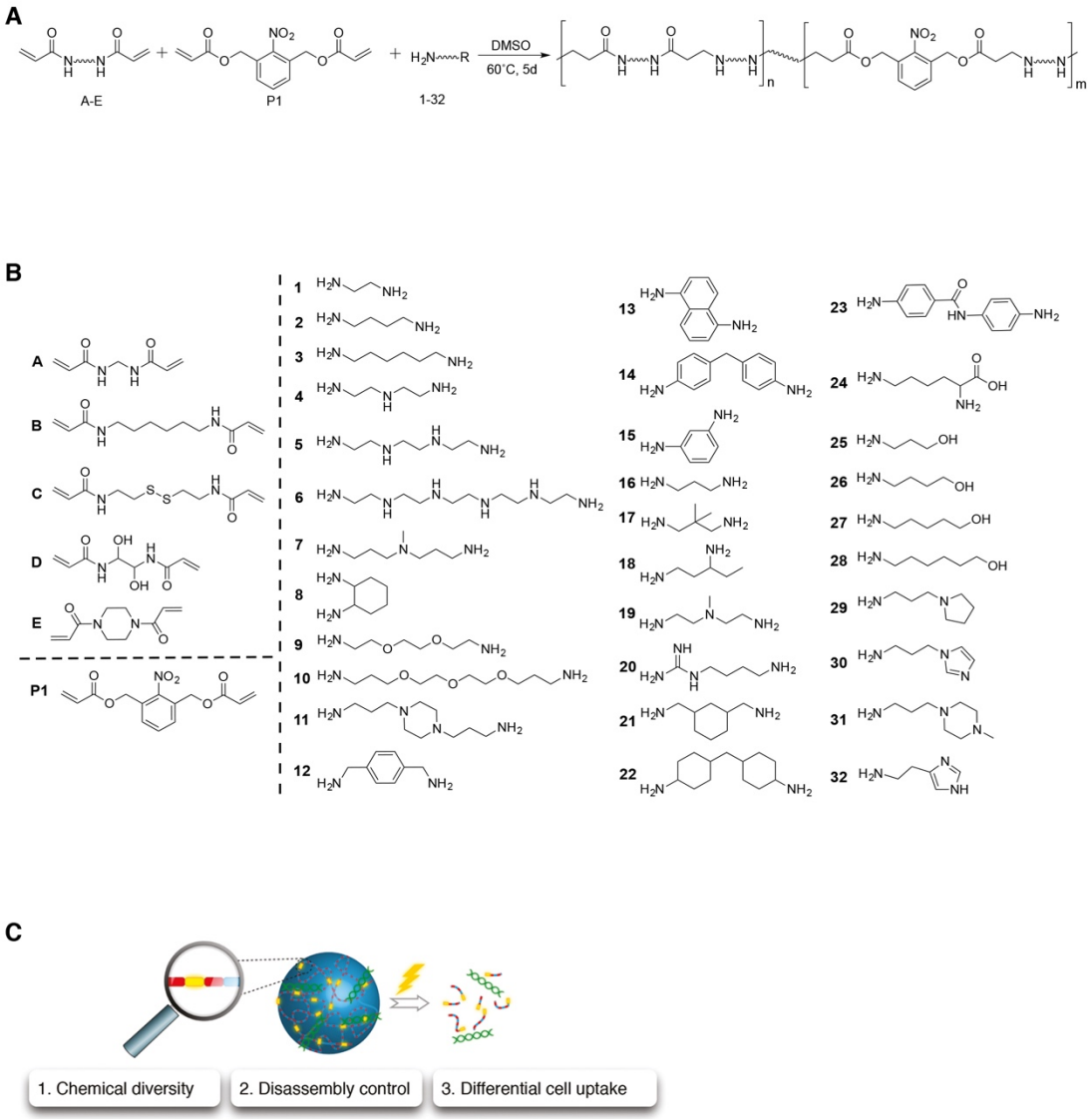

Figure 27: Light-triggerable NP library and gene knockdown activity. (A) Reaction scheme for the preparation of light-sensitive polymers based in the reaction of bisacrylamides (A-E), photo-cleavable diacrylate (P1) and amines (1-32). (B) Monomers used for the synthesis of the library. (C) Schematic representation of the light disassembly of the NPs.

as well as skin fibroblast survival in ischemic conditions[330]. To our knowledge, there are only three studies reporting the use of light-triggerable formulations for the delivery of miRNAs *in vivo*. In one of the studies, the miRNA was modified with a photolabile caging group sensitive to UV-light[235] and showed limited skin regeneration at macroscopic level. The other studies reported a

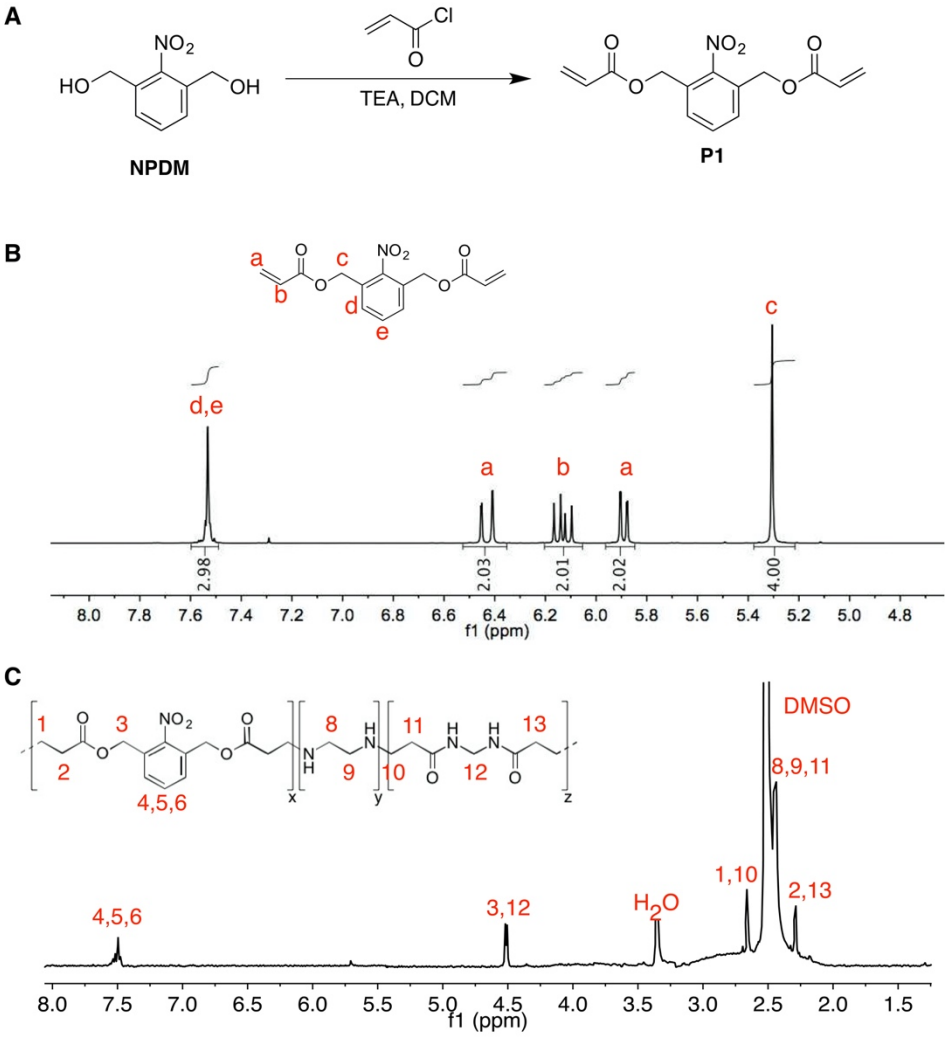

D

	X:Y:Z ratio	UV	Diameter (nm)	Counts (kcps)	Counts decrease (%)
P1A1	12.5:50:37.5	No	246.9	135.2	40.7
		Yes	188.5	80.2	
	25:50:25	No	211.1	248.3	81.6
		Yes	197.6	45.8	
P1A7	12.5:50:37.5	No	298.8	359.4	55.1
		Yes	213.4	161.2	
	25:50:25	No	168.6	215.0	77.8
		Yes	252.7	47.7	

Figure 28: Synthesis of a photo-cleavable linker and its incorporation in polymers. (A) Reaction scheme for the synthesis of the photo-cleavable linker P1. (B) ^{1}H spectrum of P1 in $CDCl_3$. (C) ^{1}H spectrum of P1A1 in DMSO-d6 with P1 (x): amine (y): bisacrylamide (z) ratio of 25:50:25. (D) Optimisation of the ratio between P1, bisacrylamide and amine in P1A1 and P1A7 NPs, to obtain NPs that are highly light responsive, and thus photo-cleavable.

formulation sensitive to NIR light for the delivery of miRNAs[185,351]; however, the inorganic nature of the formulation raises some issues for a potential clinical translation. Here we have identified a biodegradable NP formulation that is able to transfect efficiently *in vivo* miRNAs and enhance significantly wound healing kinetics.

3.1 Synthesis and characterisation of the light-triggerable NP library

To confer the light sensitivity to the polymers, a photo-cleavable linker P1 was introduced in polymer backbone (Figure 28A and 28B). The library was prepared by the addition of monomers (P1, amine and bisacrylamide monomers) in dimethyl sulphoxide (DMSO), for 5 days, at 60 ºC (Figure 27A - 27C). To confer high light sensitivity to the synthesised polymers (and consequently NPs) the ratio of P1 per repeating unit of the polymer was 25 (P1):25 (bisacrylamide):50 (diamine) (Figure 28C and 28D). At the end of the reaction, the unreacted acrylamide groups were capped with amines since previous studies have demonstrated that amine-terminated polymers had higher transfection efficiencies[136]. The efficiency of the capping procedure was high as no measurable acrylate proton signals (5 – 7 ppm) were observed by ^{1}H-NMR (Figure 28C and Figure 29). The synthesised polymer library had (i) a large variety of side groups (ii) disulphide bonds that were relative stable in physiological conditions (pH 7.4) but were

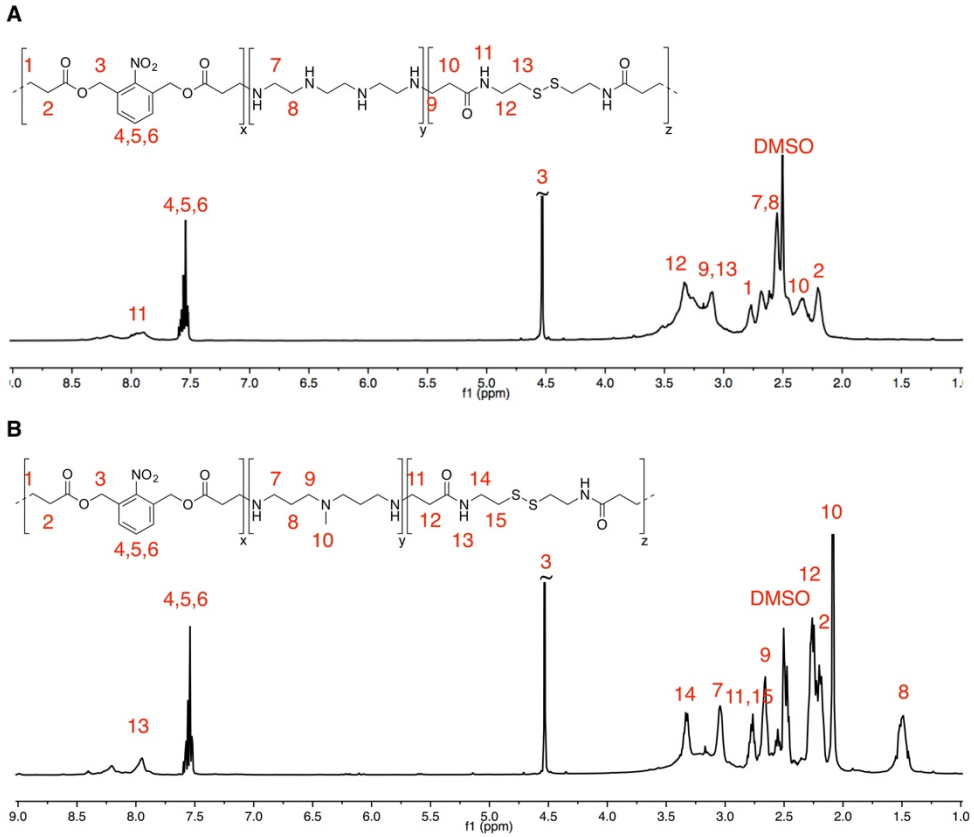

Figure 29: ^{1}H spectra of P1C5 (A) and P1C7 (B) polymers in DMSO-d6 with P1 (x): amine(y): bisacrylamide (z) ratio of 25:50:25.

rapidly degraded in intracellular reductive environments and (iii) different solubility and hydrophilicity in aqueous solution.

The library of 160 polymers was then precipitated in water to form NPs (Figure 30A). In the conditions tested, most of the polymers (90%) were able to form NPs. Polymers that failed NP formation were either soluble in water or formed large polymeric aggregates. The average yield of NP formation was 20.7 ± 15.3%, having 10% of the polymers yields above 25% (Figure 30B).

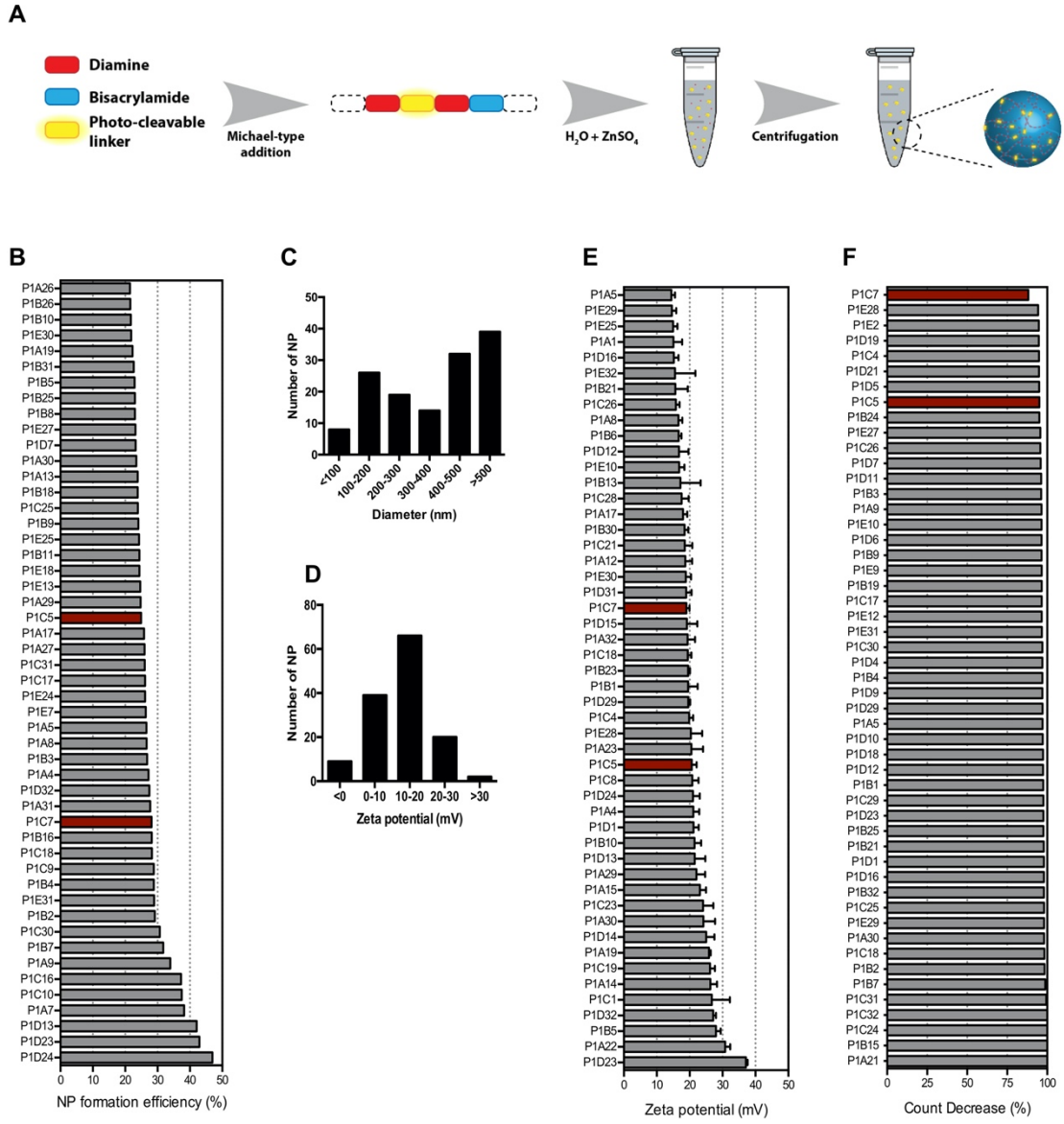

Figure 30: Physicochemical properties of the NP library. (A) Scheme illustrating the synthesis of the polymers and formation of NPs. (B) NP formation efficiency of the top 50 formulations. NP formation efficiency was calculated by the ratio between the weight of NPs after purification and the theoretical molecular weight of the polymer. (C-D) Frequency distribution of NP diameter (C) and zeta potential (D). (E)Zeta potential of the top 50 positive NP. The results are expressed as Mean ± SEM (n = 3). (F) NP count decrease of the top 50 formulations after 10 min UV irradiation (365 nm). The light dissociation of the NPs was calculated by the ratio between the counts (as determined by DLS) before and after light exposure.

90% of the NPs had a size range between 100 and 500 nm (Figure 39C) and 20% of the NPs a zeta potential above 20 mV (Figure 30D - 30E), as evaluated by dynamic light scattering (DLS). Transmission electron microscopy (TEM) analyses confirmed the size range obtained by DLS (Figure 31). The light responsiveness of the NPs was then evaluated (Figure 30F), by the quantification of number of counts per second before and after light exposure, as assessed by DLS (Figure 30F), and by TEM analyses (Figure 31). Approximately 80% of the formulations showed 50% count decrease after 10 min of UV light exposure. Light sensitivity seemed to be independent on the characteristics of the bisacrylamide monomers.

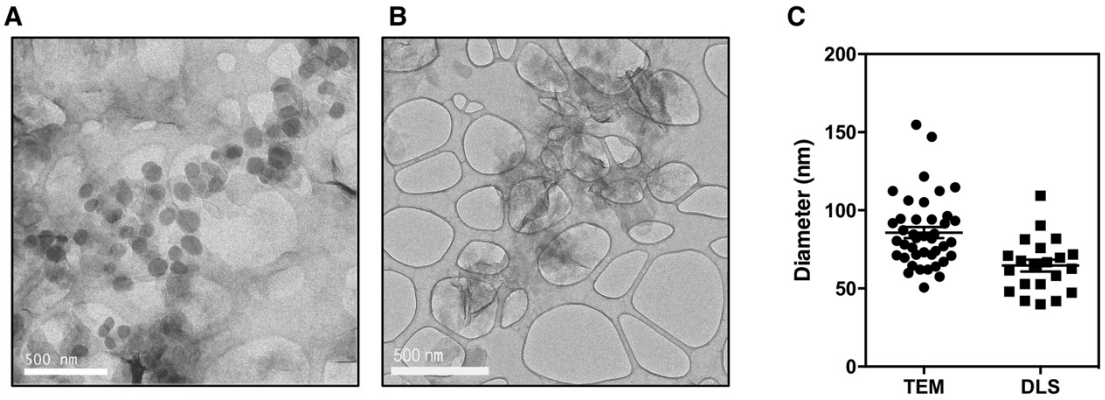

Figure 31: Characterisation of P1C7 NPs. Representative TEM images of P1C7@siRNA NPs before (A) and after irradiation (B) with UV light (10 min, 365 nm, 1 mW/cm^2). (C) NP diameter distribution as determined by TEM and DLS analyses. For DLS (Brookhaven ZetaPALS), data from five NP (50 µg/mL) samples was collected with five measurement runs (1 min) on each sample. Results are Mean ± SEM (n=5). In case of TEM analyses, NP suspensions (500 µg/mL) were applied on carbon coated 400 mesh copper grids, left to air dry and analysed (JEOL-2100-HT microscope). Up to 3 images were acquired and analysed on ImageJ. Results are Mean ± SEM (n = 3, up to 20 nanoparticles per image).

To form the NP@siRNA complexes, both NP and siRNA were mixed to promote electrostatic interactions. Based on preliminary tests with P1C5 formulation, a ratio siRNA (against GFP): NP (w/w) of 1:50, a concentration of NP@siRNA of 20 µg/mL and a transfection time of 10 min were selected for running the NP library (Figure 32). For *in vivo* applications (see below), it is desirable that the formulations are rapidly internalised by cells to reduce their washing from the place they are administered and thus a 10 min-transfection time was used for subsequent studies. To run the library, the NPs were complexed with siRNA labeled with a Cy5 tag, followed by the centrifugation of the NPs, the quantification of the concentration of siRNA not immobilised onto the NPs in the supernatant, and the use of NP@siRNA complexes for cell transfection (Figure 33A). In average, 79.0 ± 13.5% of the initial siRNA was immobilised onto the NPs. Thirty two percent of the formulations did immobilise more than 80% of the initial siRNA (Figure 33B). Formulations more effective binding siRNA were those NPs formed by bisacrylamide A, C and E and diamines 2, 3, 4, 5, 6, 7, 11, 16, 21 or 22. Our results suggested that the binding of siRNA

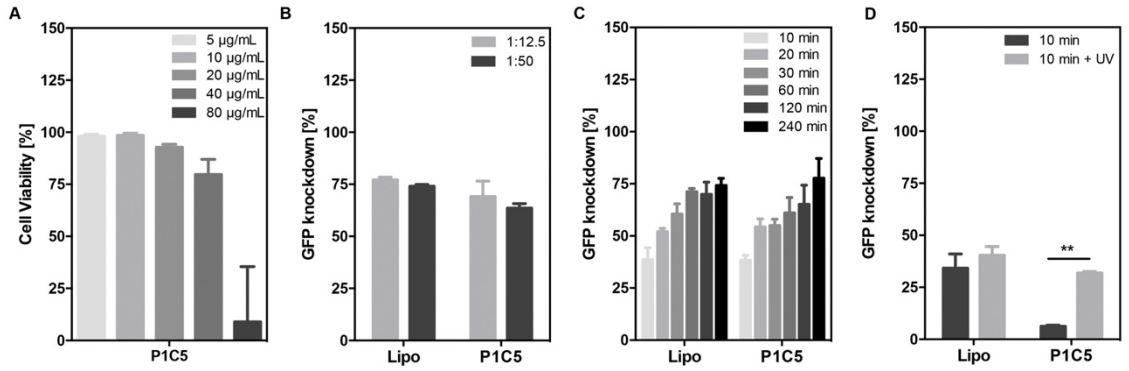

Figure 32: Determination of the siRNA@NP complex concentration, siRNA:NP ratio, kinetics and effect of light activation in gene knockdown. RNAiMAX complexed with siRNA was used as control. Viability and gene knockdown studies was performed in HeLa cells expressing GFP. GFP knockdown was monitored by high-content microscopy. (A) HeLa cell viability after transfection with NPs (siRNA:NP ratio = 1:50) at different concentrations for 4 h. Cell nuclei were stained with Hoechst H33342 and propidium iodide after 48 h. Cell viability was calculated as the % of dead nuclei from the total count of nuclei. (B) Effect of siRNA:NP (w/w) ratio keeping NPs concentration constant at 20 µg/mL in terms of GFP knockdown analysed after 48 h. (C) Effect of transfection time of NP@siRNA complexes (siRNA:NP ratio = 1:50; 20 µg/mL) in GFP knockdown analysed after 48 h. (D) Influence of UV light irradiation (365 nm, 1 mW/cm^2) on siRNA@NP complex and consequently GFP knockdown. Cell transfection was performed for 10 min followed by 10 min of UV irradiati- on. GFP knockdown was analysed at 48 h. Results are Mean ± SEM (n = 4). Statistical analysis was performed using an unpaired student t-test; **P < 0.005.

was not only dependent on positive zeta potential but also on the presence of aliphatic moieties in the polymer backbone.

3.2 High-content screening for maximum GFP silencing efficacy

To evaluate the knockdown properties of the NP@siRNA complexes, HeLa cells stably expressing eGFP were transfected with the formulations. Cells were transfected with NP@siRNA-Cy5 (siRNA:NP 1:50; 20 µg/mL) complexes for 10 min, washed to remove non-internalised complexes, either irradiated or not for 10 min and cultured for additional 48 h. Lipofectamine was used as control. High-content imaging was used to monitor simultaneous several parameters in the same screening experiment, such as cell viability, NP internalisation (from the Cy5 tag of the siRNA) and GFP knockdown (Figure 41), Material and Methods). For the concentration tested, the formulations had no significant impact in cell viability (cell viability > 90%) (Figure 33C) but they showed significant differences in the delivery of siRNA within cells (Figure 33D). It is interesting to note that although some formulations showed higher cell uptake (e.g. P1A19 formulation) than others (for example P1C7 formulation) they showed lower GFP knockdown. It is possible that differences in NP disassembly after light activation (34% decrease in P1A19 vs. 88%

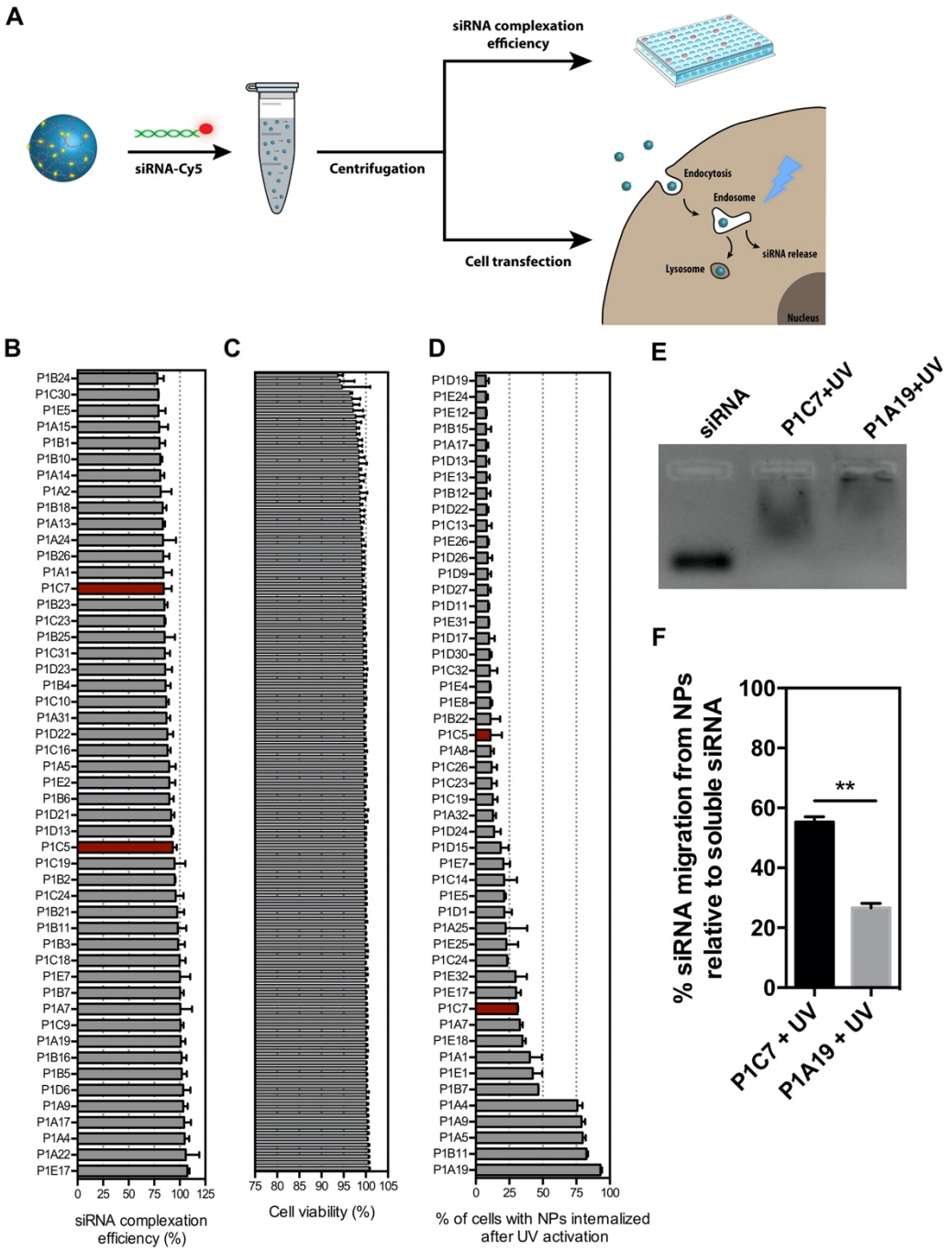

Figure 33: Complexation capacity of the NPs for siRNA as well as cytotoxicity and cellular internalisation of NP@siRNA complexes. (A) Schematic representation of siRNA complexation with NPs (siRNA:NP ratio=1:50) and cellular internalisation studies of NP@siRNA complexes (20 µg/mL) with transfection time of 10 min. (B) siRNA complexation efficiency of the top 50 formulations determined in NPs@siRNA-Cy5. (C) HeLa cell viability at 48 h post transfection without UV irradiation. Cell nuclei were stained with Hoechst H33342 and propidium iodide at 48 h, and cell viability calculated as the % of dead nuclei from the total count of nuclei. (D) Percentage of cells stained for NPs@siRNA-Cy5 at 48 h post-transfection. The top 50 conditions with higher NP internalisation in HeLa cells are displayed. Results are Mean ± SEM (n=3). (E) Gel electrophoresis of soluble siRNA or NPs@siRNA (100 µg/mL) after UV irradiation (10 min, 365 nm, 1 mW/cm^2). (F) Percentage of siRNA migration from P1C7 and P1A19 NP formulations relative to soluble siRNA (control) after UV irradiation. The calculation was done by considering the mean of each gel band. Results are Mean ± SEM (n=2). Statistical analysis was performed using an unpaired student t-test. ** P<0.01.

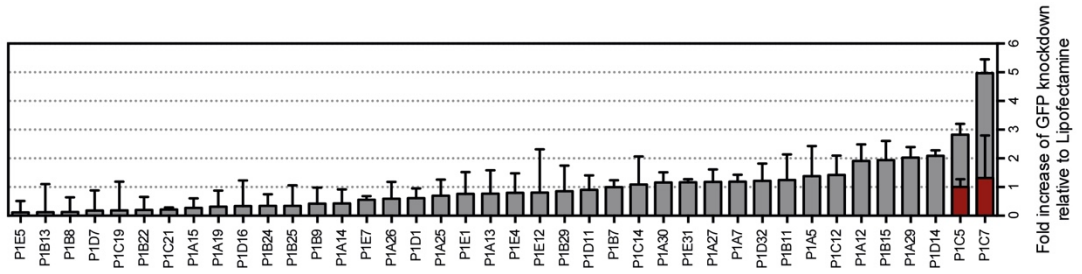

Figure 34: High-throughput screening of NPs for gene knockdown using siRNA. Fold increase of GFP knockdown after 48 h post-transfection relative to Lipofectamine (Lipo) for the best 40 formulations. Cells were transfected with the formulations for 10 min and subsequently irradiated for 10 min with a UV lamp. The red bars show GFP knockdown in the best two formulations without UV irradiation. Results are expressed as Mean ± SEM (n = 3).

Table 13: Polymer molecular weight change of purified P1C5 and P1C7 in DMSO (0.8 M) upon irradiation with a UV lamp at 365 nm for 10 min and summary of the NPs properties.

	Polymer				Nanoparticle					
Sample	UV light	M_n (kDa)	M_w (kDa)	PDI	Size (nm)	Zeta (mV)	Count decrease (%)	siRNA complexation (%)	Internalisation (%)	Fold increase rela. to Lipo with UV
P1C5	No	3.3	9.5	2.88	353.1 ± 34.6	20.6 ± 2.3	95.1 ± 3.4	93.2 ± 3.9	6.4 ± 4.7	2.8 ± 0.6
P1C5	Yes	2.4	6.4	2.67						
P1C7	No	6.8	33.0	4.85	73.5 ± 10.5	18.9 ± 3.5	88.2 ± 5.4	84.2 ± 7.8	30.0 ± 1.9	5.0 ± 0.8
P1C7	Yes	5.0	26.7	5.34						

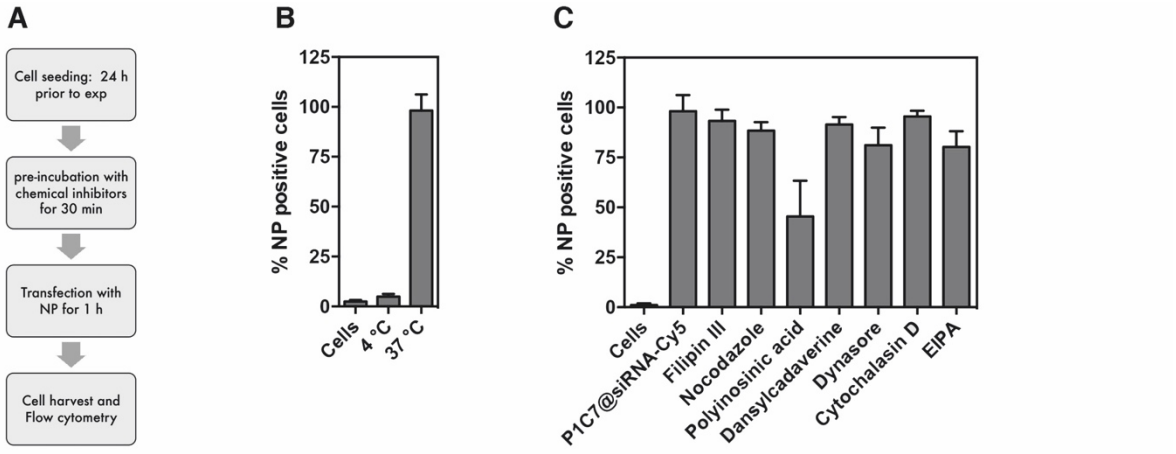

Figure 35: Internalisation mechanism of P1C7@siRNA-Cy5 NPs. (A) Schematic representation of the experimental protocol. (B) Effect of temperature in the cellular uptake of P1C7@siRNA-Cy5 NPs. (C) Uptake of P1C7@siRNA-Cy5 in the presence of several endocytosis inhibitors: filipin III inhibits cholesterol dependent internalisation mechanisms, nocodazole inhibits microtubule dependent pathways, polyinosinic acid inhibits scavenger receptors, dansylcadaverine and dynasore inhibits clathrin-mediated endocytosis, cytochalasin D inhibits all pathways dependent on actin (including macropinocytosis) and ethylisopropylamiloride (EIPA) inhibits macropinocytosis. The concentrations tested for each inhibitor were confirmed before the experiment to be non-cytotoxic. Cellular internalisation of P1C7@siRNA-Cy5 NPs was evaluated by flow cytometry. Results are expressed as Mean ± SEM (n = 3).

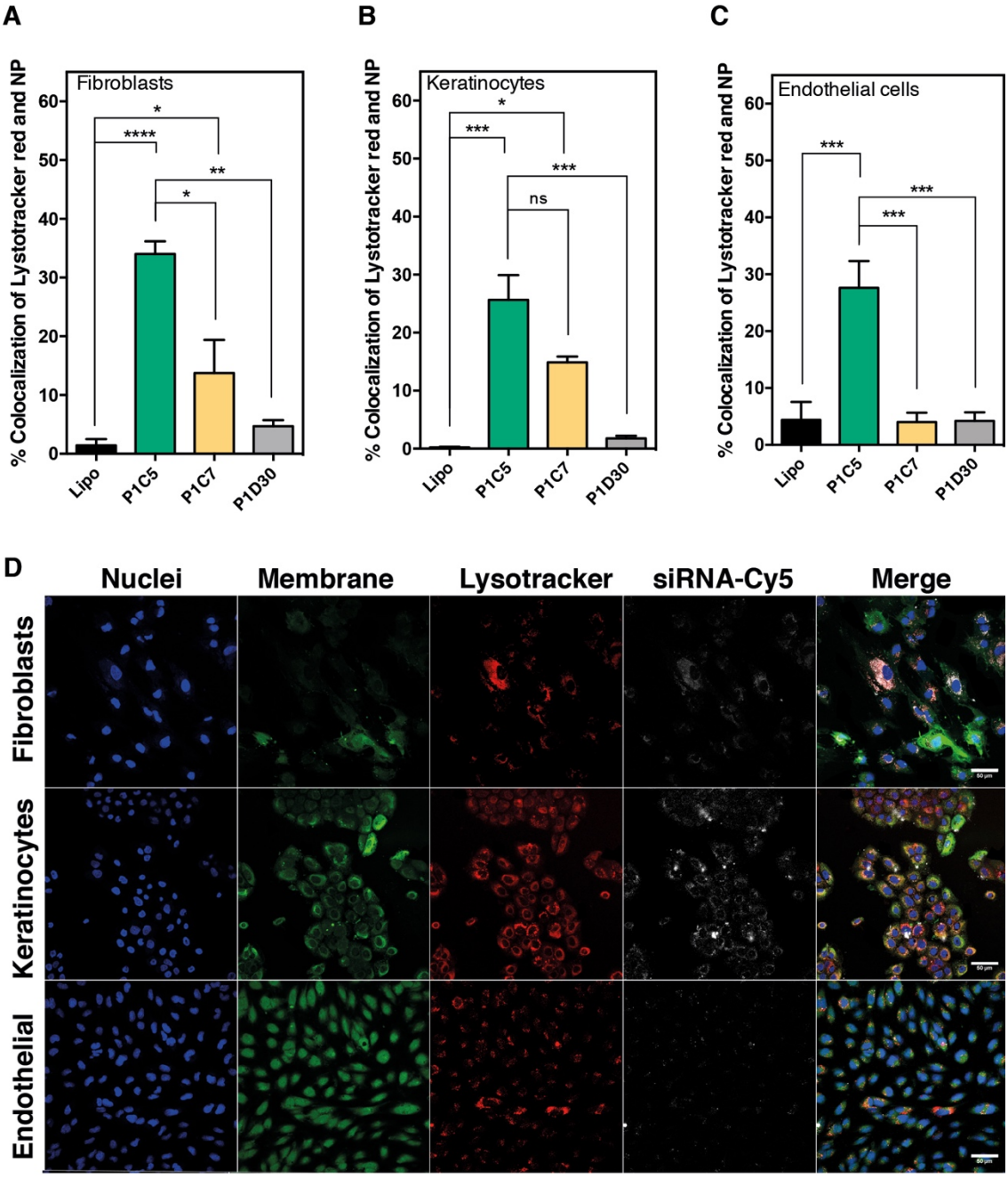

Figure 34: Internalisation in human skin cells. Fibroblasts (A), keratinocytes (B) and endothelial cells (C) were transfected with NP@siRNA-Cy5 formulations (20 µg/mL) for 1 h, washed to remove the non-internalised NPs and finally stained (CFSE for cell membrane; Lysotracker red for endolysosome; H33342 for cell nuclei) for confocal microscopy examination. Formulations with high (P1C5 and P1C7) and low (P1D30) gene knockdown efficiency as well as lipofectamine (Lipo) were evaluated for internalisation studies. Cell internalisation was monitored by the colocalisation of siRNA-Cy5 with Lysotracker red. Results are presented as Mean ± SEM (n = 2 independent samples, 3-9 microscope fields). Statistical analyses were performed by one-way ANOVA followed by a Bonferroni multi-comparison test (*P < 0.05; **P < 0.01; ***P < 0.001; ****P < 0.0001). (D) Representative confocal microscopy images showing the colocalisation of P1C7@siRNA-Cy5 formulation with endolysosomal compartment (Lysotracker red) for 3 cell types. Scale bar is 50 µm.

in P1C7) as well as in NP zeta potential (25.9 ± 0.5 mV in P1A19 vs. 18.9 ± 0.9 mV in P1C7) may result in variable siRNA release after NP disassembly (Figure 33E and Figure 33F) and ultimately biological activity. Importantly, six formulations were more efficient than commercial Lipofectamine to knockdown GFP (Figure 34). These formulations contained bisacrylamide A (shortest aliphatic), C (bioreducible disulphide bond) and diamines 1 (short aliphatic), 4-7 (increased nitrogen content) and 10-11 (ethyleneglycol containing units) (Table 15). Two formulations (P1C7 and P1C5) were selected for further characterisation due to their high ability to knock down the reporter cell line. Importantly, the knockdown activity of the formulations was superior after light activation as compared to the same formulations without light activation, highlighting the temporal control of their biological activity. P1C7 formulation was the most promising one because of its efficiency and temporal control of GFP knockdown (Table 13). The internalisation of P1C7@siRNA-Cy5 NPs in HeLa cells (was endocytic and mainly mediated by scavenger receptors (Figure 35).

3.3 Skin cell internalisation and rapid endosomal escape properties of NP@siRNA

Light-triggerable NPs might have potential use in skin applications[185,351]. Therefore, we evaluated whether some of formulations had different responses towards skin cells. For this purpose, the internalisation of two formulations with high GFP knockdown (P1C7 and P1C5) as well as one formulation with low GFP knockdown (P1D30) were tested against human skin cells, specifically, fibroblasts, keratinocytes and endothelial cells (ECs). Cells were transfected with NPs@siRNA-Cy5 or lipofectamine@siRNA-Cy5 (Figure 36). Our results show significant differences in NP internalisation according to each cell type, demonstrating that cell internalisation was dependent in the chemistry of the formulation. P1C7 formulation had higher tropism to fibroblasts and keratinocytes than ECs. Based on the knockdown efficiency (highest GFP knockdown after light irradiation, Figure 34) and skin cell internalisation pattern (high NP internalisation in keratinocytes and fibroblasts (Figure 36), which improves the bioactivity of the non-coding RNA tested below), P1C7 NPs were selected for subsequent studies.

Previous studies have demonstrated that efficacy of RNA silencing mechanism is directly correlated with endosomal escape[2,123], which is mediated by the recruitment of galectin-8 to the RNA releasing endosomes[130]. To evaluate whether efficacy of P1C7 formulation in RNA silencing is connected to the rapid endosomal escape, the kinetics of galectin-8 recruitment were measured on A7r5-Gal8YFP reporter cells[358]. Cells were transfected with P1C7@siRNA-Cy5 NPs for 10 min, after which, they were exposed to UV light for 10 min and then incubated for 60 min. Lipofectamine complexed with the same amount of siRNA-Cy5 was used as control. The area of

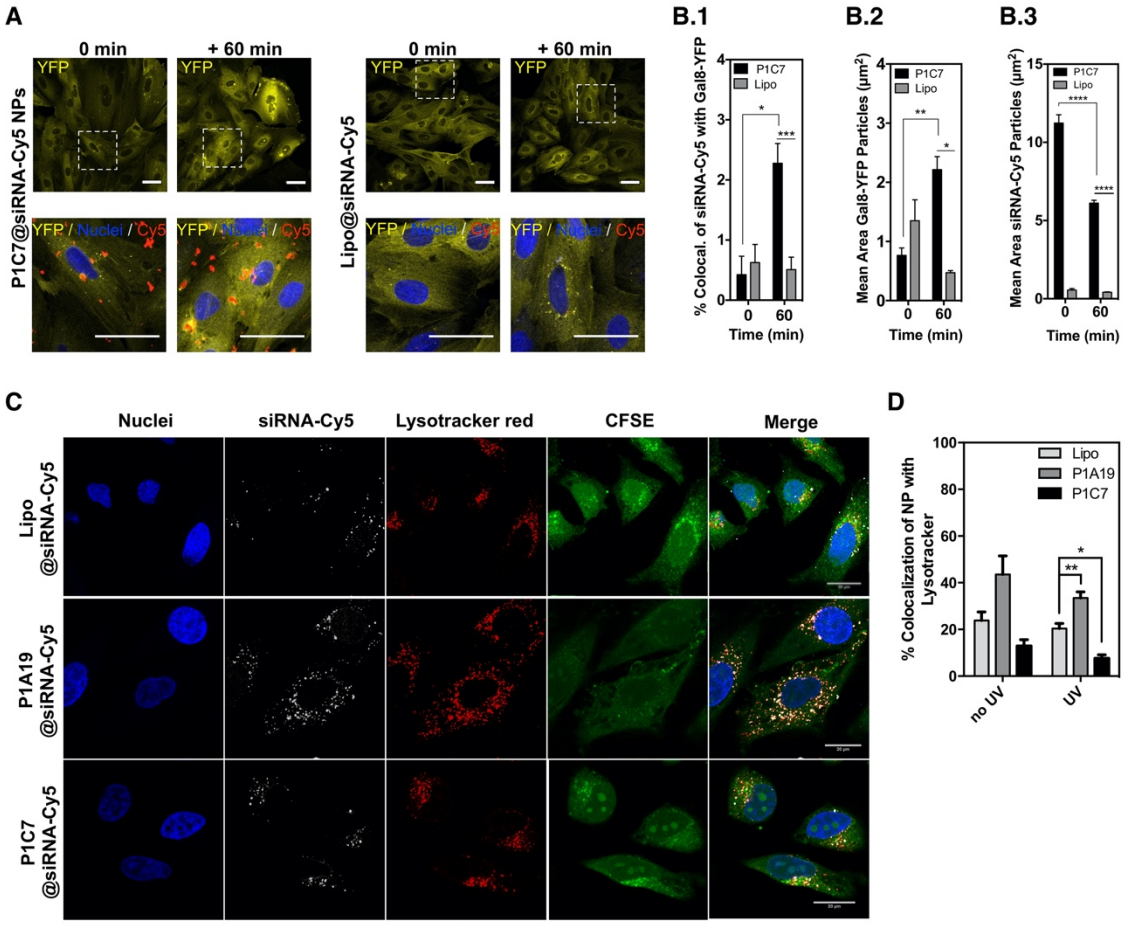

Figure 35: Intracellular trafficking of NP formulations. A) Galectin-8 recruitment in A7r5-Gal8-YFP reporter cells cultured in the presence of P1C7@siRNA-Cy5 or Lipo@siRNA-Cy5, as evaluated by confocal microscopy. Cells were transfected with the formulations for 10 min (t 10 min) and then activated by UV light (10 min, 365 nm, 1 mW cm^2; t = 0 min). The white scale bar is 50 µm. B) Colocalization of galectin- 8-YFP spots with Cy5 (B.1) as well as mean areas of bright Gal8-YFP spots (B.2), and siRNA-Cy5 (B.3). Results are mean ± SEM (n = 4-17, 2 technical replicates). C) HeLa cells were transfected with P1C7@siRNA-Cy5, P1A19@siRNA-Cy5 (20 µg/mL), or Lipo@siRNA-Cy5 for 10 min, washed to remove the non-internalised NPs, irradiated or not with UV light for 10 min and stained (CFSE for cell membrane; Lysotracker red for endolysosome; H33342 for cell nuclei) for confocal microscopy examination 1 h after the incubation. Representative confocal images showing the co-localization of siRNA-Cy5 formulation with endolysosomal compartment. Scale bar is 20 µm. D) Co-localization between NPs@siRNA-Cy5 and endolysosomal compartment expressed as the Manders' overlap coefficient quantified by ImageJ analyses. Results are presented as mean ± SEM (3-9 microscope fields). Statistical analyses were performed by one-way ANOVA followed by Tukey's post-hoc test, except for NP P1C7 against lipofectamine at 60 min, which was assessed by an unpaired student t-test. * P<0.05; ** P<0.01; *** P<0.001; ****P<0.0001.

siRNA-Cy5 NPs decreased overtime indicating the disassembly of the NPs within cells. Cells transfected with P1C7@siRNA-Cy5 showed a higher number of foci with galectin-8 than the ones transfected with Lipofectamine, and the foci number as well as the foci area increased overtime (Figure 37B.1 and Figure 37B.2). To further confirm these results, we have transfected HeLa cells for 10 min (followed or not by UV light exposure) with P1C7@siRNA-Cy5, Lipo@siRNA-Cy5

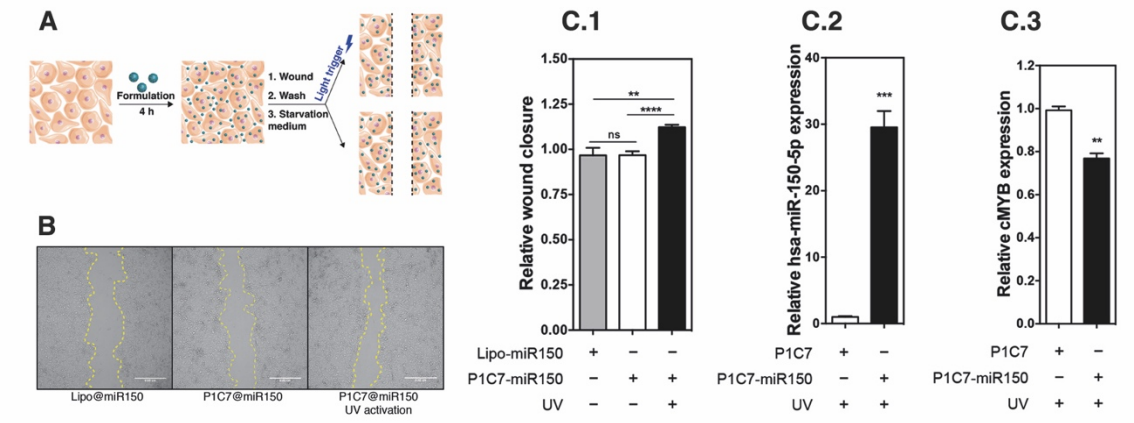

Figure 36: Bioactivity of P1C7@miR150 in in vitro wound healing. (A) Schematic representation of the experimental protocol. Confluent human keratinocytes were treated for 4 h with P1C7 NPs or P1C7@miR150 NPs. Lipofectamine complexed with miR150 was used as control. The wound was created by scratching the monolayer of cells. Cell migration was monitored by high-content microscopy. (B) Representative images of the wound healing process at 48 h post wounding. Scale is 0.05 cm. (C.1) Wound closure 48 h post-scratch. Wound area was quantified by ImageJ and normalized to the initial wound area. Results are presented as average ± SEM (n = 6-8). Quantification of miR150 (C.2) and cMYB (C.3) gene transcripts by qRT-PCR in keratinocytes treated with P1C7 NPs or P1C7@miR150 NPs, 48 h post wounding. Results are presented as Mean ± SEM (n = 6-8). Statistical analysis was performed by a student t-test, except for NP P1C7 against time at 0 min which was assessed by one-way ANOVA followed by a Bonferroni post-test. * $P < 0.05$; ** $P < 0.01$; *** $P < 0.001$; ****$P < 0.0001$.

or a formulation with high cell uptake but low capacity for GFP knockdown (P1A19@siRNA-Cy5). Confocal microscopy results showed lower co-localisation of P1C7@siRNA-Cy5 with the endolysosomal compartment (stained with Lysotracker) than Lipo@siRNA-Cy5 or P1A19@siRNA-Cy5 (Figure 37C and Figure 37D). Overall, our results indicate that P1C7 formulation delivered more efficiently the siRNA to the cell cytoplasm than lipofectamine or other NP formulations.

3.4 Application of light-triggered P1C7@miR150 promotes wound healing

To extend the application of P1C7 NPs, the formulation was used for the delivery of miRNAs. NPs were complexed with miRNA-150-5p (from now on termed as miRNA150). Cells were transfected with P1C7, P1C7@miRNA150 or Lipo@miRNA150 (Figure 38A). Cells were then wounded and cell migration was monitored. At 48 h post wounding, cells transfected with non-irradiated P1C7@miRNA150 showed increased migration as compared to NPs without miRNA150 (Figure 38C.1 and Figure 38B). Importantly, cells transfected with P1C7@miRNA150 and activated by light showed increased migration as compared to cells transfected with non-activated NPs or lipofectamine, both complexed with miRNA150. As expected, the increased migration of cells seems to be mediated by an increase in the intracellular

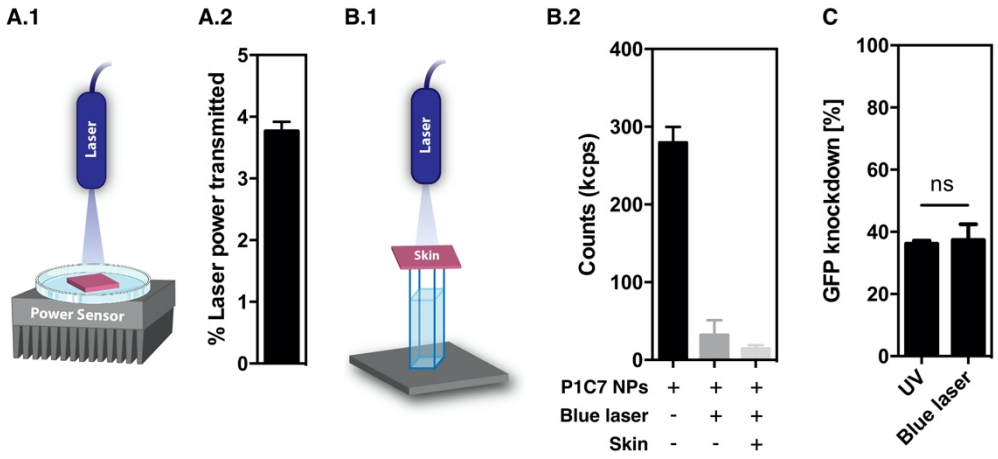

Figure 37: Photo-disassembly of NPs through a skin barrier. (A.1) Schematic representation of the experiment. A 2 cm × 2 cm skin (thickness of 260-290 µm as measured by a caliper) was placed in a plastic petri dish on top of a thermal power sensor (Thorlabs s310c). The tissue was then irradiated with a 405 nm laser at 80 mW/cm^2 during 1 min. Laser attenuation values were calculated by normalising against laser power values obtained with the empty petri dish. (A.2) Blue laser attenuation. Results are expressed as Mean ± SEM (n = 3). (B.1) Schematic representation of the methodology used. A sample of skin (thickness: 260-290 µm) was placed on top of a plastic cuvette containing an aqueous suspension of P1C7@miRNA150 complexes followed by its irradiation with a blue laser (405 nm, 80 mW/cm^2) for 10 min. As a control, a cuvette with an aqueous suspension of P1C7@miRNA150, without the skin sample on top, was irradiated by a blue laser for the same time. At the end, both NP suspensions were characterized by DLS analyses. (B.2) Blue laser disassembly of P1C7 NPs placed below skin. Results are presented as Mean ± SEM (n = 3). (C) Cells transfected with P1C7@siRNA complexes (20 µg/mL) and activated by a blue laser (405 nm at 80 mW/cm^2) yielded similar GFP knockdown efficiency as cells activated by a UV laser (365 nm at 1 mW/cm^2). Cell transfection was performed for 10 min followed by 10 min of irradiation. GFP knockdown was analysed at 48 h. Results are Mean ± SEM (n = 4). Statistical analysis was performed using an unpaired student t-test.

levels of miRNA150 (Figure 38C.2) and by the knock down of *cMYB* gene (Figure 38C.3), a direct target of the miRNA[330,359].

Next, we evaluated whether P1C7@miRNA150 NPs could function *in vivo*, in an acute wound healing animal model. Initially, we investigated whether the formulation could be activated *in vivo* by a blue laser after subcutaneous transplantation (Figure 39A, B). We have used a blue laser rather than a UV light (used in the *in vitro* tests) to prevent potential tissue damage. The blue laser (408 nm at 80 mW/cm^2) led to similar levels of gene knockdown in cells transfected with P1C7@siRNA complexes as the UV light (365 nm at 1 mW/cm^2) (Figure 39C). Our results show high NP disassembly even if the attenuation of the laser was significant (only 4% of the laser was able to cross the skin barrier of 300-400 µm) (Figure 39A.2 and 39B.2). Then, we administered P1C7@miRNA150 subcutaneously in the borders of wounds and allowed the NPs to be internalised by the skin tissue for 30 min, followed by their activation by a blue laser for 5 min (Figure 40A). P1C7@scramble miRNA or vehicle (PBS) were used as controls.

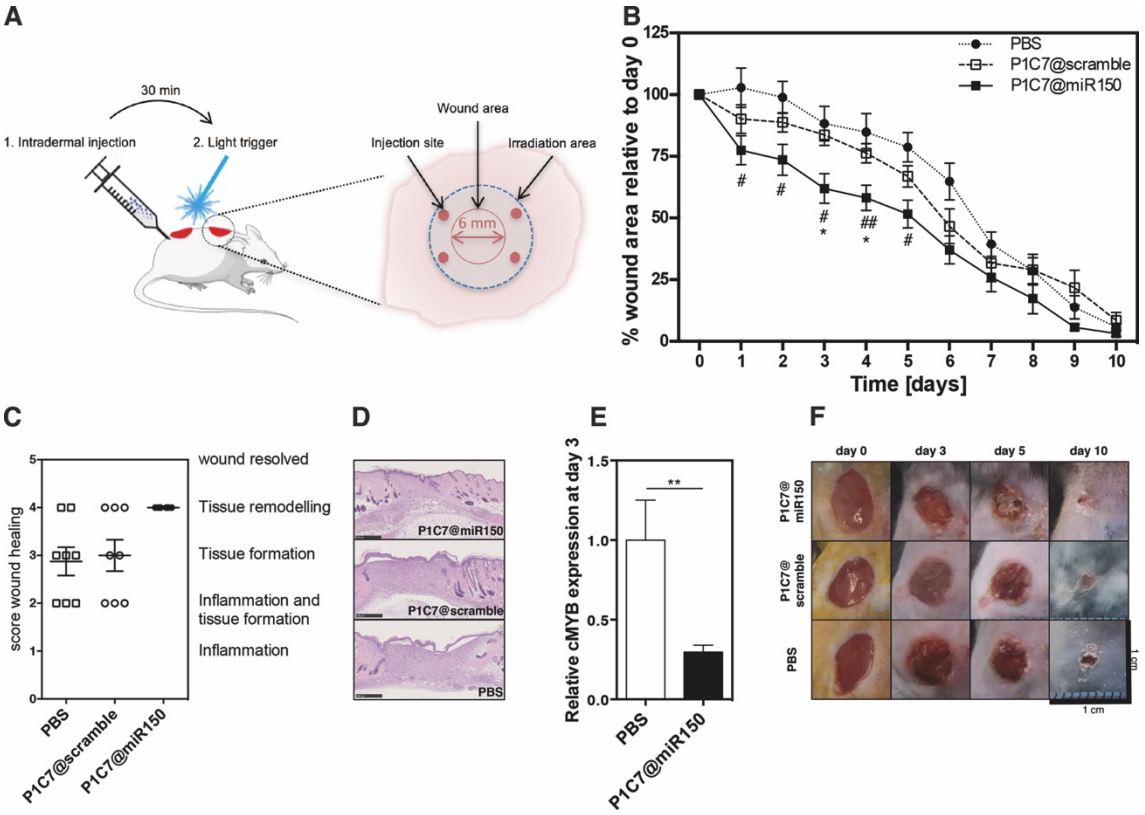

Figure 38: Acute wound healing activity of P1C7@miR150 formulation. (A) Schematic representation of the animal experimental set up. (B) Wound closure (relative to day 0) in animals treated with PBS, P1C7@scramble or P1C7@miR150. Results are Mean ± SEM (n = 8). Statistical analyses were performed by student t-test with Welch's correction. #P < 0.05, ##P < 0.01 between PBS and P1C7-miR150 groups; *P < 0.05 between P1C7-scramble and P1C7-miR150 groups. (C) Histological score regarding wound healing. Results are Mean ± SEM (n = 8). (D) Representative hematoxylin/eosin staining for wounds at day 10. Scale bar is 500 µm. (E) Expression of cMYB transcripts in skin tissue quantified by qRT-PCR analyses. Data presented as Mean ± SEM (n = 6-20). ** P < 0.01. (F) Representative images of the wound healing process immediately after the surgery and at days 3, 5 and 10.

Wounds treated with light-triggered P1C7@miRNA150 NPs healed faster as compared to wounds treated with PBS or P1C7@scramble miRNA, which was statistical significant for some of the days (Figure 40B). These results were also confirmed by histological analyses showing qualitative differences in the wound healing process and re-epithelialisation (Figure 49C and 49D). Wounds treated with PBS were in stages of inflammation and tissue formation until tissue remodelling, whereas wounds treated with P1C7@miRNA150 were all in the tissue remodelling phase (Figure 40C and 40D). To show that indeed the regenerative program was mediated by miRNA150, the expression of the *cMYB* gene, a direct target of miRNA150, was evaluated at day 3 by qRT-PCR (Figure 40E). The percentage of *cMYB* gene transcripts were 60% lower in wounds treated with P1C7@miRNA150 NPs than with P1C7 NPs.

4 CONCLUSION

In conclusion, we have successfully synthesised a light-activatable NP library for efficient *in vivo* small non-coding RNA delivery. The library screening revealed six formulations which were more efficient in cell transfection and RNA silencing as the commercial agent lipofectamine with additional temporal control over the release of the small non-coding RNA. P1C7, as leading formulation, was shown to be a rapid transfection agent with fast endosomal escape and high efficiency not only for siRNA mediated gene silencing but also for microRNAs. Moreover, we demonstrate high efficacy and significance of light-triggered microRNA delivery in a wound healing animal model. Taken together, light-triggerable NP formulations give an extra level of control in the delivery of non-coding RNAs which may enhance their bioactivity.

Acknowledgements

The authors would like to thank the financial support of ERA Chair project (ERA@UC, ref:669088) through the EU Horizon 2020 program, the POCI-01–0145-FEDER-016390 (acronym : CANCEL STEM), POCI-01-0145-FEDER- 029414 (acronym: LIghtBRARY), and UID/NEU/04539/ 2019 projects through Compete 2020 and FCT programs. NMR data was collected at the UC-NMR facility, which is supported in part by the FEDER—European Regional Development Fund through the COMPETE Programme (Operational Programme for Competitiveness) and by National Funds through the FCT—Fundacao para a Ciencia e a Tecnologia (Portuguese Foundation for Science and Technology) through grants REEQ/481/QUI/2006, RECI/ QEQ-QFI/0168/2012, CENTRO-07-CT62-FEDER-002012, and Rede Nacional de Ressonância Magnetica Nuclear (RNRMN).

Conflict of interest

The authors declare no conflict of interest.

5 MATERIALS and METHODS

Synthesis of the photocleavable linker P1. The photocleavable linker P1 (2-nitro-1,3-phenylene)bis(methylene) diacrylate was synthesised and purified according to a previously reported procedure (Biomaterials 2014, 35, 5006-5015). Briefly, to a solution of (2-nitro-1,3-phenylene)dimethanol (5.5 g, 30 mmol, ARCH Bioscience) in anhydrous dichloromethane (38 mL, Fisher Chemical), was added dropwise trimethylamine (10.5 mL, 75 mmol, Sigma-Aldrich) under argon atmosphere. Then, acryloyl chloride (9.8 mL, 120 mmol, Merck) was added dropwise into the reaction mixture using a dropping funnel over 15 min at 0 °C. The mixture was stirred for additional 18 h at room temperature. After removing the formed solid by filtration, the filtrate was dried under vacuum and then resuspended in ethyl acetate (Fisher Chemical). The resulting solution was washed with saturated sodium chloride solution and then dried overnight with sodium sulphate. The final product was obtained after purification by silica gel chromatography (hexane: ethyl acetate as eluent, 1:1, v/v) as a white crystal.

Optimisation of the photocleavable linker ratio in poly(amido amine)s. To optimise the amount of the photocleavable linker in the poly(amido amine), ratios of 25:75 and 50:50 of P1 to A (methylenebisacrylamide) were used in the synthesis of some polymers. To calculate the ratio of incorporation of P1 into the polymer, polymers were precipitated in water, lyophilised, resuspended in DMSO-d_6 and analysed by ^{1}H-NMR (Bruker Avance III 400 MHz) relative to TMS. Size and count decrease of the nanoparticles after UV exposure were measured by DLS.

Optimisation of the ratio siRNA:NP, transfection time and irradiation time for efficient gene knockdown. Several parameters were optimised for the high-throughput screening of NP@siRNA mediated gene silencing capacity of the polymeric NP library. Firstly, siRNA:NP ratio was optimised to maximise GFP knockdown. Therefore, NPs (200 µg/mL) were complexed with siRNA against GFP in ratios of 1:12.5 and 1:50 for 2 h in nuclease free sterile water shaking on an orbital shaker (250 rpm) at room temperature. To evaluate bioactivity of the complexes, HeLa-GFP cells were seeded at a density of 40.000 cells/mL for 24 h prior the experiment. Cells were transfected for 4 h with NP@siRNA complexes (20 µg/mL) in starvation (DMEM). Cells were then washed, fresh medium with reduced serum (DMEM, 5% FBS, 0.5% PenStrep) added and cells were cultured for 48 h. At the end, cells were stained with H33342 and

PI (both 0.25 µg/mL) and analysed by fluorescence microscopy on a high-content microscope (In Cell Analyzer 2200). Cell viability and GFP knockdown were quantified as described in high-content imaging section below.

In a separate experiment, the transfection time was optimised. The motivation here was to identify a time relatively short that could lead to significant gene knockdown. Cells were transfected with NP@siRNA complexes (20 µg/mL; 1:50 siRNA:NP) from 10 min to 4 h. In a separate experiment, different UV light sources were evaluated for NP activation within cells. Cells were placed (right after transfection and medium replacement) on a 20 cm support (distance from top 15 cm) in a transilluminator (UVP BioSpectrum 500) and irradiated with 365 nm light (1 mW/cm^2) from the top for 10 min. In both experiments cells were cultured in medium with reduced serum (DMEM, 5% FBS, 0.5 % PenStrep) until 48 h. Cells were stained with H33342 and PI (both 0.25 µg/mL) and analysed by fluorescence microscopy on a high-content microscope (In Cell Analyzer 2200) for GFP knockdown (described in high-content imaging section below).

Synthesis of polymers with photocleavable moieties. Prior to synthesis, diamines (1-32), bisacrylamides (A-E) and photocleavable linker P1, were diluted to 1.6 M in DMSO. Specifications of all monomers can be found in Supplementary Table 1. The monomers (25 µL of P1, 25 µL of bisacrylamides A-E, 50 µL of amines 1-32) were added to a polypropylene 96 well plate, the plate sealed with aluminum foil and then incubated at 60°C under agitation (orbital shaker, 250 rpm) for 5 days. Polymer synthesis was performed at final monomer concentration of 0.8 M. Polymers were finally end capped with 20% molar excess (10 µL to 100 µL reaction volume) of the respective diamine 1-32 for 2 h (60°C, 250 rpm) and stored at 4°C until usage.

Gel permeation chromatography (GPC) analyses. Number average molecular weights (Mn) and molecular weight distributions (Mw/Mn) were measured by GPC on a HPLC Agilent 1260 system equipped with a guard column (Agilent, Aquagel, 10 mm, 10 µm) followed by three columns: (i) Agilent, Aquagel-OH 40, 300 × 7.5 mm, 8 µm, (ii) Agilent, Aquagel-OH 50, 300 × 7.5 mm, 8 µm and (iii) Phenomenex, Polysep-GFC-P2000, 300 × 7.8 mm, range 100 – 10 k Da, connected to a UV (254 and 280 nm) and RI detector (Agilent). An acetate buffer (0.5 mol/L, pH = 4.5) was used as an eluent, at a flow rate of 0.7 mL/min and 35 °C. Polyethylene oxide standards (EasyVial PEG/PEO, range 194 – 1000 k Da) were used to calibrate the SEC, since it has been demonstrated that such eluent composition allows PEO to be a suitable calibration standard for poly(amido-amines).

NP preparation and activation. For the high-throughput screening of NPs, NPs were prepared in sterile conditions using sterilised 96-deepwell polypropylene plates (VWR). Therefore, each polymer solution (15 µL; in DMSO) was precipitated into sterile nuclease free molecular grade water (960 µL) with subsequent addition of sterile zinc sulphate (25 µL, 1M). Plates were sealed with PP adhesive seals and incubated shaking (250 rpm) on an orbital shaker at room temperature overnight. NPs were purified by centrifugation at 4 °C, 8000 g for 8 min. The mass concentration of each purified formulation was determined after lyophilizing samples. The efficiency of NP formation was up to 47%, calculated according to equation:

$$NP\ formation\ efficiency\ (\%) = \frac{M_{NP}}{M_{polymer}} \times 100$$

where M_{NP} denotes the weight of material recovered after NPs purification and freeze-drying and $M_{polymer}$ is the theoretical polymer weight.

NP size and zeta potential analyses. The size and zeta potential of NPs was measured by a ZetaPALS analyzer (Brookhaven Instruments Corp.). NPs were resuspended in 1 mM KCl and diluted to achieve average count rates about 200 kcps to perform the DLS measurement. Values were expressed as the mean of 5 measurement runs, each with a duration of 1 min. To determine light sensitivity of the NPs, a duplicate of the sample was used. NP disassembly was triggered by a UV lamp (365 nm, 100-Watt, 5 cm distance, 10 min). Samples NP size and average count rates were determined as for the non-irradiated sample. Light sensitivity is expressed as percent count decrease respective to the initial average count rate, which is an indicator for NP concentration.

TEM analyses. A suspension of P1C7 NPs (500 µg/mL) was prepared in molecular grade water. A droplet of the suspension was added to the surface of an ultrathin carbon coated 400 mesh copper grid, irradiated or not with UV light (10 min, 365 nm, 1 mW/cm2) and left air-dry for 5 h at room temperature in a closed petri dish. NPs were viewed with a JEOL-2100-HT microscope. Digital images were acquired with a fast-readout "OneView" 4k x 4k CCD camera that operates at 25 fps (300 fps with 512 x 512 pixel) and features drift correction. The diameter of NPs was analysed with the Particle Tool from ImageJ.

High-throughput complexation of NPs with siRNAs. NPs were suspended in sterile nuclease free molecular grade water to a concentration of 400 µg/mL. Complexation with siRNA against eGFP (GFP Duplex I, GE Dharmacon) was then done at a ratio of 1:50 (siRNA:NP, w:w) in a 96-deepwell polypropylene plate (VWR). From each NP formulation, an aliquot (50 µL) was added to a deep well plate, following the plate layout for subsequent cell transfection. A solution of siRNA containing 4 µg/mL siRNA and 4 µg/mL Cy5-tagged siRNA was prepared in sterile molecular grade, nuclease free water. The siRNA solution (50 µL) was added to the NPs in the same volume (50 µL) using a multichannel pipette. As control for siRNA activity and transfection, the same procedure was followed for lipofectamine RNAiMAX (15 µl/mL; Invitrogen). The plates were sealed with adhesive polypropylene seals and allowed to incubate shaking at room temperature for 2 h on an orbital shaker (250 rpm, room temperature). Samples were then diluted 1:10 with DMEM to 20 µg/mL NP concentration and directly used for cell transfection or determination of complexation efficacy. Complexation efficacy was determined indirectly from Cy5 tagged- siRNA after separating NPs and non-complexed siRNA by centrifugation (4ºC, 14000g, 15 min), quantifying Cy5 fluorescence in three replicates of the supernatant. Concentration of siRNA was determined relative to a standard curve.

High-throughput siRNA transfections. HeLa-GFP (CellBiolabs Inc.) cells were cultured DMEM (without phenol red) containing FBS (10%, v/v), PenStrep (0.5%, v/v, 50 µg/mL) and blasticidin (10 µg/mL). HeLa-GFP cells were seeded 24 h prior to experiment in 96 well plates (Costar) with a density of 4.000 cells per well. Cells were transfected with NP@siRNA complexes (20 µg/mL) or lipofectamine RNAiMAX (1.5 µL/ml) in DMEM as described above. Transfections were performed with three technical replicates and each plate in duplicate. After 10 min of transfection, the medium was replaced by DMEM containing 5% FBS (v/v, to slow down cell proliferation), PenStrep (0.5%, v/v, 50 µg/ml) and blasticidin (10 µg/ml). In one plate, NPs were activated for 10 min (using 365 nm light from top on a transilluminator UVP BioSpectrum 500 at 15 cm distance), while with the second plate (with the same NP formulations as the first plate), no activation of NPs was performed. This experiment allowed us to compare the bioactivity of released siRNA with and without application of the stimulus. At 48 h, cells were stained and placed in an automated incubator (Cytomat 2, Thermo) for further incubation and analyses by high-content imaging with an automated fluorescence microscope (In Cell 2200, GE Healthcare).

High-content imaging analyses. Cell nuclei were stained at 48 h with Hoechst H33342 (Sigma-Aldrich, 0.25 µg/mL) and propidium iodide (PI, Sigma-Aldrich, 0.25 µg/mL). Dead cells stained for both Hoechst H33342 and PI, while live cells stained only for Hoechst H33342. At 48 h and 72 h, four random fields per well were imaged on a high-content microscope (In Cell 2200, GE Healthcare) with a 20× objective. Automated image analyses were performed using the In Cell Developer software from GE Healthcare. GFP knockdown was accessed from the mean GFP fluorescence intensity in the cytoplasm of live cells. Hoechst 33342 was used to define a nuclear mask, excluding dead cells (with 10% overlap of PI and H33342 stain), which was then dilated to cover as much of the cytoplasmic region as possible (Figure 41). Removal of the original nuclear region from the dilated mask creates a ring mask that covers the cytoplasmic region outside the nuclear envelope. GFP knockdown was expressed as percentage of fluorescence on non-treated HeLa-GFP cells (after subtracting fluorescence background of HeLa cells). Cell viability was calculated from the total number of cells (quantified by cell nuclei) after subtraction of dead cells (cells presenting >10% overlap of PI and Hoechst stain). Internalisation of NPs was quantified by the fluorescence signal of NPs in cells.

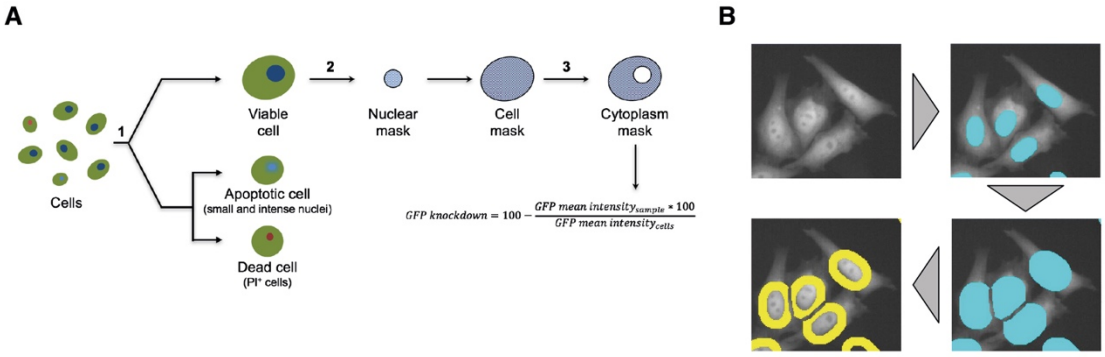

Figure 39: Schematic representation of image analysis. (A) Image analysis steps: (1) definition of healthy cell population to analyse; (2) definition of area to measure GFP levels and (3) creation of cytoplasm mask by subtracting the nuclear mask from the cell mask. (B) Image analysis was conducted using In Cell Developer Software which implements machine learning techniques. Cell viability was analyzed calculating the percen- tage of nuclei with form factor > 0.95 and at least 10% overlap with propidium iodide staining, in the total nucleus population. By subtraction of the dead masked nuclei from the total nuclei population, a healthy nucleus mask can be defined. Consecutively the healthy nucleus mask was dilated to cells and the nucleus mask was subtracted to achieve a cytoplasm mask, where GFP fluorescence can be measured minimizing artefacts from other stains (i.e. H33342) and flattening the detection pane. GFP knockdown can then be calculated as percentage decrease of GFP fluorescence signal relative to 0% GFP knockdown control from untreated HeLa- GFP cells and 100% GFP knockdown of HeLa background control cells.

siRNA release from NPs after light exposure. The release of siRNA from NPs after UV-irradiation (10 min, 365 nm, 1 mW/cm2) was investigated by 1% agarose gel electrophoresis (containing orange G (1X) in TBE buffer (1X)). siRNA (15 µL, 2 µg/mL) and NP@siRNA (100 µg/mL) solution/suspension was applied to separate gel lanes, and electrophoresis was performed for 15 min at 100 V. The gel was visualised under a UV transilluminator (Gel Doc XR+, BioRad) at an excitation wavelength of 302 nm. The obtained bands were analysed using ImageJ software 1.48 v (National institutes of Health, USA).

Cellular internalisation of NPs. NP@siRNA complexes were exposed for 1 h to human dermal keratinocytes (HaCaT cells; CLS Cell Lines Service GmbH, Eppelheim, Germany), human normal dermal fibroblast (NHDF) or human umbilical vein endothelial cells (HUVEC, Lonza) and characterised by flow cytometry or confocal microscopy. For flow cytometry, HaCaT and NHDF cells were cultured in DMEM medium while HUVECs were cultured in EGM-2 medium (Lonza). All media was supplemented with FBS (10%, v/v) and PenStrep (0.5%, v/v, 50 µg/mL). Cells were seeded in 24 well plates (HaCaT and HUVECs at 25.000 cells/well while NHDF cells at 12.000 cells/well) and allowed to adhere for 24 h. Cells were transfected for 1 h with NP@siRNA-Cy5 or lipofectamine@siRNA-Cy5 complexes in DMEM or EGM-2 media. Complexes were removed and cells were washed with PBS.

For confocal microscopy, HaCaT and NHDF cells were cultured in DMEM medium while HUVECs were cultured in EGM-2 medium. All media was supplemented with FBS (10%, v/v) and PenStrep (0.5%, v/v, 50 µg/mL). Cells (HaCaT and HUVECs: 20000 cells/well; NHDF cells: 10.000 cells/well) were seeded in black glass bottom 96 well plates (IBIDI, Germany) coated with 0.1% gelatine (Sigma) and allowed to adhere for 24 h. Prior to transfection cells were stained with CellTrace™ CFSE 488 (5 µM; Molecular Probes, Life Technologies) according to manufacturer's instructions. Cells were transfected for 1 h with NP@siRNA-Cy5 complexes in DMEM (for HaCaT or NHDF cells) or EBM-2 (for HUVECs). Cells were stained with Lysotracker Red (100 nM; Molecular Probes, Life Technologies) for 30 min during cell transfection. Complexes were removed and cells were washed twice with PBS and fixated with 4% (v/v) paraformaldehyde (Alfa Aesar) in PBS for 10 min at room temperature. Nuclei were stained with H33342 (2 µg/mL) for 10 min. Cells were then washed 3 times with PBS and analysed by confocal microscopy (Zeiss LSM710) using a 40× immersion oil objective. Each condition is represented by two technical replicates and four or more representative images per field were acquired. Colocalisation of NP@siRNA-Cy5 with Lysotracker red was performed using JaCoP on Image J.

Uptake of P1C7@siRNA-Cy5 in the presence of chemical inhibitors. HeLa cells were plated in a 24 well plate at a density of 5×10^4 cells/well and left to adhere overnight. Cells were pre-incubated with endocytosis inhibitors for 30 min followed by 1 h incubation with P1C7@siRNA-Cy5 (20 μg/mL). The following inhibitors were tested: filipin III (80 μM), nocodazole (3 μM), polyinosinic acid (100 μg/mL), dansylcadaverine (25 μM) cytochalasin D (1 μM), dynasore (30 μM) and EIPA (80 μM). As controls, we used cells without NPs and cells incubated with NPs without inhibitor at 37 °C and at 4 °C. At the end of each point, cells were centrifuged, washed three times with PBS and then resuspended for flow cytometry analysis.

Intracellular trafficking and siRNA release. Endosomal escape can be determined by galectin-8 recruitment[130]. A7r5-Gal8YFP[358] reporter cells (kindly donated by Craig Duvall's lab) were used to study the colocalisation of the Cy5 signal from the NP@siRNA-Cy5 complexes with YFP-Gal8 spots from releasing endosomes. A7r5-Gal8YFP cells were cultured in DMEM supplemented with FBS (10%, v/v), PenStrep (0.5%, v/v, 50 μg/mL) and blasticidin (10 μg/mL). For the experiment 4.000 cells were seeded in each well of a black 96 well plate with glass bottom (IBIDI), suitable for confocal microscopy and allowed to adhere overnight. Cells were transfected for 10 min with NPs (20 μg/mL) or L2000 complexes with siRNA-Cy5 in DMEM. Cells were then washed, and cell culture medium was added to the cells. UV light (365 nm, 1 mW/cm^2) activation was performed for 10 min followed by cell culture. Cells were fixated (4% PFA for 10 min) at different times (t=-10 immediately after transfection, t=0 after light activation and t=+15, 30. 45, 60 min post light activation), washed with PBS, cell nuclei stained with H33342 (1 μg/mL, Sigma) and analysed by a confocal microscope (Zeiss LSM710, 40x immersion oil objective). Each condition is represented by two technical replicates and 4 or more images per field were acquired representing the total cell population. The area of YFP-Gal8 and Cy5-NPs spots were analysed with the Particle Plugin from ImageJ. Colocalisation of Cy5-labelled NPs with YFP-Gal8 spots was performed using JaCoP on Image J.

Complexation of miR150 to the NPs. The complexation of miR150 (GE Dharmacon) to P1C7 NPs followed the same procedure previously described for siRNA. Briefly, miR150 and P1C7 NPs were mixed in molecular grade nuclease free, sterile water (Fisher Bioreagents) in a ratio of 1:50 (w/w, miRNA to NPs), and the suspension agitated on an orbital shaker for 2 h at room temperature. After complexation, the NP suspension was diluted in cell culture medium before use.

Bioactivity of P1C7@miRNA150 formulation. Human keratinocytes were cultured in DMEM supplemented with 10% FBS and 0.5% PenStrep, harvested and then seeded in a 96 well plate at a density of 25.000 cells/well to grow to a monolayer in approximately 48 h. Cells were then inhibited by mitomycin (5 µg/mL, in cell culture medium, Tocris Bioscience) for 2 h, transfected for 4 h with P1C7 NPs (40 µg/mL in DMEM) or P1C7 NPs@miRNA150 complexes (40 µg/mL in DMEM), washed with PBS to remove non-internalised NPs, exposed or not to UV light (10 min, 365 nm, 1 mW/cm^2). The cell monolayer was then scratched with a pipette tip and then cultured in cell culture medium for 48 h. As controls, cells were transfected for 4 and 24 h with the commercial agent lipofectamine RNAiMAX or RNAiMAX-miR150 complexes. In both cases (NPs and lipofectamine), wound closure was monitored by an automated fluorescence microscope (In Cell 2000, GE Healthcare, 4× objective) every 12 h. Wound closure was analysed from the image field in the center of the well, measuring the wound area with Image J. The percentage of wound closure was calculated by well considering the initial wound area and then normalised to the control of the respective group.

Quantitative analyses of miR150 transfection. To demonstrate that HaCaT cells were successfully transfected with P1C7 NPs@miRNA150 complexes, cells were transfected with P1C7 NPs or P1C7@miRNA150 NPs for 4 h, washed with PBS to remove non-internalised NPs, light activated, and finally cultured for 48 h. Next, cells were harvested, lysed and RNA isolated by a miRCURY™ RNA isolation kit (Exiqon) following manufacturer´s instructions. The cDNA was then synthesised using the Mir-X™ miRNA First Strand Synthesis (Exiqon). Expression of miRNA was quantified by quantitative RT-PCR (7500 Fast Real-Time PCR System, Applied Biosystems, Carlsbad, CA, USA) using Mir-X™ SYBR qRT-PCR kit (Clontech, California, USA) and NZYSpeedy qPCR Green Master Mix (NZYTech, Portugal). For normalisation of microRNA expression levels, RNU6 was used as (housekeeping) control (Supplementary Table 3). Results were analysed using the $\Delta\Delta C_T$ method to indicate relative miR150 expression from light activated miR-carrying to non-carrying P1C7 NPs.

Quantitative analysis of target gene knockdown. HaCaT cells transfected with P1C7 NPs or P1C7@miRNA150 NPs (see section before) were analysed for the expression of *cMYB*, a target gene of miR150. Therefore, cDNA was synthesised from 1 µg total RNA using TaqMan™ reverse transcription reagents (Applied Biosystems, CA, USA). Quantitative RT-PCR was performed using NZYSpeedy qPCR Green Master Mix (NZYTech, Portugal) on a RT-PCR (7500 Fast Real-Time PCR System, Applied Biosystems, Carlsbad, CA, USA). Quantification of

the target gene was analysed relative to GAPDH as housekeeping gene: $relative\ expression = 2^{[-(C_T\ Sample - C_T\ GAPDH)]}$. Minimal cycle threshold values (C_T) were calculated from at least 3 independent reactions. $\Delta\Delta C_T$ was calculated to determine relative *cMYB* expression from light activated miR-carrying to non-carrying P1C7 NPs.

***In vivo* wound healing experiments**. Animal protocol was approved by the Ethics Committee of the Faculty of Medicine of the University of Coimbra (ORBEA_159_2017/05052017). Male C57BL/6 mice (8 weeks) were purchased from Charles River (Wilmington, MA, USA). Mice were separated on individual cages 24 h prior the induction of the skin wounds. They were anesthetised with xylazine/ketamine (xylazine hydrochloride - Rompun, 10 mg/kg of body weight; ketamine hydrochloride – Imalgene 1000, 80 mg/kg of body weight), shaved with an electric clipper on the back and remaining hair removed with depilatory cream (Dove), the skin was disinfected with betadine and two 6 mm-diameter dorsal full-thickness excisional wounds were created with a sterile biopsy punch in each animal. The treatments (P1C7@miRNA150, P1C7@scramble, PBS; n=8) were administered as intradermal injection at 4 locations around the wound. Light (5 min; 5 sec on/off; 405 nm blue laser; Thorlabs, Dachau, Germany) activation of the NPs was performed 30 min post-injection, to allow the NPs to be internalised by the skin cells. During the first 2 days, the mice received every 8 h buprenorphine (0.05 mg/Kg of body weight, Bupaq) to relief the animals from any pain or distress caused by the procedure. The animals were observed daily and wound area was measured. At day 3 and 10 mice were sacrificed by cervical dislocation after an overdose of anesthesia. Skin biopsies were taken for histological and gene expression analyses.

Histological analyses of skin wounds. Skin wounds were excised with a margin of epidermis outside the wound (approx. 2 mm) and processed for routine histology. Therefore, freshly excised wounds were placed onto a small piece of cardboard, with the subcutaneous tissue facing down, and immersed in 10% neutral buffered formalin for 24 h. After fixation, trimming was performed longitudinally, in the direction of the hair flow and centered on the wound. Samples were embedded in paraffin, sectioned at 4 µm, and stained with hematoxylin and eosin. Histological analysis was performed by a pathologist blinded to experimental groups and measurements were performed using NDP.view2 software coupled to Nanozoomer SQ slide scanner (Hamamatsu).

Quantitative analysis of miRNA150 target gene in skin wounds. To quantify downregulation of miR150 gene targets in the skin wounds, samples at day 3 post-surgery were analysed. RNA was isolated using TRIzol (500 µL, Invitrogen) reagent from 15-50 mg of tissue. Samples on ice were homogenised by a TissueLyser (Qiagen) operated at 30 Hz in three cycles of 2 min. Samples were then processed according to manufacturer´s instructions for RNA isolation and RNA was quantified on a NanoDrop™ (Thermo Scientific). cDNA was prepared from 1 µg total RNA using TaqMan™ reverse transcription reagents (Applied Biosystems, CA, USA). Quantitative RT-PCR (qRT-PCR) of murine cMYB was performed using NZYSpeedy qPCR Green Master Mix (NZYTech, Portugal) and detection on a RT-PCR (7500 Fast Real-Time PCR System, Applied Biosystems, Carlsbad, CA, USA) equipment. Quantification of the target gene was analysed relative to mouse GAPDH as housekeeping gene: $relative\ expression = 2^{[-(C_T\ Sample - C_T\ GAPDH)]}$. Minimal cycle threshold values (C_T) were calculated from at least 3 independent reactions. $\Delta\Delta C_T$ was calculated to determine downregulation of *cMYB* relative to control skin (tissue day 0).

Light activation of P1C7 NPs though a skin barrier. To demonstrate that NPs can be dissociated by a 405 nm laser through the skin barrier, back skin from C57BL/6 mice was used as barrier between the light source and the NPs. Briefly, hair was removed from mouse skin with depilation cream and washed several times with PBS and mounted on a cardboard plate with a 1 cm^2 hole with the geometry of DLS cuvettes. A 405 nm laser (Thorlabs, Germany) was used for the experiment. Laser power intensity by cm^2 was measured with a digital optical power and energy meter (Thorlabs, Germany) with and without the skin barrier (skin thickness 0.26-0.29

Table 14: Sequence of primers used in qRT-PCR experiments.

Gene		Sequence	Species
h-MYB	FW RW	CCGAATATTCTTACAAGCTCC GGACCTGTTTTTAGGTACTG	human
h-GAPDH	FW RW	AGCCACATCGCTCAGACACC GTACTCAGCGCCAGCATCG	human
m-MYB	FW RW	CACAAAACATCTCCAGTCAC TCTTCGTCGTTATAGTGTCTC	mouse
m-GAPDH	FW RW	AAGGTCATCCCAGAGCTGAA CTGCTTCACCACCTTCTTGA	mouse
hsa-miR-150-5p	FW	TCTCCCAACCCTTGTACC	human
RNU6	FW	ACACGCAAATTCGTGAAG	human

mm). P1C7 NPs (50 µg/mL) were activated for 10 min with the laser with or without the skin barrier and then measured by DLS. Laser power transmission and NP count decrease were analysed for 3 individual samples.

Table 15: Information about the chemical name, CAS and vendor of the monomers used to generate the NP library.

Monomer	Chemical Name IUPAC	CAS	Vendor
A	Methylenebisacrylamide	110-26-9	Aldrich
B	Hexamethylenebisacrylamide	7150-41-6	Polyscience
C	Cystaminebisacrylamide	6098-457-8	Polyscience
D	Dihydroxyethylenebisacrylamide	868-63-3	Aldrich
E	Bisacryloylpiperazin	6342-17-2	Sigma
P1	(2-Nitro-1,3-phenylene)bis(methylene)diacrylate	1599460-50-0	Synthesized
1	Ethylenediamine	107-15-3	Merck
2	1,4-Diaminobutan	110-60-1	Aldrich
3	1,6-Diaminohexan	124-09-4	Alfa Aesar
4	Diethylenetriamine	111-40-0	Alfa Aesar
5	Triethylenetetraamine	112-24-3	Acros Organics
6	Pentaethylenehexamine	4067-16-7	Aldrich
7	3,3'-Diamino-N-methyldipropylamine	105-83-9	Aldrich
8	1,2-Diaminocyclohexane	694-83-7	Aldrich
9	1,8-Diamino-3,6-dioxaoctane	929-59-9	Acros Organics
10	1,13-Diamino-4,7,10-trioxatridecane	4246-51-9	Aldrich
11	1,4-Bis(aminopropyl)piperazine	7209-38-3	Aldrich
12	1,4-Phenylenedimethanamine	539-48-0	Merck
13	1,5-Diaminonaphthalene	2243-62-1	Aldrich
14	4,4'-methylenedianiline	101-77-9	Aldrich
15	1,3-Phenylenediamine	108-45-2	TCI Chemicals
16	1,3-Diaminopropane	109-76-2	TCI Chemicals
17	2,2-Dimethyl-1,3-propanediamine	7328-91-8	TCI Chemicals
18	1,3-Diaminopentane	589-37-7	TCI Chemicals
19	2,2'-Diamino-N-methyldiethylamine	4097-88-5	TCI Chemicals
20	Agmatine sulfate	2482-00-0	TCI Chemicals
21	1,4-Bis(aminomethyl)cyclohexane	2579-20-6	TCI Chemicals
22	4,4'-Methylenebis(cyclohexylamine)	1761-71-3	Aldrich
23	4,4'-Diaminobenzanilide	785-30-8	Aldrich
24	DL-Lysine	70-53-1	Aldrich
25	3-Amino-1-propanol	156-87-6	Aldrich
26	4-Amino-1-butanol	13325-10-5	Aldrich
27	5-Amino-1-pentanol	2508-29-4	Sigma Aldrich
28	6-Amino-1-hexanol	4048-33-3	Alfa Aesar
29	1-(3-Aminopropyl)pyrrolidine	23159-07-1	Alfa Aesar
30	1-(3-Aminopropyl)imidazole	5036-48-6	Aldrich
31	1-(3-Aminopropyl)-4-methylpiperazine	224-954-4	Alfa Aesar
32	Histamine	51-45-6	Sigma Aldrich

CHAPTER IV – A LIGHT-TRIGGERABLE FORMULATION TO CONTROL THE STABILITY OF PRO-ANGIOGENIC TRANSCRIPTION FACTOR HYPOXIA INDUCIBLE FACTOR 1a (HIF-1a)

Josephine Blersch[a], Vitor Francisco[a,b], Catarina Rebelo[a,b], Adrian Jiménez-Balsa[a], Helena Antunes[a,b], Sandra Pinto[a], Susana Simões[a], Akhilesh Rai[b], Lino Ferreira[a,b]

[a]Center for Neuroscience and Cell Biology, University of Coimbra, Coimbra, Portugal

[b]Faculty of Medicine, University of Coimbra, 3000-548, Coimbra, Portugal

Published in: ***Nanoscale***, 2020,**12**, 9935-9942†

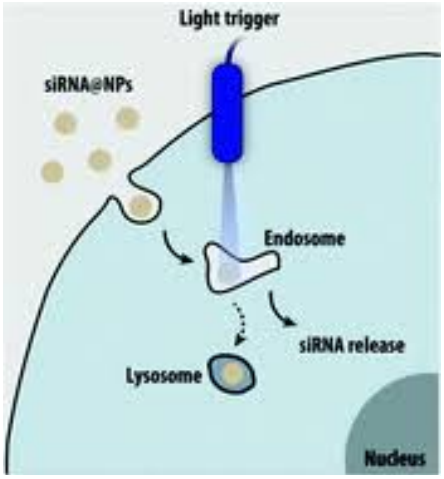

Figure 40: Graphical Abstract depicting schematically light activation of NPs in endosomal compartment with subsequent siRNA release.

1 ABSTRACT

The control of vascular remodelling mediated by transcription factor HIF-1α is critical in several diseases including cancer, retinopathies, chronic wounds, ischemic heart disease, among others. Gene silencing using small interfering RNA (siRNA) is a promising therapeutic strategy to regulate HIF-1α; however, the delivery systems developed so far have limited endothelial targeting and efficiency. Herein, we have synthesised a light-triggerable polymeric nanoparticle (NP) library composed by 110 formulations which showed variable morphology, charge and disassembly rates after UV exposure. More than 35% of the formulations of the library were more efficient in gene knockdown than siRNA delivered by a commercial transfection agent (lipofectamine RNAiMAX). The most efficient siRNA delivery formulations were tested against different cell types to identify one with preferential targeting to endothelial cells. Using a two-steps methodology, we have identified a formulation that shows exquisite targeting to endothelial cells and is able to deliver more efficiently the siRNA that modulates HIF-1α than commercial

† Reproduced from Blersch et al.[384] with permission from the Royal Society of Chemistry

transfection agents. Overall, the strategy reported here increases the specificity in tissue regulation and the efficiency in the intracellular delivery of siRNAs.

2 INTRODUCTION

The abnormal activation of hypoxia inducible factor-1a (HIF-1α) pathway leads to the overexpression of angiogenic growth factors that causes undesirable neovascularisation in tissues such as retina and primary tumours[312]. Moreover, despite the ischemia in several diseases, HIF-1α is destabilised in diabetic wounds[360], critical limb ischemia[361] and ischemic heart disease[312]. HIF-1α is regulated by an enzyme called prolyl hydroxylase domain protein 2 (PHD2)[312,362]. This enzyme is active in normoxia conditions and thus triggers the degradation of the transcription factor while inactive in hypoxia conditions and thus the stabilisation of the transcription factor induces the expression of pro-angiogenic growth factors such as vascular endothelial growth factor (VEGF), basic fibroblast growth factor (bFGF), among others[312,362]. The inhibition of PHD2 has been attempted with small molecules; however, these drugs have shown off-targets[363]. siRNAs have emerged as an attractive tool for regulating gene expression and thus to inhibit HIF-1α. Indeed, studies have demonstrated the inhibitory properties of PHD2 siRNA in the context of wound healing[315,364] and cancer[365]; however, with limited efficacy and the targeting to endothelial cells, important in the context of cancer[366] and ischemic diseases[367], was not demonstrated.

A large variety of siRNA delivery system have been developed relying on cell penetrating peptides, lipid-based formulations and polymeric NPs[347,368,369], some of them identified by high-throughput screening approaches[112,158,370,371]. A limited number of these strategies have progressed to clinical trials and some of them reached the market[372]. Despite the significant progresses in the delivery of siRNA, two major issues have yet not been completely addressed: (i) limited cell targeting of the formulations increasing the concerns about potential off target effects and (ii) low endosomal escape limiting its efficacy[373,374]. Although lipidic NPs able to release more efficiently siRNA to endothelial cells have been described[354], the molecular mechanism is not yet known. Experimental *in vitro* data indicate that the endosomal escape of siRNA should take place during the early stages of the intracellular trafficking (minutes range after formulation uptake) to prevent their accumulation in the lysosomes[2,3,130]. In the current study, we hypothesize that enhanced endothelial cell targeting might be achieved by the use of NP libraries with physico-chemical diversity, being the cell targeting controlled by a combination of NP size, geometry, charge and composition. We further hypothesize that enhanced endosomal escape might be achieved by using light-triggerable formulations that are taken up by cells and disassemble rapidly (minutes range) by light releasing the siRNA.

3 RESULTS and DISCUSSION

Herein, we have designed a light-triggerable formulation that shows preferential accumulation in endothelial cells while releasing more efficiently PHD2 siRNA in cell cytoplasm than other commercial transfection agents. To identify that formulation, we have prepared a library of light-triggerable polymeric NPs for the delivery of siRNA. Then, the polymers were conjugated with a light sensitive molecule to increase their hydrophobicity as well as to confer light responsiveness properties. The conjugated polymers were then precipitated in water to form NPs and then complexed with siRNA. The NPs were characterised for their size, zeta potential, light disassembly properties, cellular internalisation and gene knockdown activity. The top hits were then tested against different cell types to identify a formulation with the highest tropism to endothelial cells. Finally, the hit formulation was tested regarding its efficacy in the inhibition of endothelial cell PHD2 gene.

3.1 HT synthesis and characterisation of light activatable poly(amido amine) NPs

The library of poly(amido amine)s was prepared by Michael-type addition[3,130,353] of bisacrylamides with diamines in dimethyl sulfoxide (DMSO) for 5 days at 60 °C (Figure 43A). Monomers were selected based in their chemical properties (hydrophobicity/hydrophilicity, composition, structure) or by the fact that they have been used with success in previous NP libraries (Figure 43B and 43C). This strategy allowed us the preparation of polymers with (i) a large variety of side groups (structure: linear, ring, branched; reactivity: primary, secondary and tertiary amines; molecular weight), (ii) disulphide bonds that were relative stable in physiological conditions (pH 7.4) but likely degraded in intracellular reductive environments and (iii) different solubility in aqueous solution. In the final stage of reaction, an excess of the amine monomer was added to ensure that acrylamide end groups were capped with amines in order to increase transfection efficiency[136]. To confer light responsiveness properties to the polymers, a light sensitive pendant group was attached to the polymer backbone. Therefore, the polymer library was reacted with 4,5-dimethoxy-2-nitrobenzyl chloroformate (NVOC), in the presence of trimethylamine as a catalyst. NVOC was selected because it responds rapidly to UV/blue light and the degradation products are relatively non-cytotoxic[375].

To validate the overall synthetic strategy, we randomly selected one polymer and characterised it by NMR (Figure 44A). ^{1}H-NMR spectrum of A4 showed the absence of acrylate protons (5.5 to 7.0 ppm) indicating complete reaction of the acrylamide with the amines.

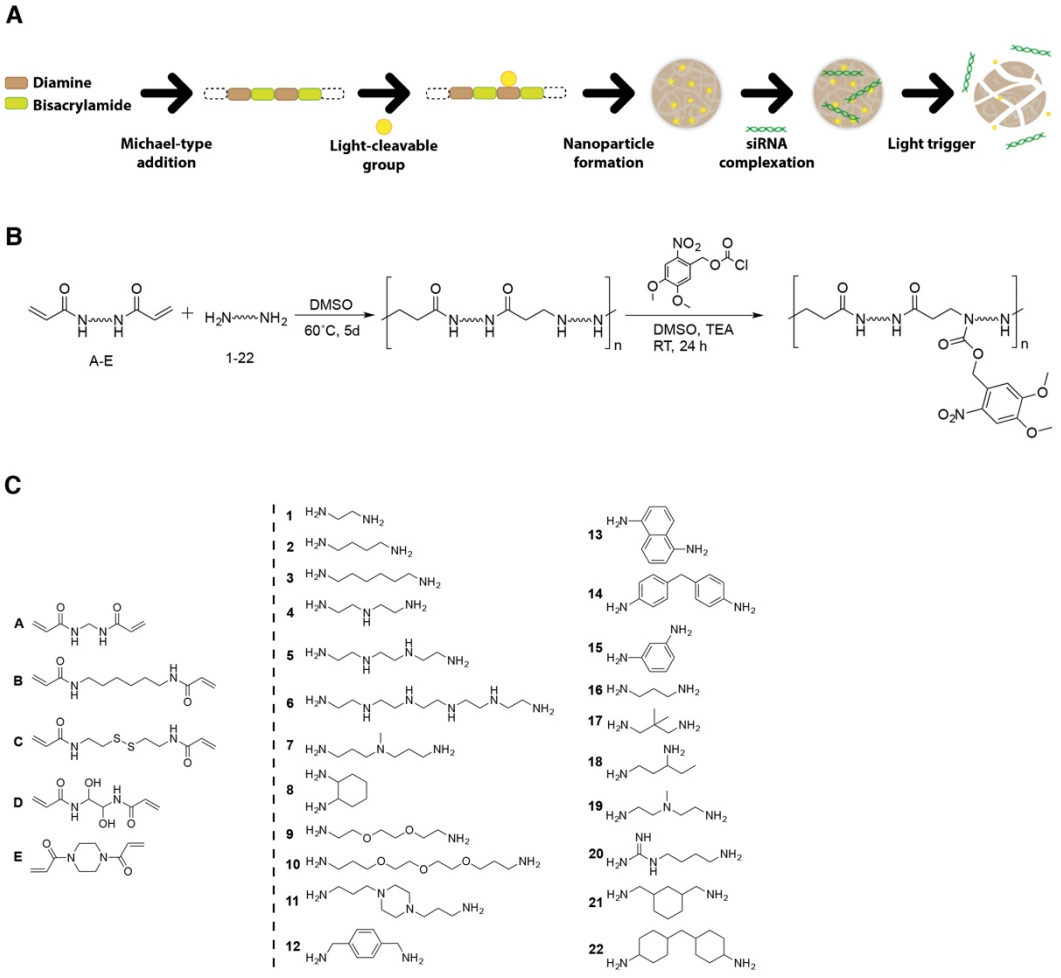

Figure 41: Light-activatable NP library and gene knockdown activity. (A) Scheme illustrating the formation of light-activatable polymers and formation of nanoparticles. (B) Reaction scheme for the combinatorial synthesis of the poly(amino amine)s, followed by the conjugation of NVOC. The mechanism of photocleavage is also presented. (C) Monomers used for the synthesis of the library: bisacrylamides (A-E) and diamines (1-22).

Moreover, the spectrum of A4 showed the expected peaks of NVOC protons at δ 7.9, 7.7, 5.1 and 3.8-3.9 ppm. Successful conjugation of A4 with NVOC was also confirmed by spectrophotometry (Figure 44B). As expected, the absorbance spectrum of A4 showed an absorbance maximum at 354 nm after NVOC conjugation. After UV irradiation of the polymer for 10 min, there is the cleavage of the NVOC moiety of the polymer (approximately 50%; for a polymer with an experimental degree of substitution (DSexp) of 20%) and the consequent decrease in the absorbance at 354 nm. A4 NPs were obtained by nanoprecipitation of A4 polymer conjugated with NVOC in aqueous solution, followed by the addition of zinc sulphate to stabilize the NPs[376]. To form light-responsive NPs, a compromise between hydrophobicity (which impacts in NP yield by the nanoprecipitation process) and light-responsiveness (high conjugation of the polymer with NVOC slows down the NP photo-disassembly) process should be optimised. To

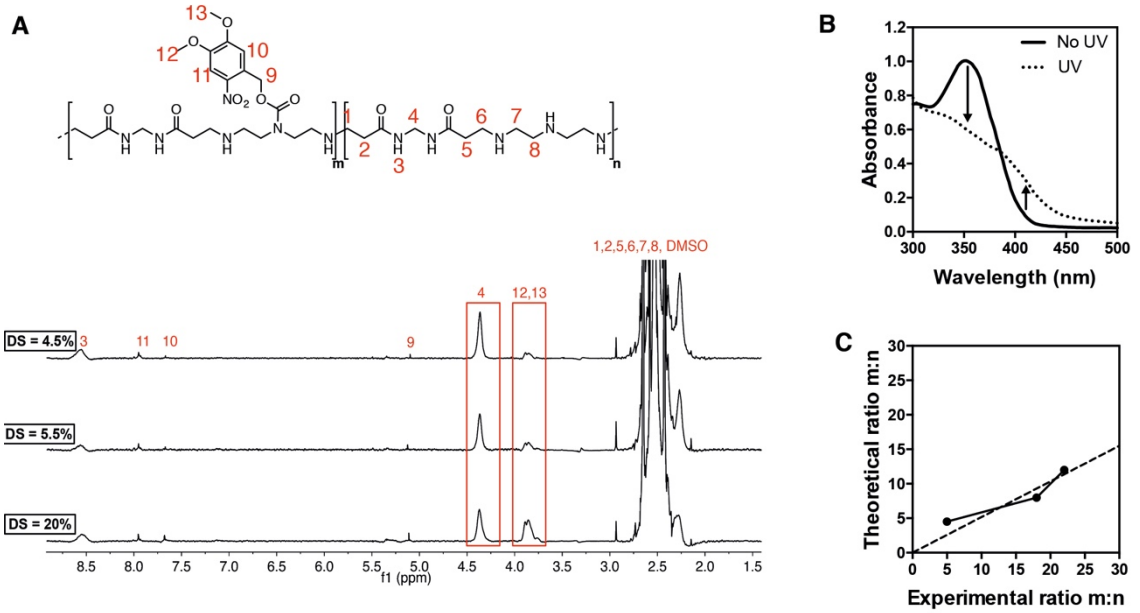

Figure 42: Optimisation of the light-cleavable moiety (NVOC) ratio in the polymer A4. After the synthesis, the polymer was reacted with NVOC at the following theoretical molar ratio (NVOC:diamine): 1:4, 1:8 and 1:12. To calculate the ratio of incorporation of NVOC into the polymer, polymers were precipitated in water, lyophilized, resuspended in DMSO-d6 and analysed by ^{1}H-NMR. (A) NMR spectra (in DMSO-d6) of A4 polymers with different NVOC-Cl:diamine molar ratios. The results show a degree of substitution of 20 %, 5.5% and 4.5%. (B) Effect of UV light (10 min, 365 nm, 200 mW/cm^2) in the absorbance of the polymer A4 (DSexp = 20%). The decrease in absorption at 350 nm (NVOC) and the increase at 420 nm (nitroso product) indicate the photo-cleavage of NVOC. (C) Theoretical and experimental NVOC:diamine molar ratio´s ratio by NMR.

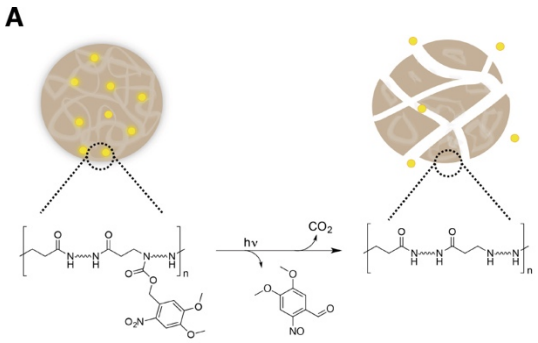

B

	UV	Diameter (nm)	Count (kcps)	C.decrease (%)
DS = 20%	No	165.7	124.0	87.7
	Yes	2.2	15.2	
DS = 5.5%	No	140.2	170.8	85.1
	Yes	176.1	25.4	
DS = 4.5%	No	306.8	230.5	80.8
	Yes	579.5	44.2	

Figure 43: (A) Schematic illustration of NPs disassembly upon UV light irradiation. (B) Optimisation of the NVOC to amine ratio in the nanoparticle A4, to obtain the higher nanoparticle count decrease after UV irradiation. The formulation (50 µg/mL) was irradiated with UV light (365 nm, 200 mW/cm^2) for 10 min.

address this issue, A4 polymer was conjugated with three different molar ratios of NVOC: diamine (Figure 45C) and then the individual polymers precipitated in aqueous solution. The NP efficiency for A4 with a DSexp of NVOC of 20% was 16% (i.e., percentage of mass recovered from the initial monomers used for polymer synthesis and derivatisation). After activation with UV light, NVOC is cleaved from the polymer, which changes the hydrophobic-hydrophilic balance in the NPs resulting in its disassembly. This response is expressed in the percentage count decrease of NPs, as monitored by dynamic light scattering (DLS). The NPs formed by polymers with a DSexp of 20% (i.e. the molar ratio of NVOC: diamine was 1:5) showed the highest NPs count decrease after UV irradiation (Figure 45). Therefore, this molar ratio was adopted to synthesize the library with 110 possible polymers.

Next, we have synthesised the NP library and characterize the properties of NPs according to size, zeta potential and light responsiveness. Most of the polymers (90%) were able to form NPs by nanoprecipitation, while 10% were either soluble in water or formed aggregates that rapidly flocculated and deposited. The high-water solubility of some polymers was likely due to the low conjugation of the polymer with NVOC because of the low amine groups in the polymer. Next, we determined the NP formation efficiency taking into account the mass of monomers used for the synthesis and conjugation of the polymers and the resulting NP mass after freeze-drying (Figure 46A). The median NP formation efficiency was 27 ± 15%. The NPs were then characterised by DLS, to obtain NPs size (Figure 46B, C, E) and zeta potential (Figures 46D and 46F). Ninety percent of NPs had a size between 50 and 500 nm, while 65% of the NPs showed positive charge (zeta potential>10 mV). NPs composed by crosslinkers A and C had narrow size distribution and highly positive zeta potential. NPs composed by diamines 5-8 and 15-18 had the highest positive zeta potential. Next, we evaluated the light responsiveness of the NP library (Figure 46G). More than 90% of the formulations were sensitive to UV irradiation. Approximately 79% of the formulations had a 50% decrease after 10 min of UV irradiation. The light responsiveness of the NPs formulations was likely influenced by the presence of aromatic moieties, the hydrophobicity of the polymer before NVOC conjugation, among others. It was largely independent of the characteristics of the crosslinker but dependent in the diamine's composition, since aromatic diamines (12-15 and 23), negatively affected the light-response of the formulation.

3.2 High RNA silencing efficacy and temporal control with light sensitive NP@siRNA complexes

To evaluate the capacity of NPs to complex siRNA, each NP formulation was mixed with a GFP-silencing siRNA for 2 h to promote electrostatic interactions. The ratio siRNA to NP was optimised to yield the highest knockdown efficiency in HeLa-GFP cells, being the ratio siRNA:NP

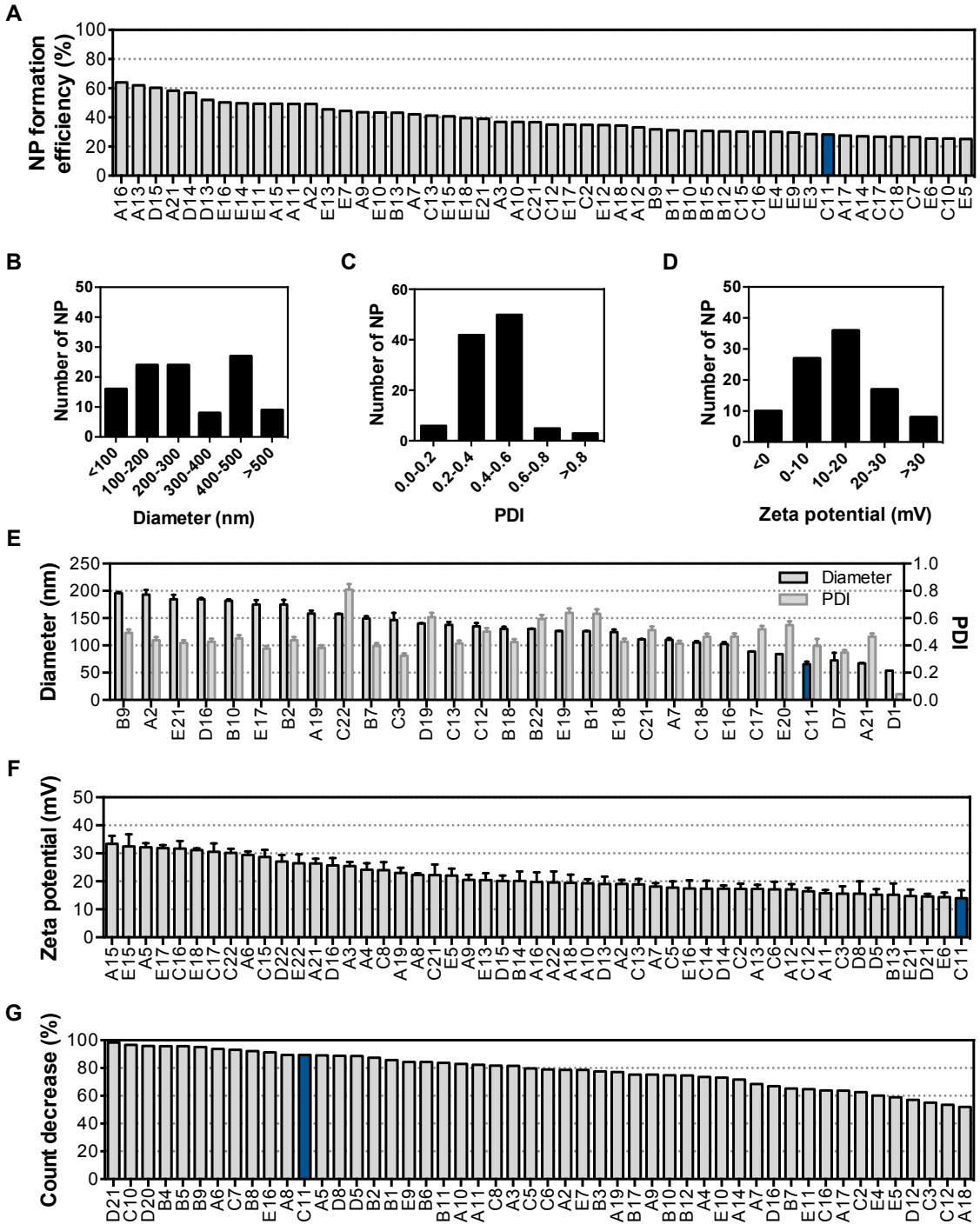

Figure 44: Physicochemical properties of the 50 top NP formulations. (A) Efficiency of NP formation calculated from the ratio of theoretical polymer weight and weight of NP after purification. (B) Diameter frequency distribution. (C) PDI frequency distribution. (D) Zeta potential frequency distribution. (E) Size and PDI of nanoparticles within size range between 50 and 200 nm. (F) Zeta potential of the NPs measured by DLS. In E and F, results are Mean ± SEM (n = 3). (G) NP disassembly by light. Count decrease was determined by DLS after 10 min UV irradiation (365 nm, 100 mW/cm2).

of 1:50 (w/w) the most effective (Figure 47). This ratio is a compromise between NP charge (accounting for cell uptake) and siRNA concentration (accounting for bioactivity). Therefore, all the subsequent steps were done with this siRNA:NP ratio. Next, we quantified the complexation efficiency of siRNA with the library of NPs by fluorescence spectroscopy. NPs were centrifuged after the complexation and the concentration of labelled siRNA (tagged with a Cy5 dye) quantified in the supernatant. For all the formulations, the median efficiency was 70±27%, being 40% of the formulations able to complex more than 75% of the siRNA (Figure 48B). The most effective formulations in binding siRNA were composed by crosslinker A, C or E and diamines with higher aliphatic contribution (2, 3, 11, 16, 21, 22) or high amine content (4, 5, 6, 7, 11). These results indicated that the binding of siRNA was not only dependent on positive zeta potential (mostly caused by amines) but also by the presence of aliphatic domains.

After demonstrating the capacity of NPs to complex siRNA and disassemble after UV exposure, we evaluated NP@siRNA mediated gene knockdown upon light activation using siRNA against eGFP in HeLa-GFP cells. For that purpose, cells were transfected with NP@siRNA (siRNA:NP 1:50 (w/w), 20 µg/mL) complexes for 10 min (Figure 48A), washed to remove non-internalised complexes, light-activated for 10 min and cultured for additional 48 h. Non-treated HeLa-GFP and HeLa-GFP cells transfected with lipofectamine RNAiMAX complexed with siRNA were used as controls. Cell viability (evaluated by propidium iodide (PI)

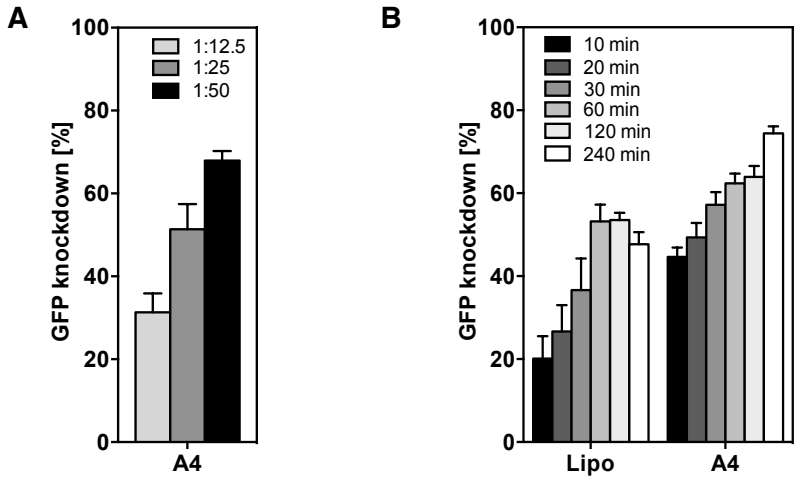

Figure 45: Evaluation of the influence of siRNA:NP ratio and transfection time in the knockdown efficiency of the formulations. (A) Effect of the ratio siRNA:NP in the knockdown efficiency. HeLa-GFP cells were transfected for 4 h with a NP formulation (formulation A4; 20 µg/mL) containing siRNA-Cy5 against GFP at different ratios siRNA:NP (w/w) (1:12.5; 1:25 and 1:50). Lipofectamine RNAiMAX (Lipo) was used as a control transfection agent. GFP knockdown was quantified at 48 h post-transfection. (B) Effect of transfection time in the knockdown efficiency. Cells were transfected for various times (between 10 and 240 min) with A4 NP@siRNA-Cy5 complexes (20 µg/mL; 1:50 siRNA:NP). GFP knockdown was analysed at time 48 h after transfection by high-content microscopy. All results are presented as Mean ± SEM (n = 3).

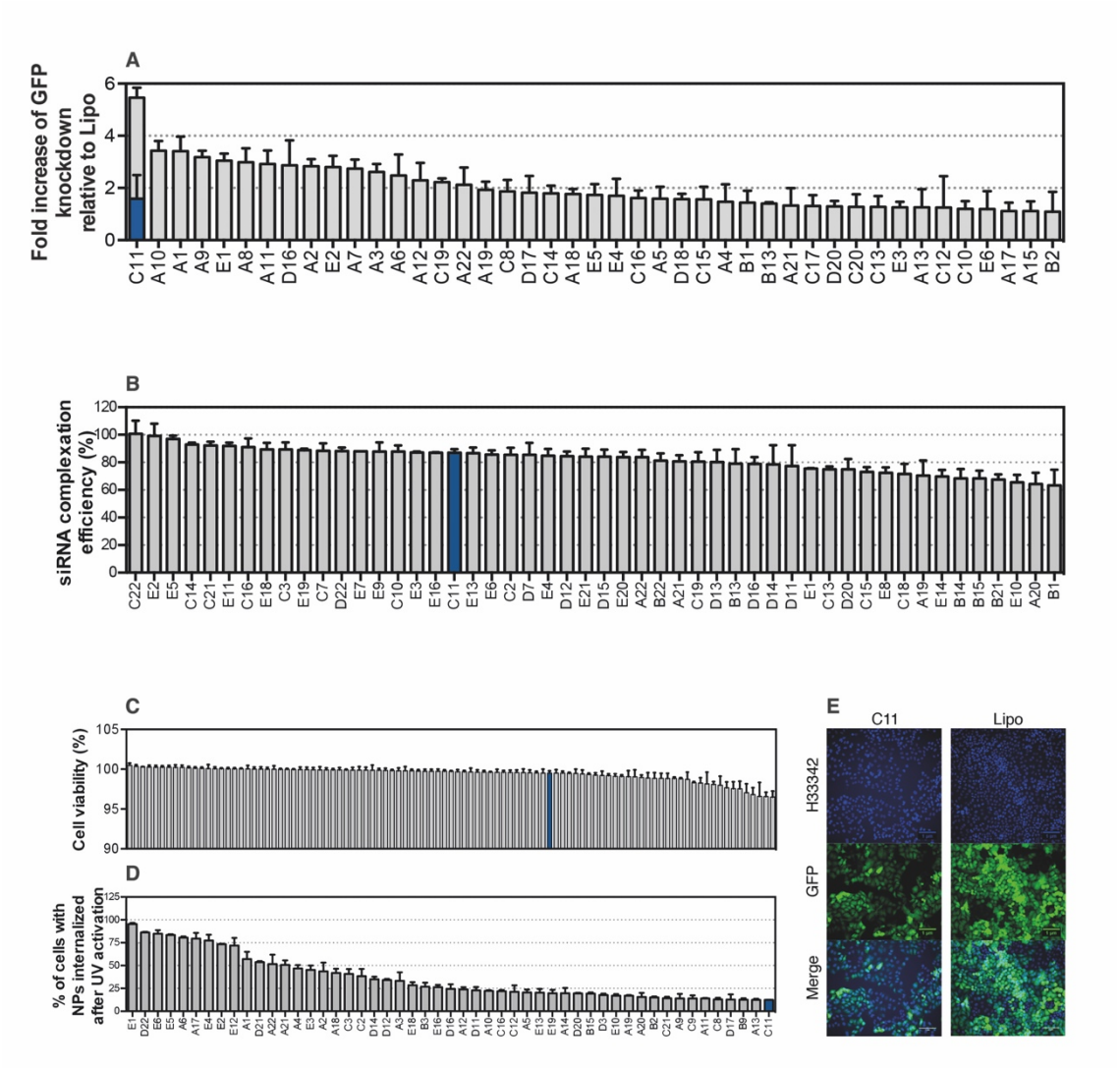

Figure 46: Results from high-throughput screening of the photo-antenna library. HTS of NPs for maximal GFP silencing efficacy after transfecting in HeLa-GFP cells for 10 min with 20 µg/mL NP@siRNA complexes with ratios of 1:50 siRNA:NP (w/w) and 10 min light activation with a UV lamp. (A) Gene silencing efficacy of the 43 best NP formulations. Efficacy was measured as fold increase GFP knockdown relative to Lipofectamine RNAiMAX (Lipo), 48 h post transfection. The blue bar shows GFP knockdown of the best formulation without UV activation. (B) Efficiency of siRNA complexation in the top 50 formulations of NP@siRNA-Cy5. (C) Cell viability at 48 h post transfection without UV irradiation. Cell nuclei were stained with Hoechst H33342 and dead cells with propidium iodide. Cell viability was calculated as the % of dead nuclei from the total count of nuclei. (D) Percentage of cells stained for NPs@siRNA-Cy5 (siRNA:NP ratio = 1:50) at 48 h post-transfection. The graph shows the top 50 NP formulations with high cell internalisation. In A, B, C and D results are Mean ± SEM (n = 3). (E) Representative images of gene knockdown in HeLa-GFP cells 48 h post-transfection with C11 formulation containing a siRNA against GFP. Scale bar corresponds to 1 µm.

staining), NP internalisation (evaluated by the Cy5 tag of the siRNA) and GFP knockdown results were obtained by high-content microscopy analyses. GFP knockdown was calculated as percentage decrease of GFP fluorescence signal relative to non-treated HeLa-GFP cells and HeLa-GFP cells transfected with lipofectamine complexed with siRNA. No significant impact in cell viability was observed for all the NPs of the library (cell viability>90%) (Figure 48C). NP formulations were internalised by HeLa cells and accumulated in the cell cytoplasm for at least 48 h (Figure 48D). To further demonstrate the delivery of siRNA to the cell cytoplasm, we have transfected HeLa cells for 10 min with C11@siRNA-Cy5 or with Lipo@siRNA-Cy5 followed by irradiation or not with UV light (Figure 49). The intracellular trafficking of the formulations was monitored by confocal microscopy using a general endolysosomal staining (LysoTracker). The results showed lower co-localisation of C11@siRNA-Cy5 with endolysosomes after irradiation than before irradiation indicating that the rapid NP disassembly favoured the escape of siRNA from the endolysosomal compartment (Figure 49).

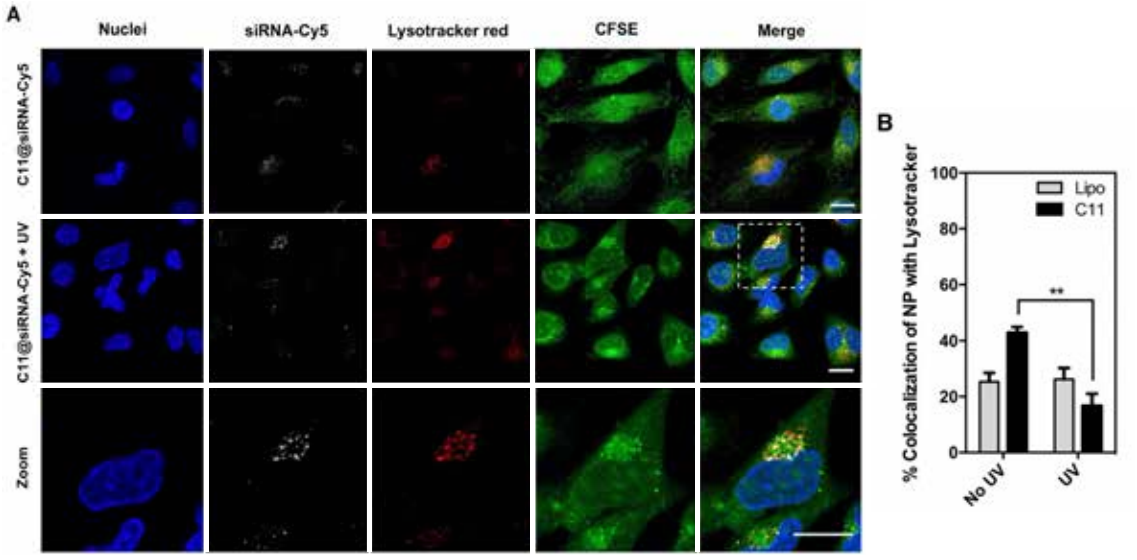

Figure 47: C11@siRNACy5 colocalisation with LysoTracker Red. HeLa cells were transfected with C11@siRNA-Cy5 (20 µg/ml) or Lipo@siRNA-Cy5 for 10 minutes. Cells were then washed and NPs were activated with UV light (10 min, 1 mW/cm^2). The cells were stained with CFSE for cell membrane, LysoTracker red for endolysosome, H333342 for cell nuclei and analysed 1 h after transfection by confocal microscopy. (A) Representative confocal microscopy images showing the colocalization of C11@siRNA-Cy5 formulation irradiated or not with UV light with Lysotracker Red. White scale bar is 20 µm. (B) Colocalization of Lysotracker Red with siRNA-Cy5 expressed as the Manders' overlap coefficient quantified using JACoP on ImageJ. Results are resented as Mean ± SEM. Statistical analysis was assessed by unpaired student t-test with Welch's correction. ** P <0.01.

Importantly, more than 35% of the formulations were more efficient in GFP knockdown than lipofectamine RNAiMAX (fold increase>1) (Figure 48A, 48E). Formulations containing crosslinkers A, C or E and diamines 1, 4-7 or 10-11 showed the highest GFP knockdown activity. Five formulations (C11, A10, A1, A9 and E1) showed more than 3-fold increase relative to lipofectamine RNAiMAX in GFP knockdown and were selected for further studies.

3.3 Skin cell tropism of NP@siRNA

The uptake of NPs by cells is dependent on multiple factors such as NP size[95], NP shape[93], NP surface chemistry[90,94,96], and the type of cell and its machinery, since each cell type may internalize the same NP by different endocytic pathways. For example, polystyrene NPs are highly taken up by endothelial and hepatocyte cells and less by macrophages and epithelial cells[100]. To identify NPs able to target more preferentially endothelial cells, we evaluated NP@siRNA-Cy5 internalisation in different type of cells through colocalisation with the endolysosomal compartment (Lysotracker) by confocal microscopy. Because one of the potential applications of these light-triggerable NPs is for skin applications[185] we have chosen human keratinocytes, dermal fibroblasts and endothelial cells as cell models to investigate endothelial cell-specific NP uptake. Six efficient gene silencing formulations (A1, A9, A10, C11, E1, E2) and one non-efficient formulation (E21, which presented lower knockdown activity than lipofectamine) were chosen to assess cell uptake (Figure 50). Cells were transfected either with NP@siRNA-Cy5 or Lipo@siRNA-Cy5 for 1 h, washed to remove the NPs that were not internalised, and analysed by confocal microscopy. From all the formulations tested, C11 formulation was the highest taken up by endothelial cells while showing low uptake by keratinocytes and fibroblasts.

Based in the high efficacy of C11 to transfect endothelial cells and in the knockdown activity demonstrated in HeLa-GFP cells, this formulation was selected for subsequent studies. Initially, the physical-chemical properties of C11 formulation were investigated. The polymer had a DSexp of 24%, as measured by ^{1}H-NMR (Figure 51A), a Mw of 12.700 Da, as evaluated by GPC, and was responsive to UV irradiation, as measured by spectrophotometry (Figure 51B). When C11 was complexed with siRNA yielded NPs with an average diameter of ~60 nm and a zeta potential of 13.9 ± 1.2 mV, as demonstrated by DLS and TEM analysis (Figure 51C and D). The NPs disassembled after UV (365 nm, 10 min) light irradiation (more than 80%) (Figure 51E) due to the cleavage of NVOC moiety and the disruption of the hydrophobic/hydrophilic balance in the NP and release the siRNA (Figure 51F). We also investigated whether UV light could cross skin tissue and trigger the release of siRNA from the C11 formulation. Indeed, UV radiation is able to cross the skin tissue at the necessary level to disassemble the NP formulation (Figure 53).

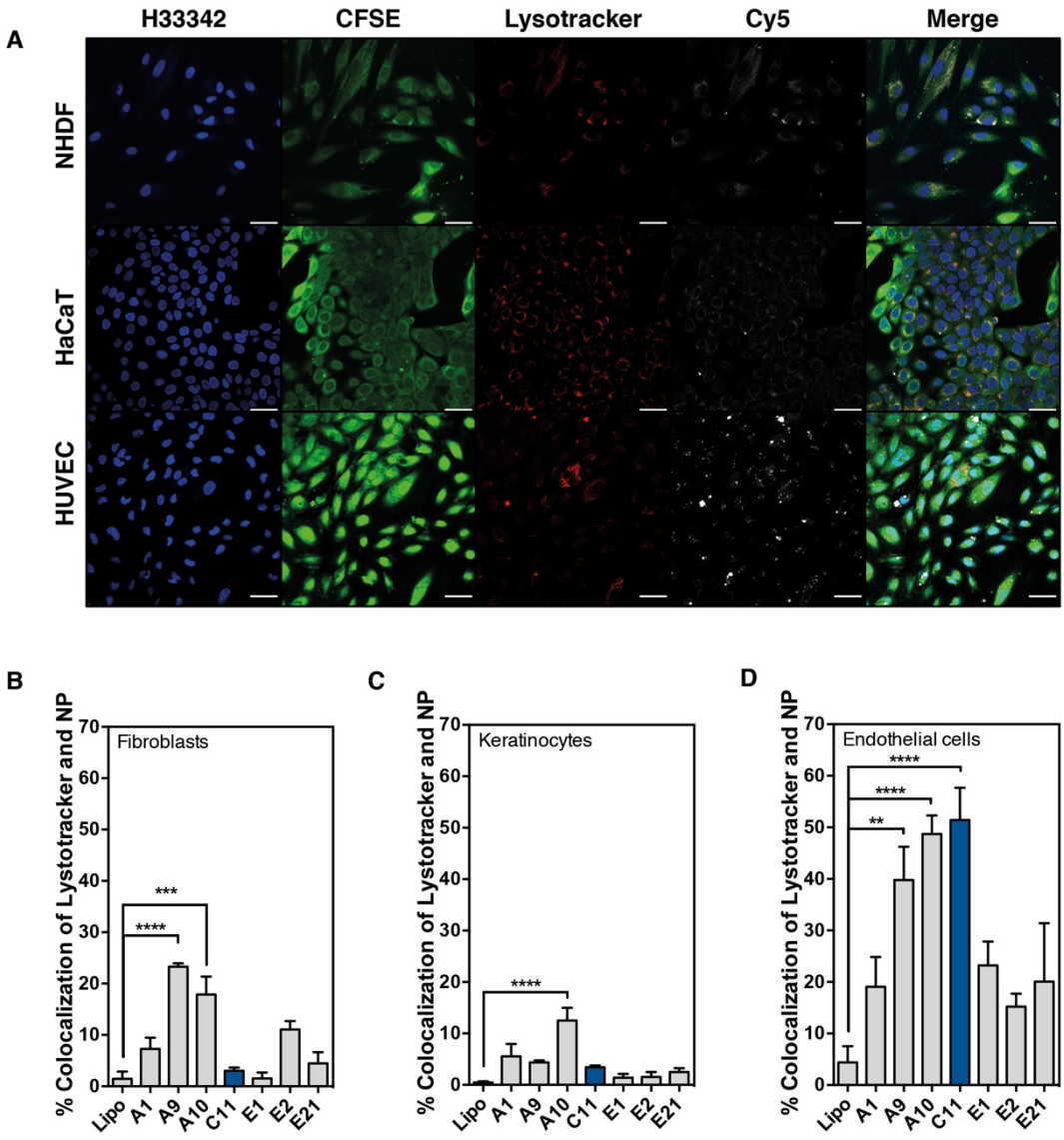

Figure 48: NP internalisation studies in human skin cells. (A) Representative images from confocal microscopy showing colocalisation of C11@siRNA-Cy5 with Lysotracker red (endolysosomal compartment) in the three cell types. Scale bar corresponds to 50 µm. Human fibroblasts (B), keratinocytes (C) and endothelial cells (D) were used for internalisation studies. The following formulations have been tested: (i) high gene silencing formulations (six) identified in the high-throughput screening (A1, A9, A10, C11, E1, E2), (ii) lipofectamine RNAiMAX (Lipo; positive control) and (iii) a low gene silencing formulation (E21, negative control). Cells were transfected for 1 h with NP@siRNA-Cy5 (20 µg/mL) complexes, washed to remove non-internalised NPs, stained (cytoplasm with CFSE; endolysosomal compartment with Lysotracker Red; nuclei with H33342) and analysed by confocal microscopy using a 40x objective. Internalisation was quantified through colocalisation of siRNA-Cy5 with Lysotracker red. Results are represented as Mean ± SEM (n = 2 independent samples, 3-9 microscope fields per independent sample). Statistical analyses were performed by one-way ANOVA followed by a Bonferroni multi-comparison test (*P < 0.05; **P < 0.01; ***P < 0.001; ****P < 0.0001) against Lipo.

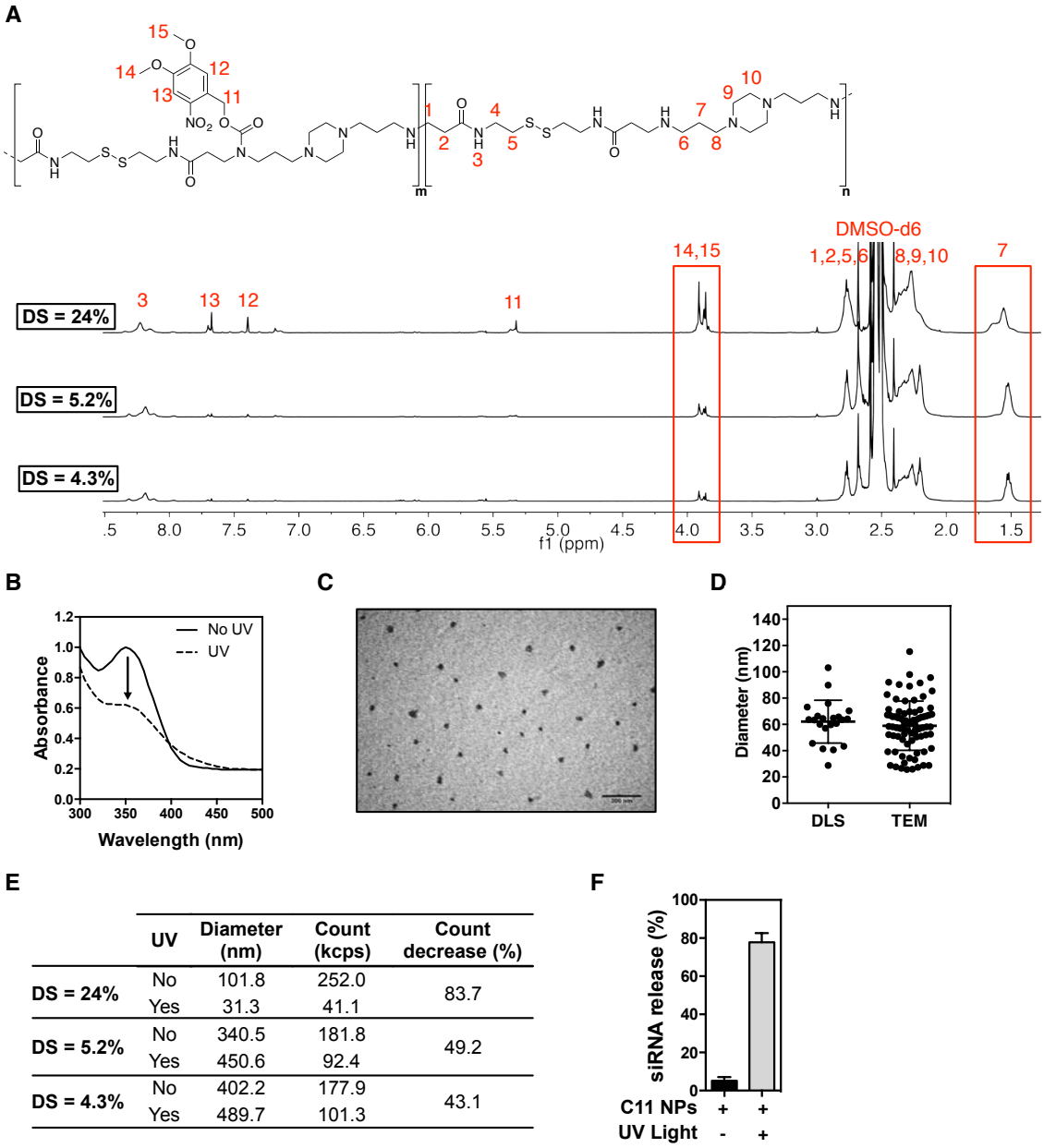

	UV	Diameter (nm)	Count (kcps)	Count decrease (%)
DS = 24%	No	101.8	252.0	83.7
	Yes	31.3	41.1	
DS = 5.2%	No	340.5	181.8	49.2
	Yes	450.6	92.4	
DS = 4.3%	No	402.2	177.9	43.1
	Yes	489.7	101.3	

Figure 49: Characterisation of C11 polymer and NPs. (A) NMR spectra (in DMSO-d6) of C11 polymers with different NVOC:diamine molar ratios. The results show a DSexp of 24.0 %, 5.2% and 4.3% (DStheo = 25%, 12.5% and 8.3%, respectively). (B) Effect of UV light (10 min, 365 nm, 100 mW/cm^2) in the absorbance of the polymer C11 (DSexp = 24%). The decrease in absorption at 350 nm (NVOC) and the increase at 420 nm (nitroso product) indicate the photo-cleavage of NVOC. (C) Representative image of NPs obtained by TEM (DSexp = 24%). Bar corresponds to 200 nm. (D) Distribution of NP diameters as evaluated by TEM and DLS analyses. For DLS analyses, a suspension of NPs at a concentration of 50 µg/mL was used. For TEM analyses, a NP suspension at a concentration of 500 µg/mL was applied on carbon coated 200 mesh copper grids, left to air dry and analysed (FEI-Tecnai Spirit BioTwinG2). The images were acquired and analysed on ImageJ. Results are Mean ± SEM (n = 2-5, up to 5 images per replicate). (E) Disassembly of C11 NPs with different ratios of NVOC after UV irradiation. The formulations (50 µg/mL) were irradiated with UV light (365 nm, 10 min, 100 mW/cm^2) for 10 min and analysed by DLS. (F) siRNA-Cy5 release from C11 NPs (50 µg/mL) after UV light irradiation (10 min, 1 mW/cm^2). siRNA-Cy5 was determined in the supernatant relative to a standard curve. Results are presented as Mean ± SEM (n = 3).

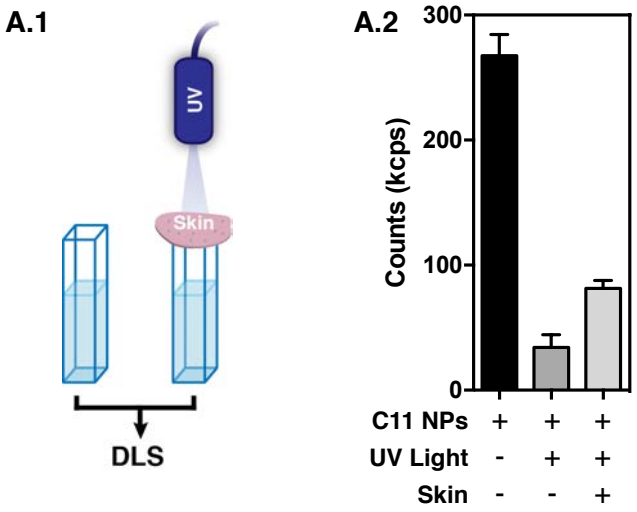

Figure 51: Photo-disassembly of C11@siRNA NPs. (A.1) Schematic representation of the methodology used to evaluate the photo-disassembly of C11@siRNA NPs beneath a mouse skin biopsy. A skin fragment (diameter ~1.7 cm placed on a cardboard with a 1 cm^2 hole; thickness of 200-230 µm as measured by a caliper) was placed above a cuvette containing a suspension of C11@siRNA (50 µg/mL, 2 mL). The cuvette was irradiated with UV light at 1 mW/cm^2 during 10 min and then analysed by DLS to determine NP count (A.2). In A.2, results are presented as Mean ± SEM (n = 3).

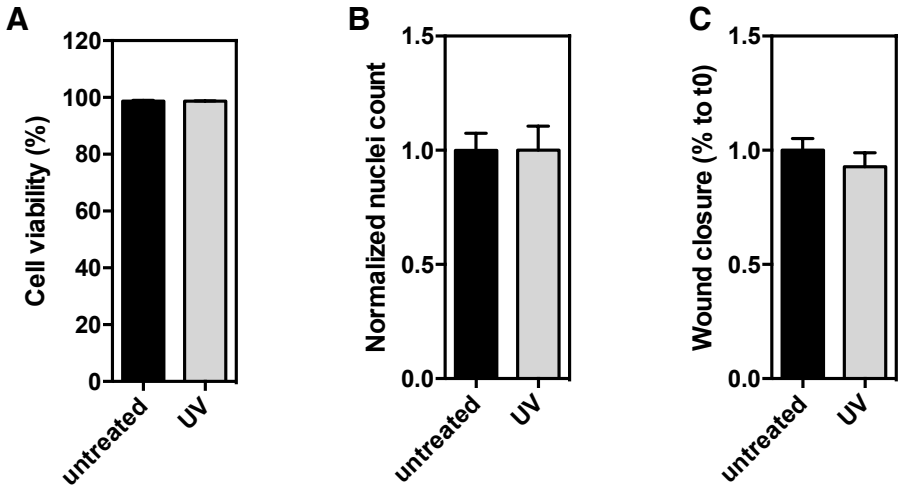

Figure 50: Influence of UV light on cell viability and activity. Cells were irradiated or not with UV light (10 min, 1 mW/cm^2) and analysed at 48 h. (A) Cell viability of HeLa-GFP cells. Cell nuclei were stained with Hoechst H33342 and propidium iodide at 48 h, and cell viability calculated as the % of dead nuclei from the total count of nuclei. (B) Endothelial cell proliferation. Nuclei were stained with H33342 and analysed by high content imaging at time 48 h. The number of cells at time 48 h was normalized by the one at time 0. (C) Endothelial cell migration. Wound area was quantified in ImageJ and normalised to the initial wound area. All results are presented as Mean ± SEM (n = 3).

3.4 Efficiency of C11 NPs to deliver HIF-1a stabilizing PHD2 siRNA

To demonstrate the utility of C11, we have complexed the NP with PHD2 siRNA and tested the formulation in endothelial cells. It has been shown that HIF-1α stabilisation in endothelial cells by PHD2 inhibition induces VEGF upregulation, which leads to proliferation and migration of the cells (Figure 54A)[362,377,378]. We have performed the experiments in normoxia since mRNA and protein expression of HIF-1α was higher in normoxia than in hypoxia after cell transfection with shPHD2[186]. The effect of UV in cell viability and activity was initially evaluated. Our results showed no influence in viability, proliferation or migration in cells exposed to UV light (365 nm, 10 min) relatively to non-exposed cells (Figure 52)). Next, we evaluated cell

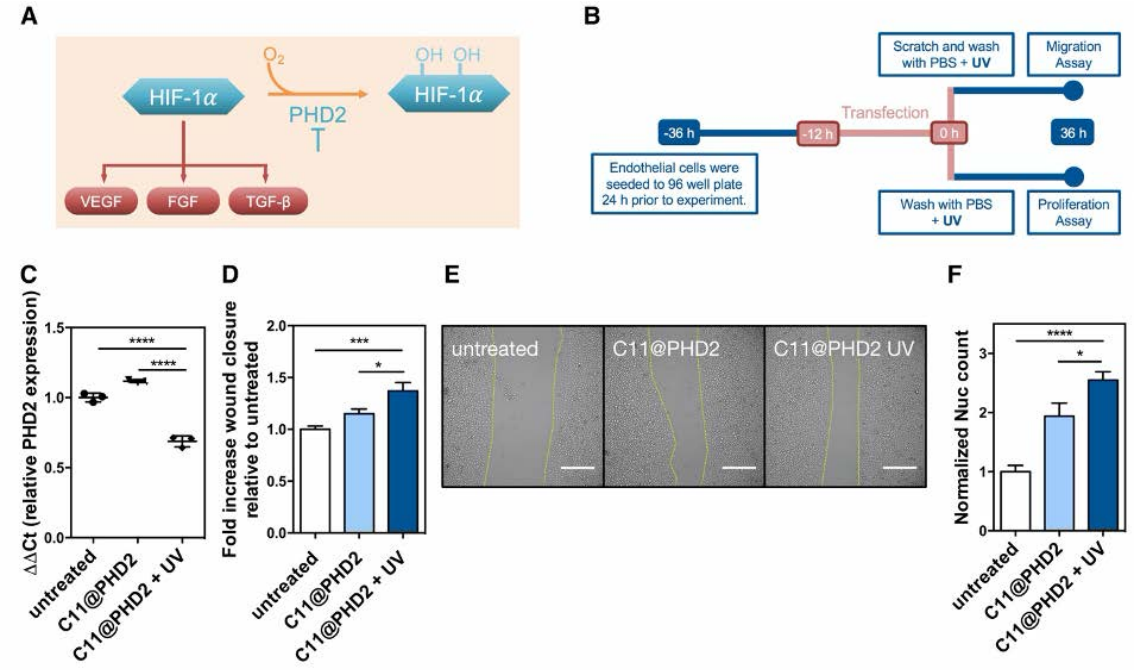

Figure 52: Bioactivity of C11@PHD2 NPs in endothelial cells. (A) Stabilization of HIF-1a by siRNA silencing PHD2 can be used as therapeutic strategy to control endothelial cell proliferation and migration, by the upregulation of VEGF and TGF-b growth factors[362, 377, 378] (B) Schematic representation of the experimental protocol for the migration and proliferation assays. Endothelial cells were grown to confluence and transfected with C11@PHD2 for 12 h. In the migration assay, non-internalised complexes were washed, the cell monolayer was wounded with a pipette tip and irradiated or not with UV light (365 nm, 10 min, 1 mW/cm^2). Cell migration in the wounded area was monitored by high content imaging. In the proliferation assay, non-internalised complexes were removed, cells were either or not irradiated with a UV light, and then cultured for additional 36 h. (C) Cells were harvested 24 h post-transfection and evaluated for PHD2 mRNA expression by qRT-PCR analyses and expressed relatively to GAPDH mRNA. Results are presented as Mean ± SEM (n=3). (D) Relative scratch closure 36 h post wounding. Wound area was quantified in ImageJ and normalised to the initial wound area. Results are presented as Mean ± SEM (n = 3-8 wells). (E) Representative images of wounds 36 h post scratch. Scale bar corresponds to 50 µm. (F) Cell proliferation at 36 h post transfection. Nuclei were stained with H33342 and analysed by high content imaging. Relative nucleus count is presented as Mean ± SEM (n = 3-6). All Statistical analyses were performed using One-Way Anova followed by a Tukey post-test (*P<0.05; *** P<0.001; ****P<0.0001).

migration and proliferation after transfection with C11@PHD2 NPs. Cells were transfected for 12 h with C11@PHD2 NPs, activated or not with a UV light for 10 min, and cell migration evaluated in a wounded monolayer of endothelial cells (Figure 54B). Our qRT-PCR analyses indicate that PHD2 mRNA available in the cytoplasm was lower in cells transfected with C11@PHD2 NPs and activated by light as result of the inhibition of the siRNA (Figure 54C). Endothelial cell migration was significantly increased when cells were treated with C11@PHD2 NPs after light activation as compared to cells treated with C11@PHD2 NPs without light activation or non-treated cells (Figures 54D and 54E). Therefore, our results indicate that C11@PHD2 NPs efficiently delivered the siRNA to endothelial cells and the exposure to light improved PHD2 siRNA release from C11 NPs. Next, we evaluated the biological activity of siRNA delivered by C11@PHD2 NPs in a cell proliferation assay (Figure 54B and 54F). Cells were transfected for 12 h with C11@PHD2 NPs, activated or not with a UV light for 10 min, and cell proliferation evaluated for 36 h by cell counting using a high-content microscope. Our results indicate that cells transfected with C11@PHD2 NPs and then activated by light proliferated at higher extent than cells treated with C11@PHD2 NPs but not exposed to light. Although C11 formulation has disulphide bonds incorporated in polymer backbone (monomer C), and therefore can be cleaved by intracellular glutathione, the results show that light activation is required to maximize its biological effect (cell migration and proliferation).

4 CONCLUSION

In conclusion, we have developed a formulation that has preferential accumulation in endothelial cells and release more efficiently siRNA in the cell cytoplasm than a conventional transfection agent. The formulation has been identified by a two-step methodology comprising a high-throughput screening of a new light-triggerable NP library and then testing the top hits against several cell types to identify a formulation that has more accumulation in endothelial cells. The NP library proposed here had higher gene knock-down activity (30% of the formulations showed higher knock-down activity than lipofectamine) than another NP library (10% of the formulations showed higher knock-down activity than lipofectamine) recently reported by us[379]. In this study, the light-responsive library of NPs was based in a simple principle, i.e., conjugation of a light-sensitive pendant molecule (NVOC) to polymers synthesised by high-throughput while in the previous study we have incorporated a light-responsive monomer in the core of the polymer. In addition, using the current synthetic scheme we could identify formulations with higher endothelial cell accumulation than the top hits tested in the previous study. It is currently not

known the factors that mediate endothelial cell targeting and future studies should address this issue. It is possible that a combination of NP cell internalisation, kinetics of NP disassembly and intrinsic NP physico-chemical properties may account for the differential NP uptake and gene knockdown activity among formulations. The best formulation identified in this study (C11) shows a balance between these 3 properties. Importantly, our results showed that the rapid disassembly (in the first 10 min after transfection) of formulations after cell transfection enhanced their gene knockdown activity. Future studies should evaluate the *in vivo* efficacy of the current formulation. Overall, our results report a new strategy to identify formulations for efficient endothelial RNA delivery and specifically to inhibit the activity of PHD2, an enzyme that controls the stability of HIF-1α.

Acknowledgements

The authors would like to thank the financial support of ERA Chair project (ERA@UC, ref:669088) through EU Horizon 2020 program, the POCI-01-0145-FEDER-016390 (acronym: CANCEL STEM), POCI-01-0145-FEDER-029414 (acronym: LIghtBRARY) and UID/NEU/04539/2019 projects through Compete 2020 and FCT programs.

Conflict of interest

The authors declare no conflict of interest

5 MATERIALS and METHODS

Synthesis of polymers. The library of poly(amido amine)s with light-cleavable moiety (NVOC) was synthesised via Michael addition reaction. Prior to synthesis, diamines (1-22), bisacrylamides A-E were diluted to 1.6 M in anhydrous DMSO (Sigma-Aldrich). Specifications of all monomers can be found in supplementary Table 1. After designing the plate layout for the 110 combinations between monomers A-E and 1-22, 100 µL aliquots of bisacrylamides and 100 µL aliquots of diamines were added to each well of a 96-deepwell plate (polypropylene (PP), VWR). The plates were sealed with aluminum foil and incubated for reaction at 60 ºC shaking for five days on an orbital shaker (250 rpm). Polymers were finally end capped with 20% molar excess (10 µL to 100 µL reaction volume) of the respective diamine 1-22 for 2 h (60ºC, 250 rpm). Next, the polymers were functionalised with 4,5-dimethoxy-2-nitrobenzyl chloroformate (NVOC, Sigma-Aldrich) in the presence of triethylamine (10% molar ratio, Sigma-Aldrich). The reaction was performed overnight under shaking at room temperature. Finally, the plates were stored at 4ºC until usage.

Determination of the best photocleavable group ratio in poly(amido amine)s. To optimize the amount of the photocleavable group in the poly(amido amine), ratios of 1:4, 1:8 and 1:12 of NVOC to diamine were used in the synthesis of A4 polymer. To obtain the degree of substitution of NVOC in the polymer, A4 was purified by precipitation in water, lyophilised, resuspended in DMSO-d6 and analysed by ^{1}H-NMR (Bruker Avance III 400 MHz) relative to TMS. After preparation of nanoparticle with the polymers with different NVOC ratio, size and count decrease of the nanoparticles before and after UV irradiation (10 min, 365 nm, 100 mW/cm2) were measured by DLS.

Evaluation of the best ratio siRNA:NP and transfection time in the gene knockdown efficiency. siRNA:NP ratio was optimised with formulation A4 to maximize GFP knockdown. A suspension of A4 NPs (200 µg/mL) was complexed for 2 h with siRNA against GFP in ratios of 1:12.5, 1:25 and 1:50 (w/w) in nuclease free sterile water under shaking on an orbital shaker (250 rpm) at room temperature. To bioactivity of the complexes were evaluated in HeLa-GFP cells which were seeded at a density of 40.000 cells/mL for 24 h prior the experiment. Cells were transfected for 4 h with NP@siRNA complexes (20 µg/mL) in starvation (DMEM), washed, fresh medium with reduced serum (DMEM, 5% FBS, 0.5% PenStrep) added and

cultured for additional 48 h. After 48 h, cells were stained with H33342 and PI (both 0.25 μg/mL) and analysed by fluorescence microscopy on a high-content microscope (In Cell Analyzer 2200). The quantification of cell viability and GFP knockdown is described in high content imaging section below.

The transfection time was optimised to identify a time relatively short that could lead to significant gene knockdown. In this way, cells were transfected with NP@siRNA complexes (20 μg/mL; 1:50 siRNA:NP (w/w)) from 10 min to 4 h. After a washing step, cells were cultured in medium with reduced serum (DMEM, 5% FBS, 0.5 % PenStrep) until 48 h. Cells were stained with H33342 and PI (both 0.25 μg/mL) and analysed by fluorescence microscopy on a high-content microscope (In Cell Analyzer 2200) for GFP knockdown (described in high content imaging section below).

Gel permeation chromatography (GPC) analyses. Molecular weights (Mn) and molecular weight distributions (Mw/Mn) of selected polymers were measured by GPC on a HPLC Agilent 1260 system equipped with a guard column (Agilent, Aquagel, 10 mm, 10 μm) followed by three columns: (i) Agilent, Aquagel-OH 40, 300 × 7.5 mm, 8 μm, (ii) Agilent, Aquagel-OH 50, 300 × 7.5 mm, 8 μm and (iii) Phenomenex, Polysep-GFC-P2000, 300 × 7.8 mm, range 100 – 10 k Da, connected to a UV (254 and 280 nm) and RI detector (Agilent). The GPC eluent was acetate buffer (0.5 mol/L, pH = 4.5), and the polymers were eluted at 0.7 mL/min. The temperature was set at 35 °C. Polyethylene oxide standards (EasyVial PEG/PEO, range 194 – 1000 k Da) were used to calibrate the SEC, since it has been demonstrated that such eluent composition allows PEO to be a suitable calibration standard for poly(amido amines).[380]

NP library preparation. Nanoparticle library was prepared in sterilised 96-deepwell plates by precipitation 15 μL of each polymer in water (960 μL, molecular biology grade, Fisher Bioreagents) and further addition of 25 μL of zinc sulfate (1M, Sigma-Aldrich). Plates were sealed with PP adhesive seals and left stirring on an orbital shaker (250 rpm) at 25 °C. After a step of purification (centrifugation at 4 °C, 8000 g for 8 min), the samples were resuspended in water (molecular biology grade) and lyophilised to determine the mass concentration of each nanoparticle. The efficiency of NP formation was calculated according to equation:

$$NP\ formation\ efficiency\ (\%) = \frac{M_{NP}}{M_{polymer}} \times 100$$

where MNP denotes the weight of material recovered after NPs purification and freeze-drying and Mpolymer is the theoretical polymer weight.

Characterisation of NP size and zeta potential. The diameter and zeta potential of NPs was measured by photon correlation spectroscopy (PCS) using quasi-elastic light scattering equipment (ZetaPALS analyser, Brookhaven Instruments Corp., Holtsville, NY) and ZetaPlusTM Particle Sizing Software (version 4.03). The scattered light was collected at fixed angle of 90º. To measure NPs size, a suspension of NP in water (molecular biology grade) was added to a cuvette (50 µg/mL, 2 mL), allowed to stabilize for 10 minutes and then analysed at room temperature (3 times). To assess the percentage of NPs disassembly upon UV light irradiation (10 min, 365 nm, 100 mW/cm2), a duplicate of the samples was used and the values of NP diameter and NP counts (Kcps) were recorded. The zeta potential of NPs was determined in a 1 mM KCl solution at 25 ºC (50 µg/mL, 2 mL). All data were recorded as the mean of 5 measurements runs.

TEM analyses. The analysis was carried out on a FEI-Tecnai Spirit BioTwinG2 electron microscope. Aqueous dispersion of C11 NPs (500 µg/mL) was added on the surface of carbon coated 200 mesh copper grid and left air-dry for 5 h at room temperature in a closed petri dish. Digital images were acquired with coupled side mounted CCD camera MegaView III-SIS and the diameter of NPs was analysed with the Particle Tool from ImageJ.

High-throughput complexation of siRNAs with NPs. In a 96-deepwell plate, the NPs (50 µL, 400 µg/mL) were complexed with siRNA against eGFP (50 µL, 4 µg/mL siRNA and 4 µg/mL Cy5-tagged siRNA, GFP Duplex I, GE Dharmacon) at a weight ratio 1:50 (siRNA:NP). As control for siRNA activity and transfection, the same procedure was followed for lipofectamine RNAiMAX (15 µL/mL; Invitrogen). The plates were sealed (PP seals) and allowed to incubate at room temperature for 2 h on an orbital shaker (250 rpm). Samples were then diluted 1:10 with DMEM to 20 µg/mL NP concentration and directly used for cell transfection or determination of complexation efficacy. Complexation efficacy was determined indirectly from Cy5 tagged-siRNA after separating NPs and non-complexed siRNA by centrifugation (4ºC, 14.000g, 15 min), quantifying Cy5 fluorescence in three replicates of the supernatant. Concentration of siRNA was determined relative to a standard curve.

High-throughput transfections with NP@siRNA. Stable transfected HeLa-GFP (CellBiolabs Inc.) reporter cells were cultured in DMEM (without phenol red) containing FBS (10%, v/v), PenStrep (0.5%, v/v, 50 µg/mL) and blasticidin (10 µg/mL). 24 hours prior to the experiment, HeLa-GFP cells were seeded in 96 well plates (Costar) with a density of 4.000 cells per well. NP@siRNA complexes (20 µg/mL) or lipofectamine RNAiMAX (1.5 µL/ml) were prepared in DMEM as described above. Cell transfections were performed with three technical replicates and plates in duplicate. After 10 min of cell material contact for transfection, medium was replaced by DMEM containing 5% FBS (v/v), PenStrep (0.5%, v/v, 50 µg/mL) and blasticidin (10 µg/mL). One plate duplicate was used for activation of the NP using a transilluminator (10 min, 365 nm, UVP BioSpectrum 500). The second plate of the duplicate (with same sample layout) remained without NP activation, allowing comparison of the bioactivity of released siRNA with and without activation by the light trigger. 48 h post transfection, cells were stained and placed in an automated incubator (Cytomat 2, Thermo) for high-content imaging analysis with an automated fluorescence microscope (In Cell 2200, GE Healthcare).

High-content imaging analyses. To distinguish viable cells from dead cells, cell nuclei were stained with Hoechst 33342 (Sigma-Aldrich, 0.25 µg/mL) and propidium iodide (PI, Sigma-Aldrich, 0.25 µg/mL). Dead cell nuclei are permeable for PI and show staining for H33342 and PI, where live cells are stained only with H33342. 48 h and 72 h post transfection, cells were analysed on a high-content microscope (In Cell 2200, GE Healthcare) with a 20× objective, where 4 random image fields per well were imaged. Image analysis was performed with In Cell Developer software (GE Healthcare), applying machine learning algorithms. H33342 staining was used for definition of a nuclear mask (nuclei). Dead cell masks, with PI and H33342 staining overlapping 10% (dead nuclei) were subtracted from H33342 nuclear mask, resulting in viable nuclear population (viable nuclei). That mask was then dilated to cover as much of the cell region possible (cell). Next, nuclear mask was subtracted from the cell mask, resulting in a ring that masks the cytoplasm. GFP fluorescence intensity was measured in that cytoplasm mask of live cells. GFP knockdown was calculated as percentage of fluorescence on non-treated HeLa-GFP cells (after subtracting HeLa cell fluorescence background). From the difference of the total count of nuclei and dead nuclei count, cell viability was calculated. By quantification of the Cy5 tagged siRNA in the cytoplasm, internalisation of the NP was quantified.

siRNA release from C11 NPs after UV light irradiation. The release of siRNA from C11 (50 µg/mL, weight ratio 1:50 siRNA:NP, molar ratio 1:58 siRNA:NP) after UV-irradiation (10 min, 365 nm, 1 mW/cm2) was determined by quantification of Cy5 tagged-siRNA in the supernatant after centrifugation (4°C, 14000g, 15 min). The concentration of siRNA-Cy5 was determined by fluorescence in a microplate reader (Synergy H1) relative to a standard curve ($y = 3978.3x - 61.87$; $R2 = 0.9869$).

Cellular internalisation profiling of NPs. Human dermal keratinocytes (HaCaT cells; CLS Cell Lines Service GmbH, Eppelheim, Germany), human normal dermal fibroblast (NHDF) or human umbilical vein endothelial cells (HUVEC, Lonza) were used to quantify internalisation of NP@siRNA complexes by colocalisation with the endolysosomal compartment. HaCaT and NHDF cells were cultured in DMEM medium, HUVECs were cultured in EGM-2 medium (Lonza). All media was supplemented with FBS (10%, v/v) and PenStrep (0.5%, v/v, 50 µg/mL). Twenty-four hours prior to the experiment, cells were seeded to each well in black glass bottom 96 well plates (IBIDI, Germany) coated with 0.1% gelatine (Sigma) with densities of HaCaT and HUVECs at 20.000 cells/well, NHDF cells at 10.000 cells/well. Cells were stained with CellTrace™ CFSE 488 (5 µM; Molecular Probes, Life Technologies) according to manufacturer's instructions prior to the experiment. For cell transfection, cells were incubated for 1 h with NP@siRNA-Cy5 or lipofectamine@siRNA-Cy5 complexes in DMEM or EGM-2 media. Lysotracker Red (100 nM; Molecular Probes, Life Technologies) staining was added for 30 min during cell transfection. Next, complexes were removed, and cells were washed twice with PBS. After fixation with 4% (v/v) paraformaldehyde (Alfa Aesar) in PBS for 10 min at room temperature, cell nuclei were stained with H33342 (2 µg/mL) for 10 min and subsequent washes with PBS. Cells were analysed by confocal microscopy (Zeiss LSM710) using a 40× immersion oil objective with two technical replicates per condition and a minimum of four representative image fields per replicate. Colocalisation of NP@siRNA-Cy5 with Lysotracker red was analysed using JaCoP on ImageJ.

Complexation of PHD2 to the NPs. The complexation of PHD2 (GE Dharmacon) to C11 NPs followed the same procedure previously described for siRNA. Briefly, PHD2 and C11 NPs were mixed in molecular grade nuclease free, sterile water (Fisher Bioreagents) in a ratio of 1:50 (w/w, siRNA to NPs), and the suspension agitated on an orbital shaker for 2 h at room temperature. After complexation, the NP suspension was suspended in cell culture medium before use.

Proliferation of endothelial cells. To assess cell proliferation, EOMA-GFP cells cultured in DMEM medium containing FBS (10%, v/v) and PenStrep (0.5%, v/v, 50 µg/mL), were seeded in 24 well plates (7.500 cells/well; pre-coated for 10 min with 0.1% gelatine) and allowed to adhere overnight. Cells were transfected with C11@PHD2 complexes (20 µg/mL) for 12 h in DMEM with reduced FBS (2.5%, v/v and PenStrep). We have chosen 12 h because shorter transfection times did not translate in measurable functional activity (data not shown). Non-internalised NPs were removed, and medium was replaced by complete medium with 10% FBS (v/v) and PenStrep. NPs were activated with UV light, using a transilluminator (365 nm, 10 min, 1 mW/cm2; UVP BioSpectrum 500). Cell growth was analysed at 36 h post transfection by staining the cells with H33342 (1 µg/mL, Sigma) and fluorescence imaging (In Cell 2000). Nuclei were counted from H33342 nucleus staining on In Cell Developer. Each experimental condition was performed with at least three technical replicates. Six images per well were analysed.

Angiogenesis - Tube formation in matrigel. EOMA-GFP cells were seeded at 30.000 cells/well to 24 well plate pre-coated for 10 min with 0.1% gelatine. Cells were transfected for 12 hours with 20 µg/mL C11-PHD2 in DMEM with reduced FBS (2.5%, v/v) and PenStrep (0.5%, v/v, 50 µg/mL). Non-internalised NPs were removed by washing with PBS. Cells were treated with trypsin (conc.) for 1 minute. Trypsin was blocked by adding DMEM containing 10% FBS (v/v). Cells from each condition were collected, centrifuged (250 rpm, 3 min) and resuspended in complete medium. Cells from each experimental condition were counted and 4000 cells/well were seeded into each well of Angiogenesis 15-µ-slides (IBIDI) previously prepared containing 10 µL Matrigel, which was polymerised for 1h at 37 ºC. NPs were activated with blue light, using a transilluminator (365 nm, 10 min, 1 mW/cm^2; UVP BioSpectrum 500). At 6 hours post cell inoculation, cells were imaged by brightfield microscopy. Tube length, Loop count and branching points were analysed by IBIDI angiogenesis analyser.

***In vitro* wound healing assay.** EOMA-GFP cells (15.000 cells/well) were seeded in 96 well plates (pre-coated for 10 min with 0.1% gelatine) 24 h prior to experiment to allow cells to grow to a complete monolayer in full medium (DMEM with FBS (10%, v/v) and PenStrep (0.5%, v/v, 50 µg/mL)). Cells were then inhibited by mitomycin (5 µg/mL, in cell culture medium, Tocris Bioscience) for 2 h and then transfected for 12 h with C11@PHD2 NPs (20 µg/mL) in DMEM with FBS (2.5%, v/v) and PenStrep (0.5%, v/v, 50 µg/mL). We have chosen 12 h because shorter transfection times did not translate in measurable functional activity (data not shown). NPs were then removed from the cells and washed with PBS. The monolayer was wounded, by scratching the cells with a yellow (200 µL) pipette tip. Cell debris and detached cells were removed by gently washes with PBS. Fresh medium (DMEM with FBS (1%, v/v) and PenStrep (0.5%, v/v, 50 µg/mL)) was added. NPs were then activated with UV light, using a transilluminator (365 nm, 10 min, 1 mW/cm2; UVP BioSpectrum 500). Wound healing was monitored until 36 h post-scratch using brightfield microscopy (4x objective) on an automated microscope (In Cell 2000). Wound area was quantified by measuring cell free area with ImageJ. Relative wound closure was calculated at 36 h post wounding relative to time 0 h and normalised to control condition.

Quantitative analysis of PHD2 transfection by qRT-PCR. EOMA-GFP cells were seeded at 30.000 cells/well to 24 well plate pre-coated for 10 min with 0.1% gelatine. Cells were transfected for 12 h with C11-PHD2 (20 µg/mL) in DMEM with reduced FBS (2.5%, v/v) and PenStrep (0.5%, v/v, 50 µg/mL). Non-internalised NPs were removed by washing with PBS and further incubation with fresh medium (DMEM, 10% FBS, v/v 0.5% PenStrep). NPs were activated with UV light, using a transilluminator (365 nm, 10 min, 1 mW/cm2; UVP BioSpectrum 500). After 24 h, cells from each condition were harvested after application of lysis buffer. RNA extraction was performed using RNeasy Plus Micro Kit (Quiagen) following manufacturers instruction. RNA was quantified on NanoDrop (Thermo Scientific). 1 µg total RNA was used to synthesize cDNA with qScript cDNA SuperMix (Quantabio). Quantitative RT-PCR was performed using NZYSpeedy qPCR Green Master Mix (NZYTech, Portugal) on a RT-PCR (CFX Connect Real-Time System, BioRad). Quantification of the target gene (PHD2) was analysed relative to GAPDH as housekeeping gene: $relative\ expression = 2^{[-(C_T\ Sample - C_T\ GAPDH)]}$ (Table 16). Minimal cycle threshold values (CT) were calculated from at least 3 independent reactions. ΔΔCT was calculated to determine relative PHD2 expression.

C11 NPs disassembly after UV light irradiation through a skin barrier. To demonstrate that NPs placed under a skin biopsy can be disassembled by UV light, a skin fragment (taken from the back of the mouse) was placed in a 1 cm2 hole of a cardboard and a cuvette with a suspension of C11@siRNA (50 µg/mL) placed beneath the skin. The cuvette was irradiated with UV light (365 nm, 10 min, 1 mW/cm2) and the number of NPs monitored by DLS. As control, a cuvette with C11@siRNA (50 µg/mL) was used in the same set up but without skin.

Table 16: Sequence of primers used in qRT-PCR experiments.

Gene		Sequence	Species
m-PHD2	FW RW	CCACTGGCACTCAACTAACTCA CCGAGTTCATTTAGTGCCCGTCA	mouse
m-GAPDH	FW RW	AAGGTCATCCCAGAGCTGAA CTGCTTCACCACCTTCTTGA	mouse

Table 17: Detailed description of name, CAS, Vendor of library monomers.

Monomer	Chemical Name IUPAC	CAS	Vendor
A	Methylenebisacrylamide	110-26-9	Aldrich
B	Hexamethylenebisacrylamide	7150-41-6	Polyscience
C	Cystaminebisacrylamide	6098-457-8	Polyscience
D	Dihydroxyethylenebisacrylamide	868-63-3	Aldrich
E	Bisacryloylpiperazin	6342-17-2	Sigma
P1	(2-Nitro-1,3-phenylene)bis(methylene)diacrylate	1599460-50-0	Synthesized
1	Ethylenediamine	107-15-3	Merck
2	1,4-Diaminobutan	110-60-1	Aldrich
3	1,6-Diaminohexan	124-09-4	Alfa Aesar
4	Diethylenetriamine	111-40-0	Alfa Aesar
5	Triethylenetetraamine	112-24-3	Acros Organics
6	Pentaethylenehexamine	4067-16-7	Aldrich
7	3,3'-Diamino-N-methyldipropylamine	105-83-9	Aldrich
8	1,2-Diaminocyclohexane	694-83-7	Aldrich
9	1,8-Diamino-3,6-dioxaoctane	929-59-9	Acros Organics
10	1,13-Diamino-4,7,10-trioxatridecane	4246-51-9	Aldrich
11	1,4-Bis(aminopropyl)piperazine	7209-38-3	Aldrich
12	1,4-Phenylenedimethanamine	539-48-0	Merck
13	1,5-Diaminonaphthalene	2243-62-1	Aldrich
14	4,4'-methylenedianiline	101-77-9	Aldrich
15	1,3-Phenylenediamine	108-45-2	TCI Chemicals
16	1,3-Diaminopropane	109-76-2	TCI Chemicals
17	2,2-Dimethyl-1,3-propanediamine	7328-91-8	TCI Chemicals
18	1,3-Diaminopentane	589-37-7	TCI Chemicals
19	2,2'-Diamino-N-methyldiethylamine	4097-88-5	TCI Chemicals
20	Agmatine sulfate	2482-00-0	TCI Chemicals
21	1,4-Bis(aminomethyl)cyclohexane	2579-20-6	TCI Chemicals
22	4,4'-Methylenebis(cyclohexylamine)	1761-71-3	Aldrich

CHAPTER V – CONCLUSION

1 DISCUSSION

Globally increasing prevalence and cost for treatments of chronic or non-healing wounds together with associated medical complications are one of the most challenging issues for healthcare systems around the world with wealth growing societies[286–289]. RNA-based therapies have emerged recently as promising drugs for skin regeneration (Table 9). RNAi drugs as microRNA and short interference RNA (siRNA) are very potent therapeutics due to their high specificity and selectivity for targets that are independent of the cellular expression system, giving the possibility to interfere in the regulation of any mRNA target[1]. Delivery vehicles are necessary to protect RNAi therapeutics from degradation, to promote cell and tissue uptake[32] and to avoid toxicity. From the discovery of the mechanism[6] until the clinical approval of the first siRNA drug it took almost twenty years[7]. Most of the clinical studies with siRNA were performed without carrier. Clinical trials with microRNAs reached maximum phase II[68], so far. Failure of clinical trials are associated to high toxicity (infusion/ immune reaction) and lack of efficacy. Strategies for efficient RNAi delivery are still limited due to obstacles related to cellular targeting and intracellular delivery. The first clinically approved formulation for RNAi therapy comprises an LNP-GalNAc siRNA formulation[7], which was found through development of pH sensitive libraries of lipids[112,159] and lipid-like materials[158] (see also Table 6) in high-throughput screenings for silencing firefly luciferase reporter in HeLa cells. However, the endosomal escape of leading LNP formulations for siRNA delivery was shown to be as low as 2% *in vitro* and *in vivo*[129], limited by a very short timeframe after endocytosis[3] and restricted to the liver as target organ. Despite severe immune reactions[381], LNPs and LNP-GalNAc conjugates are the most frequent carriers in clinical trials with siRNA therapeutics (see analysis in Figure 4B). Therefore, it is imperative to invest more in the development of non-toxic carriers for effective intracellular small non-coding RNA delivery. Especially in the area of local and topical delivery to eye and skin for which more than 70% of clinical trials are registered with naked siRNA. Nanoparticles allowing controlled drug release through activation with an external trigger are intensively studied for this purpose[133]. Especially light-triggered materials seem to be promising for efficient *in vivo* delivery of bioactive compounds and small non-coding RNAs[185,236,330].

This thesis focused on the development of a library of light-activatable, biocompatible polymeric nanoparticles for the delivery of small non-coding RNAs as siRNA and microRNA.

The main hypothesis of this thesis is that light-activatable nanoparticles allow precise control of the timing and spatial release of the RNA molecule which in turn enhances gene silencing efficacy and would accelerate translation of the technology. By using NP libraries with high diversity in terms of chemical composition, size and geometry, formulations can be identified for enhanced cell targeting. Lacking hypothesis of structures beneficial to increase endosomal escape of NPs make the design and screening of NP libraries favorable to identify the most efficient carrier for rapid and effective intracellular siRNA release[111,112]. For this purpose, two libraries with high physico-chemical diversity were designed to create light sensitive polymers, following two synthetic strategies, including a (i) photo-cleavable linker as presented in Chapter 3, or a (ii) photo-responsive antenna as described in Chapter 4.

For the library design we have selected Michael-type addition reaction, which gives the possibility through a simple synthetic scheme and high diversity of monomers (hydrophobic, hydrophilic, increased O-, N-content, bioreducible disulphide bonds) to synthesize polymers with high physico-chemical diversity. Compounds identified in previous high-throughput screens were included[111,136,137]. Most of the previous library screens for efficient gene (including DNAs and RNAs) delivery vehicles prepared for the transfection polyplex[111,136,137,256] or lipoplex[112,158,159] by mixing soluble polymers/lipid with the gene material. In this work NPs were produced from the polymer libraries by nanoprecipitation. It is important to highlight, that in this work NPs were synthesized before addition of small ncRNAs and no polyplex were formed. In order to achieve light sensitivity of the NP, stability of the NPs needs to be dependent on the interaction with the light sensitive compound. The photo-cleavable crosslinker (P1) and the photo-antenna (NVOC) contain both a hydrophobic, aromatic ring. The hydrophobic-hydrophilic interactions between hydrophobic photo-sensitive compound and hydrophilic (amine endcapped) polymer determine stability and light sensitivity of the NPs, as shown in this work by substitution of crosslinkers with different ratios of photo-sensitive P1 (Figure 28D), or different degree of amine substitution with NVOC (Figure 45B). Highest rates of disassembly (80%, as percentage count decrease relative to before light activation) were achieved when half of the crosslinker was substituted by P1 in two formulations. 70% of the NP library respond to the light trigger with more than 75% count decrease to the stimulus. For the photo-antenna library this population only comprised 30% of the NP formulations. When analysing NPs with different rates of amine substitution with NVOC, dissociation rates are almost similar (80-90%) between 4.5 and 20% of DS, but NP diameter changes to more condensed NPs with highest DS (165 nm) and smallest fragments after photo-activation and disassembly (2.2 nm). Comparing the NP populations with sizes below 300 nm in both libraries, almost 60% of the NVOC library show diameters below 300 nm, whereas only 38% of the formulations of the P1 library are in that size range. These results indicate that

hydrophobic-hydrophilic interactions and other intramolecular forces in NPs with NVOC are stronger in comparison to P1 containing NPs, leading to generally smaller NPs with lower efficacy in the light response with the same energy for activation. This issue requires further investigation. The data shows in zeta potential measurements from both libraries, values accumulating around 12.8 mV with 10% of NPs above 25 mV. Most of those formulations are from the photo-antenna library, predominantly composed of crosslinker A or C and diamines with high amine content (triethylenetetraamine), aliphatic domains (1,4-bis(aminomethyl)cyclohexane) or aromatic moieties (1,5-diaminonaphthalene). Through positive surface charge of the NPs, net negatively charged small non-coding RNAs can be immobilised by electrostatic interaction on the NPs. Mostly positive zeta potential translated in complexation efficacy of more than 75% of initially applied siRNA (in ratio 1:50, w:w, siRNA:NP) for a third of the NPs. However, only few correlations between both data sets exist. NPs with complexation efficacies above 90% are predominantly constituted by crosslinker P1, C and diamines with higher amine content and aliphatic moieties (triethylene tetraamine and 3,3‘-diamino-N-methyldipropylamine) in the polymer backbone.

One of the innovative aspects of this work is the focus of the high-throughput screening (HTS) on short times of cell-material contact for transfection and the use of high-content imaging for analysis. Previous library screens for RNAi transfection agents have been typically using single or dual luciferase reporters to screen for luciferase silencing[112,157]. In case of the dual reporter, gene silencing and cell viability can be analysed from the same experiment[155]. In this work, high-content imaging with automated image analysis was implemented to obtain cell-based information about multiple parameters of bioactivity caused by siRNA conjugated NPs. Few studies are published using HCI for nanoparticle mediated RNAi screening[129]. A model-system of GFP reporter with Cy5-tagged anti GFP siRNA was used with nucleus and PI live cell stains, to analyse GFP silencing, cell viability and internalisation from the same experiment by multiparametric image analysis. Procedures for HTS were standardised starting from cell culture and sample handling and several parameters were optimised, such as NP dose, ratio of siRNA:NP, and HT light activation to boost GFP silencing efficacy. Short timeframes for endosomal escape identified in previous work from Sahay et al.[3] took us to carry out the screening with short times of cell-material contact for transfection. Therefore, GFP silencing from NP@siRNA complexes with incubation for transfection below 4 hours were analysed with a subset of the library beforehand the screening. Those results showed, that 10 min of cell-material contact were sufficient to cause 50% bioactivity achieved with 4 hours of transfection time with NP@siRNA complexes. A commercial standard (Lipofectamine RNAiMAX) was used to compare transfection efficacy directly. By using 20 µg/ mL NP@siRNA, and 10 min light activation at 365 nm, almost

40% of the NPs from the library bearing the photo-antenna were identified with increased GFP silencing efficacy in comparison to a commercial transfection standard, without compromising cell viability. Bioreducible C11 was identified with highest global gene silencing efficacy applying the light trigger and two-fold increased silencing through light activation. In general, 18% of the NPs were identified with higher gene silencing efficacy and modulation through application of the light trigger. Constituted predominantly from crosslinker A or C and diamines with aliphatic domains. This data shows that NPs from polymers containing an NVOC-antenna are highly efficient transfection agents allowing temporal control over siRNA release. From the library with the photo-cleavable linker less than 10% of the formulations were found with higher GFP silencing efficacy as the commercial agent, with eight of those formulations showing increased bioactivity after light activation. As in the NVOC-library, C (N,N'-cystaminebisacrylamide) is the predominant crosslinker. The disulphide containing, bioredu1acible crosslinker N,N'-cystaminebisacrylamide was already identified in previous screenings to promote siRNA gene silencing efficacy[185-187, 191]. From that library, P1C7 and P1C5 were identified as lead formulations with high magnitude and temporal control over GFP silencing. One major difference between photo-antenna bearing and photo-cleavable crosslinker libraries are the dissociation products. Where NVOC is cleaved from the polymer chain, photo-activation of P1 causes fragmentation of the polymer backbone. The hypothesis might be that those short polymer fragments can protect the small non-coding RNA until loading in the RISC and consequently lead to higher GFP silencing efficacy. However, looking to overall response of the formulations, a higher quantity of NVOC containing formulations shows increased GFP silencing efficacy in comparison to the commercial agent, which would not support this hypothesis. Whereas, a formulation from the photocleavable-crosslinker library was identified with absolute highest GFP silencing and temporal control. This data also shows increased efficiency of siRNA delivery by using an external trigger in comparison to internal stimulus sensitive materials only[165,166,168].

The present thesis is one of the first studies proving transfection with less than one hour of cell material contact and early timepoints for endosomal escape and siRNA release for polymeric nanoparticles. After cellular internalisation, endosomal escape of siRNA carrying formulations was shown to be the main parameter limiting siRNA bioactivity *in vitro* and *in vivo*[2,3]. Internalisation of P1C7 (in HeLa cells) was shown to be driven mainly by scavenger receptor dependent endocytosis. Vesicles from the endosomal compartment that release siRNA (using LNP or lipoplex) were shown to recruit the autophagy marker galectin-8 within 15 min after internalisation[130]. Colocalisation of Cy5-tagged siRNA on P1C7 NPs with bright galectin-8 vesicles was visible after transfection and increased significantly until 60 min. For the commercial agent this was not the case. Increasing galectin-8 recruitment (measured by colocalisation and

galectin-8 particles) confirms endosomal escape of the formulation from transfection on. Analysis of the mean area of siRNA-Cy5 particles, high cellular internalisation of P1C7@siRNA-Cy5 was demonstrated in comparison to Lipofectamine@siRNA-Cy5. Notably, the mean area of those particles decreases about 50% right after light activation (0 min) and again about 50% 15 min post activation. This data indicates disintegration of the NPs and possibly dilution of the signal through release in the cytoplasm.

Library NPs are rapidly internalised in skin cells and show different tropism for specific cell types. The most important cell types for reepithelialisation of wounded tissue are keratinocytes, dermal fibroblasts and endothelial cells. For successful application of light-activatable RNAi therapeutics in skin regeneration, carriers need to be internalised in the cell type, where RNAi targets alter cell function. Lead formulations from the high-content screening were used and NP uptake in skin cells through colocalisation with endolysosomal compartment after one hour of cell transfection was evaluated and compared to commercial agent and a non-hit NP. The non-hit NP results are with generally higher magnitude in comparison to Lipofectamine as commercial agent. We have identified one formulation without tropism for a specific cell type (A10), one NP with tropism for endothelial cells (C11) and P1C7 with tropism for migratory cells (keratinocytes and fibroblasts). Bioreducible C11, with almost six-fold increased gene silencing efficacy relative to commercial standard and tropism for endothelial cells was combined with PHD2 siRNA, a regulator of the hypoxic cell response. Microvasculature disruption in injuries are the cause for ischemia, triggering HIF-1α signalling. PHD2 silencing causes HIF-1α stabilisation and activation of hypoxia response with increased angiogenesis, migration, proliferation through higher expression of VEGF and TGF-β among others. Endothelial cell response after treatment with C11@PHD2 and light activation was evaluated and confirmed increased PHD2 silencing through light activation by qRT-PCR. Boosted bioactivity of PHD2 siRNA released from C11@PHD2 NPs was observed in *in vitro* wound healing and proliferation assays. Those results turn C11@PHD2 a promising candidate to accelerate wound healing in acute and chronic wounds *in vivo* and translation of the technology for application in regenerative medicine.

Another novelty of this work is the application of a light-triggerable nanoparticle to efficiently deliver microRNA for wound healing *in vivo* with only a single intervention. Few studies are known with light activatable nanoparticles for *in vivo* micro-RNA delivery[185,235,351]. Photo-caged miR-92a showed limited potential in diabetic wounds, with no statistical differences in the wound healing kinetics. Other studies involve NIR activated nanoparticles with inorganic Au core, which could be an issue for clinical translation[185,351]. Wound closure kinetics are dependent on strongly migrating cells from the wound edge. The stimulatory effect of pro-migratory

microRNA-150 was shown by treating human keratinocytes with P1C7@miR150 NPs and light activation. Pro- proliferative effect of miR-150[330] was inhibited to not dilute the signal. Without application of the light trigger P1C7@miR150 shows similar migratory levels as transfection of miR-150 with a commercial agent. This highlight the boost in bioactivity of the small RNA by light activation. Accelerated wound healing kinetics *in vitro* were confirmed through treatment of full thickness excisional wounds in an acute wound healing mouse model (with statistical differences from day 1-5). Analysis of histological sections at day 10 showed progression to tissue remodelling stage of all wounds in the treatment group. Sustained silencing of miR-150 target MYB was confirmed by qRT-PCR in tissue at day 3. Those results show a novel strategy and high translational potential of light-activatable NPs to deliver topically non-coding RNAs.

This thesis describes a powerful platform with the first light-activatable nanoparticle library with remote activation and efficient *in vivo* non-coding RNA delivery in wound healing. Lower doses and significantly less material-cell contact is needed for efficient cell transfection and only one administration is necessary to create high bioactivity *in vivo*.

2 FUTURE WORK and PERSPECTIVE

One major contribution of this work is the demonstration of rapid transfection of different kind of cells. The material developed also serves as platform for transfection of cell lines, primary cells and hard to transfect cells (as shown by transfection of keratinocytes). Hereby strategies of *ex vivo* treatment with RNAi and re-implantation cells are possible to reprogram a diseased cell phenotype. For instance, by treatment of EPCs with NP conjugated to miR-155. *Ex vivo* treatment of pre-miR-155 was already shown to revert cellular malfunction of $CD34^+$ cells[382].

To better understand mechanisms of endosomal escape of polymeric siRNA and microRNA carriers, live cell imaging experiments following galectin-8 recruitment need to be conducted for longer time to clearly identify the full window of endosomal escape and from which time on NP@ siRNA formulations stay trapped in the endolysosomal compartment.

This work shows successful delivery of siRNA and microRNA with increased bioactivity after light activation. Through the structural and physico-chemical diversity, immobilisation of many kinds of RNAs (i.e. sgRNA for CRISPR/Cas gene editing[368]) are possible. Recently mRNA have emerged as therapeutic tool for reprogramming disease phenotypes[160]. New screening technologies for mRNA delivery for LNPs were developed[139]. The screening of polyplex using the photo-triggerable PAA library developed in this work shows promising results *in vitro* for cellular reprogramming.

The results presented here are an exciting first step towards the translation of light-triggerable polymeric carriers for RNA-based therapeutics delivery. The next steps to bring this technology from bench to the market are extensive toxicity tests to accomplish data required from regulatory authorities. As well as *in vivo* application in a clinically relevant context. For the use of P1C7 conjugated to miR-150 in a chronic wound healing model (such as full thickness excisional wounds in diabetic mice) we predict significant results in comparison to commercial agents for miR-150 delivery. In general, we envision topical application of the formulation which could be, for light penetration reason, to the eye or the skin. For ocular application (immobilised in a matrix or by intravitreal injection), ambient UV could be sufficient for sustained release of therapeutic small non-coding RNAs. Antunes et al. describe the use of a photo-cleavable linker where ambient UV is sufficient to promote photo-cleavage in a hyaluronic acid gel[330]. Furthermore, depending on the application, NPs with different light responses can be selected from the libraries. Especially for an application as wound healing, where the biological response follows a well-orchestrated process, combinations of bioactive molecules in a defined temporal pattern are interesting. Mainly

for microRNAs, that show very defined temporal pattern[345]. Therefore, NP formulations with different release profiles can be selected and combined with the corresponding bioactive molecule to achieve superior biological activity, fitting with natures' orchestra.

This work shows the successful development of a potent system for spatio-temporally controlled RNAi therapeutics drug delivery *in vivo* to their target site with high bioactivity. Barriers and limitations for RNAi delivery can be overcome with light-triggerable polymeric NPs, paving the way for the translation of RNAi therapeutics to the clinic.

BIBLIOGRAPHY

1. Howard, K. Unlocking the money-making potential of RNAi. *Nat. Biotechnol.* **21**, 1441–1446 (2003).
2. Gilleron, J. *et al.* Image-based analysis of lipid nanoparticle – mediated siRNA delivery, intracellular trafficking and endosomal escape. *Nat. Biotechnol.* **31**, 638–646 (2013).
3. Sahay, G. *et al.* Efficiency of siRNA delivery by lipid nanoparticles is limited by endocytic recycling. *Nat. Biotechnol.* **31**, 653–658 (2013).
4. Perrie, Yvonne; Rades, T. Controlling drug delivery. in *Pharmaceutics: Drug Delivery and Targeting* 1–24 (1999).
5. Yun, Y. H., Lee, B. K. & Park, K. Controlled Drug Delivery: Historical perspective for the next generation. *J. Control. Release* **219**, 2–7 (2015).
6. Fire, A. *et al.* Potent and specific genetic interference by double-stranded RNA in Caenorhabditis elegans. *Nature* **391**, 806–811 (1998).
7. Mullard, A. FDA approves landmark RNAi drug. *Nat. Rev. Drug Discov.* **17**, 613–613 (2018).
8. Morrison, C. Alnylam prepares to land first RNAi drug approval. *Nat. Rev. Drug Discov.* **17**, 156–157 (2018).
9. Mohr, S. E., Smith, J. A., Shamu, C. E., Neumüller, R. A. & Perrimon, N. RNAi screening comes of age: Improved techniques and complementary approaches. *Nat. Rev. Mol. Cell Biol.* **15**, 591–600 (2014).
10. Kanasty, R. L., Whitehead, K. A., Vegas, A. J. & Anderson, D. G. Action and reaction: The biological response to sirna and its delivery vehicles. *Mol. Ther.* **20**, 513–524 (2012).
11. Fabian, M. R., Sonenberg, N. & Filipowicz, W. Regulation of mRNA Translation and Stability by microRNAs. *Annu. Rev. Biochem.* **79**, 351–379 (2010).
12. Shin, C. *et al.* Expanding the MicroRNA Targeting Code: Functional Sites with Centered Pairing. *Mol. Cell* **38**, 789–802 (2010).
13. Fedorov, Y. *et al.* Off-target effects by siRNA can induce toxic phenotype. *RNA* **12**, 1188–1196 (2006).
14. Jackson, A. L. *et al.* Expression profiling reveals off-target gene regulation by RNAi. *Nat. Biotechnol.* **21**, 635–638 (2003).
15. Tschuch, C. *et al.* Off-target effects of siRNA specific for GFP. *BMC Mol. Biol.* **9**, 1–14 (2008).
16. Wang, X. *et al.* Selection of hyperfunctional siRNAs with improved potency and specificity. *Nucleic Acids Res.* **37**, 1–9 (2009).
17. Khvorova, A., Reynolds, A. & Jayasena, S. D. Functional siRNAs and miRNAs exhibit strand bias. *Cell* **115**, 209–216 (2003).
18. Grimm, D. *et al.* Fatality in mice due to oversaturation of cellular microRNA/short hairpin RNA pathways. *Nature* **441**, 537–541 (2006).

19. Castanotto, D. *et al.* Combinatorial delivery of small interfering RNAs reduces RNAi efficacy by selective incorporation into RISC. *Nucleic Acids Res.* **35**, 5154–5164 (2007).

20. Giering, J. C., Grimm, D., Storm, T. A. & Kay, M. A. Expression of shRNA from a tissue-specific pol II promoter is an effective and safe RNAi therapeutic. *Mol. Ther.* **16**, 1630–1636 (2008).

21. Sledz, C. A., Holko, M., De Veer, M. J., Silverman, R. H. & Williams, B. R. G. Activation of the interferon system by short-interfering RNAs. *Nat. Cell Biol.* **5**, 834–839 (2003).

22. Bridge, A. J., Pebernard, S., Ducraux, A., Nicoulaz, A. L. & Iggo, R. Induction of an interferon response by RNAi vectors in mammalian cells. *Nat. Genet.* **34**, 263–264 (2003).

23. Gantier, M. P. & Williams, B. R. G. The response of mammalian cells to double-stranded RNA. *Cytokine Growth Factor Rev.* **18**, 363–371 (2007).

24. Judge, A. D. *et al.* Sequence-dependent stimulation of the mammalian innate immune response by synthetic siRNA. *Nat. Biotechnol.* **23**, 457–462 (2005).

25. Deleavey, G. F. & Damha, M. J. Designing chemically modified oligonucleotides for targeted gene silencing. *Chem. Biol.* **19**, 937–954 (2012).

26. Gooding, M., Malhotra, M., Evans, J. C., Darcy, R. & O'Driscoll, C. M. Oligonucleotide conjugates – Candidates for gene silencing therapeutics. *Eur. J. Pharm. Biopharm.* **107**, 321–340 (2016).

27. Watts, J. K., Deleavey, G. F. & Damha, M. J. Chemically modified siRNA: tools and applications. *Drug Discov. Today* **13**, 842–855 (2008).

28. Jackson, A. L. *et al.* Position-specific chemical modification of siRNAs reduces 'off-target' transcript silencing. *RNA* **12**, 1197–1205 (2006).

29. Amarzguioui, M., Holen, T., Babaie, E. & Prydz, H. Tolerance for mutations and chemical modifications in a siRNA. *Nucleic Acids Res.* **31**, 589–595 (2003).

30. Allerson, C. R. *et al.* Fully 2'-Modified Oligonucleotide Duplexes with Improved in Vitro Potency and Stability Compared to Unmodified Small Interfering RNA. *J. Med. Chem.* **48**, 901–904 (2005).

31. Shen, W., Liang, X. H., Sun, H. & Crooke, S. T. 2'-Fluoro-modified phosphorothioate oligonucleotide can cause rapid degradation of P54nrb and PSF. *Nucleic Acids Res.* **43**, 4569–4578 (2015).

32. Dowdy, S. F. Overcoming cellular barriers for RNA therapeutics. *Nat. Biotechnol.* **35**, 222–229 (2017).

33. Kigasawa, K. *et al.* Noninvasive delivery of siRNA into the epidermis by iontophoresis using an atopic dermatitis-like model rat. *Int. J. Pharm.* **383**, 157–160 (2010).

34. Lee, W.-R., Shen, S.-C., Zhuo, R.-Z., Wang, K.-C. & Fang, J.-Y. Enhancement of Topical Small Interfering RNA Delivery and Expression by Low-Fluence Erbium:YAG Laser Pretreatment of Skin. *Hum. Gene Ther.* **20**, 580–588 (2009).

35. Inoue, T. *et al.* Modulation of scratching behavior by silencing an endogenous cyclooxygenase-1 gene in the skin through the administration of siRNA. *J. Gene Med.* **9**, 995–1001 (2007).

36. Robbins, P. D. & Ghivizzani, S. C. Viral vectors for gene therapy. *Pharmacol. Ther.* **80**, 35–47 (1998).

37. Chen, Y., Zhao, H., Tan, Z., Zhang, C. & Fu, X. Bottleneck limitations for microRNA-based therapeutics from bench to the bedside. *Pharmazie* **70**, 147–154 (2015).

38. Thomas, C. E., Ehrhardt, A. & Kay, M. A. Progress and problems with the use of viral vectors for gene therapy. *Nat. Rev. Genet.* **4**, 346–358 (2003).

39. Goswami, R. *et al.* Gene Therapy Leaves a Vicious Cycle. *Front. Oncol.* **9**, 1–25 (2019).

40. Senior, M. After Glybera's withdrawal, what's next for gene therapy? *Nat. Biotechnol.* **35**, 491–492 (2017).

41. Morrison, C. $1-million price tag set for Glybera gene therapy. *Nat. Biotechnol.* **33**, 217–218 (2015).

42. Meade, B. R. & Dowdy, S. F. Enhancing the cellular uptake of siRNA duplexes following noncovalent packaging with protein transduction domain peptides. *Adv. Drug Deliv. Rev.* **60**, 530–536 (2008).

43. Patlolla, R. R., Desai, P., Belay, K. & Singh, M. Translocation of Cell Penetrating Peptide Engrafted Nanoparticles Across Skin Layers. *Biomaterials* **31**, 5598–5607 (2010).

44. Wheeler, L. A. *et al.* Inhibition of HIV transmission in human cervicovaginal explants and humanised mice using CD4 aptamer-siRNA chimeras. *J. Clin. Invest.* **121**, 2401–2412 (2011).

45. Li, S. D. & Huang, L. Gene therapy progress and prospects: Non-viral gene therapy by systemic delivery. *Gene Ther.* **13**, 1313–1319 (2006).

46. Zimmermann, T. S. *et al.* Clinical Proof of Concept for a Novel Hepatocyte-Targeting GalNAc-siRNA Conjugate. *Mol. Ther.* **25**, 71–78 (2017).

47. Spiess, M. Perspectives in Biochemistry The Asialoglycoprotein Receptor : A Model for Endocytic Transport Receptors. *Biochemistry* **29**, (1990).

48. Schwartz, A. L., Fridovich, S. E. & Lodish, H. F. Kinetics of Internalisation and Recycling of Transferrin Receptor in a Human Hepatoma Cell Line. *J. Biol. Chem.* **257**, 4230–4237 (1982).

49. Cedillo, I. *et al.* Synthesis of 5-GalNAc-conjugated oligonucleotides: A comparison of solid and solution-phase conjugation strategies. *Molecules* **22**, 1–12 (2017).

50. Huang, Y. Preclinical and Clinical Advances of GalNAc-Decorated Nucleic Acid Therapeutics. *Mol. Ther. - Nucleic Acids* **6**, 116–132 (2017).

51. Adams, D. *et al.* Patisiran, an RNAi Therapeutic, for Hereditary Transthyretin Amyloidosis. *N. Engl. J. Med.* **379**, 11–21 (2018).

52. Jensen, S. A. *et al.* Spherical Nucleic Acid Nanoparticle Conjugates as an RNAi- Based Therapy for Glioblastoma. *Sci Transl Med* **30**, 209ra152 (2013).

53. Randeria, P. S. *et al.* siRNA-based spherical nucleic acids reverse impaired wound healing in diabetic mice by ganglioside GM3 synthase knockdown. *PNAS* **112**, 5573–5578 (2015).

54. Davis, M. E. The first targeted delivery of siRNA in humans via a self-assembling, cyclodextrin polymer-based nanoparticle: From concept to clinic. *Mol. Pharm.* **6**, 659–668 (2009).

55. Van Niel, G., D'Angelo, G. & Raposo, G. Shedding light on the cell biology of extracellular vesicles. *Nat. Rev. Mol. Cell Biol.* **19**, 213–228 (2018).

56. Fitzgerald, K. *et al.* A Highly Durable RNAi Therapeutic Inhibitor of PCSK9. *N. Engl. J. Med.* **376**, 41–51 (2016).

57. Scherer, L. J. & Rossi, J. J. Approaches for the sequence-specific knockdown of mRNA. *Nat. Biotechnol.* **21**, 1457–1465 (2003).

58. Kleinman, M. E. *et al.* Sequence- and target-independent angiogenesis suppression by siRNA via TLR3. *Nature* **452**, 591–597 (2008).

59. DeVincenzo, J. *et al.* A randomised, double-blind, placebo-controlled study of an RNAi-based therapy directed against respiratory syncytial virus. *Proc. Natl. Acad. Sci.* **107**, 8800–8805 (2010).

60. Crooke, S. T., Witztum, J. L., Bennett, C. F. & Baker, B. F. RNA-Targeted Therapeutics. *Cell Metab.* **27**, 714–739 (2018).

61. Couzin-Frankel, J. Roche exits RNAi field, cuts 4800 jobs. *Science (80-.).* **330**, 1163 (2010).

62. Bouchie, A. Markets, venture investors and big pharma interest in RNAi soars. *Nat. Biotechnol.* **32**, 203–204 (2014).

63. Walsh, G. Biopharmaceutical benchmarks 2018. *Nat. Biotechnol.* **36**, 1136- (2018).

64. Watchdog Research, Inc. Alnylam Pharmaceuticals , Price and Volume History. (2019).

65. Garber, K. Alnylam launches era of RNAi drugs. *Nat. Biotechnol.* **36**, 777–778 (2018).

66. Khorkova, O. & Wahlestedt, C. Oligonucleotide therapies for disorders of the nervous system. *Nat. Biotechnol.* **35**, 249–263 (2017).

67. Garber, K. & Arbor, A. Worth the RISC? *Nat. Biotechnol.* **35**, 198–202 (2017).

68. Wu, X. & Turnbull, A. P. Current trends in RNA-based therapeutic development. *Drug Discovery World Fall* 16–23 (2018).

69. Tabernero, J. *et al.* First-in-humans trial of an RNA interference therapeutic targeting VEGF and KSP in cancer patients with liver involvement. *Cancer Discov.* **3**, 406–417 (2013).

70. Coelho, T. *et al.* Safety and Efficacy of RNAi Therapy for Transthyretin Amyloidosis. *N. Engl. J. Med.* **369**, 819–829 (2013).

71. Zuckerman, J. E. *et al.* Correlating animal and human phase Ia/Ib clinical data with CALAA-01, a targeted, polymer-based nanoparticle containing siRNA. *Proc. Natl. Acad. Sci.* **111**, 11449–11454 (2014).

72. Khvorova, A. & Watts, J. K. The chemical evolution of oligonucleotide therapies of clinical utility. *Nat. Biotechnol.* **35**, 238–248 (2017).

73. Setten, R. L., Rossi, J. J. & Han, S. ping. The current state and future directions of RNAi-based therapeutics. *Nat. Rev. Drug Discov.* **18**, 421–446 (2019).

74. Fambrough, D. Weathering a storm. *Nat. Biotechnol.* **30**, 1166–1168 (2012).

75. Lai, W. & Wong, W. Design of Polymeric Gene Carriers for Effective Intracellular Delivery. *Trends Biotechnol.* **36**, 713–728 (2018).

76. Barenholz, Y. Doxil® - The first FDA-approved nano-drug: Lessons learned. *J. Control. Release* **160**, 117–134 (2012).

77. Bobo, D., Robinson, K. J., Islam, J., Thurecht, K. J. & Corrie, S. R. Nanoparticle-Based

Medicines: A Review of FDA-Approved Materials and Clinical Trials to Date. *Pharm. Res.* **33**, 2373–2387 (2016).

78. Pan, L. *et al.* Nuclear-Targeted Drug Delivery of TAT Peptide-Conjugated Monodisperse Mesoporous Silica Nanoparticles Limin. *J. Am. Chem. Soc.* **134**, 5722–5725 (2012).

79. Paulo, C. S. O., Vidal, M. & Ferreira, L. S. Antifungal nanoparticles and surfaces. *Biomacromolecules* **11**, 2810–2817 (2010).

80. Comune, M. *et al.* Antimicrobial peptide-gold nanoscale therapeutic formulation with high skin regenerative potential. *J. Control. Release* **262**, 58–71 (2017).

81. Suk, J. S., Xu, Q., Kim, N., Hanes, J. & Ensign, L. M. PEGylation as a strategy for improving nanoparticle-based drug and gene delivery. *Adv. Drug Deliv. Rev.* **99**, 28–51 (2016).

82. Nguyen, V. H. & Lee, B. J. Protein corona: A new approach for nanomedicine design. *Int. J. Nanomedicine* **12**, 3137–3151 (2017).

83. Cedervall, T. *et al.* Understanding the nanoparticle–protein corona using methods to quantify exchange rates and affinities of proteins for nanoparticles. *PNAS* **104**, 2050–2055 (2007).

84. Lundqvist, M., Stigler, J., Lynch, I., Cedervall, T. & Dawson, K. A. Nanoparticle size and surface properties determine the protein corona with possible implications for biological impacts. *PNAS* **105**, 14265-14270 (2008).

85. Salvati, A. *et al.* Transferrin-functionalised nanoparticles lose their targeting capabilities when a biomolecule corona adsorbs on the surface. *Nat. Nanotechnol.* **8**, 137–143 (2013).

86. Stolnik, S., Illum, L. & Davis, S. S. Long circulating microparticulate drug carriers ☆. *Adv. Drug Deliv. Rev.* **64**, 290–301 (2012).

87. Müller, L. K. *et al.* Pre-coating with protein fractions inhibits nano-carrier aggregation in human blood plasma. *RSC Adv.* **6**, 96495–96509 (2016).

88. Huang, L. & Liu, Y. In Vivo Delivery of RNAi with Lipid-Based Nanoparticles. *Annu. Rev. Biomed. Eng.* **13**, 507–530 (2011).

89. Bae, Y. H. & Park, K. Targeted drug delivery to tumours: Myths, reality and possibility. *J. Control. Release* **153**, 198–205 (2011).

90. Chou, L. Y. T., Ming, K. & Chan, W. C. W. Strategies for the intracellular delivery of nanoparticles. *Chem. Soc. Rev.* **40**, 233–245 (2011).

91. Saraiva, C. *et al.* Nanoparticle-mediated brain drug delivery: Overcoming blood-brain barrier to treat neurodegenerative diseases. *J. Control. Release* **235**, 34–47 (2016).

92. Pei-Hui Yang, Xuesong Sun, Chiu, J., Sun, H. & Qing-Yu He. Transferrin-mediated gold nanoparticle cellular uptake. *Bioconjug. Chem.* **16**, 494–496 (2005).

93. Venkataraman, S. *et al.* The effects of polymeric nanostructure shape on drug delivery. *Adv. Drug Deliv. Rev.* **63**, 1228–1246 (2011).

94. Oh, N. & Park, J. H. Endocytosis and exocytosis of nanoparticles in mammalian cells. *Int. J. Nanomedicine* **9**, 51–63 (2014).

95. Zhang, S., Li, J., Lykotrafitis, G., Bao, G. & Suresh, S. Size-dependent endocytosis of nanoparticles. *Adv. Mater.* **21**, 419–424 (2009).

96. Walkey, C. D., Olsen, J. B., Guo, H., Emili, A. & Chan, W. C. W. Nanoparticle size and surface chemistry determine serum protein adsorption and macrophage uptake. *J. Am. Chem. Soc.* **134**, 2139–2147 (2012).

97. Mukherjee, S., Gosh, R. N. & Maxfield, F. R. Endocytosis. *Physiol Rev* **77**, 759–803 (1997).

98. Sahay, G., Alakhova, D. Y. & Kabanov, A. V. Endocytosis of nanomedicines. *J. Control. Release* **145**, 182–195 (2010).

99. Conner, S. D. & Schmid, S. L. Regulated portals of entry into the cell. *Nature* **422**, 37–44 (2003).

100. Xia, T., Kovochich, M., Liong, M., Zink, J. I. & Nel, A. E. Cationic Polystyrene Nanosphere Toxicity Depends on Cell-Specific Endocytic and Mitochondrial Injury Pathways. *ACS Nano* **2**, 85–96 (2008).

101. Dos Santos, T., Varela, J., Lynch, I., Salvati, A. & Dawson, K. A. Quantitative assessment of the comparative nanoparticle-uptake efficiency of a range of cell lines. *Small* **7**, 3341–3349 (2011).

102. Voigt, J., Christensen, J. & Shastri, V. P. Differential uptake of nanoparticles by endothelial cells through polyelectrolytes with affinity for caveolae. *Proc. Natl. Acad. Sci.* **111**, 2942–2947 (2014).

103. Boussif, O. *et al.* A versatile vector for gene and oligonucleotide transfer into cells in culture and in vivo: Polyethylenimine. *PNAS* **92**, 7297–7301 (1995).

104. Andreason, G. L. & Evans, G. A. Optimisation of electroporation for transfection of mammalian cell lines. *Anal. Biochem.* **180**, 269–275 (1989).

105. Chu, G., Hayakawa, H. & Berg, P. Electroporation for the efficient transfecdon of mammalian cells with DNA. *Nucleic Acids Res.* **15**, 1311–1326 (1987).

106. Zhao, Y. *et al.* High-efficiency transfection of primary human and mouse T lymphocytes using RNA electroporation. *Mol. Ther.* **13**, 151–159 (2006).

107. Kooijmans, S. A. A. *et al.* Electroporation-induced siRNA precipitation obscures the efficiency of siRNA loading into extracellular vesicles. *J. Control. Release* **172**, 229–238 (2013).

108. Boukany, P. E. *et al.* Nonendocytic delivery of lipoplex nanoparticles into living cells using nanochannel electroporation. *Adv. Healthc. Mater.* **3**, 682–689 (2014).

109. Davis, A. A., Farrar, M. J., Nishimura, N., Jin, M. M. & Schaffer, C. B. Optoporation and genetic manipulation of cells using femtosecond laser pulses. *Biophys. J.* **105**, 862–871 (2013).

110. Xiong, R. *et al.* Laser-assisted photoporation: fundamentals, technological advances and applications. *Adv. Phys. X* **1**, 596–620 (2016).

111. Anderson, D. G., Lynn, D. M. & Langer, R. Semi-Automated Synthesis and Screening of a Large Library of Degradable Cationic Polymers for Gene Delivery. *Angew. Chemie - Int. Ed.* **42**, 3153–3158 (2003).

112. Akinc, A. *et al.* A combinatorial library of lipid-like materials for delivery of RNAi therapeutics. *Nat. Biotechnol.* **26**, 561–569 (2008).

113. Simeoni, F., Morris, M. C., Heitz, F. & Divita, G. Insight into the mechanism of the peptide-based gene delivery system MPG: Implications for delivery of siRNA into

mammalian cells. *Nucleic Acids Res.* **31**, 2717–2724 (2003).

114. Suckfuell, M. *et al.* Efficacy and Safety of AM-111 in the Treatment of Acute Sensorineural Hearing Loss. *Otol. Neurotol.* **35**, 1317–1326 (2014).

115. Bates, E. *et al.* Intracoronary KAI-9803 as an adjunct to primary percutaneous coronary intervention for acute ST-segment elevation myocardial infarction. *Circulation* **117**, 886–896 (2008).

116. Touchard, E. *et al.* A peptide inhibitor of c-Jun n-terminal kinase for the treatment of endotoxin-induced uveitis. *Investig. Ophthalmol. Vis. Sci.* **51**, 4683–4693 (2010).

117. Guidotti, G., Brambilla, L. & Rossi, D. Cell-Penetrating Peptides: From Basic Research to Clinics. *Trends Pharmacol. Sci.* **38**, 406–424 (2017).

118. Moschos, S. A. *et al.* Lung delivery studies using siRNA conjugated to TAT(48-60) and penetratin reveal peptide induced reduction in gene expression and induction of innate immunity. *Bioconjug. Chem.* **18**, 1450–1459 (2007).

119. Kanazawa, T. *et al.* Suppression of tumour growth by systemic delivery of anti-VEGF siRNA with cell-penetrating peptide-modified MPEG-PCL nanomicelles. *Eur. J. Pharm. Biopharm.* **81**, 470–477 (2012).

120. Kanazawa, T., Akiyama, F., Kakizaki, S., Takashima, Y. & Seta, Y. Delivery of siRNA to the brain using a combination of nose-to-brain delivery and cell-penetrating peptide-modified nano-micelles. *Biomaterials* **34**, 9220–9226 (2013).

121. Benjaminsen, R. V, Mattebjerg, M. A., Henriksen, J. R., Moghimi, S. M. & Andresen, T. L. The Possible " Proton Sponge " Effect of Polyethylenimine (PEI) Does Not Include Change in Lysosomal pH. *Mol. Ther.* **21**, 149–157 (2013).

122. Lu, J. J., Langer, R. S. & Chen, J. A Novel Mechanism Is Involved in Cationic Lipid-Mediated Functional siRNA Delivery. *Mol. Pharm.* **6**, 763–771 (2009).

123. Sahay, G. *et al.* Efficiency of siRNA delivery by lipid nanoparticles is limited by endocytic recycling - Supporting Information. *Nat. Biotechnol.* **31**, Supporting Information (2013).

124. Martens, T. F., Remaut, K., Demeester, J., De Smedt, S. C. & Braeckmans, K. Intracellular delivery of nanomaterials: How to catch endosomal escape in the act. *Nano Today* **9**, 344–364 (2014).

125. Jere, D. *et al.* Poly(β-amino ester) as a carrier for si/shRNA delivery in lung cancer cells. *Biomaterials* **29**, 2535–2547 (2008).

126. Sakurai, Y. *et al.* Endosomal escape and the knockdown efficiency of liposomal-siRNA by the fusogenic peptide shGALA. *Biomaterials* **32**, 5733–5742 (2011).

127. Akita, H. *et al.* Nanoparticles for ex vivo siRNA delivery to dendritic cells for cancer vaccines: Programmed endosomal escape and dissociation. *J. Control. Release* **143**, 311–317 (2010).

128. Akinc, A. *et al.* Targeted delivery of RNAi therapeutics with endogenous and exogenous ligand-based mechanisms. *Mol. Ther.* **18**, 1357–1364 (2010).

129. Gilleron, J. *et al.* Identification of siRNA delivery enhancers by a chemical library screen. *Nucleic Acids Res.* **43**, 7984–8001 (2015).

130. Wittrup, A. *et al.* Visualizing lipid-formulated siRNA release from endosomes and target gene knockdown. *Nat. Biotechnol.* **33**, 1–9 (2015).

131. Roberts, R. *et al.* Autophagy and formation of tubulovesicular autophagosomes provide a barrier against nonviral gene delivery. *Autophagy* **9**, 13–14 (2013).

132. Vercauteren, D. *et al.* Dynamic Colocalisation Microscopy To Characterize Intracellular Trafficking of Nanomedicines. *ACS Nano* **5**, 7874–7884 (2011).

133. Li, Y. *et al.* Stimuli-Responsive Polymeric Nanocarriers for Efficient Gene Delivery. *Top. Curr. Chem.* **375**, https://doi.org/10.1007/s41061-017-0119-6 (2017).

134. Mura, S., Nicolas, J. & Couvreur, P. Stimuli-responsive nanocarriers for drug delivery. *Nat. Mater.* **12**, 991–1003 (2013).

135. Kelley, E. G., Albert, J. N. L., Sullivan, M. O. & Epps, T. H. Stimuli-responsive copolymer solution and surface assemblies for biomedical applications. *Chem. Soc. Rev.* **42**, 7057–7071 (2013).

136. Akinc, A., Anderson, D. G., Lynn, D. M. & Langer, R. Synthesis of poly(beta-amino ester)s optimised for highly effective gene delivery. *Bioconjug. Chem.* **14**, 979–88 (2003).

137. Akinc, A., Lynn, D. M., Anderson, D. G. & Langer, R. Parallel synthesis and biophysical characterisation of a degradable polymer library for gene delivery. *J. Am. Chem. Soc.* **125**, 5316–5323 (2003).

138. Green, J. J. *et al.* Biodegradable Polymeric Vectors for Gene Delivery to Human Endothelial Cells. *Bioconjug. Chem.* **17**, 1162–1169 (2006).

139. Sago, C. D. *et al.* High-throughput in vivo screen of functional mRNA delivery identifies nanoparticles for endothelial cell gene editing. *Proc. Natl. Acad. Sci.* **115**, 201811276 (2018).

140. Heras-Palou, C. Patisiran' s path to approval. *Nature* **574**, S7 (2019).

141. Kost, J. & Langer, R. Responsive polymeric delivery systems. *Adv. Drug Deliv. Rev.* **64**, 327–341 (2012).

142. Kato, Y. *et al.* Acidic extracellular microenvironment and cancer. *Cancer Cell Int.* **13**, 1 (2013).

143. Lim, E.-K., Chung, B. & Chung, S. Recent Advances in pH-Sensitive Polymeric Nanoparticles for Smart Drug Delivery in Cancer Therapy. *Curr. Drug Targets* **19**, 300–317 (2018).

144. Tang, H., Zhao, W., Yu, J., Li, Y. & Zhao, C. Recent Development of pH-Responsive Polymers for Cancer Nanomedicine. *Molecules* **24**, 1–24 (2019).

145. Kocak, G., Tuncer, C. & Bütün, V. PH-Responsive polymers. *Polym. Chem.* **8**, 144–176 (2017).

146. Godbey, W. T., Wu, K. K. & Mikos, A. G. Size matters: Molecular weight affects the efficiency of poly(ethylenimine) as a gene delivery vehicle. *J. Biomed. Mater. Res.* **45**, 268–275 (1999).

147. Abdallah, B. *et al.* A powerful nonviral vector for in vivo gene transfer into the adult mammalian brain: polyethylenimine. *Hum. Gene Ther.* **7**, 1947–1954 (1996).

148. Kunath, K. *et al.* Low-molecular-weight polyethylenimine as a non-viral vector for DNA delivery: Comparison of physicochemical properties, transfection efficiency and in vivo distribution with high-molecular-weight polyethylenimine. *J. Control. Release* **89**, 113–125 (2003).

149. Anderson, D. G. *et al.* A polymer library approach to suicide gene therapy for cancer. *PNAS* **101**, 16028–16033 (2004).

150. Anderson, D. G., Akinc, A., Hossain, N. & Langer, R. Structure/property studies of polymeric gene delivery using a library of poly(beta-amino esters). *Mol. Ther.* **11**, 426–434 (2005).

151. Zugates, G. T. *et al.* Rapid Optimisation of Gene Delivery by Parallel End-modification of Poly(β-amino ester)s. *Mol. Ther.* **15**, 1306–1312 (2007).

152. Zugates, G. T. *et al.* Gene delivery properties of end-modified poly(beta-amino ester)s. *Bioconjug. Chem.* **18**, 1887–1896 (2007).

153. Green, J. J. *et al.* Nanoparticles for gene transfer to human embryonic stem cell colonies. *Nano Lett.* **8**, 3126–3130 (2008).

154. Kim, J., Sunshine, J. C. & Green, J. J. Differential Polymer Structure Tunes Mechanism of Cellular Uptake and Transfection Routes of Poly(β -amino ester) Polyplexes in Human Breast Cancer Cells. *Bioconjug. Chem.* **25**, 43–51 (2014).

155. Siegwart, D. J. *et al.* Combinatorial synthesis of chemically diverse core-shell nanoparticles for intracellular delivery. *PNAS* **108**, 12996–13001 (2011).

156. Khan, O. F. *et al.* Dendrimer-inspired nanomaterials for the in vivo delivery of siRNA to lung vasculature. *Nano Lett.* **15**, 3008–3016 (2015).

157. Zhou, K. *et al.* Modular degradable dendrimers enable small RNAs to extend survival in an aggressive liver cancer model. *Proc. Natl. Acad. Sci.* **113**, 520–525 (2016).

158. Love, K. T. *et al.* Lipid-like materials for low-dose, in vivo gene silencing. *Proc. Natl. Acad. Sci.* **107**, 9915–9915 (2010).

159. Alabi, C. A. *et al.* Multiparametric approach for the evaluation of lipid nanoparticles for siRNA delivery. *Proc. Natl. Acad. Sci.* **110**, 12881–12886 (2013).

160. Arteta, M. Y. *et al.* Successful reprogramming of cellular protein production through mRNA delivered by functionalised lipid nanoparticles. *PNAS* **115**, E3351-3360 (2018).

161. Jones, D. P. *et al.* Glutathione measurement in human plasma Evaluation of sample collection, storage and derivatisation conditions for analysis of dansyl derivatives by HPLC. *Clin. Chim. Acta* **275**, 175–184 (1998).

162. Lin, C. & Engbersen, J. F. J. Effect of chemical functionalities in poly(amido amine)s for non-viral gene transfection. *J. Control. Release* **132**, 267–272 (2008).

163. Lin, C. *et al.* Linear poly(amido amine)s with secondary and tertiary amino groups and variable amounts of disulphide linkages: Synthesis and in vitro gene transfer properties. *J. Control. Release* **116**, 130–137 (2006).

164. Won, Y., Ankoné, M., Engbersen, J. F. J., Feijen, J. & Kim, S. W. Poly (Amido Amine) s Containing Agmatine and Butanol Side Chains as Efficient Gene Carriers. *Macromol. Biosci.* **16**, 619–626 (2016).

165. Tzeng, S. Y., Hung, B. P., Grayson, W. L. & Green, J. J. Cystamine-terminated poly(beta-amino ester)s for siRNA delivery to human mesenchymal stem cells and enhancement of osteogenic differentiation. *Biomaterials* **33**, 8142–8151 (2012).

166. Kozielski, K. L., Tzeng, S. Y. & Green, J. J. A bioreducible linear poly(β-amino ester) for siRNA delivery. *Chem. Commun.* **49**, 5319–21 (2013).

167. Christensen, L. V. *et al.* Reducible poly(amido ethylenimine)s designed for triggered intracellular gene delivery. *Bioconjug. Chem.* **17**, 1233–1240 (2006).

168. Vader, P., Van Der Aa, L. J., Engbersen, J. F. J., Storm, G. & Schiffelers, R. M. Disulphide-based poly(amido amine)s for siRNA delivery: Effects of structure on siRNA complexation, cellular uptake, gene silencing and toxicity. *Pharm. Res.* **28**, 1013–1022 (2011).

169. Piest, M. *et al.* Novel poly(amido amine)s with bioreducible disulphide linkages in their diamino-units: Structure effects and in vitro gene transfer properties. *J. Control. Release* **130**, 38–45 (2008).

170. Lee, J. S. *et al.* Gold, poly(beta-amino ester) nanoparticles for small interfering RNA delivery. *Nano Lett.* **9**, 2402–2406 (2009).

171. Zhu, L., Perche, F., Wang, T. & Torchilin, V. P. Matrix metalloproteinase 2-sensitive multifunctional polymeric micelles for tumour-specific co-delivery of siRNA and hydrophobic drugs. *Biomaterials* **35**, 4213–4222 (2014).

172. Kumar, B., Koul, S., Khandrika, L., Meacham, R. B. & Koul, H. K. Oxidative stress is inherent in prostate cancer cells and is required for aggressive phenotype. *Cancer Res.* **68**, 1777–1785 (2008).

173. Shim, M. S. & Xia, Y. A reactive oxygen species (ROS)-responsive polymer for safe, efficient, and targeted gene delivery in cancer cells. *Angew. Chemie - Int. Ed.* **52**, 6926–6929 (2013).

174. Nardecchia, S., Sánchez-Moreno, P., Vicente, J. de, Marchal, J. A. & Boulaiz, H. Clinical Trials of Thermosensitive Nanomaterials: An Overview. *Nanomaterials* **9**, 191 (2019).

175. Kim, Y. M., Park, M. R. & Song, S. C. Injectable polyplex hydrogel for localised and long-term delivery of siRNA. *ACS Nano* **6**, 5757–5766 (2012).

176. Lee, S. H., Choi, S. H., Kim, S. H. & Park, T. G. Thermally sensitive cationic polymer nanocapsules for specific cytosolic delivery and efficient gene silencing of siRNA: Swelling induced physical disruption of endosome by cold shock. *J. Control. Release* **125**, 25–32 (2008).

177. Wang, Y. & Kohane, D. S. External triggers and triggered targeting strategies for drug delivery. *Nat. Rev. Mater.* **2**, 17020 (2017).

178. Riviere, J. E. & Heit, M. C. Electrically-Assisted Transdermal Drug Delivery. *Pharm. Res.* **14**, 687–697 (1997).

179. Eloy, J. O., Petrilli, R., Lopez, R. F. V & Lee, R. J. Stimuli-Responsive Nanoparticles for siRNA Delivery. *Curr. Pharm. Des.* **21**, 4131–4144 (2015).

180. Gautier, C., Cougnon, C., Pilard, J. F., Casse, N. & Chénais, B. A poly(cyclopentadithiophene) matrix suitable for electrochemically controlled DNA delivery. *Anal. Chem.* **79**, 7920–7923 (2007).

181. Potter, H. & Heller, R. Transfection by Electroporation. *Curr Protoc Mol Biol* **62**, 9.3.1.-9.3.6 (2003).

182. Boukany, P. E. *et al.* Nanochannel electroporation delivers precise amounts of biomolecules into living cells. *Nat. Nanotechnol.* **6**, 747–754 (2011).

183. Oleson, J. R. Hyperthermia by magnetic induction: I. Physical characteristics of the technique. *Int. J. Radiat. Oncol. Biol. Phys.* **8**, 1747–1756 (1982).

184. Derfus, A. M. *et al.* Remotely triggered release from magnetic nanoparticles. *Adv. Mater.* **19**, 3932–3936 (2007).

185. Lino, M. M. *et al.* Modulation of Angiogenic Activity by Light-Activatable miRNA-Loaded Nanocarriers. *ACS Nano* **12**, 5207–5220 (2018).

186. Zhang, L. *et al.* Ultrasound-Targeted Microbubble Destruction (UTMD) Assisted Delivery of shRNA against PHD2 into H9C2 Cells. *PLoS One* **10**, e0134629 (2015).

187. Zhang, L. *et al.* Localised Delivery of shRNA against PHD2 Protects the Heart from Acute Myocardial Infarction through Ultrasound-Targeted Cationic Microbubble Destruction. *Theranostics* **7**, 51–66 (2017).

188. Chen, G., Roy, I., Yang, C. & Prasad, P. N. Nanochemistry and Nanomedicine for Nanoparticle-based Diagnostics and Therapy. *Chem. Rev.* **116**, 2826–2885 (2016).

189. Silva, J. M., Silva, E. & Reis, R. L. Light-triggered release of photocaged therapeutics - Where are we now? *J. Control. Release* **298**, 154–176 (2019).

190. Yang, Y. *et al.* In vitro and in vivo uncaging and bioluminescence imaging by using photocaged upconversion nanoparticles. *Angew. Chemie - Int. Ed.* **51**, 3125–3129 (2012).

191. Beauté, L., McClenaghan, N. & Lecommandoux, S. Photo-triggered polymer nanomedicines: From molecular mechanisms to therapeutic applications. *Adv. Drug Deliv. Rev.* **Dec 13**, doi: 10.1016/j.addr.2018.12.010 (2018).

192. Demmig-Adams, B. & Adams, W. W. Photoprotection and other Responses of Plants To High Light Stress. *Annu. Rev. Plant Physiol. Plant Mol. Biol.* **43**, 599–626 (1992).

193. Neckers, D. C. Photochemical Reactions of Natural Macromolecules. *J. Chem. Educ.* **50**, 164–168 (1973).

194. Neer, R. M. The evolutionary significance of vitamin D, skin pigment, and ultraviolet light. *Am. J. Phys. Anthropol.* **43**, 409–416 (1975).

195. Veleva, B. I., van Bezooijen, R. L., Chel, V. G. M., Numans, M. E. & Caljouw, M. A. A. Effect of ultraviolet light on mood, depressive disorders and well-being. *Photodermatol. Photoimmunol. Photomed.* **34**, 288–297 (2018).

196. Castaño Picó, M. J., Sánchez Maciá, M. & Soler, L. M. Variability of neonatal hyperbilirubinemia of non-immune cause in the clinical practice. *J. Neonatal Nurs.* **24**, 126–133 (2018).

197. Muchowski, K. E. Evaluation and treatment of neonatal hyperbilirubinemia. *Am. Fam. Physician* **89**, 873–878 (2014).

198. Olsen, E. A. *et al.* Guidelines for phototherapy of mycosis fungoides and Sézary syndrome: A consensus statement of the United States Cutaneous Lymphoma Consortium. *J. Am. Acad. Dermatol.* **74**, 27–58 (2016).

199. Garritsen, F. M., Brouwer, M. W. D., Limpens, J. & Spuls, P. I. Photo(chemo)therapy in the management of atopic dermatitis: An updated systematic review with implications for practice and research. *Br. J. Dermatol.* **170**, 501–513 (2014).

200. Lai, H. C., Lin, C. S., Wu, C. S. & Lan, C. C. E. The impact of irradiance on UVB-induced cutaneous immunosuppression: Implications on administering most efficient phototherapy. *J. Dermatol. Sci.* **93**, 116–122 (2019).

201. Zhang, P. & Wu, M. X. A clinical review of phototherapy for psoriasis. *Lasers Med. Sci.* **33**, 173–180 (2018).

202. Bekkenk, M. W. *et al.* Patient reported outcomes for intensified versus conventional NB-UVB treatment in non-segmental vitiligo. *J. Dermatolog. Treat.* **Nov 29**, 1–4 (2018).

203. Elman, M. & Lebzelter, J. Light therapy in the treatment of acne vulgaris. *Dermatol Surg* **30**, 139–146 (2004).

204. Gupta, A., Avci, P., Dai, T., Huang, Y.-Y. & Hamblin, M. R. Ultraviolet Radiation in Wound Care: Sterilisation and Stimulation. *Adv. Wound Care* **2**, 422–437 (2013).

205. Rigel, D. S. Cutaneous ultraviolet exposure and its relationship to the development of skin cancer. *J. Am. Acad. Dermatol.* **58**, S129–S132 (2008).

206. Lan, C. C. E., Wang, Y. T., Lu, C. Y., Fang, A. H. & Wu, C. S. The effect of interaction of heat and UVB on human keratinocyte: Novel insights on UVB-induced carcinogenesis of the skin. *J. Dermatol. Sci.* **88**, 207–215 (2017).

207. Nehl, C. L. & Hafner, J. H. Shape-dependent plasmon resonances of gold nanoparticles. *J. Mater. Chem.* **18**, 2415–2419 (2008).

208. Rui, Y. *et al.* Near-infrared light-activatable siRNA delivery by microcapsules for combined tumour therapy. *Artif. Cells, Nanomedicine Biotechnol.* **46**, 15–24 (2018).

209. Shim, G. *et al.* Light-switchable systems for remotely controlled drug delivery. *J. Control. Release* **267**, 67–79 (2017).

210. Lajunen, T. *et al.* Light activated liposomes : Functionality and prospects in ocular drug delivery. *J. Control. Release* **244**, 157–166 (2016).

211. Yavlovich, A., Smith, B., Gupta, K., Blumenthal, R. & Puri, A. Light-sensitive lipid-based nanoparticles for drug delivery : design principles and future considerations for biological applications. *Mol. Membr. Biol.* **27**, 364–381 (2010).

212. Bansal, A. & Zhang, Y. Photocontrolled Nanoparticle Delivery Systems for Biomedical Applications. *Acc. Chem. Res.* **47**, 3052–3060 (2014).

213. Lee, S. E., Liu, G. L., Kim, F. & Lee, L. P. Remote optical switch for localised and selective control of gene interference. *Nano Lett.* **9**, 562–570 (2009).

214. Heinemann, D. *et al.* Gold Nanoparticle Mediated Laser Transfection for Efficient siRNA Mediated Gene Knock Down. *PLoS One* **8**, 1–9 (2013).

215. Braun, G. B. *et al.* Laser-Activated Gene Silencing via Gold Nanoshell-siRNA Conjugates. *ACS Nano* **3**, 2007–2015 (2015).

216. Yang, C. *et al.* Theranostic Niosomes for Efficient siRNA/MicroRNA Delivery and Activatable Near-Infrared Fluorescent Tracking of Stem Cells. *ACS Appl. Mater. Interfaces* **10**, 19494–19503 (2018).

217. Berg, K. *et al.* Photochemical internalisation: A novel technology for delivery of macromolecules into cytosol. *Cancer Res.* **59**, 1180–1183 (1999).

218. Nomoto, T. *et al.* Three-layered polyplex micelle as a multifunctional nanocarrier platform for light-induced systemic gene transfer. *Nat. Commun.* **5**, 1–10 (2014).

219. Yuan, Y., Zhang, C. J. & Liu, B. A Photoactivatable AIE Polymer for Light-Controlled Gene Delivery: Concurrent Endo/Lysosomal Escape and DNA Unpacking. *Angew. Chemie*

- *Int. Ed.* **54**, 11419–11423 (2015).

220. Ji, J., Li, X., Wu, T. & Feng, F. Spiropyran in nanoassemblies as a photosensitiser for photoswitchable ROS generation in living cells. *Chem. Sci.* **9**, 5816–5821 (2018).

221. Chen, G. *et al.* NIR-induced spatiotemporally controlled gene silencing by upconversion nanoparticle-based siRNA nanocarrier. *J. Control. Release* **282**, 148–155 (2018).

222. Li, W. *et al.* Light-regulated host-guest interaction as a new strategy for intracellular PEG-detachable polyplexes to facilitate nuclear entry. *Chem. Commun.* **48**, 10126–10128 (2012).

223. Deka, S. R., Yadav, S., Mahato, M. & Sharma, A. K. Azobenzene-aminoglycoside: Self-assembled smart amphiphilic nanostructures for drug delivery. *Colloids Surfaces B Biointerfaces* **135**, 150–157 (2015).

224. Li, Y., Yang, J., Sun, L., Wang, W. & Liu, W. UV light-triggered unpacking of DNA to enhance gene transfection of azobenzene-containing polycations. *J. Mater. Chem. B* **2**, 3868–3878 (2014).

225. Asanuma, H. *et al.* Synthesis of azobenzene-tethered DNA for reversible photo-regulation of DNA functions: hybridisation and transcription. *Nat. Protoc.* **2**, 203–212 (2007).

226. Ogasawara, S. & Maeda, M. Straightforward and reversible photoregulation of hybridisation by using a photochromic nucleoside. *Angew. Chemie - Int. Ed.* **47**, 8839–8842 (2008).

227. Zhang, Y. *et al.* Photo-tearable tape close-wrapped upconversion nanocapsules for near-infrared modulated efficient siRNA delivery and therapy. *Biomaterials* **163**, 55–66 (2018).

228. Brown, P. K., Qureshi, A. T., Moll, A. N., Hayes, D. J. & Monroe, W. T. Silver Nanoscale Antisense Drug Delivery System for Photoactivated Gene Silencing. *ACS Nano* **7**, 2948–2959 (2013).

229. Li, H.-J., Wang, H.-X., Sun, C.-Y., Du, J.-Z. & Wang, J. Shell-detachable nanoparticles based on a light-responsive amphiphile for enhanced siRNA delivery. *RSC Adv.* **4**, 1961–1964 (2014).

230. Foster, A. A., Greco, C. T., Green, M. D., Epps, T. H. & Sullivan, M. O. Light-mediated activation of siRNA release in diblock copolymer assemblies for controlled gene silencing. *Adv. Healthc. Mater.* **4**, 760–770 (2015).

231. Green, M. D. *et al.* Catch and release: Photocleavable cationic diblock copolymers as a potential platform for nucleic acid delivery. *Polym. Chem.* **5**, 5535–5541 (2014).

232. Lai, Y. Sen *et al.* Photodegradable self-assembling PAMAM dendrons for gene delivery involving dendriplex formation and phototriggered circular DNA release. *New J. Chem.* **40**, 2601–2608 (2016).

233. Huynh, C. T. *et al.* Light-triggered RNA release and induction of hMSC osteogenesis via photodegradable, dual-crosslinked hydrogels. *Nanomedicine (Lond).* **11**, 1535–1551 (2016).

234. Zheng, G., Cochella, L., Liu, J., Hobert, O. & Li, W. H. Temporal and spatial regulation of microRNA activity with photoactivatable cantimirs. *ACS Chem. Biol.* **6**, 1332–1338 (2011).

235. Lucas, T. *et al.* Light-inducible antimiR-92a as a therapeutic strategy to promote skin repair in healing-impaired diabetic mice. *Nat. Commun.* **8**, 15162 (2017).

236. Schäfer, F., Wagner, J., Knau, A., Dimmeler, S. & Heckel, A. Regulating angiogenesis with light-inducible antimirs. *Angew. Chemie - Int. Ed.* **52**, 13558–13561 (2013).

237. Dolmans, D. E. J. G. J., Fukumura, D. & Jain, R. K. Photodynamic therapy for cancer. *Nat. Rev. Cancer* **3**, 380–387 (2003).

238. Liao, J. C., Roider, J. & Jay, D. G. Chromophore-assisted laser inactivation of proteins is mediated by the photogeneration of free radicals. *Proc. Natl. Acad. Sci.* **91**, 2659–2663 (1994).

239. Dabrowski, J. M. & Arnaut, L. G. Photodynamic Therapy (PDT) of Cancer: From a Local to a Systemic Treatment. *Photochem. Photobiol. Sci.* **14**, 1765–1780 (2015).

240. Oliveira, S., Fretz, M. M., Høgset, A., Storm, G. & Schiffelers, R. M. Photochemical internalisation enhances silencing of epidermal growth factor receptor through improved endosomal escape of siRNA. *Biochim. Biophys. Acta - Biomembr.* **1768**, 1211–1217 (2007).

241. Sakai, K., Imaizumi, Y., Oguchi, T., Sakai, H. & Abe, M. Adsorption characteristics of spiropyran-modified cationic surfactants at the silica/aqueous solution interface. *Langmuir* **26**, 9283–9288 (2010).

242. Jiang, J., Tong, X., Morris, D. & Zhao, Y. Toward photocontrolled release using light-dissociable block copolymer micelles. *Macromolecules* **39**, 4633–4640 (2006).

243. Tabor, R. F., McCoy, T. M., Hu, Y. & Wilkinson, B. L. Physicochemical and biological characterisation of azobenzene-containing photoswitchable surfactants. *Bull. Chem. Soc. Jpn.* **91**, 932–939 (2018).

244. Kumar, G. S. & Neckers, D. C. Photochemistry of Azobenzene-Containing Polymers. *Chem. Rev.* **89**, 1915–1925 (1989).

245. Weis, P. & Wu, S. Light-Switchable Azobenzene-Containing Macromolecules: From UV to Near Infrared. *Macromol. Rapid Commun.* **39**, 1–12 (2018).

246. Wang, G., Tong, X. & Zhao, Y. Preparation of azobenzene-containing amphiphilic diblock copolymers for light-responsive micellar aggregates. *Macromolecules* **37**, 8911–8917 (2004).

247. Takenaka, T. *et al.* Photoresponsive DNA nanocapsule having an open/close system for capture and release of nanomaterials. *Chem. - A Eur. J.* **20**, 14951–14954 (2014).

248. Jiang, J., Tong, X. & Zhao, Y. A new design for light-breakable polymer micelles. *J. Am. Chem. Soc.* **127**, 8290–8291 (2005).

249. Hansen, M. J., Velema, W. A., Lerch, M. M., Szymanski, W. & Feringa, B. L. Wavelength-selective cleavage of photoprotecting groups: Strategies and applications in dynamic systems. *Chem. Soc. Rev.* **44**, 3358–3377 (2015).

250. Gaplovsky, M. *et al.* Photochemical reaction mechanisms of 2-nitrobenzyl compounds: 2-nitrobenzyl alcohols form 2-nitroso hydrates by dual proton transfer. *Photochem. Photobiol. Sci.* **4**, 33–42 (2005).

251. Piant, S., Bolze, F. & Specht, A. Two-photon uncaging, from neuroscience to materials. *Opt. Mater. Express* **6**, 1679 (2016).

252. Oliveira, H. *et al.* Critical Considerations on the Clinical Translation of Upconversion Nanoparticles (UCNPs): Recommendations from the European Upconversion Network (COST Action CM1403). *Adv. Healthc. Mater.* **8**, 1801233 (2019).

253. Fomina, N., McFearin, C., Sermsakdi, M., Edigin, O. & Almutairi, A. UV and near-IR triggered release from polymeric nanoparticles. *J. Am. Chem. Soc.* **132**, 9540–9542 (2010).

254. Huu, V. A. N. *et al.* Light-responsive nanoparticle depot to control release of a small molecule angiogenesis inhibitor in the posterior segment of the eye. *J. Control. Release* **200**, 71–77 (2015).

255. Li, H.-J., Wang, H.-X., Sun, C.-Y., Du, J.-Z. & Wang, J. Shell-detachable nanoparticles based on a light-responsive amphiphile for enhanced siRNA delivery - Supplementary Information. *RSC Adv.* **4**, 1961–1964 (2014).

256. Deng, X., Zheng, N., Song, Z., Yin, L. & Cheng, J. Trigger-responsive, fast-degradable poly(b-amino ester)s for enhanced DNA unpackaging and reduced toxicity. *Biomaterials* **35**, 5006–5015 (2014).

257. Boto, C. *et al.* Prolonged intracellular accumulation of light-inducible nanoparticles in leukemia cells allows their remote activation. *Nat. Commun.* **8**, (2017).

258. Huynh, C. T. *et al.* Photocleavable Hydrogels for Light-Triggered siRNA Release. *Adv. Healthc. Mater.* **5**, 305–310 (2016).

259. Griepenburg, J. C., Ruble, B. K. & Dmochowski, I. J. Caged oligonucleotides for bidirectional photomodulation of let-7 miRNA in zebrafish embryos. *Bioorganic Med. Chem.* **21**, 6198–6204 (2013).

260. Connelly, C. M., Uprety, R., Hemphill, J. & Deiters, A. Spatiotemporal control of microRNA function using light-activated antagomirs. *Mol. Biosyst.* **8**, 2987–2993 (2012).

261. Brieke, C., Rohrbach, F., Gottschalk, A., Mayer, G. & Heckel, A. Light-controlled tools. *Angew. Chemie - Int. Ed.* **51**, 8446–8476 (2012).

262. Vicentini, F. T. M. de C. *et al.* Delivery Systems and Local Administration Routes for Therapeutic siRNA. *Pharm. Res.* **30**, 915–931 (2013).

263. Duvvuri, S., Majumdar, S. & Mitra, A. K. Drug Delivery to the Retina: Challenges and opportunities. *Expert Opin. Biol. Ther.* **3**, 45–56 (2003).

264. Gaudana, R., Jwala, J., Boddu, S. H. S. & Mitra, A. K. Recent perspectives in ocular drug delivery. *Pharm. Res.* **26**, 1197–1216 (2009).

265. Gaudana, R., Ananthula, H. K., Parenky, A. & Mitra, A. K. Ocular drug delivery. *AAPS J.* **12**, 348–360 (2010).

266. Patel, A., Cholkar, K., Agrahari, V. & Mitra, A. K. Ocular drug delivery systems: An overview. *World J. Pharmacol.* **2**, 47–64 (2013).

267. Cho, W. G. *et al.* Small interfering RNA-induced TLR3 activation inhibits blood and lymphatic vessel growth. *Proc. Natl. Acad. Sci.* **106**, 7137–7142 (2009).

268. Feinstein, E. *et al.* PF-04523655 (REDD14), an siRNA Compound Targeting RTP801, Penetrates Retinal Cells Producing Target Gene Knockdown and Avoiding TLR3 Activation. *Invest. Ophthalmol. Vis. Sci.* **50**, 5693 (2009).

269. Nguyen, Q. D. *et al.* Evaluation of the siRNA PF-04523655 versus ranibizumab for the treatment of neovascular age-related macular degeneration (MONET Study). *Ophthalmology* **119**, 1867–1873 (2012).

270. Bishop, P. N. Structural Macromolecules and Supramolecular Organisation of the Vitreous Gel. *Prog. Retin. Eye Res.* **19**, 323–344 (2000).

271. Ly, S. *et al.* Visualisation of self-delivering hydrophobically modified siRNA cellular internalisation. *Nucleic Acids Res.* **45**, 15–25 (2017).

272. Byrne, M. *et al.* Novel Hydrophobically Modified Asymmetric RNAi Compounds (sd-rxRNA) Demonstrate Robust Efficacy in the Eye. *J. Ocul. Pharmacol. Ther.* **29**, 855–864 (2013).

273. Saraiva, S. M., Castro-Lpoez, V., Paneda, C. & Alonso, M. J. Synthetic nanocarriers for the delivery of polynucleotides to the eye. *Eur. J. Pharm. Sci.* **103**, 5–18 (2017).

274. Bisht, R., Mandal, A., Jaiswal, J. K. & Rupenthal, I. D. Nanocarrier mediated retinal drug delivery: overcoming ocular barriers to treat posterior eye diseases. *Wiley Interdiscip. Rev. Nanomedicine Nanobiotechnology* **10**, 1–21 (2018).

275. Joseph, R. R. & Venkatraman, S. S. Drug delivery to the eye: What benefits do nanocarriers offer? *Nanomedicine* **12**, 683–702 (2017).

276. Vercauteren, D. *et al.* Flotillin-dependent endocytosis and a phagocytosis-like mechanism for cellular internalisation of disulphide-based poly(amido amine)/DNA polyplexes. *Biomaterials* **32**, 3072–3084 (2011).

277. Martens, T. F. *et al.* Coating nanocarriers with hyaluronic acid facilitates intravitreal drug delivery for retinal gene therapy. *J. Control. Release* **202**, 83–92 (2015).

278. Hilberg, F. *et al.* BIBF 1120: Triple angiokinase inhibitor with sustained receptor blockade and good antitumour efficacy. *Cancer Res.* **68**, 4774–4782 (2008).

279. Khurana, M. *et al.* Quantitative in vitro demonstration of two-photon photodynamic therapy using Photofrin® and Visudyne®. *Photochem. Photobiol.* **83**, 1441–1448 (2007).

280. Sepahvandi, A., Eskandari, M. & Moztarzadeh, F. Drug Delivery Systems to the Posterior Segment of the Eye: Implants and Nanoparticles. *Bionanoscience* **6**, 276–283 (2016).

281. Bisht, R., Jaiswal, J. K., Chen, Y., Jin, J. & Rupenthal, D. I. Light-responsive in situ forming injectable implants for effective drug delivery to the posterior segment of the eye. *Expert Opin. Drug Deliv.* **7**, 953–962 (2016).

282. Tyagi, P., Barros, M., Stansbury, J. W. & Kompella, U. B. Light-activated, in situ forming gel for sustained suprachoroidal delivery of bevacizumab. *Mol. Pharm.* **10**, 2858–2867 (2013).

283. Minutti, C. M., Knipper, J. A., Allen, J. E. & Zaiss, D. M. W. Tissue-specific contribution of macrophages to wound healing. *Semin. Cell Dev. Biol.* **61**, 3–11 (2017).

284. Juzeniene, A. *et al.* Solar radiation and human health. *Reports Prog. Phys.* **74**, 66701 (2011).

285. Hickerson, R. P. *et al.* Use of self-delivery siRNAs to inhibit gene expression in an organotypic pachyonychia congenita model. *J. Invest. Dermatol.* **131**, 1037–1044 (2011).

286. Nussbaum, S. R. *et al.* An Economic Evaluation of the Impact, Cost, and Medicare Policy Implications of Chronic Nonhealing Wounds. *Value Heal.* **21**, 27–32 (2018).

287. Martinengo, L. *et al.* Prevalence of chronic wounds in the general population: systematic review and meta-analysis of observational studies. *Ann. Epidemiol.* **29**, 8–15 (2019).

288. Vos, T. *et al.* Global, regional, and national incidence, prevalence, and years lived with disability for 328 diseases and injuries for 195 countries, 1990-2016: A systematic analysis for the Global Burden of Disease Study 2016. *Lancet* **390**, 1211–1259 (2017).

289. Sen, C. K. Human Wounds and Its Burden: An Updated Compendium of Estimates. *Adv. Wound Care* **8**, 39–48 (2019).

290. Gurtner, G. C., Werner, S., Barrandon, Y. & Longaker, M. T. Wound repair and regeneration. *Nature* **453**, 314–321 (2008).

291. Falanga, V. The chronic wound: Impaired healing and solutions in the context of wound bed preparation. *Blood Cells, Mol. Dis.* **32**, 88–94 (2004).

292. Frykberg, R. G. & Banks, J. Challenges in the Treatment of Chronic Wounds. *Adv. Wound Care* **4**, 560–582 (2015).

293. Laiva, A. L., O'Brien, F. J. & Keogh, M. B. Innovations in gene and growth factor delivery systems for diabetic wound healing. *J. Tissue Eng. Regen. Med.* **12**, e296–e312 (2018).

294. Blersch, E. Tierexperimentelle Untersuchungen zur Beeinflussung der Wundheilung durch hormonelle Faktoren. (Ulm University, 1983).

295. Fahs, F., Bi, X., Yu, F.-S., Zhou, L. & Mi, Q.-S. New insights into microRNAs in skin wound healing. *IUBMB Life* **67**, 889–896 (2015).

296. Miller, K. J., Brown, D. A., Ibrahim, M. M., Ramchal, T. D. & Levinson, H. MicroRNAs in skin tissue engineering. *Adv. Drug Deliv. Rev.* **88**, 16–36 (2015).

297. Mulholland, E. J., Dunne, N. & McCarthy, H. O. microRNA as Therapeutic Targets for Chronic Wound Healing. *Mol. Ther. Nucleic Acid* **8**, 46–55 (2017).

298. Larouche, J., Sheoran, S., Maruyama, K. & Martino, M. M. Immune Regulation of Skin Wound Healing: Mechanisms and Novel Therapeutic Targets. *Adv. Wound Care* **7**, 209–231 (2018).

299. Witte, M. B. & Barbul, A. Role of nitric oxide in wound repair. *Am. J. Surg.* **183**, 406–412 (2002).

300. Connelly, L., Jacobs, A. T., Palacios-Callender, M., Moncada, S. & Hobbs, A. J. Macrophage endothelial nitric-oxide synthase autoregulates cellular activation and pro-inflammatory protein expression. *J. Biol. Chem.* **278**, 26480–26487 (2003).

301. Förstermann, U. & Sessa, W. C. Nitric oxide synthases: Regulation and function. *Eur. Heart J.* **33**, 829–837 (2012).

302. Luo, J. D., Wang, Y. Y., Fu, W. L., Wu, J. & Chen, A. F. Gene therapy of endothelial nitric oxide synthase and manganese superoxide dismutase restores delayed wound healing in type 1 diabetic mice. *Circulation* **110**, 2484–2493 (2004).

303. Marrotte, E. J., Chen, D. D., Hakim, J. S. & Chen, A. F. Manganese superoxide dismutase expression in endothelial progenitor cells accelerates wound healing in diabetic mice. *J. Clin. Invest.* **120**, 4207–4219 (2010).

304. Luo, J.-D. *et al.* Sonic hedgehog improves delayed wound healing via enhancing cutaneous nitric oxide function in diabetes. *Am. J. Physiol. Metab.* **297**, E525–E531 (2009).

305. Asai, J. *et al.* Topical sonic hedgehog gene therapy accelerates wound healing in diabetes by enhancing endothelial progenitor cell-mediated microvascular remodelling. *Circulation* **113**, 2413–2424 (2006).

306. Park, H. J. *et al.* Sonic hedgehog intradermal gene therapy using a biodegradable poly(ß-amino esters) nanoparticle to enhance wound healing. *Biomaterials* **33**, 9148–9156 (2012).

307. Soares, M. A. *et al.* Restoration of Nrf2 signaling normalizes the regenerative niche. *Diabetes* **65**, 633–646 (2016).

308. Rabbani, P. S. *et al.* Novel lipoproteoplex delivers Keap1 siRNA based gene therapy to accelerate diabetic wound healing. *Biomaterials* **132**, 1–15 (2017).

309. Weidemann, A. & Johnson, R. S. Biology of HIF-1α. *Cell Death Differ.* **15**, 621–627 (2008).

310. Sano, H. & Ichioka, S. Influence of oxygen on wound healing dynamics in healing-impaired diabetic mice. *J. Plast. Surg. Hand Surg.* **49**, 135–140 (2015).

311. Lee, J.-W., Bae, S.-H., Jeong, J.-W., Kim, S.-H. & Kim, K. Hypoxia-inducible factor (HIF-1)α: its protein stability and biological functions. *Exp. Mol. Med.* **36**, 1–12 (2004).

312. Semenza, G. L. Hypoxia-Inducible Factor 1 and Cardiovascular Disease. *Annu Rev Physiol* **76**, 39–56 (2014).

313. Harnoss, J. M. *et al.* Therapeutic inhibition of prolyl hydroxylase domain-containing enzymes in surgery: putative applications and challenges. *Hypoxia* **3**, 1–14 (2015).

314. Zhang, X. *et al.* Wound Healing Improvement with PHD-2 Silenced Fibroblasts in Diabetic Mice. *PLoS One* **8**, 1–11 (2013).

315. Martin, J. R. *et al.* Local Delivery of PHD2 siRNA from ROS-Degradable Scaffolds to Promote Diabetic Wound Healing. *Adv. Healthc. Mater.* **21**, 2751–2757 (2016).

316. Thanik, V. D. *et al.* Topical matrix-based siRNA silences local gene expression in a murine wound model. *Gene Ther.* **14**, 1305–1308 (2007).

317. Nguyen, P. D. *et al.* Improved diabetic wound healing through topical silencing of p53 is associated with augmented vasculogenic mediators. *Wound Repair Regen.* **18**, 553–559 (2010).

318. Ghatak, S. *et al.* AntihypoxamiR functionalised gramicidin lipid nanoparticles rescue against ischemic memory improving cutaneous wound healing. *Nanomedicine Nanotechnology, Biol. Med.* **12**, 1827–1831 (2016).

319. Liu, Y. *et al.* Increased matrix metalloproteinase-9 predicts poor wound healing in diabetic foot ulcers. *Diabetes Care* **32**, 117–119 (2009).

320. Moor, A. N., Vachon, D. J. & Gould, L. J. Proteolytic activity in wound fluids and tissues derived from chronic venous leg ulcers. *Wound Repair Regen.* **17**, 832–839 (2009).

321. Castleberry, S. A. *et al.* Self-Assembled Wound Dressings Silence MMP-9 and Improve Diabetic Wound Healing in Vivo. *Adv. Mater.* **28**, 1809–1817 (2016).

322. Li, N. *et al.* Efficiency and Safety of β-CD-(D3)7 as siRNA Carrier for Decreasing MMP-9 Expression and Improving Wound Healing in Diabetic Rats. *ACS Appl. Mater. Interfaces* **9**, 17417–17426 (2017).

323. Okizaki, S. ichiro *et al.* Suppressed recruitment of alternatively activated macrophages reduces TGF-β1 and impairs wound healing in streptozotocin-induced diabetic mice. *Biomed. Pharmacother.* **70**, 317–325 (2015).

324. Toulon, A. *et al.* A role for human skin–resident T cells in wound healing. *J. Exp. Med.* **206**, 743–750 (2009).

325. Bitar, M. S. Insulin-like growth factor-1 reverses diabetes-induced wound healing impairment in rats. *Horm. Metab. Res.* **29**, 383–386 (1997).

326. Li, Q., Zhao, H., Chen, W., Huang, P. & Bi, J. Human Keratinocyte-derived Microvesicle miRNA-21 Promotes Skin Wound Healing in Diabetic Rats Through Facilitating Fibroblast Function and Angiogenesis. *Int. J. Biochem. Cell Biol.* 105570 (2019). doi:10.1016/j.biocel.2019.105570

327. Icli, B. *et al.* Regulation of impaired angiogenesis in diabetic dermal wound healing by microRNA-26a. *J. Mol. Cell. Cardiol.* **91**, 151–159 (2016).

328. Li, X. *et al.* MicroRNA-132 with Therapeutic Potential in Chronic Wounds. *J. Invest. Dermatol.* **137**, 2630–2638 (2017).

329. Zgheib, C. *et al.* Use of Cerium Oxide Nanoparticles Conjugated with MicroRNA-146a to Correct the Diabetic Wound Healing Impairment. *J. Am. Coll. Surg.* **228**, 107–115 (2019).

330. Henriques-Antunes, H. *et al.* The Kinetics of Small Extracellular Vesicle Delivery Impacts Tissue Regeneration. *ACS Nano* DOI: 10.1021/acsnano.9b00376 (2019). doi:10.1021/acsnano.9b00376

331. Yang, L. *et al.* miR-155 promotes cutaneous wound healing through enhanced keratinocytes migration by MMP-2. *J. Mol. Histol.* **48**, 147–155 (2017).

332. Saleh, B. *et al.* Local Immunomodulation Using an Adhesive Hydrogel Loaded with miRNA-Laden Nanoparticles Promotes Wound Healing. *Small* **1902232**, 1902232 (2019).

333. Li, H. *et al.* Anti-microRNA-378a enhances wound healing process by upregulating integrin beta-3 and vimentin. *Mol. Ther.* **22**, 1839–1850 (2014).

334. Wang, X. Q. *et al.* Ganglioside GM3 depletion reverses impaired wound healing in diabetic mice by activating IGF-1 and insulin receptors. *J. Invest. Dermatol.* **134**, 1446–1455 (2014).

335. Shaw, T. J. & Martin, P. Wound repair: A showcase for cell plasticity and migration. *Curr. Opin. Cell Biol.* **42**, 29–37 (2016).

336. Charafeddine, R. A. *et al.* Fidgetin-Like 2: A Microtubule-Based Regulator of Wound Healing. *J. Invest. Dermatol.* **135**, 2309–18 (2015).

337. Mukherjee, S. *et al.* Human fidgetin is a microtubule severing enzyme and minus-end depolymerase that regulates mitosis. *Cell Cycle* **11**, 2359–2366 (2012).

338. Charafeddine, R. A., Nosanchuk, J. D. & Sharp, D. J. Targeting Microtubules for Wound Repair. *Adv. Wound Care* **5**, 444–454 (2016).

339. Daniels, J. T. *et al.* Mediation of Transforming Growth Factor-β1-Stimulated Matrix Contraction by Fibroblasts. *Am. J. Pathol.* **163**, 2043–2052 (2003).

340. Frazier, K., Williams, S., Kothapalli, D., Klapper, H. & Grotendorst, G. R. Stimulation of fibroblast cell growth, matrix production, and granulation tissue formation by connective tissue growth factor. *J. Invest. Dermatol.* **107**, 404–411 (1996).

341. Igarashi, A., Okochi, H., Bradham, D. M. & Grotendorst, G. R. Regulation of connective tissue growth factor gene expression in human skin fibroblasts and during wound repair. *Mol. Biol. Cell* **4**, 637–645 (1993).

342. Cho, K. H. *et al.* Local Delivery of CTGF siRNA with Poly(sorbitol-co-PEI) Reduces Scar Contraction in Cutaneous Wound Healing. *Tissue Eng. Regen. Med.* **14**, 211–220 (2017).

343. Castleberry, S. A. *et al.* Nanolayered siRNA delivery platforms for local silencing of CTGF

reduce cutaneous scar contraction in third-degree burns. *Biomaterials* **95**, 22–34 (2016).

344. Libertine, L. *et al.* Update on phase 2 clinical trial results of RXI-109 treatment to reduce the formation of hypertrophic dermal scars. *J. Am. Acad. Dermatol.* **72**, AB273 (2015).

345. Madhyastha, R., Madhyastha, H., Nakajima, Y., Omura, S. & Maruyama, M. MicroRNA signature in diabetic wound healing: Promotive role of miR-21 in fibroblast migration. *Int. Wound J.* **9**, 355–361 (2012).

346. Juliano, R. L. The delivery of therapeutic oligonucleotides. *Nucleic Acids Res.* **44**, 6518–6548 (2016).

347. Kanasty, R., Dorkin, J. R., Vegas, A. & Anderson, D. Delivery materials for siRNA therapeutics. *Nat. Mater.* **12**, 967–977 (2013).

348. Huschka, R. *et al.* Gene Silencing by Gold Nanoshell-Mediated Delivery and Laser-Triggered Release of Antisense Oligonucleotide and siRNA. *ACS Nano* **6**, 7681–7691 (2012).

349. Chang, Y. T. *et al.* Near-Infrared light-responsive intracellular drug and sirna release using au nanoensembles with oligonucleotide-capped silica shell. *Adv. Mater.* **24**, 3309–3314 (2012).

350. Yang, Y., Liu, F., Liu, X. & Xing, B. NIR light controlled photorelease of siRNA and its targeted intracellular delivery based on upconversion nanoparticles. *Nanoscale* **5**, 231–238 (2013).

351. Wang, H. *et al.* A Near-Infrared Laser-Activated 'nanobomb' for Breaking the Barriers to MicroRNA Delivery. *Adv. Mater.* **28**, 347–355 (2016).

352. Whitehead, K. A. *et al.* Degradable lipid nanoparticles with predictable in vivo siRNA delivery activity. *Nat. Commun.* **5**, 1–10 (2014).

353. Kozielski, K. L., Tzeng, S. Y., Mendoza, B. A. H. de & Green, J. J. Bioreducible Cationic Polymer-Based Environmentally Triggered Cytoplasmic siRNA Delivery to Primary Human Brain Cancer Cells. *ACS Nano* **8**, 3232–3241 (2014).

354. Dahlman, J. E. *et al.* In vivo endothelial siRNA delivery using polymeric nanoparticles with low molecular weight. *Nat. Nanotechnol.* **9**, 648–655 (2014).

355. Gehin, C. *et al.* Dynamic amphiphile libraries to screen for the 'fragrant' delivery of siRNA into HeLa cells and human primary fibroblasts. *J. Am. Chem. Soc.* **135**, 9295–9298 (2013).

356. Zhou, Y., Ye, H., Chen, Y., Zhu, R. & Yin, L. Photoresponsive Drug/Gene Delivery Systems. *Biomacromolecules* **19**, 1840–1857 (2018).

357. Klán, P. *et al.* Photoremovable protecting groups in chemistry and biology: Reaction mechanisms and efficacy. *Chem. Rev.* **113**, 119–191 (2013).

358. Kilchrist, K. V., Evans, B. C., Brophy, C. M. & Duvall, C. L. Mechanism of Enhanced Cellular Uptake and Cytosolic Retention of MK2 Inhibitory Peptide Nano-polyplexes. *Cell. Mol. Bioeng.* **9**, 368–381 (2016).

359. Xiao, C. *et al.* MiR-150 Controls B Cell Differentiation by Targeting the Transcription Factor c-Myb. *Cell* **131**, 146–159 (2007).

360. Botusan, I. R. *et al.* Stabilisation of HIF-1 is critical to improve wound healing in diabetic mice. *Proc. Natl. Acad. Sci.* **105**, 19426–19431 (2008).

361. Sarkar, K., Fox-Talbot, K., Steenbergen, C., Bosch-Marcé, M. & Semenza, G. L. Adenoviral transfer of HIF-1α enhances vascular responses to critical limb ischemia in diabetic mice. *PNAS* **107**, 514 (2010).

362. Forsythe, J. A. *et al.* Activation of vascular endothelial growth factor gene transcription by hypoxia-inducible factor 1. *Mol. Cell. Biol.* **16**, 4604–13 (1996).

363. Fraisl, P., Aragonés, J. & Carmeliet, P. Inhibition of oxygen sensors as a therapeutic strategy for ischaemic and inflammatory disease. *Nat. Rev. Drug Discov.* **8**, 139–152 (2009).

364. Nelson, C. E. *et al.* Tunable Delivery of siRNA from a Biodegradable Scaffold to Promote Angiogenesis In Vivo. *Adv. Mater.* **26**, 607–614 (2014).

365. Bordoli, M. R. *et al.* Prolyl-4-hydroxylase PHD2- and hypoxia-inducible factor 2-dependent regulation of amphiregulin contributes to breast tumourigenesis. *Oncogene* **30**, 548–560 (2011).

366. Mazzone, M. *et al.* Heterozygous Deficiency of PHD2 Restores Tumour Oxygenation and Inhibits Metastasis via Endothelial Normalisation. *Cell* **136**, 839–851 (2009).

367. Wong, B. W., Marsch, E., Treps, L., Baes, M. & Carmeliet, P. Endothelial cell metabolism in health and disease: impact of hypoxia. *EMBO J.* **36**, 2187–2203 (2017).

368. Miller, J. B. & Siegwart, D. J. Design of synthetic materials for intracellular delivery of RNAs: From siRNA-mediated gene silencing to CRISPR/Cas gene editing. *Nano Res.* **11**, 5310–5337 (2018).

369. Shukla, R. S., Qin, B. & Cheng, K. Peptides used in the delivery of small noncoding RNA. *Mol. Pharm.* **11**, 3395–3408 (2014).

370. Mahon, K. P. *et al.* Combinatorial approach to determine functional group effects on lipidoid-mediated siRNA delivery. *Bioconjug. Chem.* **21**, 1448–1454 (2010).

371. Whitehead, K. A. *et al.* Synergistic silencing: Combinations of lipid-like materials for efficacious siRNA delivery. *Mol. Ther.* **19**, 1688–1694 (2011).

372. Kim, H. J., Kim, A., Miyata, K. & Kataoka, K. Recent progress in development of siRNA delivery vehicles for cancer therapy. *Adv. Drug Deliv. Rev.* **104**, 61–77 (2016).

373. EBioMedicine. RNA-based therapies have their day. *Lancet* **34**, 1 (2018).

374. Lönn, P. *et al.* Enhancing Endosomal Escape for Intracellular Delivery of Macromolecular Biologic Therapeutics. *Sci. Rep.* **6**, 1–9 (2016).

375. Dvir, T., Banghart, M. R., Timko, B. P.-, Langer, R. & Kohane, D. S. Photo-Targeted Nanoparticles. *Nano Lett.* **10**, 250–254 (2010).

376. Tiyaboonchai, W., Woiszwillo, J. & Middaugh, C. R. Formulation and characterisation of DNA-polyethylenimine-dextran sulfate nanoparticles. *Eur. J. Pharm. Sci.* **19**, 191–202 (2003).

377. Peter Carmeliet, Yuval Dor, Jean-Marc Herbert, Dai Fukumura, K. B. E. Al *et al.* Role of HIF-1A in hypoxia mediated apoptosis, cell proliferation and tumour angiogenesis. *Nature* **394**, 485–490 (1998).

378. Ryan, H. E., Lo, J. & Johnson, R. S. HIF-1α is required for solid tumour formation and embryonic vascularisation. *EMBO J.* **17**, 3005–3015 (1998).

379. Blersch, J. *et al.* A Light-Triggerable Nanoparticle Library for the Controlled Release of Non-Coding RNAs. *Angew. Chemie - Int. Ed.* **59**, 1985–1991 (2020).

380. Xing, H. *et al.* Molecular weight determination of a newly synthesised guanidinylated disulphide-containing poly(amido amine) by gel permeation chromatography. *Asian J. Pharm. Sci.* **12**, 292–298 (2017).

381. Chen, W. C., May, J. P. & Li, S. D. Immune responses of therapeutic lipid nanoparticles. *Nanotechnol. Rev.* **2**, 201–213 (2013).

382. Spinetti, G. *et al.* Global remodelling of the vascular stem cell niche in bone marrow of diabetic patients: Implication of the microRNA-155/FOXO3a signaling pathway. *Circ. Res.* **112**, 510–522 (2013).

383. Blersch, J. *et al.* A light-triggerable formulation to control the stability of pro-angiogenic transcription factor hypoxia inducible factor-1a (HIF-1α). *Nanoscale.* **12**, 9935-9942 (2020).